

UNIVERSITY OF BIRMINGHAM

Controlling the microstructure of a random copolymer of poly (lactic acid) and its composite with hydroxyapatite for bone repair

By

Zeinab Salary

A thesis submitted to the University of Birmingham for the degree of Doctor of Philosophy

School of Metallurgy and Materials

College of Engineering and Physical Sciences

University of Birmingham

April 2019

UNIVERSITY OF
BIRMINGHAM

University of Birmingham Research Archive

e-theses repository

This unpublished thesis/dissertation is copyright of the author and/or third parties. The intellectual property rights of the author or third parties in respect of this work are as defined by The Copyright Designs and Patents Act 1988 or as modified by any successor legislation.

Any use made of information contained in this thesis/dissertation must be in accordance with that legislation and must be properly acknowledged. Further distribution or reproduction in any format is prohibited without the permission of the copyright holder.

Abstract

Poly (lactic acid) or PLA and its composites have been extensively used for different biomedical applications. However, there has been limited research in controlling the microstructure and crystallisation behaviour of PLA as the microstructure of the polymer could have an effect on the performance of the material.

In this study, the microstructure and crystallinity of a semi-crystalline random copolymer of poly (L-lactic acid) with 4% D-isomer were controlled by using Differential Scanning Calorimetry (DSC) and Hot Stage Microscopy (HSM) under both nonisothermal and isothermal conditions. From the nonisothermal crystallisation studies, it was found that by controlling the cooling rate of the polymer after melting, polymers with different microstructures and degree of crystallinity can be obtained. Additionally, according to the isothermal studies, increasing the isothermal temperature resulted in an increase in the size of spherulites, while their number decreased. The n values obtained from the Avrami model was around 3, indicating a three-dimensional crystal growth mechanism with spherical crystals geometry. In addition, PLA and hydroxyapatite (HA) composites were prepared by using three different procedures; hot pressing, injection moulding and solution casting in order to improve the bioactivity of the polymer and investigate the effect of HA particles on the crystallisation behaviour of the composite. The hot pressing preparation method was the most effective technique in terms of blending the PLA and HA particles homogeneously. According to DSC, HSM studies and Avrami analysis of the crystallisation of the composite materials, the HA particles acted as nucleating agents to facilitate the crystallisation process of PLA. Mechanical testing results revealed that the stiffness of the composites increased with increasing the HA content.

Dichloromethane (DCM) was also used to etch the surface of PLA samples in order to introduce porosity by etching the surfaces for various periods of time. Pores were formed on the surfaces of the PLA samples evidenced by scanning electron microscopy (SEM) and therefore etching could be an easy and simple way of adding porosity on the polymer surfaces aiming to better interaction of the surfaces with mammalian cells.

The effect of different spherulitic microstructures on the nano-hardness of PLA surfaces was investigated. The values of nano-hardness and Young's modulus of the PLA samples containing larger spherulites were higher (0.377and 7.79 GPa, respectively) in comparison with the samples containing smaller spherulites (0.343 and 7.31GPa, respectively) due to the increase in the thickness of lamellae of the samples containing larger spherulites. Furthermore, the effect of secondary crystallisation on the wear behaviour of PLA samples was explored. It was found that the amount of mass loss was less in a semi-crystalline sample compared to an amorphous one. However, by introducing the secondary crystallisation, wear resistance of the PLA samples was reduced.

Hydrolytic degradation studies were performed on PLA samples under both static and dynamic conditions. By increasing the temperature of the degradation medium, the hydrolysis rate and mass loss were increased under static conditions. However, the mass of all samples did not change under dynamic conditions because the pH was almost unchanged during the experiment due to the circulation of the aqueous environment. According to the Size Exclusion Chromatography (SEC) results of the samples under dynamic conditions, the PLA samples with the small size of spherulites showed a smaller change in the molecular weight compared to the samples with the larger size of PLA spherulites, suggesting a possible increase of stability of PLA with smaller spherulites size in reaction with the buffer. Furthermore, introducing HA into PLA samples would increase the stability of the samples in the buffer due to the alkaline effect of HA particles that leads to neutralisation of the acidic degradation products of PLA.

DSC results revealed that the degree of crystallinity of all PLA and PLA-HA samples increased significantly after the hydrolytic degradation under dynamic conditions. Additionally, according to the X-ray Diffraction (XRD) results, the amorphous PLA sample crystallised during hydrolytic degradation.

Acknowledgements

I sincerely wish to thank my supervisors, Dr. Mike Jenkins and Dr. Artemis Stamboulis, for their supervision, guidance and support throughout my PhD. A special thanks to Mr. Frank Biddlestone for his technical assistance, knowledge and advice.

I would also like to thank the following individuals who collaborated during this project helping, supporting and providing technical assistance: Dr. David Grossin and Dr. Fabien Brouillet, our collaborators on the degradation studies (Phosphates, Pharmacotechnie, Biomaterials /CIRIMAT INPT-UPS-CNRS, Université de Toulouse, France); Professor Tony McNally and Mr. Martin Worrall (Nanocomposites Group at WMG, University of Warwick) for allowing access to their injection moulding equipment and technical assistance; Professor Hanshang Dong and Dr. Zhenxue Zhang (School of Metallurgy and Materials, University of Birmingham) for allowing access to the nano-indentation equipment and technical assistance, Dr Karl Dearn (school of mechanical and civil engineering, University of Birmingham) our collaborator on the tribology studies. I also must acknowledge Professor Tim Button, Professor Alison Davenport and Professor Moataz Attallah (School of Metallurgy and Materials, University of Birmingham) for their advice and support during my PhD. I would also like to thank the School of Metallurgy and Materials/University of Birmingham for financial support during my PhD. Great appreciation to all my family and friends who have supported me during my PhD. Special thanks to Dr. Parastoo Jamshidi for her pure friendship, kindness, advice and support throughout my PhD.

Finally, my utmost appreciation goes to my parents, for their constant emotional support, encouragement and unconditional love not only during my PhD but also throughout my life so far. I would not be where I am today without their help and support.

LIST OF ABBREVIATIONS

BCP – Biphasic calcium phosphate

BSE – Backscattered electron

β-TCP – β -tricalcium phosphate

CoCr – Cobalt-chromium

Co-PLA – Co-poly (lactic acid)

DCM – Dichloromethane

DMTA – Dynamic mechanical thermal analysis

DRI – Differential refractometric index

DSC – Differential scanning calorimetry

DTA – Differential thermal analysis

E_a – Activation energy

E' – Storage modulus

E_f – Flexural modulus

ECM – Extracellular matrix

FDM – Fused deposition modelling

GPC – Gel permeation chromatography

HA – Hydroxyapatite

HSM – Hot Stage Microscopy

K_{IC} – Critical stress intensity factor

LDR – Light dependent resistance

LS – Light scattering

MAF – Mobile amorphous fraction

Mn – Number-average molecular weight

Mw – Weight-average molecular weight

PCL – Polycaprolactone

PDI – Polydispersity

PGA – Poly (glycolic acid)

PHB – Polyhydroxybutyrate

pKa – Acid dissociation constant

PLA – Poly (lactic acid)

PLGA – Poly (lactic-co-glycolic acid)

PO_4^3 – Phosphate

POM – Polyoxymethylene

PP – Polypropylene

PTFE – polytetrafluoroethylene

PUR – Polyurethane

RAF – Rigid amorphous fraction

ROP – Ring-opening polymerisation

RT – Room temperature

SE – Secondary electron

SEC – Size Exclusion Chromatography

SEM – Scanning Electron Microscopy

TGA – Thermogravimetric analysis

THF – Tetrahydrofuran

UHMWPE – Ultra-high-molecular-weight polyethylene

UTS – Ultimate tensile strength

$\mathbf{X_c}$ – Degree of crystallinity

$\mathbf{X_t}$ – Relative crystallinity

$\mathbf{\Delta H_c}$ – Heat of crystallisation

$\mathbf{\Delta C_p}$ – Heat capacity

$\mathbf{\Delta H_m}$ – Heat of fusion

$\mathbf{\sigma_f}$ – Flexural strength

TABLE OF CONTENTS

Chapter 1: Introduction and literature review 1
1.1 Bone tissue 1
1.2 Physical Macrostructure of bone 1
1.3 Physical Microstructure of bone 2
1.4 Chemical composition of the bone 4
1.5 Bone defects and different established treatments 4
1.6 Scaffold requirements for tissue engineering 5
1.7 Biomaterials used for bone scaffolds 6
1.7.1 Metals 6
1.7.2 Ceramics 7
1.7.3 Polymers 7
1.7.3.1 Natural Polymers 7
1.7.3.2 Synthetic Polymers 8
1.7.4 Composites 8
1.8 Poly (Lactic Acid) 9
1.9 Polymer Microstructure 12
1.10 Semi-crystalline and amorphous polymers 12
1.11 Mechanism of Crystallisation 14
1.11.1 Nucleation 14
1.11.2 Growth 15
1.12 Crystallisation Kinetics by Avrami analysis 17
1.13 The Glass Transition temperature 18
1.14 Physical Ageing phenomenon 19
1.15 Degradation mechanism of polymers 20
1.16 Effect of microstructure on tribological behaviour of polymers 23
1.17 Effect of microstructure on the hardness of polymers 24
1.18 Controlling the microstructure of PLA 24
1.19 Polylactic acid (PLA)/hydroxyapatite (HA) composites for tissue and bone repair applications 26
1.20 Project aims and objectives 29

Chapter 2: Materials and methods 31
2.1 Materials 31
2.1.1 Poly (lactic acid) 31
2.1.2 Hydroxyapatite 31
2.1.3 Dichloromethane 31
2.2 Sample preparation 31
2.2.1 Solid-dispersion and hot pressing 31
2.2.2 Injection moulding 32
2.2.3 Solution casting 32
2.3 Differential Scanning Calorimetry (DSC) 33
2.3.1 Experimental procedure 34
2. 4 Hot Stage Microscopy (HSM) 37
2.4.1 Experimental procedure 37
2.5 Scanning Electron Microscopy (SEM) 38
2.5.1 Experimental procedure 39
2.6 Thermogravimetric analysis (TGA) 39
2.6.1 Experimental procedure 40
2.7 Tensile testing 40
2.7.1 Experimental procedure 41
2.8 Three-point bending flexural testing 42
2.8.1 Experimental procedure 42
2.9 Dynamic Mechanical Thermal Analysis (DMTA) 43
2.9.1 Experimental procedure 43
2.10 Nano-indentation (nano-hardness) testing 43
2.10.1 Experimental procedure 44
2.11 Tribological experiment 46
2.11.1 Experimental procedure 46
2.12 Hydrolytic degradation studies 48
2.12.1 Preparation of Tris buffer solution 48
2.12.2 Degradation testing under static conditions 49
2.12.3 Degradation testing under dynamic conditions 49
2.12.3.1 Experimental procedure 51
2.12.4 Size Exclusion Chromatography (SEC) coupling with static light scattering (LS) ..53

2.12.4.1 Experimental procedure 53
2.12.5 X-ray Diffraction (XRD) 54
2.12.5.1 Experimental procedure 54
Chapter 3: Controlling the microstructure and crystallisation behaviour of PLA 55
3.0 Introduction 55
3.1 Results and discussion 55
3.1.1 Thermal characterisation of the as-received PLA pellet 55
3.1.2 Influence of different heating rates on the glass transition temperature 58
3.1.3 Influence of various cooling rates on the crystallinity of the polymer 60
3.1.4 Influence of various cooling rates on the glass transition temperature 63
3.1.5 Correlation between the cooling rate and morphology of the PLA studied under hot stage microscopy (HSM) 67
3.1.6 Isothermal crystallisation kinetics of PLA samples studies by DSC 72
3.1.7 Isothermal crystallisation kinetics of PLA samples via HSM 77
3.1.8 Isothermal crystallisation kinetics and the Avrami analysis 82
3.2 Conclusions 87
Chapter 4: Controlling the microstructure and crystallisation behaviour of PLA-HA composites 89
4.0 Introduction 89
4.1 Results and discussion 89
4.1.1 SEM morphology of PLA and HA powders as well as hot pressed samples 89
4.1.2 Nonisothermal DSC studies of PLA powder and hot pressed samples 92
4.1.3 Isothermal crystallisation studies of hot pressed samples by DSC 97
4.1.4 Isothermal crystallisation kinetics and Avrami analysis of hot pressed samples 104
4.1.5 Isothermal crystallisation kinetics of PLA-HA samples via HSM 110
4.1.6 Thermogravimetric analysis (TGA) of hot pressed samples 113
4.1.7 SEM of injection moulded samples 115
4.1.8 DSC analysis of injection moulded samples 118
4.1.9 Mechanical properties of injection moulded samples 119
4.1.10 Dynamic mechanical thermal analysis (DMTA) of injection moulded samples 123
4.1.11 TGA analysis of injection moulded samples 128
4.1.12 Imaging and SEM analysis of samples achieved by solution casting 130
4.1.13 Etching the samples in DCM 132

4.1.13.1 Investigation of the Porous Surface Structure 133
4.2 Conclusions 139
Chapter 5: The effect of microstructure on the hardness and tribology behaviour of PLA 140
5.0 Introduction 140
5.1 Results and discussion 140
5.1.1 Hot Stage Microscopy (HSM) 140
5.1.2 Differential scanning calorimetry (DSC) 143
5.1.3 Nano-Indentation (nano-hardness) analysis 146
5.1.4 The effect of secondary crystallisation on tribology behaviour of PLA 154
5.2 Conclusions 161
Chapter 6: The effect of hydrolytic degradation on different microstructures of PLA 162
6.0 Introduction 162
6.1 Results and discussion 162
6.1.1 Mass loss measurements under static and dynamic conditions 162
6.1.2 Size exclusion chromatography (SEC) analysis 167
6.1.3 The effect of degradation on the microstructure of polymers 171
6.2 Conclusions 181
Chapter 7: Conclusions and Future Work 182
7.1 Conclusions 182
7.2 Future Work 186

LIST OF FIGURES

Figure 1.1 Structure of the human femur illustrating regions of cortical and cancellous bone 2
Figure 1.2 Microstructure of cortical bone 3
Figure 1.3 Microstructure of cancellous bone 3
Figure 1.4 Chemical structure of Polylactic acid (PLA).....10
Figure 1.5 Different chiral stereoisomers of Lactic acid including L-lactide, D-Lactide and meso-lactide 10
Figure 1.6 Schematic of the microstructure of a semi-crystalline polymer. Spherulites composed of plate-shaped crystals. The crystal plates consist of several chains folded lamellae and between lamella, unordered amorphous materials are trapped.....13
Figure 1.7 Disordered structure of an amorphous polymer 13
Figure 1.8 Three types of Crystal Nuclei.....15
Figure 1.9 Dependence of crystallisation rate on temperature.....16
Figure 1.10 Different erosion mechanisms: a) surface erosion, b) bulk erosion with autocatalysis, and c) bulk erosion without autocatalysis 22
Figure 2.1 Measurement of the Tg using the midpoint of the transition 35
Figure 2.2 Schematic illustration of the Richardson method for calculating the Tg 35
Figure 2.3 Determination of the heat of fusion ΔHm 36
Figure 2.4 A Linkam TMHS 600 hot stage connected with a Zeiss polarising microscope ..37
Figure 2.5 An example of a stress strain plot and the calculation of the mechanical properties from it.....41
Figure 2.6 An amorphous hot pressed PLA sample ready for conditioning for nano-indentation experiment.....45
Figure 2.7 An image of the small spherulite specimen provided by the NanoTest Vantage machine 45
Figure 2.8 An amorphous hot pressed PLA sample ready for conditioning for wear experiment.....46
Figure 2.9 Degraded PLA specimen after holding it in the oven at 125 °C for 36 hours.....47
Figure 2.10 Schematic illustration of a) closed-loop and b) open-loop configurations of flow-through cell apparatus 50
Figure 2.11 Sotax CH-4008 Basel flow-through cell apparatus 52
Figure 3.1 DSC graphs of as-received PLA pellet first, second and third heating 56
Figure 3.2 DSC graphs of as-received PLA pellet first, second and third cooling.....57
Figure 3.3 Effect of heating rate on heat flow and glass transition temperature 59
Figure 3.4 The dependence of obtained Tg on the heating rate 59
Figure 3.5 The effect of different cooling rates on the melting behaviour of PLA 61
Figure 3.6 Influence of different cooling rates on the heat of fusion (ΔHm) and fractional crystallinity of PLA pellet. The error bars are very small (± 0.5-1) up to 1 ºC min^{-1}cooling rate and afterwards almost 0; Thus, they are not obvious in the graph. 62
Figure 3.7 Cooling DSC processes of PLA pellet under different cooling rates 63

Figure 3.8 Glass transition temperatures of PLA on subsequent heating processes after cooling it at different cooling rates 64
Figure 3.9 The relationship between different cooling rates and the established T_g. The red area (Semi-crystalline samples, the dependence of T_g on crystallinity) and the blue area (amorphous samples, the dependence of T_g on cooling rate). 65
Figure 3.10 Arrhenius curve of log (cooling rate) versus the reciprocal temperature for amorphous PLA samples 66
Figure 3.11 The relationship between the glass transition temperature and crystallinity for semi-crystalline PLA samples 67
Figure 3.12 HSM micrographs showing growth of spherulites during the cooling process at a cooling rate of 0.1 ºC min^{-1}. The white scale bars represent 40 μm 68
Figure 3.13 HSM micrographs showing growth of spherulites during the cooling process at a cooling rate of 0.5 ºC min^{-1}. The white scale bars represent 40 μm 69
Figure 3.14 HSM micrographs showing growth of spherulites during the cooling process at a cooling rate of 1 ºC min^{-1}. The white scale bars represent 40 μm 70
Figure 3.15 HSM micrographs showing growth of spherulites during the cooling process at a cooling rate of 2 ºC min^{-1}. The white scale bars represent 40 μm 71
Figure 3.16 HSM micrographs showing growth of spherulites during the cooling process at a cooling rate of 3 ºC min^{-1}. The white scale bars represent 40 μm 71
Figure 3.17 Melting endotherm produced after Isothermal crystallisation at a) 95 °C, b) 110 °C and c) 125 °C 73
Figure 3.18 Heat flow against the time of Isothermal process for different time periods, at (a) 95 °C, (b)110 °C and (c) 125 °C 76
Figure 40. Optical micrographs showing growth of spherulites during melt crystallisation at 95°C- The white scale bars represent 40 μm 77
Figure 3.19 HSM micrographs showing growth of spherulites during melt crystallisation at 95 °C. The white scale bars represent 40 μm 78
Figure 3.20 HSM micrographs showing growth of spherulites during melt crystallisation at 110 °C. The white scale bars represent 40 μm 79
Figure 3.21 HSM micrographs showing growth of spherulites during melt crystallisation at 125 °C. The white scale bars represent 40 μm 80
Figure 3.22 Relative crystallinity (X_t) against crystallisation time of PLA held at different isothermal temperatures 83
Figure 3.23 Variation in half-life with crystallisation temperature 84
Figure 3.24 The Avrami plots of PLA at different isothermal temperatures 86
Figure 3.25 Variation in half-life with crystallisation temperature obtained from the Avrami 87
Figure 3.26 Crystallisation rate constant (Z) of PLA at different isothermal temperatures ... 87
Figure 4.1 SEM images of PLA powders obtained via cryogenic grinding 90
Figure 4.2 SEM images of the as-received HA powders 90
Figure 4.3 SEM micrographs of hot pressed PLA-HA samples with different wt% of HA ... 91
Figure 4.4 DSC graphs of as-received PLA pellet and powder (after cryogenic grinding) first heating, cooling and second heating (reheating) processes 92

Figure 4.5 Subsequent heating scans of hot pressed HA-PLA composites with different HA loadings after cooling at 20 ºC min.....94
Figure 4.6 Subsequent heating scans of hot pressed a) pure PLA and b) 10% HA-PLA after cooling at 20 ºC min^{-1} using different heating rates (20 and 50 ºC min^{-1}).....95
Figure 4.7 The effect of HA loading on the T_g of hot pressed composite samples 96
Figure 4.8.a Melting endotherms produced after Isothermal crystallisation process at 95 °C - PLA.....98
Figure 4.8.b Melting endotherms produced after Isothermal crystallisation process at 95 °C - PLA-HA (5 wt%).....98
Figure 4.8.c Melting endotherms produced after Isothermal crystallisation process at 95 °C - PLA-HA (10 wt%).....99
Figure 4.8.d Melting endotherms produced after Isothermal crystallisation process at 95 °C - PLA-HA (20 wt%).....99
Figure 4.8.e Melting endotherms produced after Isothermal crystallisation process at 95 °C - PLA-HA (30 wt%).....100
Figure 4.8.f Melting endotherms produced after Isothermal crystallisation process at 95 °C - PLA-HA (40 wt%).....100
Figure 4.9 Melting endotherms produced after 60 minutes of Isothermal crystallisation process at 110 °C for PLA-HA samples with different HA loadings.....101
Figure 4.10.a Melting endotherms produced after 60 minutes of Isothermal crystallisation process at 125 °C for PLA-HA samples with different HA loadings.....102
Figure 4.10.b Melting endotherms produced after 180 minutes of Isothermal crystallisation process at 125 °C for PLA-HA samples with different HA loadings.....102
Figure 4.11 Relative crystallinity (Xt) against crystallisation time of samples with different HA wt% loadings, a) 0% b) 5% c) 10% d) 20% e) 30% f) 40% held at different isothermal temperatures.....105
Figure 4.12 Half time crystallisation of hot pressed PLA-HA composites at different isothermal temperatures.....107
Figure 4.13 Avrami plots of the hot pressed PLA-HA composites with different HA wt% loadings, a) 0% b) 5% c) 10% d) 20% e) 30% f) 40% held at different isothermal temperatures.....108
Figure 4.14 Crystallisation rate constant of hot pressed PLA-HA composites at different isothermal temperatures. The error bars are small (around 3%).....109
Figure 4.15 Half time crystallisation of hot pressed PLA-HA composites at different isothermal temperatures obtained from the Avrami equation. The error bars are small (around 4%).....110
Figure 4.16 Final microstructure of hot pressed PLA-HA composites with different HA wt% loadings under HSM, a) 0 % HA, b) 10 % HA c) 20 % HA d) 40 % HA at 95, 110 and 125 °C from left to the right - The white scale bars represent 40 μm.....112
Figure 4.17 TGA of hot pressed PLA-HA composites, Mass loss (%) versus temperature.114
Figure 4.18 First derivative mass loss (%/°C) versus temperature for hot pressed PLA-HA composites.....115

Figure 4.19 SEM micrographs of fracture surfaces of the injection moulded PLA-HA composites with different HA wt% loadings a) 0 % HA, b) 5 % HA c) 12 % HA d) 20 % HA and e) 35 % HA.....117
Figure 4.20 Second heating DSC scan of injection moulded HA-PLA composites with different HA loadings 118
Figure 4.21 The effect of HA content on the Tg of injection moulded PLA-HA composites 119
Figure 4.22 Evolution of the tensile strength as a function of HA wt%.....120
Figure 4.23 Evolution of the elongation at break as a function of HA wt%.....121
Figure 4.24 Evolution of tensile modulus as a function of the HA wt%. The error bars are very small (± 0.03-0.05) and are not recognisable in the figure. 121
Figure 4.25 Evolution of flexural modulus as a function of the HA wt% 122
Figure 4.26 Evolution of flexural strength as a function of the HA wt% 123
Figure 4.27 Storage modulus vs. temperature for PLA and PLA-HA injection moulded samples.....124
Figure 4.28 Comparing the storage modulus of 20 wt% HA before and after heat treatment at 70 ºC.....125
Figure 4.29 The effect of HA wt % loading on the storage modulus for injection moulded samples.....126
Figure 4.30 Tan Delta vs. temperature for PLA and PLA-HA injection moulded samples .127
Figure 4.31 The effect of HA content on the T_g of injection moulded PLA-HA composites obtained from DMTA 127
Figure 4.32 TGA of injection moulded PLA/HA composites, Mass loss (%) versus temperature 129
Figure 4.33 First derivative mass loss (%/°C) versus temperature for hot pressed PLA-HA composites.....129
Figure 4.34 PLA film sample obtained by solution casting.....131
Figure 4.35 PLA-HA film samples with 5 and 20 wt% HA from left to right obtained by solution casting 131
Figure 4. 36 SEM images of a) PLA and b) PLA-HA (40 wt% HA) film samples obtained by solution casting 132
Figure 4.37 SEM images of PLA-HA (40 wt% HA) film sample obtained by solution casting after 10 minutes etching in DCM.....133
Figure 4.38 SEM images of an etched amorphous hot pressed PLA sample a) after 10 seconds etching, b) after 30 seconds etching and c) after 2 minutes etching 135
Figure 4.39 Semi-crystalline PLA obtained by solution casting, etched in DCM for 60 seconds.....136
Figure 4.40 SEM morphology of the fracture surfaces of PLA after etching in DCM for various periods including a) 1 min, b) 2 min and c) 4 min.....138
Figure 5.1 HSM images of spherulites formation at 95 °C via cold crystallisation for different periods: a) 0 minutes, b) 10 minutes, and c) 20 minutes. The white scale bars represent 40 μm. 142

Figure 5.2 Melting peaks of PLA samples produced (a) via cold crystallisation at 95°C and (b) via melt crystallisation at 125°C 144
Figure 5.3 The values obtained for a) nano-hardness and b) Young's modulus for PLA samples with different microstructures 148
Figure 98. (a) Mean nano-hardnes and (b) Mean young's modulus (± standard deviation) for all samples 148
Figure 5.4 Amorphous sample. Graph of nano-hardness values against the location of indentations on the sample (top), the HSM micrograph of the sample (middle) – (The white scale bars represent 40 μm) and SEM micrograph of the indentations on the polymer surface (bottom) 149
Figure 5.5 Small spherulites sample. Graph of nano-hardness values against the location of indentations on the sample (top), the HSM micrograph of the sample (middle) – (The white scale bars represent 40 μm) and SEM micrograph of the indentations on the polymer surface (bottom) 150
Figure 5.6 Large spherulites sample. Graph of nano-hardness values against the location of indentations on the sample (top), the HSM micrograph of the sample (middle) – (The white scale bars represent 40 μm) and SEM micrograph of the indentations on the polymer surface (bottom) 151
Figure 5.7 Melting peaks of PLA samples produced via secondary crystallisation 155
Figure 5.8 The relationship between the extent of secondary crystallisation and the square root of the isothermal heat treatment time 156
Figure 5.9 Relationship between coefficient of friction and sliding time for polyamide 6, POM and UHMWPE (load 30N, sliding speed = 0.88m/s) [178] 157
Figure 5.10 SEM micrographs of the middle of the wear scar; a) amorphous sample 1, b) amorphous sample 3, c) semi-crystalline 2 hours at 95°C sample 2, d) semi-crystalline 2 hours at 95°C sample 3 (direction of friction from top to bottom), x40 magnification 158
Figure 5.11 SEM micrographs of the middle of the wear scar; a) amorphous sample 3, b) semi-crystalline 2 hours at 95°C sample 3, and SEM micrographs of the wear scar boundary; c) amorphous sample 3, d) semi-crystalline 2 hours at 95°C sample 2 (direction of friction from top to bottom), x200-300 magnification 159
Figure 5.12 The relationship between increasing isothermal treatment time and wear mass loss (Amorphous samples are not included) 160
Figure 6.1 Mass % as a function of time during 60 days of the degradation of the PLA pellet at 50 °C 164
Figure 6.2 Mass % as a function of time during 60 days of the degradation process of the PLA pellet at 70 °C 165
Figure 6.3 pH changes as a function of time during 60 days of degradation process at 50 degree for PLA pellet in static conditions. The error bars are very small (± 0.04) and are not recognisable in the graph. 166
Figure 6.4 DSC scans (first heating scans) of as-received PLA pellet before and after degradation 171
Figure 6.5 DSC scans (first heating scans) of amorphous PLA obtained via hot pressing before and after degradation 172

Figure 6.6 DSC scans (first heating scans) of amorphous PLA-5 wt% HA obtained via hot pressing before and after degradation 172
Figure 6.7 DSC scans (first heating scans) of amorphous PLA-20 wt% HA obtained via hot pressing before and after degradation 173
Figure 6.8 DSC scans (first heating scans) of 40% semi-crystalline sample with small spherulites before and after degradation 173
Figure 6.9 DSC scans (first heating scans) of 40% semi-crystalline sample with large spherulites before and after degradation 174
Figure 6.10 DSC scans (first heating scans) of amorphous PLA sample conditioned in the oven at 50 °C for different periods (0 day-28 days) 179
Figure 6.11 XRD spectra of hot pressed amorphous PLA before and after degradation 180

LIST OF TABLES

Table 1.1 The Avrami Parameters for Different Crystallisation Mechanisms.....18
Table 1.2 Critical thickness values for different resorbable polymers. Above these critical dimensions, the hydrolytic degradation process could change from bulk erosion into surface erosion.....22
Table 2.1 Description of blend composition.....32
Table 2.2 The number of indentations made on each specimen.....45
Table 2.3 Determination of pH of Tris buffer solution at different temperatures.....49
Table 2.4 List of the samples prepared for dynamic degradation experiment.....52
Table 3.1 Glass transition temperatures and heat capacity values of first, second and third heating ± standard deviation.....57
Table 3.2 The effect of the heating rate on the onset, midpoint, endset and breadth of the glass transition temperature ± standard deviation.....60
Table 3.3 Measurement of X_c of PLA samples at 110 and 125 °C at various isothermal times ± standard deviation.....75
Table 3.4 The n values of PLA at different isothermal temperatures obtained from Avrami ± standard deviation.....86
Table 4.1 Comparison of properties of PLA before and after cryogenic grinding process ± standard deviation.....93
Table 4.2 Measurement of X_c of PLA-HA samples at 110 and 125 °C for various isothermal times ± standard deviation.....103
Table 4.3 The n values of hot pressed PLA-HA composites at different isothermal temperatures obtained from Avrami ± standard deviation.....109
Table 4.4 Characteristic temperatures of the thermal decomposition of hot pressed PLA-HA Composites ± standard deviation, T_x = temperature at which x % of the initial mass is lost.....115
Table 4.5 Characteristic temperatures of the thermal decomposition of injection moulded PLA-HA Composites ± standard deviation , T_x = temperature at which x % of the initial mass is lost.....130
Table 5.1 X_c values obtained for cold crystallisation at 95 °C and melt crystallisation at 125 °C for different periods ± standard deviation.....146
Table 5.2 Hardness and Young's modulus of Epofix™ resin and PLA samples with different microstructures ± standard deviation.....147
Table 5.3 Different Percentages of crystallinity at various periods at 95°C ± standard deviation.....155
Table 5.4 Mass Losses for heat-treated PLA samples (secondary crystallisation) for different periods ± standard deviation.....158
Table 6.1 SEC analysis of polymer samples before degradation under dynamic conditions168
Table 6.2 SEC analysis of polymer samples after degradation under dynamic condition....170

Table 6.3 Xc, Tm and Tg of the samples before (B) and after (A) the degradation process under dynamic conditions ± standard deviation 175

Chapter 1: Introduction and literature review

1.1 Bone tissue

Bone (also known as osseous tissue) is a hard and dense connective tissue that has a complex hierarchical structure. Bone is responsible for several critical functions of the human body such as being the structural support for the whole body, protecting the internal organs of the body, mechanical performance and joint mobility in addition to producing the blood cells. Bone is also considered as the main reservoir for different minerals which are essential for the function of the body, particularly calcium and phosphorus [1–3].

Bone contains four different types of cells, osteoprogenitor, osteoblasts, osteoclasts and osteocytes. Osteoprogenitor cells are immature progenitor cells that can differentiate into osteoblast bone cells [4]. Osteocytes are responsible for the maintenance of local bone. Osteoblasts and osteoclasts are involved with the synthesis of new bone and the resorption of old bone, respectively. Therefore, bone can regenerate and self-repair during the lifespan of an individual. However, large intraosseous wounds (critical size defects) cannot heal spontaneously [2, 5, 6].

1.2 Physical Macrostructure of bone

Bone tissue in an adult skeleton consists of two main architectural forms; cortical and cancellous. The cortical bone (also known as compact bone) has a dense structure with only 10% degree of porosity and constitutes around 80% of the total skeleton. However, only 20% of the human skeleton is composed of cancellous bone (also known as spongy bone) which has a degree of porosity of 50 – 90% [5, 7, 8]. The density of the cortical bone is about 2 mg/m^3, while the density of cancellous bone is about 0.97mg/m^3 [2]. Figure 1.1 shows the

macrostructure of the femur as a typical long bone, which consists of both cortical and cancellous bones [2].

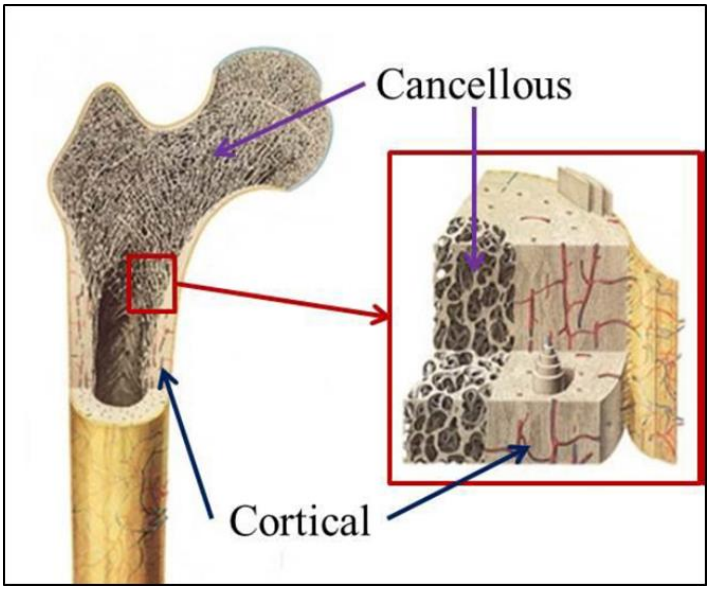


Figure 1.1 Structure of the human femur illustrating regions of cortical and cancellous bone [2]

1.3 Physical Microstructure of bone

Connective tissues, which cover the outer and inner surfaces of bones called periosteum and endosteum, respectively. The bony surface at the joints of the body is covered by articular cartilage in which the blood vessels, nerve fibres, osteoblasts and osteoclasts are located [5, 8].

Cortical bones are composed of several microscopic cylindrical structures, known as osteons or Haversian systems. These long cylinders with a diameter of 200 – 250 μm contain concentric circles of the calcified matrix (lamella) which are located parallel to the long axis of the bone. At the centre of each osteon, Haversian canals with a diameter of around 50 μm are located, which contain blood vessels and nerve filaments. At the borders of lamellae, there are some spaces (lacunae) containing osteocytes (mature bone cells). A network of microscopic channels named canaliculi connects all lacunae together. These channels can provide routes by which nutrients and waste products are transported to and from bone cells (osteocytes). There are also

some small channels (named Volkmann's canals) inside of each osteon by which all Haversian systems are connected together and to the periosteum [2, 8].

On the other hand, spongy bone resembles that of an irregular honeycomb lattice in which plates of trabeculae with the thickness of 50 – 400 μm are located. Also, there are several pores between these plates, which are filled with bone marrow and blood vessels by which nutrients can be transferred into all bone cells and lamellae [2]. The microstructure of cortical and cancellous bones is shown in Figures 1.2 and 1.3, respectively [2].

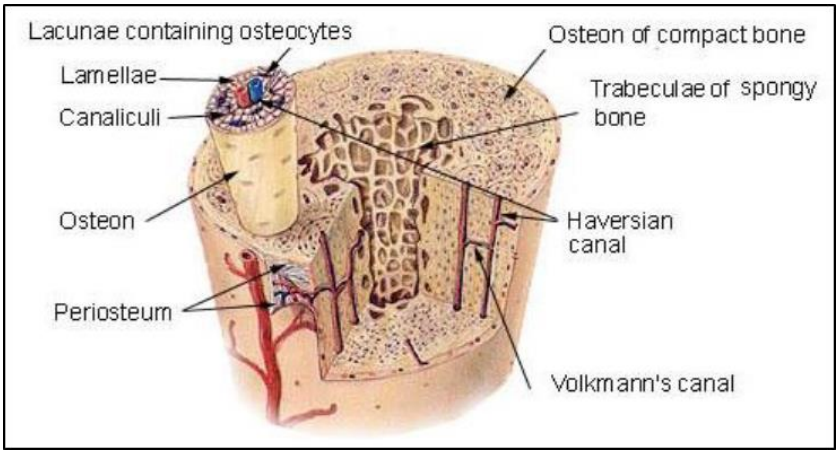


Figure 1.2 Microstructure of cortical bone [2]

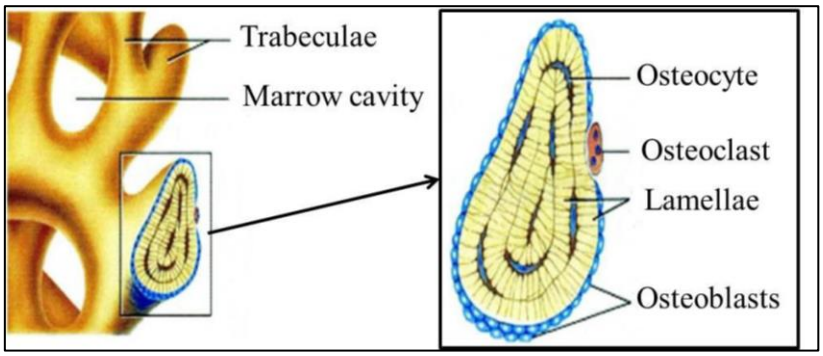


Figure 1.3 Microstructure of cancellous bone [2]

1.4 Chemical composition of the bone

Bone is a composite material, which comprises of both organic and inorganic constituents. The organic component, which contributes to about 30% (by weight) of the bone, contains type I collagen (90%) as well as other types of proteins such as glycoproteins and growth factors. The inorganic constituent is composed of crystalline apatite and makes up around 60% of the whole bone. The remaining 10% of bone tissue contains water. The tensile strength and elastic modulus of the bone are mostly attributed to the organic component, whereas the inorganic constituent contributes to the required stiffness and compressive strength of bone [2, 9].

1.5 Bone defects and different established treatments

Bone defects can occur due to different diseases such as osteoporosis, osteoarthritis, bone cancer and trauma as well as bone deformation [1, 2, 10]. Furthermore, the risk of bone-related diseases could increase with increasing age due to variations in the content of minerals and decreasing the balance between synthesising of new bone and resorption of old one [2]. Different procedures can be applied for bone replacement including autograft in which the material is sourced from the patient's own body; also, the material can come from another human body or another species, which are called allograft and xenograft, respectively. Autologous bone grafts have all required characteristics for the bone repair process such as osteoconductivity (bone can grow on its surface) and osteoinductivity (the scaffold can provide signals to induce the formation of bone). However, there are several concerns with this procedure, including the limitation in bone availability, pain and infection of the donor site, anatomical limitation in addition to a requirement for secondary surgery. In allograft approach, the material that is transferred from another person can transmit disease or can be rejected by the patient's body [1, 11, 12]. In the case of xenograft in which the material is transplanted from an animal, there is a risk of viruses transmission and immune reactions from the body

[13]. As an alternative approach, synthetic materials, which are biologically compatible within the human body can be applied as the scaffold for bone repair and regeneration [14].

1.6 Scaffold requirements for tissue engineering

An ideal scaffold for bone repair applications must meet several essential requirements. The most important ones are briefly explained below.

1. **Biocompatibility**

The scaffold must be biocompatible to reduce the inflammatory response and rejection from the host bone as much as possible [15, 16].

2. **Biodegradability**

The scaffold must be biodegradable and the degradation rate should ideally match the rate of bone tissue formation. Furthermore, the degradation products should not cause any toxicity and side effects within the host bone and surrounding tissue [15, 16].

3. **Appropriate mechanical properties**

The scaffold must be strong enough for safe handling during implantation into the tissue. Similarly, the implanted scaffold must have adequate strength and mechanical integrity to support the host bone tissue from the time of implantation up to the end of the bone regeneration process [15, 16].

4. **Porosity**

The scaffold must be porous enough and these pores must be interconnected with each other to ensure proper penetration and proliferation of cells for bone ingrowth [2, 15, 16]. Moreover, the porosity of scaffold is vital for vascularisation and metabolism [17]. However, by

increasing the porosity mechanical strength of scaffold decreases; thus, the value of total porosity must be balanced with the specific mechanical requirements for the host bone [18].

5. **Surface properties**

Scaffold surface properties such as chemical composition, surface topography and morphology can influence protein interaction, cell attachment, proliferation and growth of bone tissue [2], [15, 19]. As an example, increasing surface roughness of a scaffold can enhance its osteoconductivity and consequently improving cell adhesion [2].

1.7 Biomaterials used for bone scaffolds

Biomaterials are described as synthetic and non-vital natural materials that have the potential to influence patient's biological system in order to replace damaged tissue or develop bone regeneration [16, 20]. Generally, there are four different groups of biomaterials that can be applied for bone repair and scaffold fabrication, including ceramics, polymers, metals and composites. Each group of these materials has its own advantages and shortcomings as a biomaterial for bone regeneration [21].

1.7.1 Metals

Biocompatible metals including cobalt-chromium (CoCr), aluminium, stainless steel as well as titanium and their alloys can be applied as bone scaffolds to support the bone healing process. The benefits of these metallic scaffolds include their excellent corrosion resistance, long-term stability, high mechanical strength to be applied in load-bearing areas as well as their biocompatibility [22, 23]. However, there are some problems with metallic bone implants such as cracking, high stiffness which may result in stress-shielding and failure of the implant as well as releasing wear metal particles which could lead to inflammatory responses and allergic reaction from the host. Moreover, metallic surfaces do not have the potential to interact and

integrate with bone cells biologically; thus their surfaces usually require to be coated or treated to overcome this lack of bioactivity [22–25].

1.7.2 Ceramics

Bioceramics are classified into three different categories, including bioinert, bioactive and biodegradable/bioresorbable materials. The use of bioinert ceramics such as alumina and zirconia in the structure of bone scaffold is not usual due to their lack of interaction with bone cells, which leads to the formation of thick fibrous tissue (scar formation-fibrous encapsulation) on the surface of the implant and therefore implant failure. In contrast, bioactive ceramics have the potential to form a direct chemical bond with bone tissue and interact with osteoblast cells. Bioresorbable ceramics can be degraded over a period of time after their implantation and allow the tissue to regenerate itself [26–28]. However, ceramics cannot be applied in load-bearing applications, or they cannot be formed and shaped easily for implantation due to their brittleness [27–29].

1.7.3 Polymers

Polymers have been applied extensively in orthopaedic applications in particular for temporary implants due to their great biodegradation properties. Polymers can be classified into two different categories: natural and synthetic [30].

1.7.3.1 Natural Polymers

Polymers of natural origin such as collagen have been widely used for regeneration and healing process of various tissues including nerve, skin, cartilage and bone [16, 31]. Natural-based polymers have the advantage of good bioactivity and interaction with host tissue as well as less immunological reactions from the body compared to synthetic polymers due to their similarities with the extracellular matrix (ECM) components and biological macromolecules [32, 33]. However, natural polymers have poor mechanical properties in comparison with

synthetic polymers [34]. The other limitation of natural polymers is that their degradation behaviour is usually dependent on enzymatic activities, which can be varied among different people and different tissue sites in the same person. Consequently, the prediction of degradation performance for these polymers in vivo is more difficult compared to synthetic polymers, which can be degraded easily by water [35].

1.7.3.2 Synthetic Polymers

Different synthetic polymers including polycaprolactone (PCL), poly (lactic acid) (PLA), poly (glycolic acid) (PGA), poly(lactic-co-glycolic acid) (PLGA) as well as polyurethane (PUR) and their composites have been used for bone and tissue engineering applications [36–40]. Synthetic polymers can be degraded simply by hydrolysis into low molecular weight oligomers and then to monomers through water or serum. Therefore, the degradation rate of these polymers is almost constant among various patients and different types of tissues for the same patient and their degradation behaviour *in vivo* can be predicted and controlled by performing *in vitro* experiments [15, 35]. Moreover, their properties such as degradation rate, mechanical performance in addition to porosity can be adjusted according to a specific application [41]. However, there is a risk of tissue rejection with these polymers due to their low bioactivity [42].

1.7.4 Composites

As previously mentioned in Section 1.4, bone is described as a composite containing both mineral and organic phases. Therefore, in an attempt to closely mimic the composite structure of natural bone, various bio-composites (mostly ceramic-polymer) manufactured through different procedures for bone repair applications have been studied [43–46].

Synthetic polymers have the potential to form appropriate 3-dimensional (3D) structures for bone repair applications; however, due to their low bioactivity; these materials do not

encourage cell attachment and proliferation. In contrast, according to previous studies, calcium phosphates such as hydroxyapatite and β-tricalcium phosphate (β-TCP) are osteoconductive and can enhance cell adhesion. Consequently, polymer-calcium phosphate composites found to be an improved alternative over pure synthetic polymer scaffolds [15]. For instance, the bioactivity and cell adhesion properties of polycaprolactone can be improved by adding 20% of hydroxyapatite or β-TCP particles [43].

1.8 Poly (Lactic Acid)

Poly (lactic acid) or PLA and its copolymers are described as biodegradable synthetic polymers that have been used in various biomedical applications, including bone scaffolds, drug delivery systems, sutures and medical implants [47–49]. PLA can be produced via different procedures, including condensation polymerisation in which PLA can be synthesised directly from its basic building block (lactic acid). Lactic acid is obtained from different renewable resources such as corn and sugarcane by fermentation of their sugar. However, PLA manufactured via the condensation route has low molecular weight and mechanical properties. Consequently, in order to produce a higher molecular weight of PLA with improved mechanical properties for commercial applications ring-opening polymerisation (ROP) of the ring-formed (cyclic) dimer of lactic acid is used as an alternative route. The ROP technique is usually applied for mass production due to its capability of controlling the resulting polymer properties in a more accurate way [50]. Figure 1.4 illustrates the chemical structure of the PLA [51].

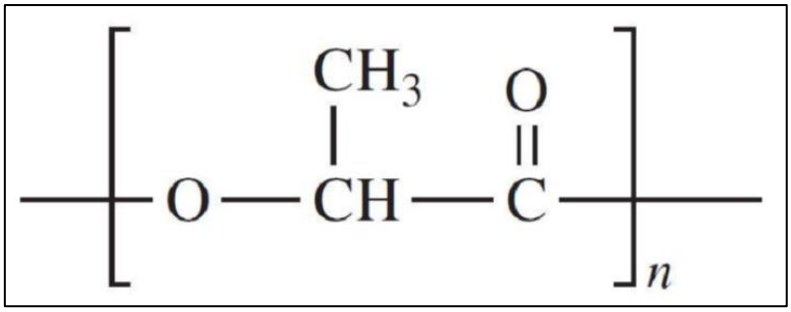


Figure 1.4 Chemical structure of Polylactic acid (PLA) [51]

The building block of PLA (lactide) has two asymmetric carbons that can be formed in three different stereoisomers including L-lactides and D-lactides in which both asymmetric carbon atoms have the same configuration L- and D- configurations, respectively. In contrast, meso-lactide possess two different configurations (one L and the other D configuration) [52]. These three different stereoisomers of lactides are shown in Figure 1.5 [51]. The difference between L and D lactic acid forms is related to their effect on polarised light such that for the L- form the plane is rotated in a clockwise direction, whereas for the D- form, the plane is rotated in an anticlockwise direction. However, the meso-lactic form is not optically active [53, 54].

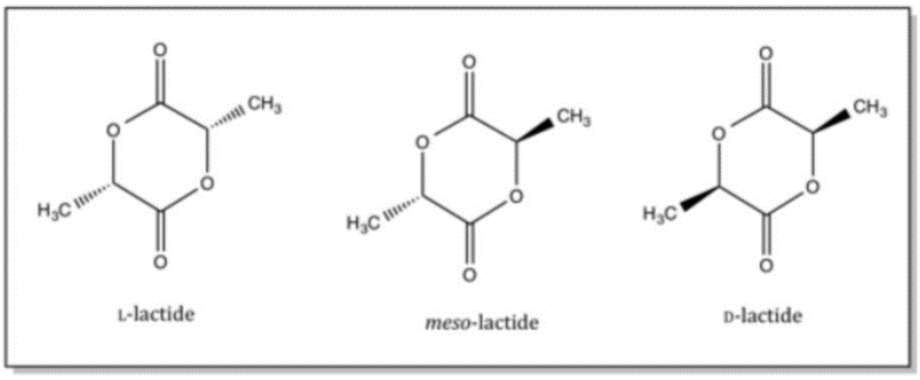


Figure 1.5 Different chiral stereoisomers of Lactic acid including L-lactide, D-Lactide and meso-lactide [51]

The resulting properties of PLA can vary significantly from a partially crystalline polymer to a completely amorphous structure due to containing different ratios of enantiomers, such as the amount of L-lactide or D-lactide [55].

PLA polymers comprising more than 90% of L-lactide tends to crystallise to some extent, whereas those with lower stereoregularity exhibit an amorphous behaviour. Additionally, by increasing the L-lactide content, the degree of crystallinity and glass transition temperature increases [56]. The crystallisation degree of pure poly(L-lactide) acid, which produced entirely from L-lactide can reach up to 45% [57]. However, introducing a small amount of D-lactide into a random copolymer of PLA can decrease the degree of crystallinity, lamella thickness as well as spherulite growth rate significantly [58]. Likewise, the addition of 1% meso-lactide into PLA can decrease its melting point around 3 ºC, which leads to a substantial reduction in the crystallisation rate [59]. Consequently, according to these observations by introducing a small amount of imperfections into the stereoregular structure of PLA, its physical properties can be changed significantly [51]. The formation of meso-lactide during the polymerisation process of PLA is unavoidable. Therefore, in order to obtain a PLA polymer with high quality, the polymerisation process must be started with monomers of higher purity (less meso-lactide amount), which can be technically and economically feasible by purification [60]. Consequently, different properties of PLA such as degree of crystallinity and degradation rate can be adjusted by controlling its stereochemical purity during fabrication [61].

1.9 Polymer Microstructure

Understanding the morphology of a polymer in the molecular level can help to recognise and define its specific properties and determine its suitable applications. A polymer substance consists of many macromolecules constructed from smaller building blocks named monomers that are connected by covalent bonds. The process by which monomers are linked together through chemical reactions is called polymerisation [62]. Polymers can be classified into two different groups based on the method of their preparation: homopolymer and heteropolymer. A polymer which is composed of a single type of monomer is considered as a homopolymer, whereas heteropolymers consist of several different types of monomers [63, 64].

1.10 Semi-crystalline and amorphous polymers

Polymers can be classified into two different categories, including semi-crystalline (partially crystalline) and amorphous. Partially crystalline polymers consist of several ordered layers of folded chains named lamella with the thickness of around 10 nm which are combined and organised into a spherical shape called spherulite. All semi-crystalline polymers contain some amorphous regions which are located between their crystalline areas. In contrast, in amorphous polymers or amorphous regions of semi-crystalline polymers, molecular chains are arranged randomly (without any order). A semi-crystalline polymer has a glass transition temperature (T_g) corresponding to its amorphous component and melting temperature (T_m) attributed to melting of the crystalline content. However, a totally amorphous polymer has only a glass transition temperature (T_g) [65, 66]. Figures 1.6 and 1.7 illustrate the structure of a semi-crystalline and an amorphous polymer, respectively [51].

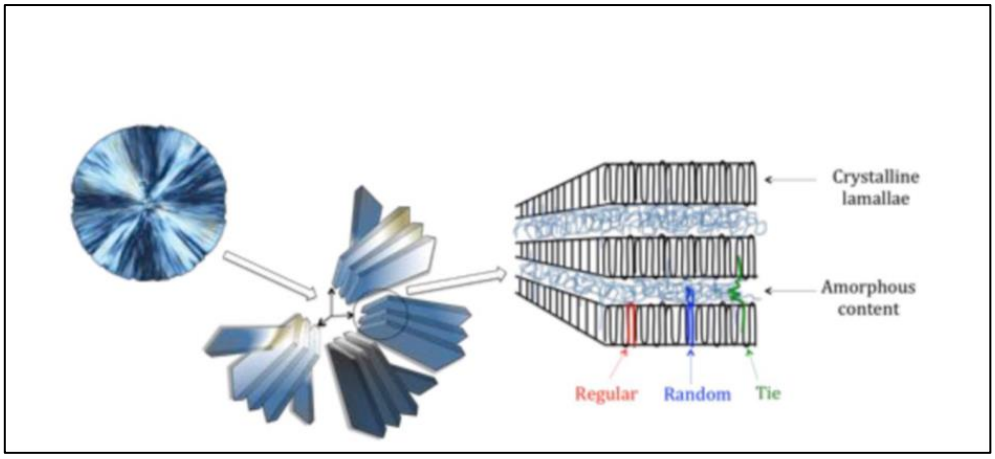


Figure 1.6 Schematic of the microstructure of a semi-crystalline polymer. Spherulites composed of plate-shaped crystals. The crystal plates consist of several chains folded lamellae and between lamella, unordered amorphous materials are trapped [51]

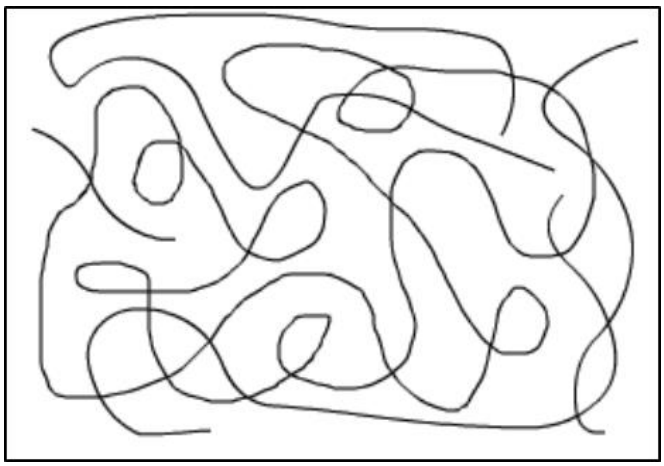


Figure 1.7 Disordered structure of an amorphous polymer [51]

1.11 Mechanism of Crystallisation

The crystallisation process of polymers involves a dynamic transition from an incredibly random and disordered structure (amorphous state) into a highly ordered microscopic structure [67]. The microstructure of a semi-crystalline polymer comprises several lamellar crystals, which combine and make a spherical particle named spherulite. The formation of spherulites continue with time until their impingement to each other and stop growing further. The final size and number of spherulites are subject to several parameters such as the previous thermal history of a polymer sample, heating and cooling rates, molecular weight of the polymer in addition to the temperature at which the polymer is crystallised [67, 68]. In reality, a 100% crystalline polymer is not achievable because the polymer chains do not have the capability to disentangle and line up completely during the crystallisation process. The crystallinity degree of many semi-crystalline polymers can vary from 40% to 75% [69]. Semi-crystalline polymers such as PLA can be obtained in either amorphous or partially crystalline form according to their molecular order and processing conditions. For instance, if the sample is quenched quite fast from the melt temperature to below the T_g the final structure would be amorphous whereas slow cooling rates provide sufficient time for the sample to develop some crystallinity (nonisothermal crystallisation) [51, 70, 71]. Additionally, a semi-crystalline polymer can be achieved isothermally from both melt and glassy states by holding the sample at a constant temperature between T_g and T_m for a certain time period [72].

1.11.1 Nucleation

Polymer crystallisation can be broken down into two distinct processes; nucleation and growth. At the first stage, the random and disordered molecular chains within the glassy state become aligned and form small ordered areas named nuclei. There are two types of nucleation; heterogeneous and homogeneous. Heterogeneous nucleation is usually due to the presence of crystalline impurities such as dust particles, which act as pre-existing nuclei and initiate the

formation of spherulites. On the other side, homogeneous nucleation is less common and usually initiated with alignment and clustering of molecular chains [51, 73].

There are three steps in the nucleation process; primary, secondary and tertiary nucleation. Primary nucleation refers to the initial production of the nucleus from melt when there is no foreign surface or pre-existing crystal. It involves combining a few molecules to form a small crystal part. Secondary nucleation is quite similar to the primary one, but it forms a new layer of material on the surface of a smooth crystal part. Tertiary nucleation takes place over a pre-existing crystal edge. Figure 1.8 illustrates the difference between the three types of nucleation [74].

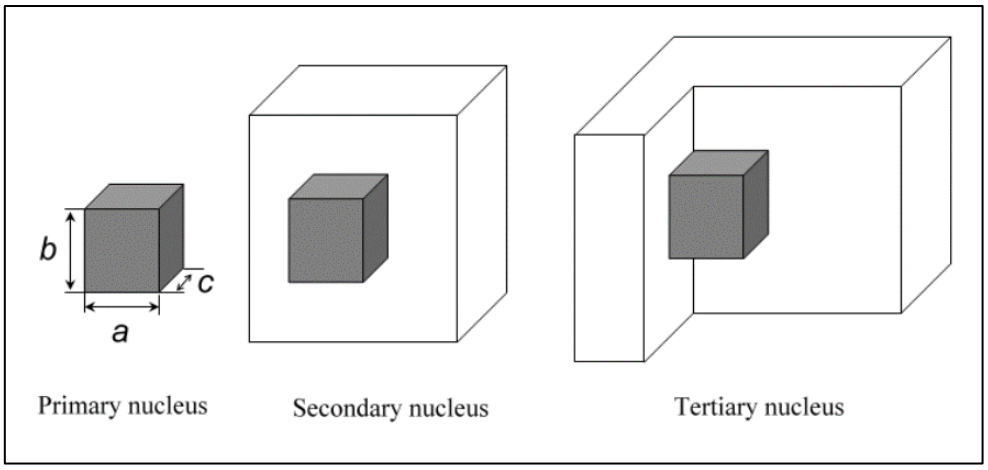


Figure 1.8 Three types of Crystal Nuclei [74]

1.11.2 Growth

At the second stage, the growth of the crystalline region occurs when additional molecular chains are aligned and clustered on the growth crystal face [51, 73]. The growth rate is highly affected by crystallisation temperature as shown in Figure 1.9 [75]. At high temperatures (near the T_m) molecular chains are too active; thus, there is little chance for the formation of stable nuclei and crystallisation growth [67, 75]. However, by decreasing the temperature below the

melting point, the viscosity of polymer increases resulting in the growth of a few crystal structures with large sizes. As the temperature decreases further and the viscosity increases more, the rate of crystallisation approaches to its maximum level at the halfway of the curve between T_g and T_m [67]. On approaching T_g, the viscosity of the polymer increases significantly leading to a decrease of the mobility of the chain segments. In this condition, there is an increased opportunity for the formation of stable nuclei. However, the growth of crystal parts reaches its minimum level because of the low molecular mobility [75].

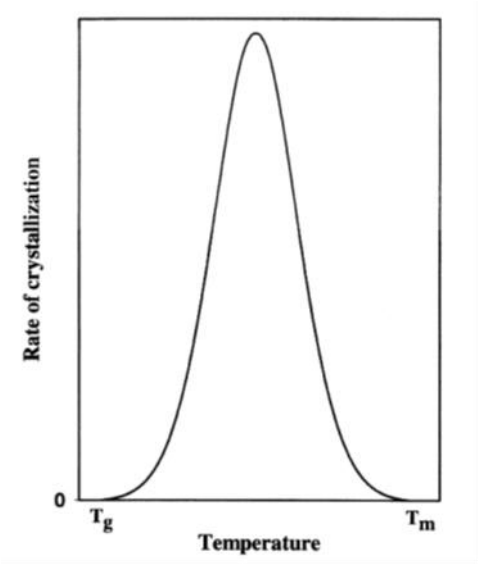


Figure 1.9 Dependence of crystallisation rate on temperature [75]

1.12 Crystallisation Kinetics by Avrami analysis

The kinetics of crystallisation is usually analysed by the Avrami model [76, 77]. It is an isothermal model relating the relative crystallinity with time, such that

$$1 - X_t = exp(-Zt^n) \qquad \textbf{(Equation 1.1)}$$

where X_t is the relative crystallinity formed during the time t, Z is a composite rate constant incorporating the characteristics of both nucleation and growth and n is the Avrami exponent. The value of n is determined according to the crystallisation mechanism and the geometry of the growing crystal. Different crystallisation mechanisms and their corresponding values of n are shown in Table 1.1. Avrami analysis has been widely used to study the isothermal crystallisation kinetics and the time dependence of the crystallisation mechanisms for different polymers such as Polypropylene (PP) [78], PCL [79] and PLA [80]. However, the Avrami model has some limitations. For instance, the n values that represent the variations in crystalline density with spherulite boundary, always take fractional values that have little or no meaning in the adopted Avrami assumptions and crystallisation kinetics of a polymer. Additionally, the results might not be very accurate due to many errors that could occur during the experimental work such as lack of appropriate conditions for the isothermal process, selecting fast rates and the existence of induction periods of time before starting the crystallisation process [74, 81]. Moreover, there are some other limitations with the Avrami assumptions as explained below [82, 83]:

1. The radial growth rate does not vary with time, whereas it is expected that the rate decreases as the spherulites start to impinge to each other.

2. The nucleation rate is constant throughout the polymer sample.

3. The primary crystallisation process is only present; however, there is evidence that two processes existed during crystallisation procedure of a polymer sample, including primary and secondary crystallisation. According to previous studies, the Avrami model provides a poor estimation for the secondary crystallisation process as the data obtained at this stage deviate from the exponential dependence.

Despite these limitations, in the absence of an alternative, the Avrami model is still widely used in the crystallisation kinetic studies.

Table 1.1 The Avrami Parameters for Different Crystallisation Mechanisms [51]

Crystallisation Mechanism	Type of Nucleation	n Value	Geometry
Spheres	Sporadic	4.0	3 dimensions
Spheres	Predetermined	3.0	3 dimensions
Discs	Sporadic	3.0	2 dimensions
Discs	Predetermined	2.0	2 dimensions
Rods	Sporadic	2.0	1 dimension
Rods	Predetermined	1.0	1 dimension

1.13 The Glass Transition temperature

Glass transition temperature (T_g) is a natural characteristic of amorphous polymers that occurs between the elastic and glassy states. Regarding the molecular structure, the T_g illustrates the relaxation phenomenon of the amorphous part of a polymer from a glassy state into a thawed state. Below the T_g of a polymer material, atoms can only vibrate in their equilibrium positions and the molecular chains have little mobility (glassy state). However, by increasing the temperature, mobility and elasticity of chain segments increase significantly up to the point that all chain segments show a viscous flow characteristic [84]. There are several factors which influence the temperature at which the glass of polymer forms (T_g) such as heating and cooling rates as well as molecular weight and crosslink density of a polymer [85, 86]. Obtained value for the T_g from different methods can vary due to the fact that T_g is a rate-dependent property.

Differential scanning calorimetry (DSC) and Differential thermal analysis (DTA) are the two most common techniques used for T_g measurement in which the changes in the specific heat of a polymer sample at the glass-to-rubber transition is determined. Extrapolative corrections are usually applied for the effects of heating or cooling rates on obtained value for T_g [87].

1.14 Physical Ageing phenomenon

Physical ageing usually occurs in polymers when they are stored below their T_g and it is associated with changes in properties of a polymer as a function of storage time at a constant temperature when there is no influence from the surrounding environment or external conditions [88]. The prefix "physical "is always emphasised in order to distinguish this ageing process from other ones such as oxidative, biological, environmental or thermal ageing. In the latter cases, polymer properties change with time irreversibly, and ageing processes modify the structure of the material permanently. On the other hand, the physical ageing process does not involve any permanent modification of the material and it is entirely reversible upon heating to above the T_g. Physical ageing can occur when the glassy polymer is in a non-equilibrium state below the T_g and ageing is caused by thermodynamic drive forces, which encourage a move towards equilibrium conditions above the Tg [88, 89].

1.15 Degradation mechanism of polymers

Biodegradable polymers such as PGA, PCL as well as PLA and its copolymers have been widely used for various medical applications such as tissue support, tissue augmentation and drug delivery systems mainly due to their high biodegradability and good compatibility of biodegradation by-products. For instance, the degradation product of PLA is its building block (lactic acid) which is produced naturally and is excreted from the body via a metabolic path from the respiratory system as carbon dioxide [15, 90, 91]. The degradation of polymers involves a chain scission process by which molecular chains are broken down gradually to form oligomers and afterwards monomers [92]. Polymers can be degraded in the body by ionic hydrolysis. Enzymatic degradation can also occur usually at the last stage of hydrolysis through which the degradation process can be catalysed with the aid of specific proteins (enzymes). This type of degradation is usually observed in the case of natural polymers. Ionic hydrolysis involves cleavage of unstable polymer bonds through the reaction with water and catalysis of degradation in the presence of ions such as PO_4^{3-}. During ionic hydrolysis, water penetrates through the whole polymer and breaks down its chemical bonds randomly. Ionic hydrolysis usually starts with the amorphous part of the polymer. Firstly, the long molecular chains are broken down to shorter ones and consequently, the molecular weight of the polymer decreases. At the second stage, the chemical bonds of the crystalline area start to cleave, resulting in a decrease in the physical and mechanical properties of the polymer [93]. The rate of ionic hydrolysis depends on several factors, including the type of chemical bond, the copolymer composition, pH and the amount of water absorption [92]. After the degradation process, erosion can occur either homogenously (known as bulk erosion) or heterogeneously (known as surface erosion). Erosion process involves loss of monomers and oligomers from the polymer, which results in a decrease in the molecular weight of the polymer. In the case of bulk erosion, material loss occurs homogeneously through the whole volume of the polymer; while in surface

erosion, the material is just removed from the surface [15, 92, 94]. There are several factors which influence the erosion and dissolution of polyesters, including the rate of hydrolysis for ester bond, the diffusion coefficient of water through the polymer as well as the amount of solubility of oligomers in degradation medium [95]. In bulk erosion, the rate of water penetration through the polymer sample is higher than the hydrolysis rate. Consequently, hydrolysis occurs from inside to outside of the sample. In contrast, during surface erosion, the material is removed from the interface of water and polymer sample; thus, the polymer is resorbed from the outer part towards the inside of it. In this type of erosion, the rate of water diffusion into the sample is less than the hydrolysis rate. Different types of erosion mechanisms are illustrated in Figure 1.10 [96]. Both types of erosion (bulk and surface) can occur in all resorbable polymers. Besides the rate of hydrolysis and the rate of water diffusion, the dimension of the sample could contribute to determining the type of erosion. A critical dimension is usually defined for each particular polymer sample (see Table 1.2) [96]. If the thickness L of the polymer matrix is less than this critical dimension, the sample can undergo bulk erosion; However, if it is larger, surface erosion could occur [97]. There is another factor, which influences the degradation behaviour of resorbable polymers known as autocatalysis. A degradation is considered autocatalytic when one or more of the hydrolysis degradation products are also the catalysts for the same degradation process. During homogeneous (bulk) erosion the oligomers obtained through hydrolysis (mostly carboxylic acids) are trapped inside of the sample which results in a local decrease of pH that would accelerate the degradation of the polymer [92, 96]. The acidic oligomers may have a harmful effect on the growth of some specific cells of the body. Therefore, during the selection of an appropriate degradable polymer for the structure of a scaffold, the effect of autocatalysis process on the growth of cells must be determined [96].

The other factors which contribute to the degradation of resorbable biopolymers are the degree of crystallinity of the polymer sample as well as the addition of fillers into the polymer. According to one study, by introducing some crystallinity through annealing and adding 2% of graphene as a filler into PLA, its degradation rate was decreased. According to these data, both crystallisation and the use of a filler in the structure of PLA can increase its hydrolytic stability [98].

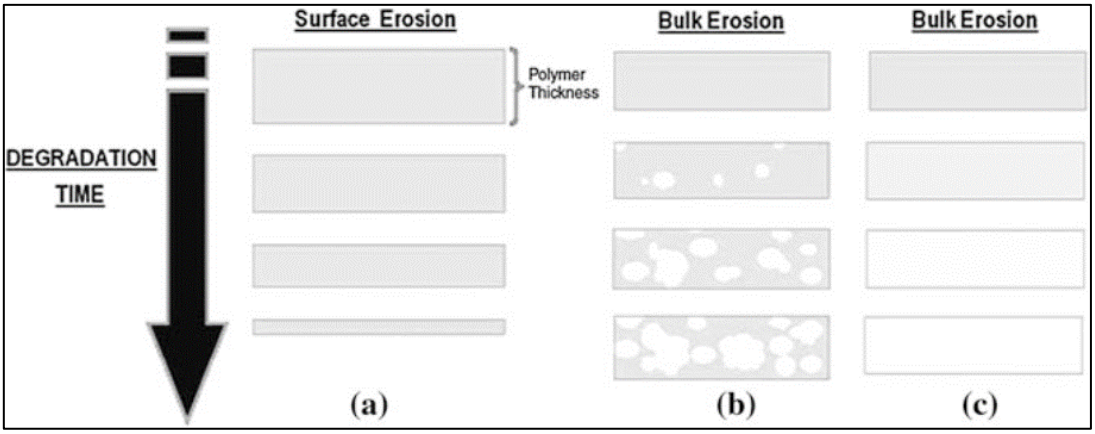


Figure 1.10 Different erosion mechanisms: a) surface erosion, b) bulk erosion with autocatalysis, and c) bulk erosion without autocatalysis [96]

Table 1.2 Critical thickness values for different resorbable polymers. Above these critical dimensions, the hydrolytic degradation process could change from bulk erosion into surface erosion [96]

Type of polymer	**Critical thickness ($L_{Critical}$)**
Poly(anhydride)	75 μm
Poly(ketal)	0.4 mm
Poly(ortho esters)	0.6 mm
Poly(acetal)	2.4 cm
Poly(e-caprolactone)	1.3 cm
Poly(α-hydroxy esters), (PLA)	7.4 cm
Poly(amides)	13.4 m

1.16 Effect of microstructure on tribological behaviour of polymers

Tribology is described as the study and engineering of interacting surfaces of materials which are in relative motion. In tribological studies, several components including wear, lubrication and friction of materials are investigated. The word 'tribology' is derived from the Greek term "tribo" which means rubbing [99]. Wear can be defined as a process in which there is a progressive loss of material from the operating surface of a solid due to the relative motion at the surface. There are several types of wear, such as adhesion and transfer, abrasion or cutting, plastic deformation and fatigue [100]. Abrasion, adhesion and fatigue are the most common types of wear in polymers [101]. Generally wear is quantified by the amount of material removal from a surface per unit time; i.e., wear rate or its inverse, the wear resistance [102]. Polymer tribology is affected by their microstructure characteristics, such as the degree of crystallinity and the spherulite dimension [103]. According to previous reports, increasing the degree of crystallinity of thermoplastic polymers enhance their mechanical properties and wear resistance [104, 105]. However, it seems that no investigation has been done for the effect of secondary crystallisation on wear properties of the polymers. Furthermore, it seems that a reduction in spherulite size can increase the rate of wear [106]. Similar results were obtained by Ainbinder et al. who investigated the effect of different spherulitic morphologies on the tribology behaviour of polypropylene (PP) by making two sets of samples (quenched and unquenched) with different degree of crystallinity. However, the increase in the rate of wear observed in the quenched PP with small spherulites might be more related to the lower crystallinity degree of it in comparison with the unquenched PP with larger spherulites and a higher degree of crystallinity [107].

1.17 Effect of microstructure on the hardness of polymers

The hardness of a polymer is defined as its resistance to local deformation [108]; thus, a polymer with lower hardness can deform more easily. The hardness of a polymer can be affected by several factors, including the molecular weight, degree of crystallinity, spherulite size and the thickness of lamellae. Generally by decreasing the amorphous content of a polymer its hardness increases. However, in some types of polymers such as gelatin, the amount of hardness is more in its amorphous state. According to previous reports, the spherulite dimension does not have a direct effect on hardness. Instead, the thickness of lamellae influences directly into the harness of a polymeric material. By increasing the thickness of lamellae of a polymer, its hardness increases significantly [108, 109].

1.18 Controlling the microstructure of PLA

As previously mentioned, PLA has a wide range of biomedical applications due to its high biocompatibility and biodegradability. Consequently controlling its microstructure is quite vital regarding improving its crystallinity and accordingly its mechanical properties in addition to the degradation rate for specific applications. There has been much effort in improving the microstructure of PLA via different methods such as copolymerisation, blending and incorporating different types of fillers into its structure [51]. Crystallisation behaviour and thermal properties of PLA can be adjusted by controlling different factors such as its molecular weight, stereoregularity, polymerisation conditions and thermal history [60]. It has been reported that the molecular weight of PLA can be controlled by the amount of hydroxyl impurities in its content; increasing hydroxyl compounds such as water and alcohol causing a reduction in its molecular weight by hydrolysis of PLA. The stereochemistry of PLA also influences the degree of crystallinity, mechanical properties and processing conditions. It can be adjusted by copolymerising with the D- or L-lactide, the D, L-lactide, the meso-lactide and

controlling the amount of each isomer in a copolymer [60, 110]. Furthermore, the crystallisation rate is very dependent on the presence or absence of a nucleating agent as well as the crystallisation temperature. According to the literature by annealing different copolymers of PLA (with various L- and D- contents), the crystallisation process can occur between 75 °C and the melting point of the polymer [110]. Generally, crystallisation of PLA occurs slowly with the fastest crystallisation rates in the temperature range of 110-130 °C [110, 111]. It has been reported that when the crystallisation process occurs at low temperatures (105-115 °C), the melting temperature appears with multiple peaks. By increasing the temperature up to around 120 °C, the double melting peaks could convert to one single peak [112]. This is in agreement with another study by Yasuniwa et al. in which the multiple melting peaks were observed at lower temperatures and low heating rates [113]. These multiple melting peaks usually related to melting-recrystallisation mechanism where small and imperfect crystals become gradually stable [112]. On the other hand, when PLA is annealed at high temperatures near to the melting point (e.g., 135 °C), a longer period is required for completing the crystallisation process in comparison with the lower temperatures [110]. Urbanovici et al. have performed isothermal crystallisation experiments of PLLA at six different crystallisation temperatures between 90-130 °C by applying DSC and using Avrami model for the analysis of the data. Regarding the Avrami data, they obtained fractional n values between 3 and 4 [110, 114]. According to previous reports, samples with low molecular weight did not show any melting or crystallisation transitions whereas samples with high molecular weight could readily crystallise and the degree of crystallinity increased as the molecular weight of the polymer went up. Also, the glass transition temperature of PLA increased by increasing the molecular weight of it. In the case of the same molecular weight partially crystalline PLA exhibited higher T_g in comparison with the amorphous sample. Generally, higher crystallinity results in better properties as well as improving the thermal stability and elastic modulus [51, 115].

1.19 Polylactic acid (PLA)/hydroxyapatite (HA) composites for tissue and bone repair applications

Generally, fillers are added into the structure of a polymer for different reasons such as reducing the final cost of a product, modification in physical, rheological and optical properties of the polymer, improving crystallinity and mechanical properties as well as controlling the degradation rate. Several factors contribute into improving the properties of a composite including the uniform dispersion of filler within the matrix, microscopic inspection of the mixture, optimisation of manufacturing properties such as temperature as well as filler particle size. There are some challenges with synthesising of composites, including the variation in the quality of raw materials, poor compatibility of the filler and matrix, increasing viscosity and reduction in molecular weight [116]. Polylactic acid (PLA)/hydroxyapatite (HA) composites have been widely used for different biomedical and tissue engineering applications [44, 117–121]. HA with the formula Ca_{10} $(PO4)_6(OH)_2$ is considered as the most stable type of calcium phosphates under normal temperatures and pH of 4-12. Its stoichiometric ratio of Ca/P is 1.67 [122]. The most common structure of HA is hexagonal in which an array of PO_4 tetrahedra held together by calcium ions in between them. Calcium ions are in two different sites. One group of them are in aligned columns and the others are in equilateral triangles in the centre of screw axis. The hydroxyl (OH^-) group are in columns on the screw axes, whereas the adjacent point of OH^- group occurs in opposite directions. Some other onions such as fluoride (F^-)and chloride (Cl^-) can replace the OH^- group [123]. HA is considered as an excellent choice for many biomedical applications such as orthopaedic and dental implants, soft tissues like skin and bone repair applications. The main advantages of HA are its great osteoconductivity and biocompatibility with tissue cells [124]. However, due to its brittleness characteristic, it cannot be applied in load-bearing applications, and it exhibits poor bioresorbability. To compensate for these limitations, composites of HA and polymers can be applied [2]. For instance, the

introduction of PLA into HA can enhance its mechanical properties considerably. On the other hand, PLA has poor bioactivity, thus by incorporation of HA into its matrix its osteoconductivity can be increased significantly [125]. Different procedures have been applied for fabrication of PLA-HA composites such as solvent casting, electrospinning, melt compounding, phase separation, surface coating [117]. However, there are still some problematic issues with effective blending process of PLA and HA. This is mainly due to the agglomeration tendency of hydroxyapatite particles, which results in poor dispersion of it in a polymer matrix and decreasing the interfacial bond between HA powders and PLA matrix [126]. This poorly dispersed composite of PLA/HA is susceptible to lose its strength quickly in the physiological environment [118]. Surface modification of hydroxyapatite could be applied to enhance the mechanical performance of PLA/HA composite [118, 126]. Cui et al. used L-lactic acid oligomer onto the surface of HA particles to improve the mechanical properties of the composite [119]. This is because polymer grafting can establish a direct chemical bonding between the polymer and inorganic filler, which results in enhancing the interfacial adhesion [120]. Other factors that influence the mechanical properties of a polymer matrix is crystallinity and thermal properties. According to one study, the addition of 20 wt% HA into the PLA matrix increased the crystallinity up to around 9% [127]. This is in contrast with another report where HA particles did not accelerate the crystallinity rate [125]. Kothapalli et al. reported that introducing 50 wt% of HA particles into the PLA matrix led to increasing the yield strength up to 150% and the compression modulus up to 100% in comparison with pure PLA. Furthermore, the glass transition temperature (T_g) was increased by about 2 °C by adding 20% HA. It was speculated that the increase in T_g could be related to the pathways along with the filler particles by which the solvent can remove entirely from the matrix. On the other hand, this increase might be because of the interfacial bonding between the filler and polymer, which restricts the chain mobility. It was observed that the HA particles

were not distributed homogenously within the matrix for composites comprising more than 40 wt% HA [121]. Nazhat et al. reported that the incorporation of HA particles into the PLA matrix increased the storage modulus both below and above the T_g of the polymer matrix. The addition of HA increased the T_g but decreased the damping of the matrix. The increase in both T_g and modulus in that report was attributed to the adsorption of polymer chains on the filler surface and restricting the mobility of molecular chains [128]. In the studies on polylactide/biphasic calcium phosphate (BCP) composites fabricated by solution blending [129], there was a reduction in both ultimate tensile strength (UTS) and failure strain as the amount of the filler increased in the composite. The decrease in UTS by incorporation of more fillers into the thermoplastic polymers is usual [130] and has also been reported by other authors [131, 132]. This is due to the decreasing of the cross-sectional area of the load-bearing polymer by adding more fillers into the composite. Furthermore, debonding of the filler from the matrix may lead to the formation of voids and the propagation of cracks, which ultimately could decrease the tensile strength. The reduction in failure strain is expected as in all polymer composites the elongation is from the polymer rather than the filler, which is rigid. Higher loadings of filler result in decreasing the elongation and failure strain of the composite [129]. Increasing the filler content in a composite could also influence the degradation rate of the polymer. Kaavessina et al. reported that the hydrolytic degradation rate of PLA was increased by introducing more HA particles into the polymer matrix [127]. On the other hand, according to a report by Sui et al. incorporating the HA particles into the PLA matrix led to a reduction in degradation rate of the polymer as a result of dissolution of alkaline HA particles and releasing the OH^- through them which might ultimately neutralise the acidic degradation products of PLA [15, 133].

1.20 Project aims and objectives

PLA has been widely used for various biomedical applications due to its biocompatibility and biodegradability. However, PLA has a limited ability to interact with human bone cells due to its low bioactivity. Therefore, in order to improve its bioactivity and cell adhesion properties for bone applications, it is usually combined with calcium phosphates such as HA. PLA-HA composites have been extensively characterised and it was found that they could improve the cell adhesion in comparison with pure PLA. However, there has been limited research in controlling the microstructure and crystallinity of PLA and PLA-HA composites. Furthermore, the majority of previous work focused on using PLLA only, while the copolymers of the PLA have the capacity to control and manipulate their microstructure and crystallinity better than the homopolymers. The microstructure and crystallisation behaviour of the polymers and composites will influence their mechanical properties and degradation behaviour, which are considered as important factors for temporary bone scaffolds. By increasing the degree of crystallinity, the mechanical strength of the scaffold could be increased, while its degradation rate decreases. Consequently, according to the final application (its required mechanical strength and degradation rate), the microstructure of the polymer and composite could be controlled and manipulated.

The main aims and objectives of this work were:

1) **To control the microstructure and crystallisation behaviour of a semi-crystalline random copolymer of poly (L-lactic acid) with 4% D-isomer**

The morphology and crystallinity of the polymer were controlled and manipulated under both isothermal and nonisothermal conditions in a differential scanning calorimetry (DSC). Furthermore, hot stage microscopy (HSM) was used to investigate the effect of thermal history on spherulites dimensions and crystallisation behaviour of the polymer.

2) **To explore the effect of HA particles on the microstructure, crystallinity, thermal stability and mechanical properties of the PLA matrix**

PLA-HA composite samples were fabricated using three different procedures, including hot pressing, injection moulding and solution casting. Composite samples were characterised using different techniques, including SEM, DSC, HSM, TGA, tensile and flexural tests as well as DMTA.

3) **To examine the effect of spherulitic microstructure on the nano-hardness (nano-indentation) characteristics of PLA**

Firstly, by using hot stage microscopy (HSM), different spherulitic microstructures were analysed and investigated. Secondly, appropriate samples required for nano-hardness testing were produced by the DSC.

4) **To explore the effect of the secondary crystallisation on the tribological behaviour of PLA**

By conditioning the PLA samples at 95 ºC for different periods ranging from 2 hours to 4 weeks, secondary crystallisation was produced within the PLA samples. The wear rate was determined by calculating the percentage of mass loss for the samples.

5) **To investigate the effect of the hydrolytic degradation on different microstructures of PLA**

The effect of hydrolysis on the mass change of PLA pellets in both static and dynamic conditions was investigated and compared. Furthermore, the effect of the hydrolytic degradation process on the changes in the molecular weight and the microstructural behaviour of PLA and PLA-HA samples under dynamic conditions was explored using SEC, DSC and XRD techniques.

Chapter 2: Materials and methods

2.1 Materials

2.1.1 Poly (lactic acid)

PLA 3052D used in this study is a random Co-PLA with around 4% D-lactic acid. It was provided by NatureWorks LLC Belgium in pellet form. Its glass transition temperature and melting region are in the range of 55-60 °C and 145-160 °C, respectively (provided by NatureWorks). PLA 3052D has a molecular weight (Mw) of around 87000 g mol^{-1}(measured by SEC).

2.1.2 Hydroxyapatite

Hydroxyapatite powder with the average size of 19 µm was supplied by Urodelia-France.

2.1.3 Dichloromethane

Dichloromethane was used as a solvent for mixing PLA and HA through solution casting procedure. It was supplied as 99.8% pure by Sigma Aldrich (Dorset, UK).

2.2 Sample preparation

2.2.1 Solid-dispersion and hot pressing

PLA pellets were converted into PLA powders with an average size of around 970 µm using cryogenic grinding. Prior to any processing, both PLA and HA powders were dried in the oven at 70 °C overnight (around 12 hours) to remove any moisture. These powders were then poured into a plastic bottle and shaken by hand for 5 minutes. The composition details are listed in Table 2.1. Afterwards, Composite plaques were produced via Moore Hydraulic Press (George E. Moore & Sons Ltd, Birmingham, UK). PLA-HA mixtures in powder form (30 grams in total for each composition) were put in the centre of a polytetrafluoroethylene (PTFE) frame (180 x

150 x 1 mm), and then enclosed between two stainless steel plates. The plates were then mounted into the press and were heated at 210 °C for 3 minutes to ensure an even temperature throughout the whole sample. Subsequently, the plates compressed and held for a further 5 minutes under 10 tonnes of pressure followed by quenching into the water to produce totally amorphous samples. Obtained sheets were cut into small pieces and used for different characterisations and thermal analysis.

Table 2.1 Description of blend composition

PLA-HA Composites Composition (wt%)	
PLA	HA
100	0
95	5
90	10
80	20
70	30
60	40

2.2.2 Injection moulding

PLA and PLA-HA samples (5-35 wt% HA) were produced for mechanical testing by a twin extrusion using the HAAKE minilab thermo scientific mini twin-screw extruder at Warwick University (WMG). The temperature of the extruder was 196 °C and the screw speed was 50 RPM. Afterwards, the extruded specimens were injection moulded into test specimens required for mechanical testing using the following conditions; cylinder temperature, 196 °C, mould temperature; 81 °C, pressure was 100 bar.

2.2.3 Solution casting

PLA and PLA-HA samples with various HA loadings (5-40 wt% HA) were produced via solution casting method by dissolving the PLA pellets in dichloromethane (DCM) and adding the HA powders gradually into the solution. The solution was stirred at room temperature using

a magnetic stirrer. Subsequently, the solution was poured into a petri dish to be dried at room temperature.

2.3 Differential Scanning Calorimetry (DSC)

A broad range of thermal characterisations for polymers and their composites could be analysed using differential scanning calorimetry (DSC) through which thermal transitions of a polymer or composite can be detected by considering the changes in heat capacity of the sample. There are different thermal properties which can be recorded from a DSC curve by measuring the differences in heat flow which occur during the experiment for a polymer specimen while it absorbs or releases heat including glass transition temperature (T_g), melting temperature (T_m) and crystallisation temperature (T_c). Furthermore, the crystallisation kinetics and morphology of the polymer as well as the miscibility of polymer blends could be analysed through this technique. Polymers which are partially crystalline usually represent all thermal properties mentioned above (T_g, T_m and T_c) while for amorphous polymers only a T_g appeared on their DSC curve.

A power compensated DSC (Perkin-Elmer DSC-7) was used in this study, which consisted of two cells, one for the sample and one for the reference. Each sample was encapsulated in an aluminium pan with a lid while an empty aluminium pan with lid was used as the reference. The temperature for each cell was controlled separately using thermocouples below each heater. A power compensated DSC has the capability to maintain the temperature for both sample and reference at the same level during cooling or heating of the whole system by adjusting the required power input (compensating the required heat). The amount of heat or energy required for the sample to be at the same level of temperature as the reference may not be equal because of the exo/endothermic thermal transitions occurring within the sample. The differential heating power required to do this is measured as heat flow versus temperature or time.

2.3.1 Experimental procedure

In order to ensure the accuracy and reliability of the results, temperature and thermal responses of the DSC instrument were calibrated using pure (99.999) indium and tin standards. The temperature of the calorimeter was calibrated by measuring the melting points of pure indium (T_m^0 =156.6 ºC) and pure tin (T_m^0 =231.9 ºC). The thermal responses of the instrument were calibrated by calculating the heat of fusion of a known mass of indium (ΔH_m^0 =28.5J/g).

In all experiments, samples with a weight of around 10 mg were cut from the as-received PLA pellets or powders after cryomilling or were sampled from a hot pressed plaque. The samples were weighted and secured inside an aluminium pan with a lid. In the first DSC scan for all experiments the thermal history of the samples was erased by heating them from RT up to 210 ºC and held for 5 minutes at this temperature before cooling them back to the RT. A heating and cooling rate of 50 ºC min^{-1} were applied for most of the experiments to avoid additional crystallisation during the process.

The glass transition temperatures (T_g) of the samples were determined by drawing tangents at the transitions to calculate the onset, midpoint and endset. The midpoint of the transition was recorded as the T_g (see Figure 2.1) [134]. However, in some instances, an endotherm peak was superimposed on the T_g. In these cases, the T_g of the sample was determined according to Richardson's method [135]. A schematic of Richardson's method for determining the T_g is illustrated in Figure 2.2 [51] where the T_g follows the path 1234 and increases between points 2 and 3. The T_g is located where areas A+C=B.

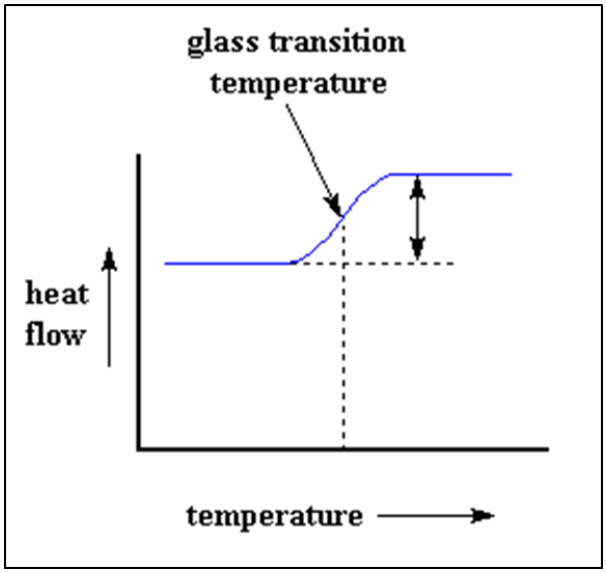


Figure 2.1 Measurement of the Tg using the midpoint of the transition [134]

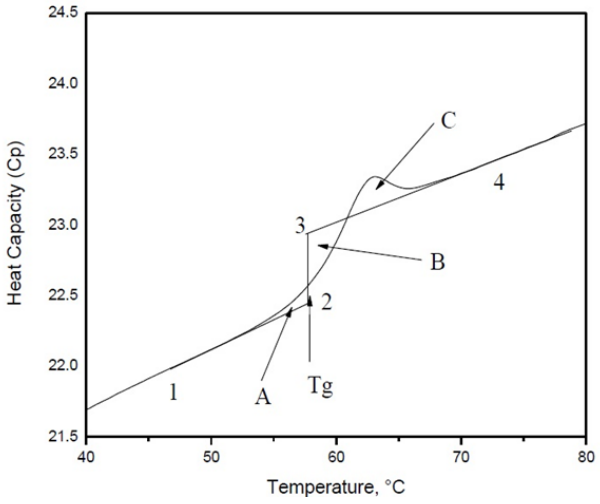


Figure 2.2 Schematic illustration of the Richardson method for calculating the Tg [51]

The method for determination of heat of fusion (ΔH_m) is shown graphically in Figure 2.3 [136] where a linear baseline was drawn from the first onset of melting to the last trace of crystallinity. The amount of ΔH_m can be obtained from the area under the endotherm (see Figure 2.3).

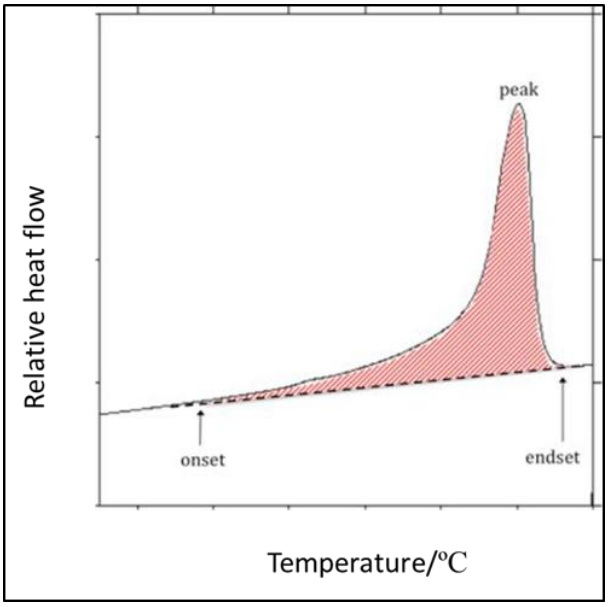


Figure 2.3 Determination of the heat of fusion ΔH_m [136]

2. 4 Hot Stage Microscopy (HSM)

Spherulitic morphology of PLA and PLA-HA samples were investigated using a Linkam TMHS 600 hot stage equipped with Zeiss polarising microscope (see Figure 2.4). A Linkam TSM94 controller that was connected to a PC thermal control software (Linksys 32) controlled the temperature of the equipment during the experiment. Images were captured using an Olympus digital camera.

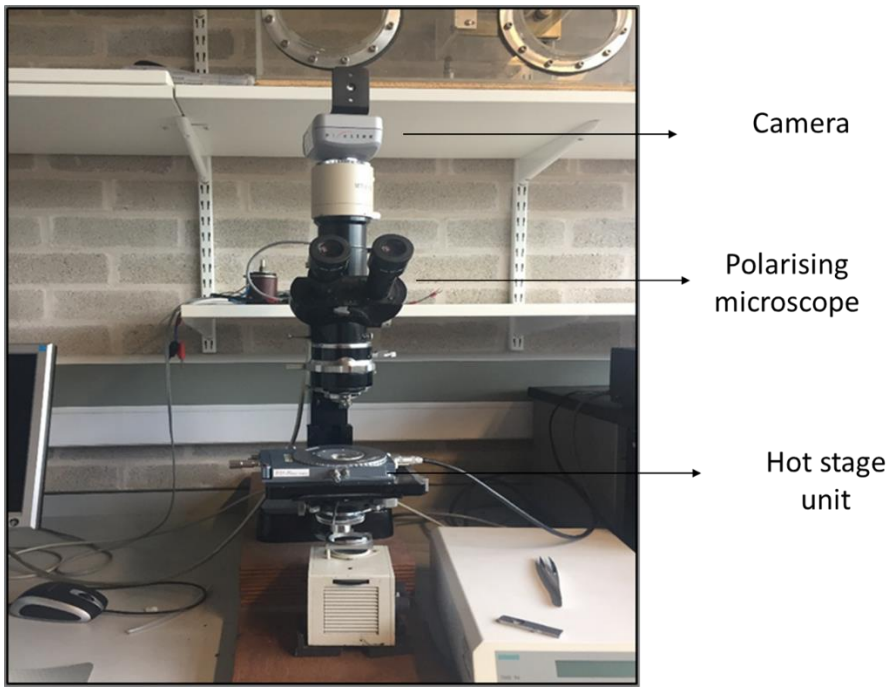


Figure 2.4 A Linkam TMHS 600 hot stage connected with a Zeiss polarising microscope

2.4.1 Experimental procedure

Thin sheet samples with approximately 10-15 μm were prepared via hot pressing and were placed between two glass slides of diameter 16 mm inside the hot stage for observation. Two types of experiments were performed, including the dynamic and isothermal crystallisation studies of the polymer. Through the dynamic process, the effect of different cooling rates on the spherulitic morphology and crystallisation behaviour of PLA was investigated by recording the micrographs as a function of time and temperature during heating and cooling of the sample.

During the isothermal procedure, the effect of crystallisation temperature and HA particles on spherulitic microstructure and nucleation behaviour of the polymer was explored.

The scale bars (black scale bars) obtained from the device (HSM) were small and not clear. Therefore, white scale bars were made by PowerPoint according to the original scale bars (black scale bars) and were used for all HSM images.

The isothermal crystallisation process was also performed using the HSM equipped with a light dependent resistance (LDR) Model ORP 12. When the light is transmitted through the sample, the resistance responds to the changes in light intensity. The voltage changes proportional to the resistance according to Ohm's law (V= IR). The output from the system is voltage as a function of time (a sigmoidal curve). Consequently, the variations of the voltage with time could be recorded to obtain the changes in relative crystallinity against time by using the equation below:

$$X_t = \frac{V_f - V_0}{\Delta V} \qquad \textbf{(Equation 2.1)}$$

where X_t is the relative crystallinity, ΔV is the changes in voltage, V_f is the final voltage and V_0 is the initial voltage. By normalising the data, the relative crystallinity (0-1) against time can be obtained.

2.5 Scanning Electron Microscopy (SEM)

Scanning electron microscopy (SEM) is a type of electron microscope used for capturing high resolution images of the samples to study their composition and surface topography. Prior to SEM characterisation of a sample, the surface of it must be coated with an electrically conductive material such as gold or platinum. During the SEM of the sample, an electron beam is scanned across the surface (which is conductive) of it resulting in the generation of low

energy secondary (SE) and reflected or backscattered (BSE) electrons. The secondary electrons that escape from the surface of the sample could provide topographical information whereas the BSE, which have higher penetration through the samples, could provide information regarding the composition and distribution of different elements within the samples. The elements that have higher atomic numbers observed brighter under the microscope, whereas those with lower atomic numbers appear darker in SEM images.

2.5.1 Experimental procedure

In order to prepare fracture surfaces for SEM characterisation, samples were scored using a scalpel, then submerged into liquid nitrogen and held (for around 3-5 minutes) up to applying a load across the score mark resulting in the fracture of the sample. The samples were then removed from the nitrogen bath by pliers and were mounted vertically on SEM stubs with the fracture surfaces facing upwards.

JEOL JSM-6060LV SEM was used for imaging analysis of all samples in this work except the samples for tribological studies, which were analysed by the Hitachi 3030 scanning electron microscope. Prior to SEM, all samples were coated with gold for about 3 minutes to be conductive. Furthermore, in order to improve the quality of the SEM images, a conductive silver paste was painted where the specimen and stub had contact.

2.6 Thermogravimetric analysis (TGA)

Thermogravimetric analysis is a useful technique for the assessment of the amount of filler content in polymer composites, residual solvent and absorbed moisture content as well as measuring the range of temperatures for degradation of the polymer. The TGA testing is carried out either dynamically at a defined heating rate or in an isothermal mode in a defined atmosphere (e.g., oxygen (air), argon or nitrogen). During the TGA experiment, the weight of

the sample is determined over time as a function of temperature using an electronic microbalance with high sensitivity.

2.6.1 Experimental procedure

TGA of PLA and PLA-HA samples were performed by a Netzsch Jupiter STA 449C thermogravimetric analyser in the air atmosphere which flowed at 50 cm^3 min^{-1}. The samples were heated from the RT up to 600 ºC at the heating rate of 10 ºC min^{-1} in order to investigate the range of temperatures where degradation occurs for each composition. During each experiment, the weight of the sample as a function of temperature was recorded. The range of temperature for degradation of the sample considered from the point where the weight of the sample dropped from the baseline (onset) up to the point where the weight of the material is almost zero (endset). Prior to all experiments, two empty ceramic crucibles were placed in the sample holder and the reference holder of TGA and the same thermal scan parameters as for the samples were applied in order to correct the baseline. The weight of the sample for each experiment was around 8 mg.

2.7 Tensile testing

Tensile testing is a fundamental material engineering test in which a load or stress is applied to the sample and the response of the sample is recorded up to fracture. Therefore, a load versus extension or stress-strain curve could be obtained through this technique by which the mechanical properties of the material including ultimate tensile strength (UTS), elongation at break and Young's Modulus could be determined. The UTS equals to the maximum stress value that occurs for a specimen during an experiment while the elongation at break is the final strain value before fracturing of a sample. The Young's Modulus value could be obtained by taking the gradient from the linear part of the stress-strain curve (see Figure 2.5) [137].

In uniaxial tensile testing (which is used here), the stress is applied into the specimen along one axis. The sample is attached at each end into the grips of the tensile testing machine. During the experiment, the sample is elongated along its axis at a constant rate, while the instantaneous load applied into the sample plus the subsequent elongation are determined by a load cell and extensometer respectively.

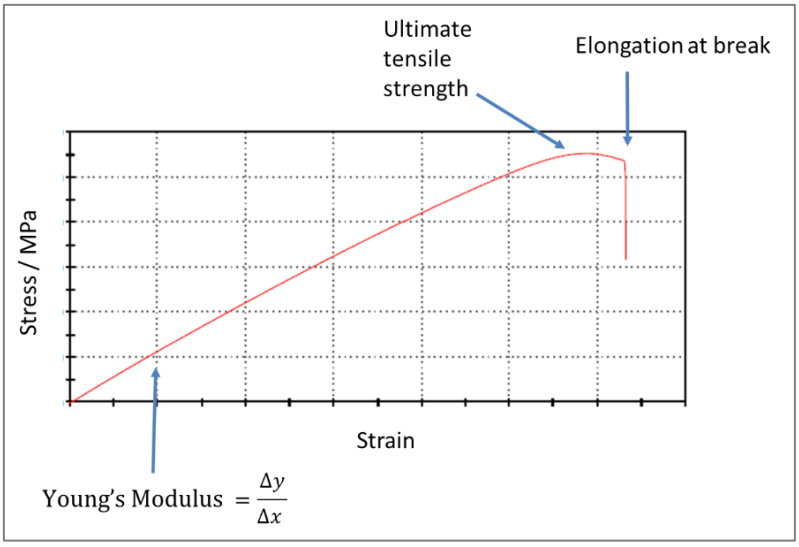


Figure 2.5 An example of a stress strain plot and the calculation of the mechanical properties from it

2.7.1 Experimental procedure

Dog-bone shaped of PLA and PLA-HA (5-35 wt% HA) specimens with a gauge length of 15 mm, width of 3.20 mm and thickness of 3.20 mm were prepared for tensile testing via injection moulding procedure.

Uniaxial tensile testing was performed on the specimens at ambient temperature (21 ºC) using an Instron 5566 mechanical tester (Instron, High Wycombe, UK) with a 10 kN load cell, a cross-head speed of 2 mm min^{-1} and 500 ms time intervals. The mechanical testing was proceeded up to the failure of the specimen and the data were collected via Merlin software. Five repeats were tested for each type of sample and the average values were quoted in the text.

2.8 Three-point bending flexural testing

The three-point bending flexural testing determines the amount of force required for bending a material under three-point loading conditions. It is a classical technique in engineering used to determine the value for Young's modulus of a material while it is flexing. During the experiment, the specimen is located on a support span while the force is applied into the centre of the specimen, which results in producing three-point bending of the specimen at a particular rate.

2.8.1 Experimental procedure

Rectangular (beam) shaped of PLA and PLA-HA (5-35 wt% HA) specimens with a length of 25 mm, width of 11 mm and thickness of 1 ± 0.1 mm were prepared for flexural testing via injection moulding procedure. Three-point bending flexural testing was performed on the specimens at ambient temperature (21 ºC) using an Instron 5566 mechanical tester (Instron, High Wycombe, UK) with a 10 kN load cell, a cross-head speed of 2 mm min^{-1} and 500 ms time intervals. The mechanical testing was continued up to the failure of the specimen and the data were collected via Merlin software. The flexural modulus (E_f) and flexural strength (σ_f) were determined using Equations 2.2 and 2.3, respectively. Five repeats were tested for each type of sample and the average values were quoted in the text.

$$E_f = \frac{L^3 m}{4bd^3} \qquad \textbf{(Equation 2.2)}$$

$$\sigma_f = \frac{1.5FL}{bd^2} \qquad \textbf{(Equation 2.3)}$$

where L is the length of the beam in mm, m is the slope of the load-deflection graph, b is the width of the beam in mm, d is the thickness of the beam in mm and F is the maximum force that sample can withstand obtained from the load-deflection graph in newton (N).

2.9 Dynamic Mechanical Thermal Analysis (DMTA)

Dynamic mechanical thermal analysis (DMTA) is a technique used to study and characterise the viscoelastic behaviour of polymeric materials. During the DMTA experiment, sinusoidal stress is applied into the specimen at a constant frequency while it is heated. Changes in temperature results in variations in properties of the material, including stiffness (storage modulus) and damping (Tan δ). Two types of modulus, including the storage modulus (in phase) and loss modulus (out of phase) could be obtained through this technique owing to sinusoidal force. The elastic behaviour of the material could be determined according to its storage modulus. By dividing the loss modulus into storage modulus, Tan δ (damping) could be obtained. Tan δ determines the energy dissipation of material and used for calculation of T_g. The T_g is considered at a point (temperature) where there is a large drop in the amount of storage modulus in a storage modulus versus temperature graph. It could also be measured at the peak of Tan δ in a Tan δ against temperature plot.

2.9.1 Experimental procedure

Rectangular shaped specimens of PLA and PLA-HA (5-35 wt% HA) with the same dimensions mentioned above for flexural testing were prepared for DMTA experiment via injection moulding procedure. Dynamic temperature three-point bend testing was carried out using the DMTA (NETZCH DMA 242 cell linked to TASC 414/3 controller). The specimens were heated from RT up to 130 ºC at a heating rate of 1 ºC min^{-1} and frequency of 25 Hz. The data were collected by NETZSCH DMA measurement channel 18 software.

2.10 Nano-indentation (nano-hardness) testing

The nano-indentation testing can be applied to determine the hardness of small volumes of material. During the nano-indentation experiment, the depth of penetration into the surface of the sample is measured as the load is applied to a known geometry indenter tip (usually a three-

sided pyramid geometry named Berkovich tip). Consequently, the area of the contact (indent) could be calculated using the known geometry of the indenter. The Young's modulus of the sample could be determined by measuring the rate of change of load and depth (slope of the load against the depth of penetration plot).

2.10.1 Experimental procedure

An amorphous PLA plaque obtained via hot pressing cut into small squares of approximately 15 mg that is suitable for conditioning in a DSC (see Figure 2.6). Three specimens were left amorphous, whereas six of them were conditioned in the DSC in order to make semi-crystalline samples ($X_c \sim 40\%$) with different spherulites dimensions (small and large sizes). Prior to nano-indentation testing the nine (three repeats of each type) PLA samples were cold mounted using an epoxy resin (Epofix^{TM}) which has a curing temperature of 40 °C [138] which is less than the T_g of the PLA to avoid any crystallisation. Each three different samples, including one amorphous, one with small spherulites and one with large spherulites were placed into one stub for cold mounting creating three epoxy stubs. After putting the samples in the mould, the Epofix^{TM} was poured on top. The mixture was then left overnight (around 12 hours) to be cured. Subsequently, the samples were polished (up to x4000 grit) to remove the top amorphous layer and to make them flat enough for the nano-indentation testing.

A NanoTest Vantage machine coupled with the NanoTest software, was used for determination of both nano-hardness and Young's modulus of the samples. The diamond 3-sided pyramid indenter (Berkovich) applied a load of 5 mN into the specimen. The time of loading and unloading was 30 seconds with 5 seconds hold in between them. The number of indentations applied at different locations in each sample in a rectangular pattern shown in Table 2.2. The gaps between these indentations were 30 and 20 μm in each row and column, respectively (see Figure 2.7 as an example).

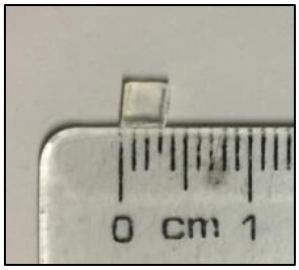


Figure 2.6 An amorphous hot pressed PLA sample ready for conditioning for nano-indentation experiment

Table 2.2 The number of indentations made on each specimen

Type of specimen	**Number of indentations (row** x **column)**
Epofix™ resin	99 (11 x 9)
Amorphous	48 (8 x 6)
Small spherulites	54 (9 x 6)
Large spherulites	30 (6 x 5)

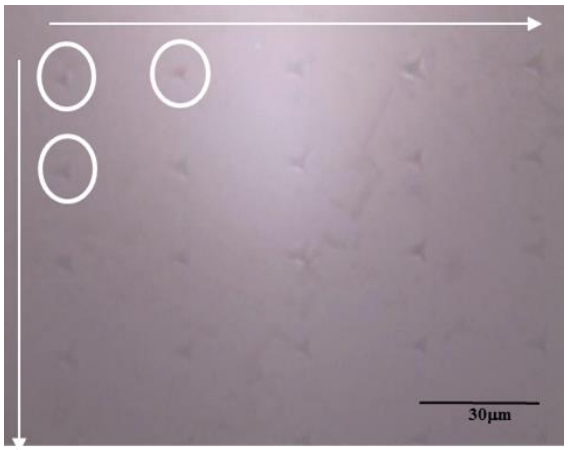


Figure 2.7 An image of the small spherulite specimen provided by the NanoTest Vantage machine

2.11 Tribological experiment

Different components such as lubrication, friction and wear rate of the materials can be investigated through tribological studies.

2.11.1 Experimental procedure

An amorphous PLA sheet obtained via hot pressing was cut into rectangular samples with the dimensions of 55 mm long and 25 mm wide, which is suitable for wear testing (see Figure 2.8).

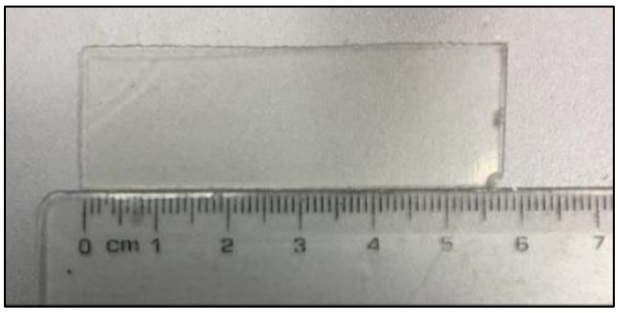


Figure 2.8 An amorphous hot pressed PLA sample ready for conditioning for wear experiment

The initial idea was to explore the effect of spherulitic microstructure on the tribological behaviour of PLA. However, due to the occurrence of degradation phenomenon during producing the PLA samples with large spherulites that are appropriate for wear experiment, this was abandoned.

In order to obtain semi-crystalline samples (approx. 40%) with small spherulites, amorphous hot pressed PLA samples were conditioned in an oven at 95 °C and held for 2 hours (cold crystallisation). Large spherulites samples were made via melt crystallisation in a furnace by which the cooling and heating rates could be controlled. The process for making large spherulites samples involved heating the amorphous hot pressed PLA samples up to 210 °C and held for 5 minutes before being cooled to 125 °C and held for 36 hours in order to produce samples with around 40% crystallinity. However, a sample with some bubbles and

discoloration was produced through this method (see Figure 2.9) indicating the degradation of the sample. Therefore, the investigations into the effect of spherulite sizes on wear behaviour of crystalline PLA samples were discontinued and instead, the effect of secondary crystallisation on tribological behaviour of the samples was explored.

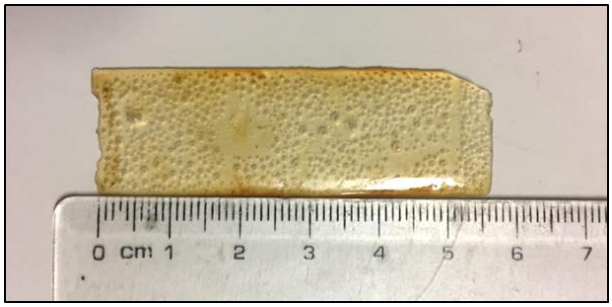


Figure 2.9 Degraded PLA specimen after holding it in the oven at 125 °C for 36 hours

Three rectangular specimens obtained via hot pressing were left amorphous whereas fifteen of them were conditioned in the oven for various periods including 2 hours, 3.5 days, 7 days, 14 days, and 28 days (three repeats for each of them) to investigate the effect of secondary crystallisation on the wear rate of the PLA.

TE 77 High-Frequency Friction Machine was applied for the measurement of friction and wear rate of the PLA samples. During the experiment, some loose debris were produced from the material, which was removed using a piece of blue roll in order to minimise the contamination. The temperature was maintained at 25 °C (below the T_g) to avoid crystallisation. Four thermocouples were used for measurement of the temperature including one attached to the outside part of the specimen and the others (three of them) were put under the surface of the specimen at the centre of the stroke and two turnaround points. A 6 mm steel ball was run across the length of the sample with a stroke length of 12.5 mm and a frequency of 5 Hz. A

constant amount of load (10 N) was applied during each test. Testing for all samples was run for 60 minutes.

2.12 Hydrolytic degradation studies

2.12.1 Preparation of Tris buffer solution

Tris buffer is an appropriate solution for studying most of the biological systems. This is because its pKa (acid dissociation constant) could be maintained at around 8 at RT, making it be as a suitable buffer for keeping the pH in the range of 7-9.

In order to make 500 mL Tris buffer solution, 6.057 g of Tris powder was added into 450mL of distilled water in a volumetric flask. Afterwards, the flask was put on a hot plate and the solution was stirred at 24 °C for around 10 minutes up to dissolving the powder through the water completely. Subsequently, the pH of the solution was measured by a pH meter and at the same time, hydrochloric acid was added to the mixture to set the appropriate pH (around 7). Since the pH values could vary by changing the temperature, they were determined according to the temperature at which the degradation experiment is going to run using the equation below:

$$\mathrm{pH}(\mathrm{T}_{\mathrm{Experimental}}) = \mathrm{pH}(\mathrm{T}_{\mathrm{Synthesise}}) + (\mathrm{T}_{\mathrm{Experimental}} - \mathrm{T}_{\mathrm{Synthesise}}) \times \alpha \qquad \textbf{(Equation 2.4)}$$

where the experimental temperatures ($\mathrm{T}_{\mathrm{Experimental}}$) are 37, 50 and 70 °C. The temperature for synthesising the Tris buffer solution ($\mathrm{T}_{\mathrm{Synthsise}}$) is 24 °C and the pH at this temperature equals to 7.4. The Temperature coefficient (α) defines the relative variation of pH in Tris buffer solution with regards to the changes in temperature (0.028 $°C^{-1}$). The final pH results are shown in Table 2.3. Finally, three containers of 500 mL Tris buffer solution at pH=7.4 for three

different temperatures, including 37, 50 and 70 °C were obtained. The final mixtures were kept in glass bottles in the fridge at around 5 °C up to running the degradation experiment.

Table 2.3 Determination of pH of Tris buffer solution at different temperatures

Temperature coefficient (α)- pH/°C	-0.028
Synthesise temperature (°C)	24
Temperature of experiment (°C)	**pH**
37	7,764
50	8,128
70	8,688

2.12.2 Degradation testing under static conditions

As-received PLA pellet sample with a weight of 0.5 g was immersed into approximately 5 mL Tris buffer solution in a 30 mL glass flask. Three repeats were performed in three different flasks for all temperatures, including 37, 50 and 70 °C (in the oven) to ensure the reliability and accuracy of the results. The experiments were run for 2 months and the mass of the samples was measured by using a balance (Sartorius model ME414S) with the accuracy of 0.0001g at different periods, including: after 2 days, after 15 days, after 30 days, after 45 days and after 60 days from the start point of the experiment. Prior to mass measurement, each sample was washed with distilled water and was dried in the oven at 37 °C for 24 hours. The pH of the buffer solution was also measured at different periods (0, 30, 45 and 60 days) during the experiment.

2.12.3 Degradation testing under dynamic conditions

“Flow-through cell apparatus” is commonly used for dissolution testing in drug development areas. Through this technique, the quality of the drugs could be ascertained by recording the process of drug release from a dosage form. In this work, we used this method to study the hydrolytic degradation behaviour of PLA and PLA-HA samples for a certain period (1 month).

The device consists of a reservoir, which contains the dissolution medium. The medium is forced from the reservoir vertically upwards through the cells using a pump. The temperature of the system is controlled by a water bath. The flow cells are made of transparent and inert materials. They have a filter system on top of them, which could prevent the escape of undissolved particles from the cells. The bottom of the cells is filled with tiny glass beads (diameter: 1 mm) up to around 5 mm from the top of the cells in order to prevent the entering of the solution into the tubes. The samples should be located on the glass beads. The flow-through cell device can operate in two different configurations, including closed-loop and open-loop configurations (see Figure 2.10) [139]. In a closed-loop configuration, a fixed volume of the medium is recycled whereas in an open-loop configuration a fresh liquid from the reservoir continuously going into the cell.

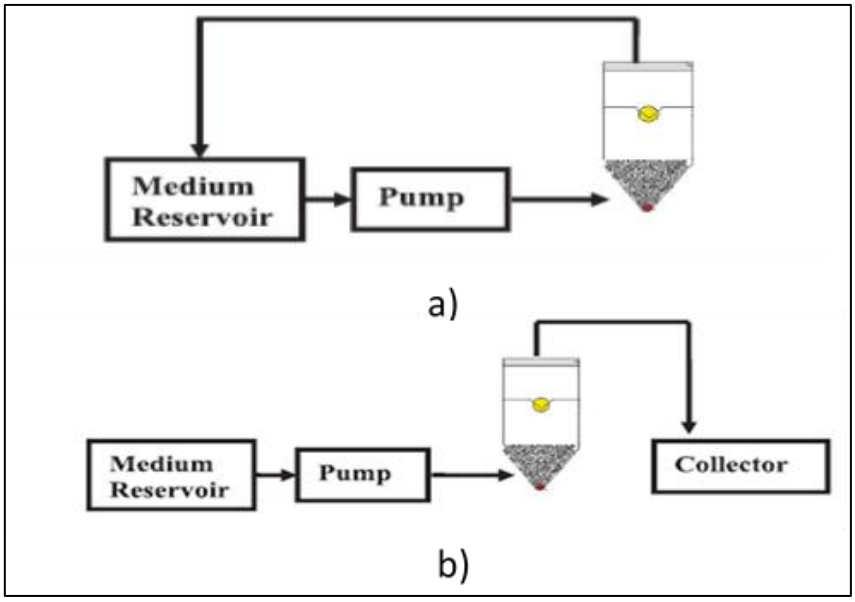


Figure 2.10 Schematic illustration of a) closed-loop and b) open-loop configurations of flow-through cell apparatus [139]

2.12.3.1 Experimental procedure

The main reason for using the flow-through cell technique for hydrolytic degradation studies here was to simulate the blood circulatory system of the human body, as the final applications of the materials are bone scaffolds used in the human body. Therefore, this in vitro testing (dynamic hydrolytic degradation) could be more similar to the actual in vivo experiment compared to the static hydrolytic degradation testing. The dynamic hydrolytic degradation was performed in a closed-loop configuration using Sotax CH-4008 Basel flow-through cell apparatus. Eleven samples were prepared for the experiment. The list of the samples is shown in Table 2.4. The same buffer solution (Tris buffer) as for static experiment was used for dynamic degradation testing. According to the results from the static degradation, there was no mass loss for the samples at 37 °C. Furthermore, at 70 °C (above the T_g), there was a possibility of occurrence of secondary crystallisation during the experiment. Therefore, the temperature of 50 °C was used during the dynamic degradation experiment. The circulation volume of Tris buffer in each cell was 100 mL (the minimum volume in a closed-loop configuration to limit evaporation at 50 °C). The speed of the circulation was 8.3 mL min^{-1}. Since the apparatus consisted of only six flow cells (see Figure 2.11), the experiment was done two times (the same condition) and each time half of the samples were tested. The degradation experiments were run only for 1 month due to the time constraints and limited access to the device. The cells for three of the sample, including 3.5 days, 7 days and 28 days of secondary crystallisation were broken during the experiments. Thus no results achieved for these samples (the results of the effect of secondary crystallisation could not be reported). It was not possible to stop the flow-through cell apparatus (degradation testing) during the experiment at different periods. Therefore, the results could be obtained only at two time intervals (before and after degradation). However, Some fractions of the solution was taken from all samples (from the solution) at different time intervals including after 2 days, 7 days, 15 days and 30 days (from

the start point) during the experiment in order to find out the degradation rate and behaviour of all samples and comparing the results of them.

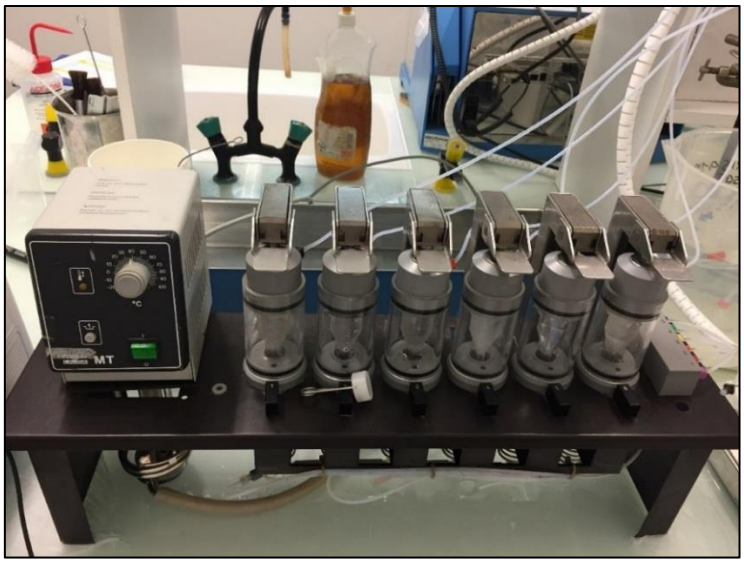


Figure 2.11 Sotax CH-4008 Basel flow-through cell apparatus

Table 2.4 List of the samples prepared for dynamic degradation experiment

Sample	Investigation
As-received PLA pellet	Reference
Amorphous hot pressed PLA	Effect of hot pressing
Amorphous hot pressed PLA-HA (5 wt% HA)	Effect of HA
Amorphous hot pressed PLA-HA (20 wt% HA)	
PLA sample with small spherulites (Xc:40%) made in DSC	Effect of spherulite dimensions
PLA sample with large spherulites (Xc:40%) made in DSC	
Secondary crystallisation process of PLA: 2 hours, 3.5 days, 7 days, 14 days, and 28 days heat treated in the oven	Effect of secondary crystallisation

2.12.4 Size Exclusion Chromatography (SEC) coupling with static light scattering (LS)

Size Exclusion Chromatography (SEC), also known as gel permeation chromatography (GPC) is a method by which dissolved polymer molecules could be separated according to their size or volume. Static light scattering is another method used to determine the intensity of the scattered light in order to measure the molecular weight of a polymer. By adding the LS detector to SEC, the absolute amount of molecular weight could be obtained without the need for a standard curve as the reference.

2.12.4.1 Experimental procedure

The molecular weight of all samples before and after degradation process under dynamic conditions was measured and analysed using size exclusion chromatography (SEC) system equipped with a multi-angle static light scattering (LS) detector and a differential refractometric index (DRI) detector. The multi-angle LS detector made it possible to have access to the absolute masses of the analysed polymers (no need for using a standard curve).

Tetrahydrofuran (THF) was used as the solvent for most of the samples. However, some of the polymers were not soluble in THF and they were dissolved instead in chloroform. The hot pressed amorphous PLA was dissolved in both solvents as a reference. In size exclusion chromatography (SEC), the species were eluted according to their size (hydrodynamic radius); the larger molecules are eluted first, the smaller ones last. The samples were solubilized in the solvent to obtain solutions of concentration close to 10 mg ml $^{-1}$. The solubilisation was long (6 days). The samples were filtered on 0.45 μm filters before being analysed by SEC. Injections have been tripled and were reproducible; only one of the results was shown in the text. ASTRA VII (Wyatt Technology) software was used for the analysis of the results.

2.12.5 X-ray Diffraction (XRD)

X-ray Diffraction (XRD) could be used for recognising different types of polymer phases including semi-crystalline and amorphous. It is also possible to measure the degree of crystallinity using this method. Three basic elements are used in the X-ray technique, including a sample holder, an X-ray tube and an X-ray detector. To generate the X-ray scan of a specimen, firstly some electrons are produced by heating a filament in a cathode ray tube. Secondly, these electrons are accelerated towards the specimen using a voltage. Thirdly, when the specimen interacts within the electrons, the X-ray spectra could be obtained.

2.12.5.1 Experimental procedure

XRD analysis was carried out for amorphous PLA sample before and after the degradation experiment under dynamic conditions using an X-ray diffractometer (INEL Equinox 1000, France) to explore the effect of the degradation process on the crystallisation behaviour of the amorphous sample. Diffraction data were collected in the 2θ range between 10º and 60º with a step size of 0.02º/2θ. The XRD experiment was run for 90 minutes.

Chapter 3: Controlling the microstructure and crystallisation behaviour of PLA

3.0 Introduction

The focus of this chapter is on the study of basic thermal characterisation, crystallisation kinetics and controlling the final microstructure of a semi-crystalline random copolymer of PLA using both Differential Scanning Calorimetry (DSC) and Hot Stage Microscopy (HSM). Controlling the microstructure and crystallisation behaviour of the polymer could have an effect on its use in bone repair.

3.1 Results and discussion

3.1.1 Thermal characterisation of the as-received PLA pellet

Samples with a weight of around 10 mg were cut from PLA pellet and secured inside aluminium pans with lids. First, samples were heated from 25 to 210 ºC at a heating rate of 20 ºC $min^{-1}$and held for 5 minutes to clear any thermal history. Secondly, they were cooled to 25 ºC at a cooling rate of 20 ºC min^{-1} before being reheated to 210 ºC in a DSC at the same heating rate. Subsequently, another cooling and heating scans (the same as previous ones) were repeated in order to prove that the samples are reproducible.

The thermal transitions associated with heating, cooling and reheating processes are shown in Figure 3.1. A step change in the heat flow that occurred at about 65 ºC during the first heating corresponds to the glass transition process. This was followed with a linear increase in the heat flow up to the onset melting temperature at 140 ºC where there was evidence of melting. The melting process was completed by 160 ºC when the heat flow continued to increase linearly with temperature due to the rise in the specific heat of the liquid amorphous phase. The degree of crystallinity of PLA based composite material can be calculated by using Equation 3.1:

$$X_c = \frac{\Delta H_m - \Delta H_c}{\Delta H_m^0 \times 1 - (\frac{\%\, wt\ filler}{100})} \times 100\%\ [140] \qquad \textbf{(Equation 3.1)}$$

where ΔH_m and ΔH_c correspond to the heat of fusion and heat of crystallisation of PLA respectively, ΔH_m^0 is the heat of fusion of the totally crystalline PLA (93.0J/g) [140] and wt% filler refers to the weight percentage of the filler. The degree of crystallinity for the as-received PLA pellet was determined to be 38%.

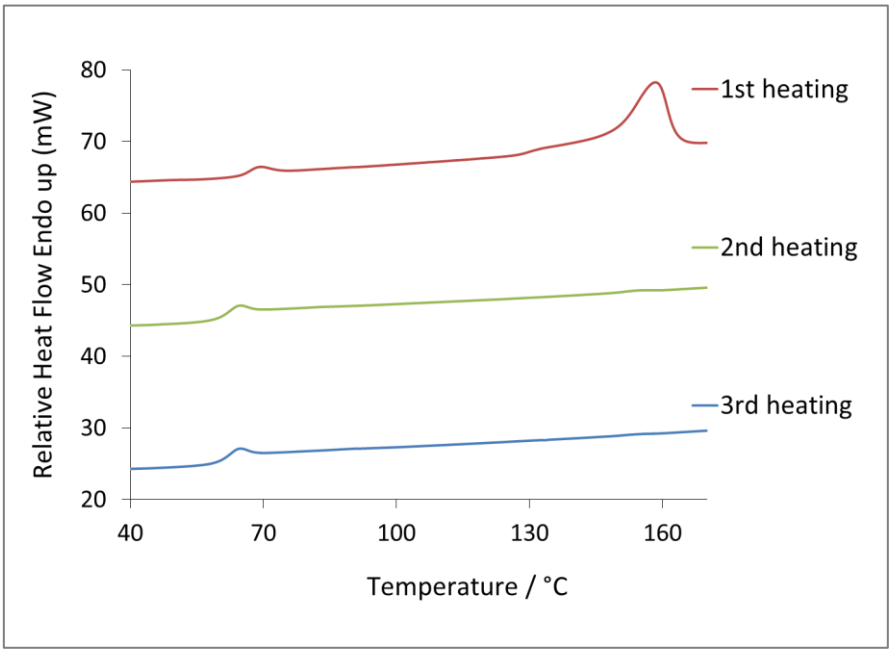


Figure 3.1 DSC graphs of as-received PLA pellet first, second and third heating

The glass transition temperature was reduced during the second and third heating to around 61 ºC. In contrast, there was an increase in the heat capacity (ΔC_p) at the T_g on subsequent heating processes (Table 3.1). These two events are due to the fact that the initial sample was partially crystalline while the cooled samples were found to be totally amorphous (no melting peak was observed). The breadth value (the difference between the onset and the endset temperature) was almost the same for all three heating scans.

Table 3.1 Glass transition temperatures and heat capacity values of first, second and third heating ± standard deviation

Process	Onset (ºC)	Midpoint (ºC)	Endset (ºC)	Breadth (ºC)	$\Delta C_p(Tg)$ (Jk^{-1})
Heat 1	63.7 ± 0.3	65 ± 0.5	67 ± 0.3	3.3 ± 0.3	0.42 ± 0.006
Heat 2	59.3 ± 0.2	61 ± 0.6	62.8 ± 0.2	3.5 ± 0.2	0.56 ± 0.005
Heat 3	59.6 ± 0.2	61 ± 0.7	62.8 ± 0.2	3.2 ± 02	0.53 ± 0.005

Figure 3.2 shows the DSC curves as obtained during the cooling process at 20 ^{0}C min^{-1}. It is apparent from Figures 3.1 and 3.2 that the PLA pellet did not recrystallise on subsequent heating and cooling processes.

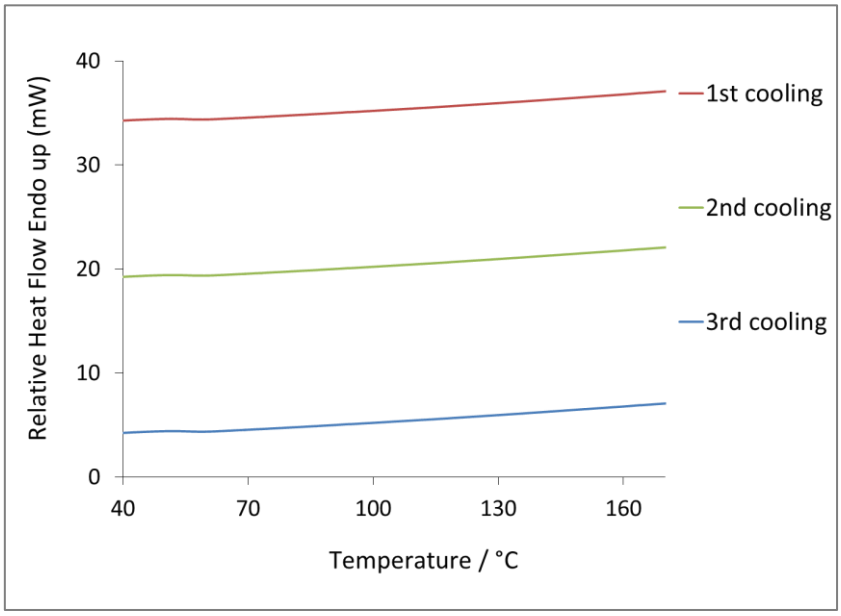


Figure 3.2 DSC graphs of as-received PLA pellet first, second and third cooling

To conclude, the as-received PLA pellet was semi-crystalline; however, there was no evidence of recrystallisation during all the subsequent heating and cooling scans. These results are consistent with other findings reported by Abdul Aziz et al. [51]. The next stage is to explore the effect of using various heating and cooling rates as a means to control the crystallinity, microstructure and T_g.

3.1.2 Influence of different heating rates on the glass transition temperature

The T_g of a polymer depends on the cooling rate at which the glass is formed [51]. The measured T_g is also dependent on the sample mass and heating rate [141]; increased values of both can increase the thermal lag (which is due to the temperature differential between the thermocouple, which shows the output temperature near to the sample and the real temperature within the sample) and the measured T_g.

Since T_g is influenced by the heating rate; it is essential to report all T_g temperatures along with the relative heating rates. Hence, it was decided to explore the effect of different heating rates on T_g values.

The experiment was conducted in three different sets of samples in order to minimise the effect of thermal degradation on the samples. On the first run of each set, PLA samples were heated up and melted completely by holding them at 210 ºC for 5 minutes before being cooled down to the RT at a constant rate of 20 ºC min^{-1}. The samples were reheated to 210 ºC with a range of heating rates from 5-50 ºC min^{-1} to investigate the effect of heating rate on the T_g. As illustrated in Figure 3.3, the glass transition temperatures became more prominent as the heating rate increased, showing that high heating rates could increase the sensitivity of the DSC. The T_g shifted towards higher temperatures with increasing heating rates due to the thermal lag effect (Figure 3.4). The effect of the thermal lag was corrected by extrapolating to zero heating rate.

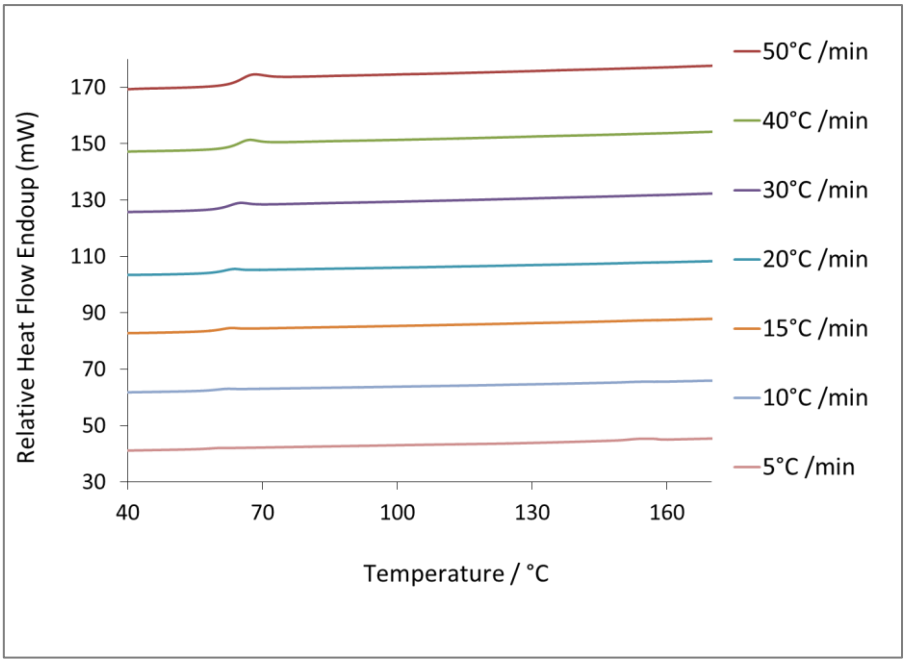


Figure 3.3 Effect of heating rate on heat flow and glass transition temperature

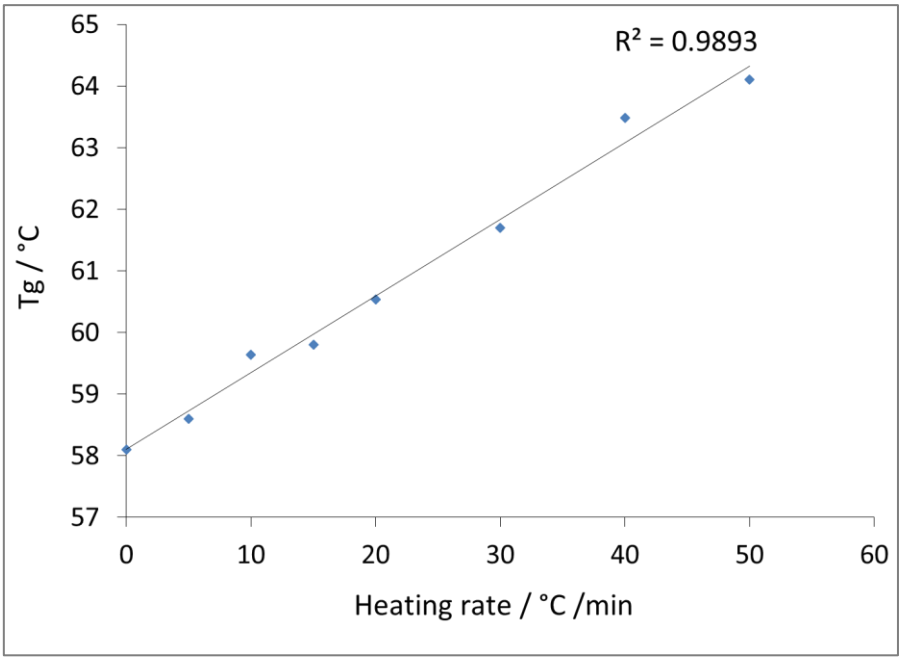


Figure 3.4 The dependence of obtained Tg on the heating rate

As can be seen in Table 3.2, the T_g value shifted around 6 ºC to a higher temperature by increasing the heating rate from 5 to 50 ºC min^{-1}. In addition, the breadth value of the glass transition temperature became larger by increasing the heating rate. Similar results were found regarding this effect for polystyrene by Foreman et al.[141].

Table 3.2 The effect of the heating rate on the onset, midpoint, endset and breadth of the glass transition temperature ± standard deviation

Heating rate(^{0}C min^{-1})	**Onset (^{0}C)**	**Midpoint (^{0}C)**	**Endset (^{0}C)**	**Breadth (^{0}C)**
5	56.7 ± 0.05	58.6 ± 0.6	59.9 ± 0.05	3 ± 0.2
10	57.6 ± 0.05	59.6 ± 0.5	61 ± 0.01	3.3 ± 0.05
15	58.2 ± 0.05	59.8 ± 0.8	61 ± 0.6	3 ± 0.4
20	58.6 ± 0.05	60.5 ± 0.4	62 ± 0.4	3.7 ± 0.07
30	59.6 ± 0.05	61.7± 0.7	63 ± 0.7	4 ± 0.1
40	61.6 ± 0.05	63.4 ± 0.5	65 ± 0.7	4 ± 0.1
50	62 ± 0.07	64 ± 0.2	66 ± 0.5	4.4 ± 0.03

In summary, by increasing the heating rate, the thermal gradient developed across the specimen leading to shifting the T_g towards higher temperatures. However, this heating rate dependence of the T_g can be normalised using a calibration curve as a correction procedure. Therefore, all T_g temperatures are reported according to their relative heating rates.

3.1.3 Influence of various cooling rates on the crystallinity of the polymer

As-received PLA pellet samples were heated in a DSC up to 210 ºC at a constant heating rate of 20 ºC min^{-1} and held for 5 minutes to be melted completely. Afterwards, they were cooled to RT at various cooling rates from 0.1 to 50 ºC min^{-1} and reheated to 210 ºC at the same heating rate to measure the degree of crystallinity according to the established melting peak. The effect of cooling rate on the melting behaviour of PLA during the subsequent heating process is shown in Figure 3.5. It is quite apparent from this figure that samples remained totally amorphous when treated under fast cooling rates whereas by applying slow cooling rates, the melting endotherm became measurable.

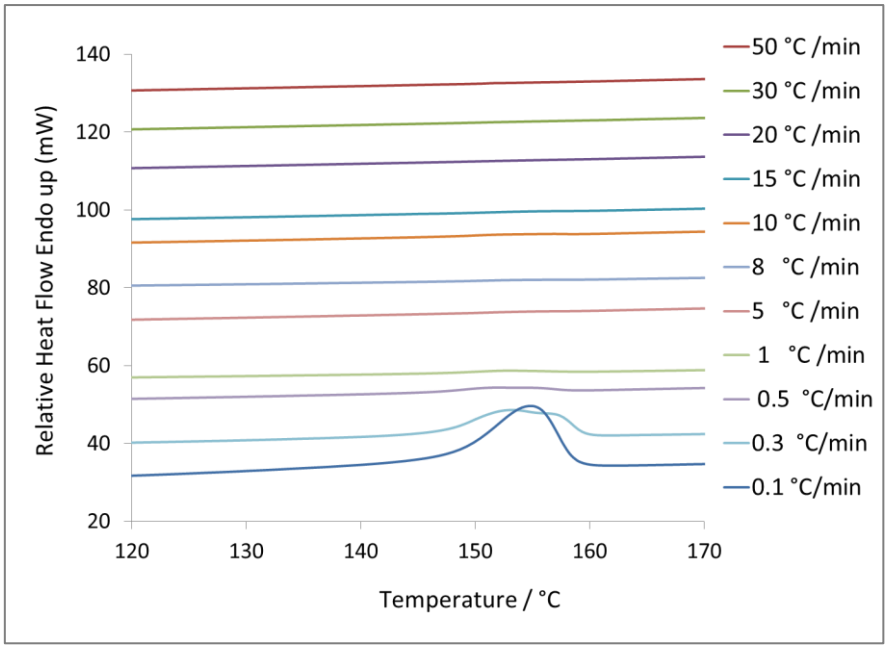


Figure 3.5 The effect of different cooling rates on the melting behaviour of PLA

Figure 3.6 shows that both the heat of fusion and the degree of crystallinity increased gradually as the value of cooling rate became smaller. The value for the degree of crystallinity obtained at 0.1 ^{o}C min^{-1} was more than 35%, which was almost equal to the one for the as-received sample. This clearly indicates that when the samples were cooled quickly, there was not enough time for any crystallinity to develop within that time-scale, whereas the low cooling rates provided sufficient time for crystallinity to increase. This is because under fast cooling rates the motion of the molecular chains cannot track the cooling temperature; thus, the chains have less mobility and they cannot diffuse into the crystalline lattice within a short time period [71].

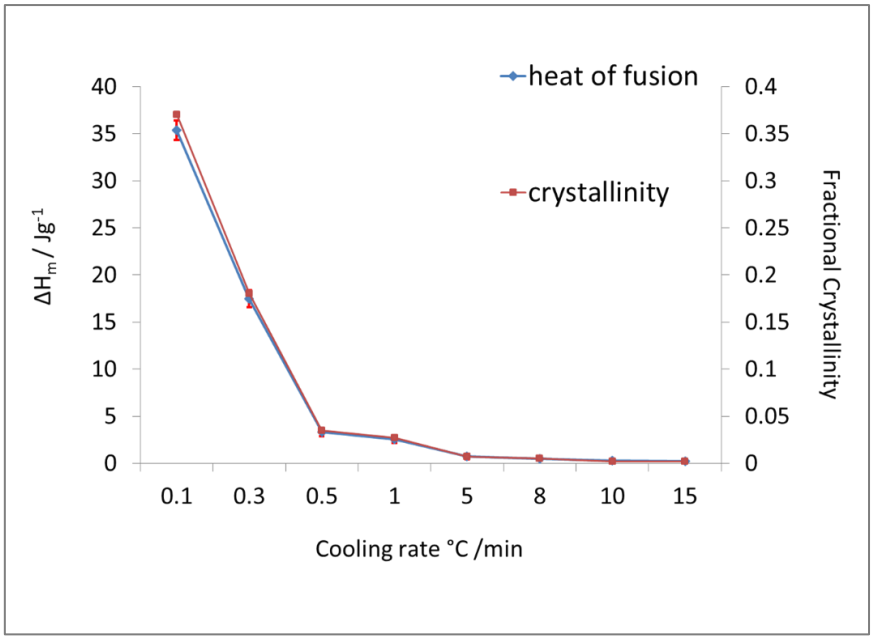


Figure 3.6 Influence of different cooling rates on the heat of fusion (ΔH_m) and fractional crystallinity of PLA pellet. The error bars are very small (± 0.5-1) up to 1 ºC min^{-1}cooling rate and afterwards almost 0; Thus, they are not obvious in the graph.

Due to a lack of sensitivity, no exothermic crystallisation was observed on the cooling run (see Figure 3.7). This indicates that although the crystallisation process has occurred under low cooling rates according to the results of subsequent heating processes, the rate of the crystallisation was too slow to be detected by DSC during the cooling processes. This is in accordance with the results found by Abdul Aziz et al. [51].

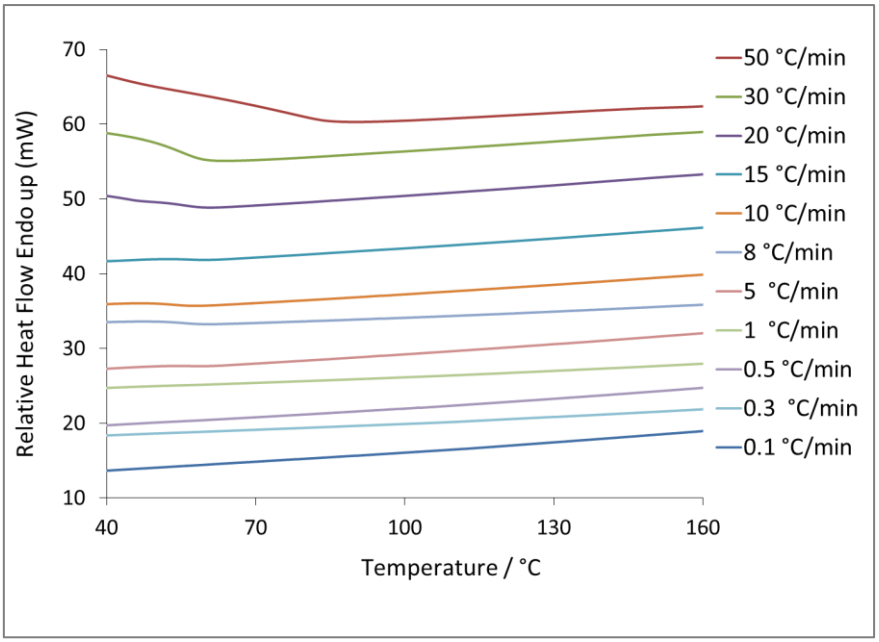


Figure 3.7 Cooling DSC processes of PLA pellet under different cooling rates

3.1.4 Influence of various cooling rates on the glass transition temperature

Figure 3.8 shows the effect of different cooling rates on the glass transition temperature. It is apparent from this figure that as the cooling rate decreased, the T_g became more pronounced. The peaks on the T_g are attributed to the physical ageing phenomenon that can occur during the cooling process of the polymer from above to below the T_g. During the cooling process, when the polymer was cooled through its T_g, the mobility of molecular chains was reduced and the material became thermodynamically unstable. Consequently, the polymer which was in non-equilibrium glassy state tended to reach equilibrium. Ageing is caused by thermodynamic drive forces which encourage a move towards equilibrium conditions above the T_g and this appears as an ageing peak on T_g [142]. Therefore, by reducing the cooling rate, there is more time for the material to be aged. However, it is quite interesting to note that no ageing peak was observed at the cooling rate of $0.1^0C\ min^{-1}$. This could be attributed to the three-phase structure of a semi-crystalline polymer containing both crystalline and amorphous areas. The amorphous region comprises of two sections, including a mobile amorphous fraction (MAF) and a rigid amorphous fraction (RAF). The RAF is highly coupled with the crystal phase

resulting in reducing the mobility of the amorphous phase [143]. On the other hand, the physical ageing process could occur when the molecular chains are mobile. In other words, the thick lamella structure and the high crystalline content of the sample at this cooling rate hindered the ageing process or slowed it down to a point which could be ignored [144].

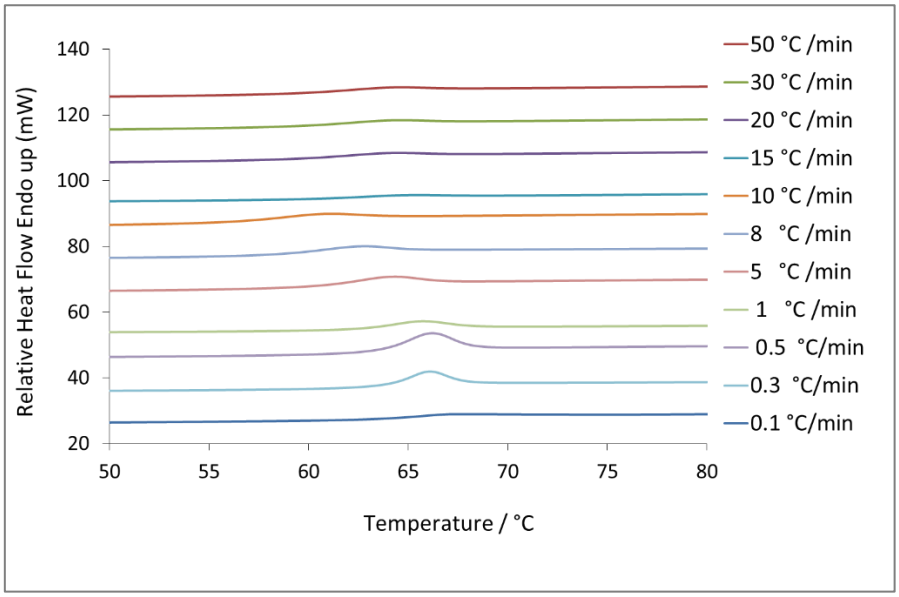


Figure 3.8 Glass transition temperatures of PLA on subsequent heating processes after cooling it at different cooling rates

Figure 3.9 shows two entirely different trends regarding the influence of cooling rate on the T_g. For the slow-cooled samples which are considered to be partially crystalline (less than 5 ºC min^{-1}) the T_g became larger as the cooling rate decreased. In contrast, for the amorphous samples (5 ºC min^{-1} and above), the T_g increased with higher cooling rates. The latter trend is related to the usual dependence of T_g on the cooling rate in a DSC measurement where the temperature at which the polymer chains lock into the glassy material is determined by the cooling rate which imposes a time-scale over which the molecular chains are allowed to move. This is because the glassy polymer is formed at a temperature, which is in equilibrium. Consequently, when the polymer cools slowly, more motions can occur and the network of chains that are moving around can rearrange themselves so that they can follow maintaining the thermal equilibrium of their environment whereas by applying fast cooling rates the

molecular mobility decreases and the structure becomes more out of equilibrium and subsequently the T_g goes up.

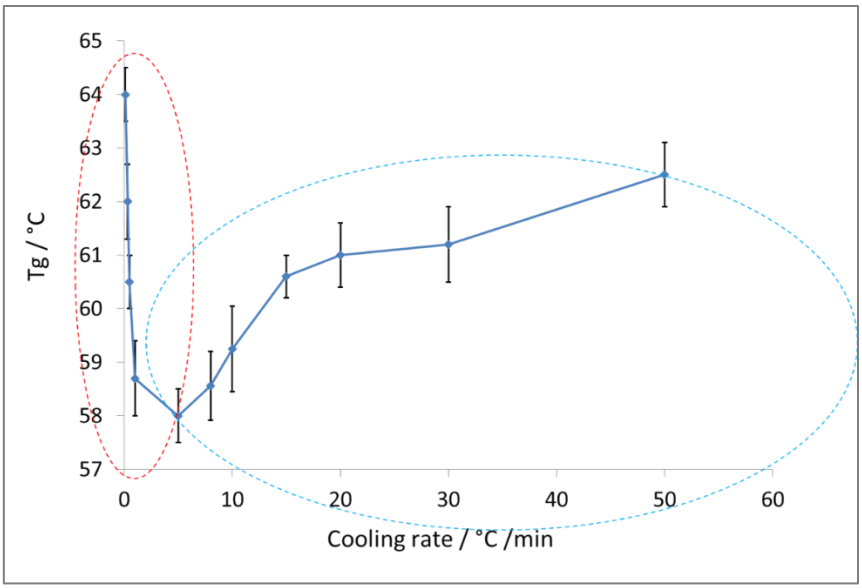


Figure 3.9 The relationship between different cooling rates and the established T_g. The red area (Semi-crystalline samples, the dependence of T_g on crystallinity) and the blue area (amorphous samples, the dependence of T_g on cooling rate).

The amorphous region of the curve (blue area) can follow an Arrhenius relationship shown below (Equation 3.2)

$$k = A \exp -\frac{E_a}{RT} \quad [51] \qquad \textbf{(Equation 3.2)}$$

where K is the cooling rate (R_c), A is a pre-exponential factor , E_a is the activation energy for molecular mobility (kJ mol^{-1}), R is the universal gas constant (8.314 J mol^{-1} K^{-1}) [145] and T is the glass transition temperature (T_g) in Kelvin. Figure 3.10 shows an Arrhenius plot of Ln (cooling rate) against the reciprocal temperature. The amount of activation energy (E_A) calculated from this equation was 448 ± 0.95 kJ mol^{-1}. According to a report by Murphy et al., the activation energy value of a PLA polymer depends on D-lactide content. According to that report, incorporation of more D-lactide into PLA decreases its T_g and E_a value due to the greater mobility of molecular chains [136]. However, the E_a values obtained by Murphy et al. for two

types of semi-crystalline PLA samples with the same amount of D-lactide content like in this study (4%) were higher (around 700-800 kJ mol^{-1}) than the amount of E_A value achieved in this study. This might be due to the lower molecular weight of the PLA in this study resulting in lower E_a values [136].

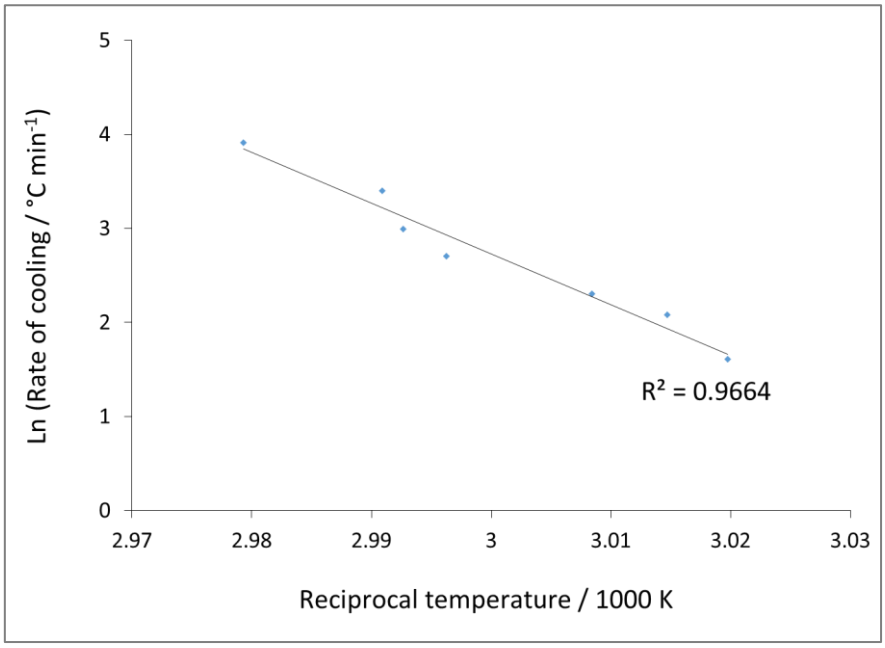


Figure 3.10 Arrhenius curve of log (cooling rate) versus the reciprocal temperature for amorphous PLA samples

Regarding the semi-crystalline samples (the red area) as mentioned before, T_g was increased inversely with the value of cooling rate. The reason is that in this region, the T_g is also influenced by the crystallinity and as can be seen in Figure 3.11, the T_g value became larger by increasing the amount of crystallinity. This is because, in a semi-crystalline polymer, the amorphous regions are trapped among many hard crystalline materials, which can reduce their segmental mobility and consequently increase the T_g [51].

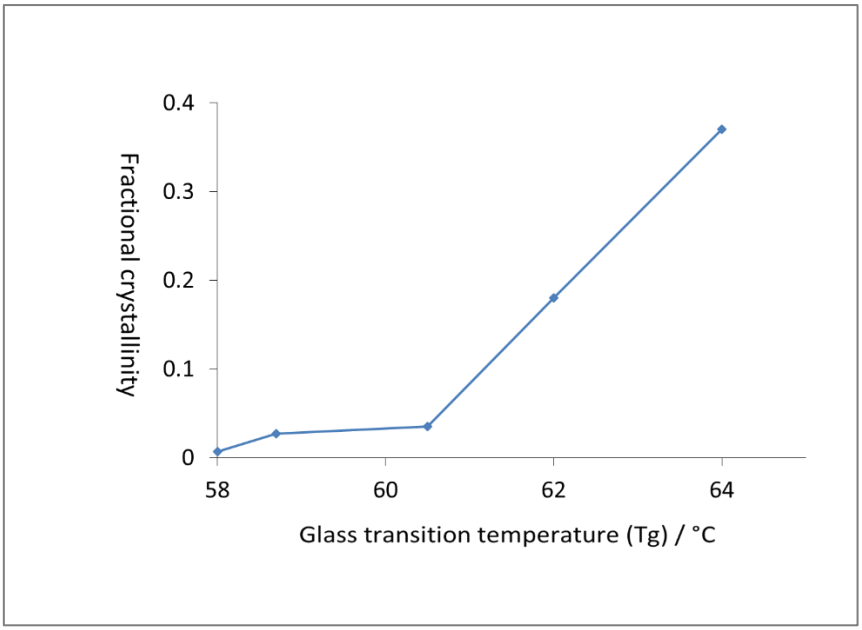


Figure 3.11 The relationship between the glass transition temperature and crystallinity for semi-crystalline PLA samples

Overall, these results indicate that the amount of cooling rate plays a vital role in the determination of T_g. However, in semi-crystalline polymers, the degree of crystallinity seems to be the dominant factor for the calculation of T_g. This is also in agreement with Abdul Aziz et al. [51].

3.1.5 Correlation between the cooling rate and morphology of the PLA studied under hot stage microscopy (HSM)

In order to investigate the correlation between the cooling rate and the resulting morphology of the PLA during the crystallisation process from the melt, thin film samples prepared by hot pressing were examined under hot stage microscopy (HSM). The same procedure as DSC was applied for the samples under HSM. First, samples were heated up to 210 °C at a rate of 20 °C min^{-1} and held for 5 minutes; afterwards they were cooled down to the RT at various cooling rates (0.1-3) °C min^{-1} before being reheated to the melt temperature at the same heating rate. There was no evidence of spherulites formation during the heating process. Thus, the heating

rate was sufficient to avoid any recrystallisation. Figures 3.12-3.16 illustrate the morphology behaviour of PLA during the cooling process from the melt at different cooling rates.

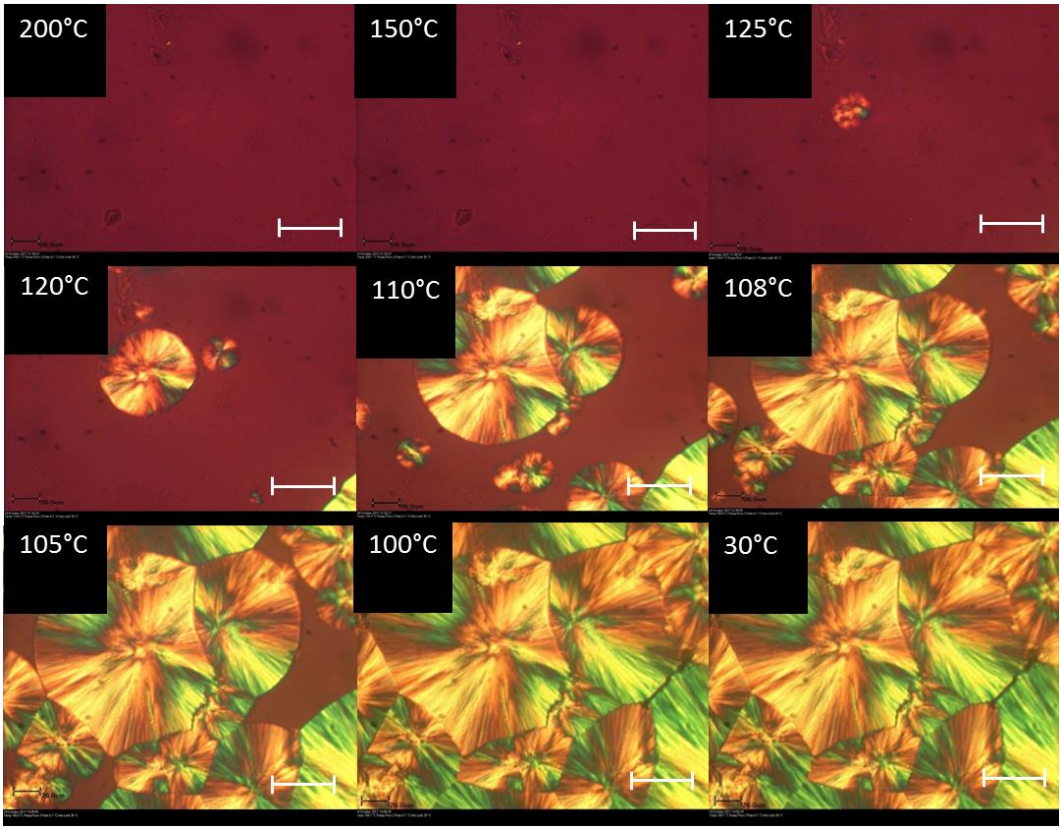


Figure 3.12 HSM micrographs showing growth of spherulites during the cooling process at a cooling rate of 0.1 ºC min^{-1}. The white scale bars represent 40 μm

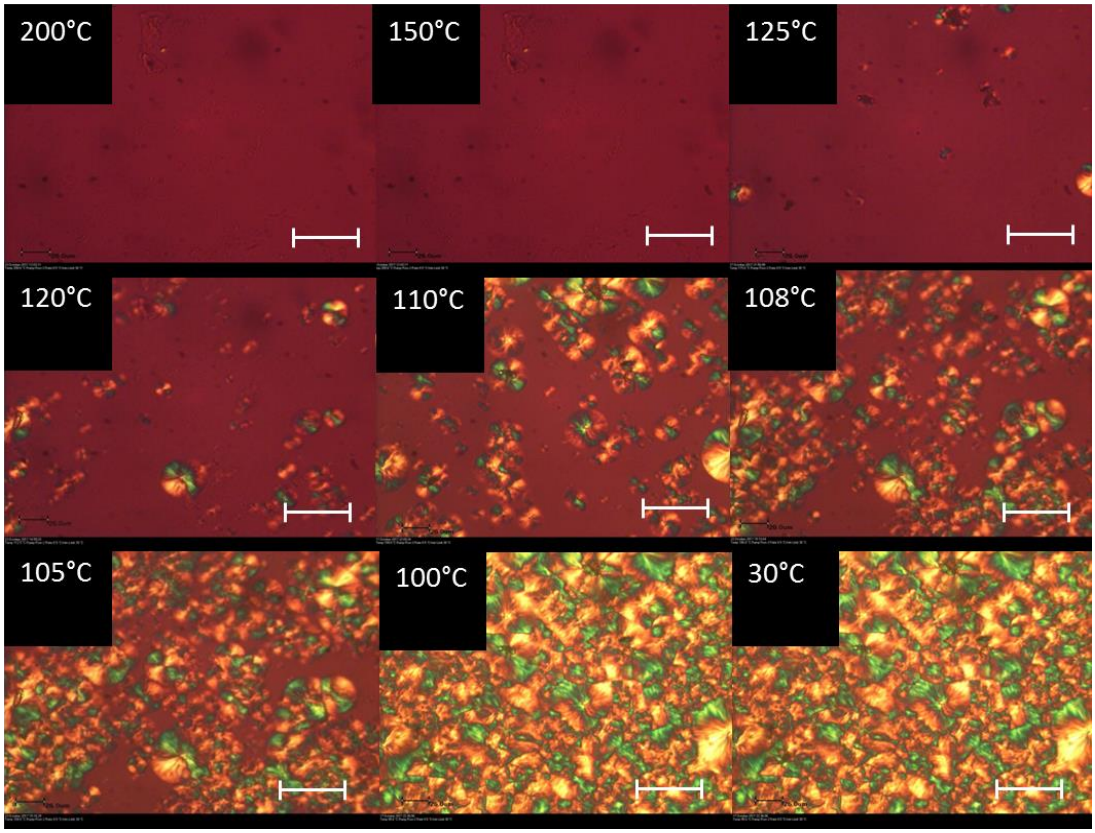


Figure 3.13 HSM micrographs showing growth of spherulites during the cooling process at a cooling rate of 0.5 ºC min^{-1}. The white scale bars represent 40 μm

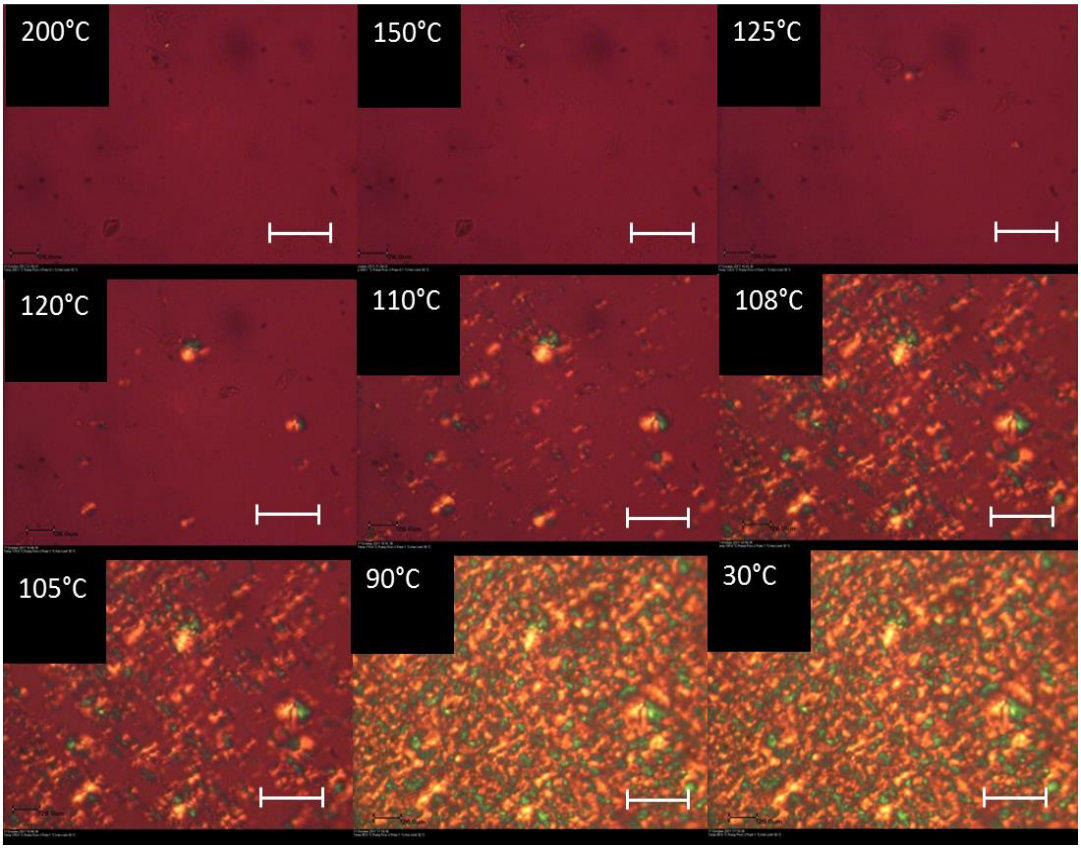


Figure 3.14 HSM micrographs showing growth of spherulites during the cooling process at a cooling rate of 1 ºC min^{-1}. The white scale bars represent 40 μm

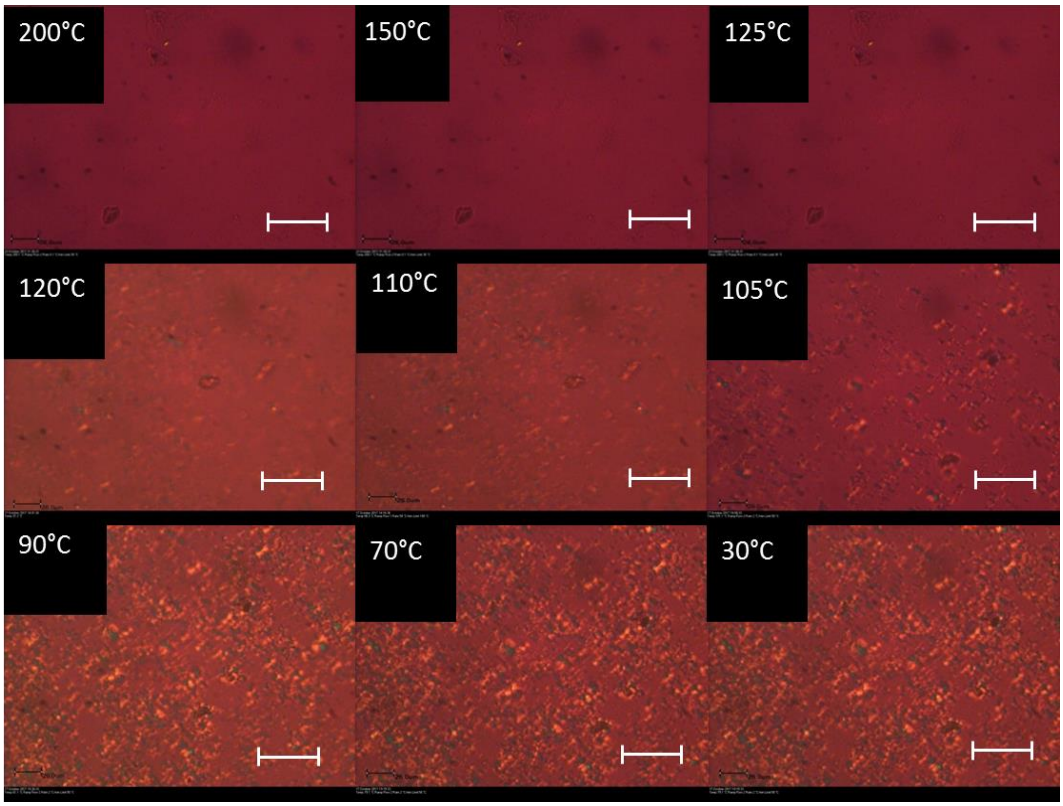


Figure 3.15 HSM micrographs showing growth of spherulites during the cooling process at a cooling rate of 2 ºC min^{-1}. The white scale bars represent 40 μm

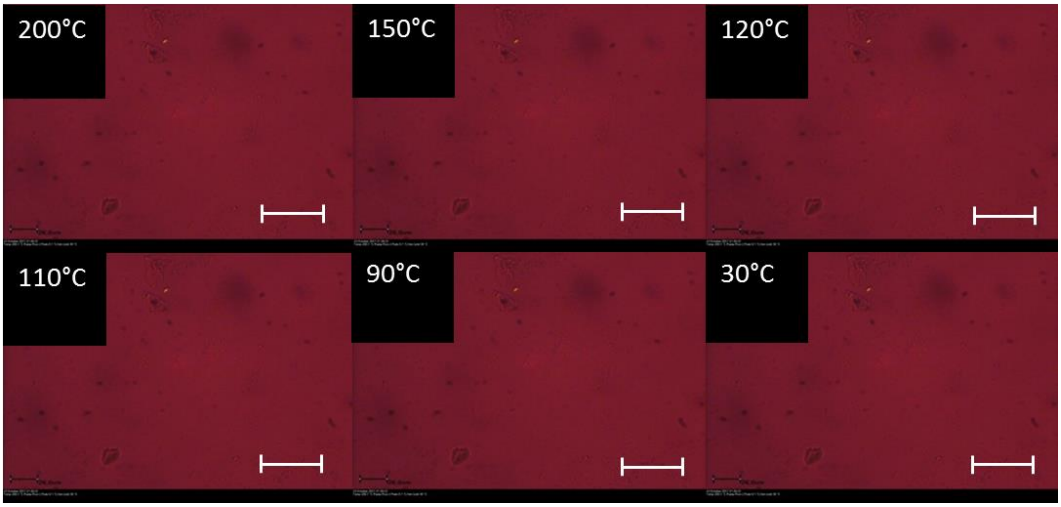


Figure 3.16 HSM micrographs showing growth of spherulites during the cooling process at a cooling rate of 3 ºC min^{-1}. The white scale bars represent 40 μm

As can be seen from the figures above the formation of spherulites for all cooling rates initiated at around 125 °C and completed at a range of 90-100 °C. It is also apparent from these figures that at slow cooling rates such as 0.1 °C min^{-1} the spherulites which were created were relatively large (80-120 μm) and as the cooling rate increased the size of spherulites became smaller up to around (5-25μm) at the cooling rate of 1 °C min^{-1}. This can be associated with the relationship between nucleation and growth rate. Faster cooling rates increased nucleation density. Therefore, the number of crystalline structures increased, but the size of them decreased as the cooling rate went up. No spherulites were observed at the cooling rate of 3 °C min^{-1}, suggesting that this rate was too fast for the growth of any crystalline structure.

These results suggest that the morphology and size of spherulites for the PLA sample can be controlled and manipulated by applying different cooling rates.

3.1.6 Isothermal crystallisation kinetics of PLA samples studies by DSC

According to the previous results from nonisothermal crystallisation studies under the HSM, the range of temperatures at which the molecular chains are sufficiently mobile to reorganise themselves and adopt the appropriate structure for crystallisation process are between 90-125 °C. Thus, using DSC, the isothermal studies of PLA samples were investigated within this range of temperatures. This procedure started by heating the samples of weight 8-10 mg secured in aluminium pans up to 210 °C, holding them for 5 minutes and rapidly cooling them down to the pre-set crystallisation temperatures (95,110 and 125) °C. The samples were then held for a period of (0.5hr-4hr) at these temperatures and afterwards were cooled down to 25 °C before being reheated to the melt to explore the effect of isothermal crystallisation process at different temperatures on the samples. Heating and cooling rates of 50 °C min^{-1} were applied during the process to avoid any additional crystallisation. Figure 3.17 illustrates the melting

endotherms produced during the subsequent heating processes, which were performed on the samples after being held at different crystallisation temperatures for various periods.

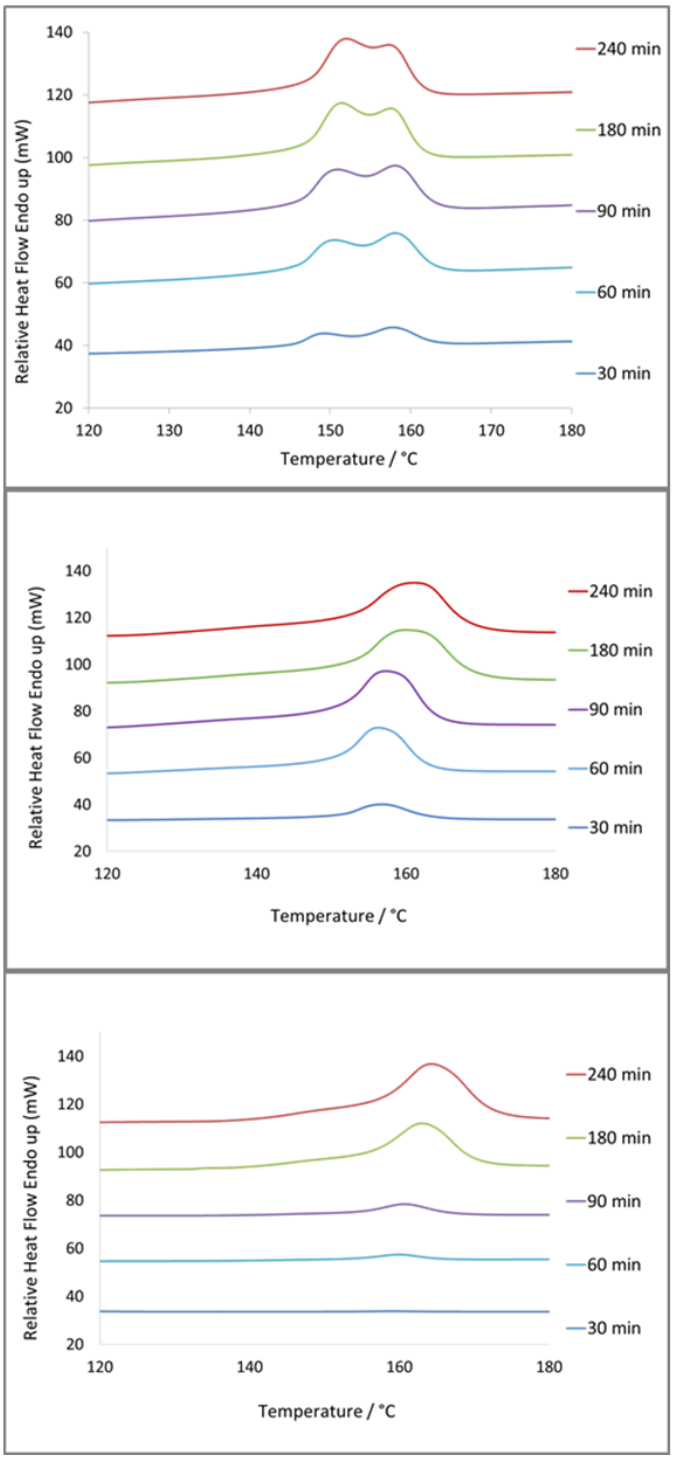


Figure 3.17 Melting endotherm produced after Isothermal crystallisation at a) 95 °C, b) 110 °C and c) 125 °C

According to this figure at low crystallisation temperature (95 °C), a double melting endotherm was detectable whereas the higher temperatures (110 °C and 125°C) produced only one single endotherm. This fact has been observed before in other reports [112, 113, 146–148]. Multiple melting peaks usually appear during the heating process when the samples are treated at low temperatures or under low heating rates. There are different explanations for this phenomenon. First, it can be related to the fact that crystal structures always have the tendency to become more stable by rearranging themselves through melting, recrystallisation and remelting process, which usually occur during the DSC heating scans. The crystallisation process at low temperatures creates small and imperfect crystal structures. Therefore, these imperfect crystals go through lots of reorganisations on heating which culminates as a multiple melting behaviour in a DSC heating scan. Furthermore, it can be associated with the polymorphism phenomenon in which there are more than one crystal structures that go through a melting and crystallisation process during the heating scan. Other factors which contribute to these multiple melting peaks phenomena are the variation in the thickness of lamella and the difference in the molecular weight of various polymer chains [146, 147].

According to Table 3.3, at both temperatures of 110 and 125 °C the degree of crystallinity (X_c) increased as the holding time at these temperatures became longer. The crystallisation process occurred much faster at 110 °C in comparison with 125 °C at which the value of X_c was very low (around 6%) up to 1.5 hours and afterwards (after 4 hours) it had a sharp increase up to around 37%. This is because by annealing the polymers at higher temperatures (near to the melting peak) only crystal structures with the highest melting point could be produced. Therefore, a longer period is required for making more perfect crystal components with a higher melting point. This is as a consequence of forming and melting less perfect crystal components with lower melting points at the beginning of the crystallisation process and then reforming these imperfect crystals into more perfect ones with higher melting peaks [110].

Table 3.3 Measurement of X_c of PLA samples at 110 and 125 °C at various isothermal times ± standard deviation

Time (Min)	**X_c (%) at 110 °C**	**X_c (%) at 125 °C**
30	8 ± 0.4	0.20 ± 0.005
60	27 ± 0.9	2 ± 0.2
90	39 ± 0.4	6 ± 0.9
180	40 ± 0.9	29 ± 0.9
240	41 ± 0.9	37 ± 0.35

Figure.3.18 shows the DSC trace of heat flow against time at three different Isothermal temperatures (95, 110 and 125 °C). As it is apparent from this figure, due to the lack of sensitivity, no isotherm was detectable at all temperatures. However, melting peaks appeared in all subsequent heating scans after the isothermal processes (as shown in Figure 3.17). This indicates that, although crystallinity had occurred during the isothermal hold, it was too low to be detectable by the DSC.

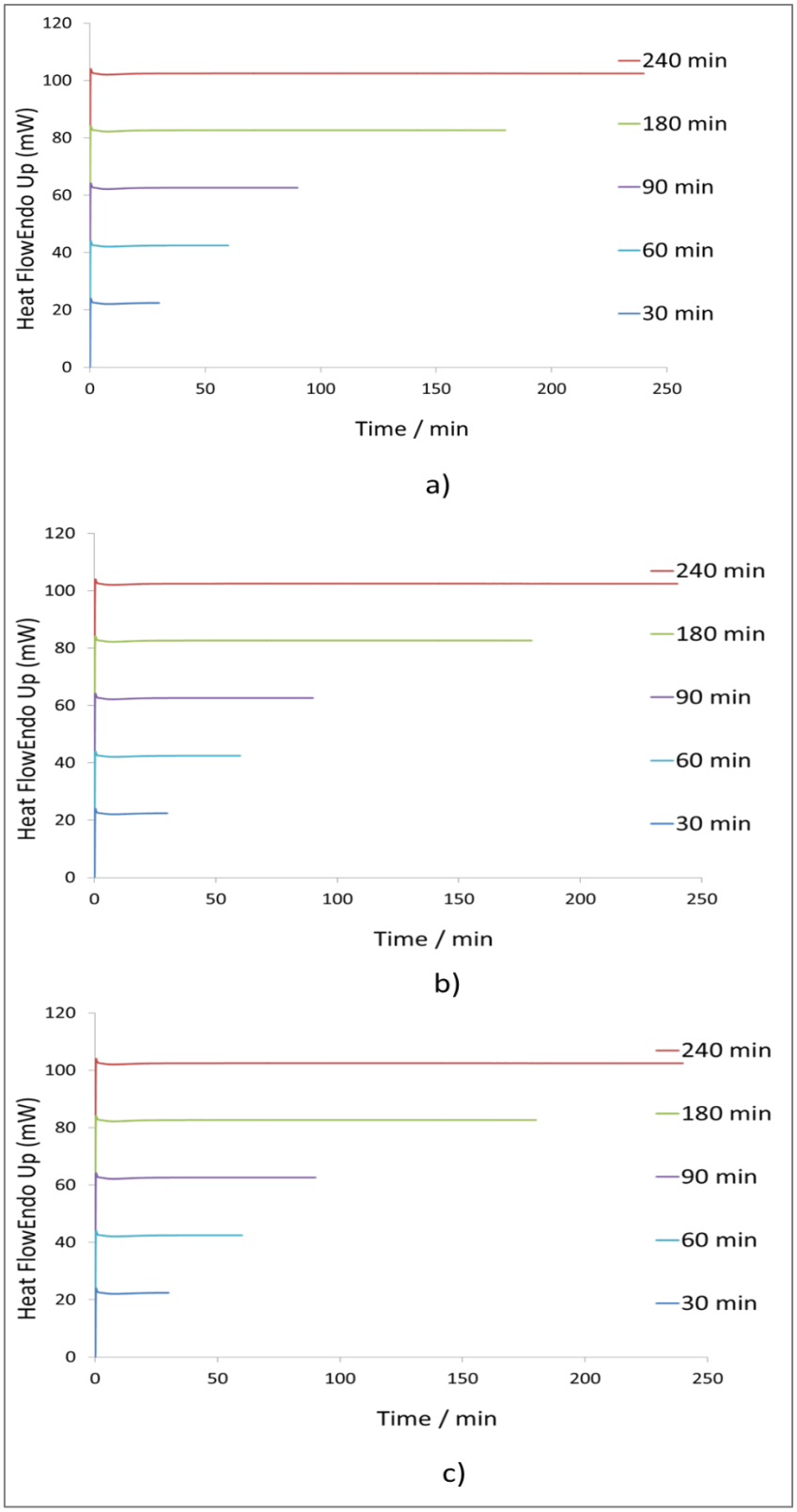


Figure 3.18 Heat flow against the time of Isothermal process for different time periods, at (a) 95 °C, (b)110 °C and (c) 125 °C

3.1.7 Isothermal crystallisation kinetics of PLA samples via HSM

In order to examine the effect of the isothermal process on the microstructure of the samples, thin film samples were analysed under HSM. The process involved melting the samples at 210 °C with a heating rate of 50 °C min^{-1} and held for 5 minutes before being cooled to the crystallisation temperatures at the same rate as heating rate. The growth of spherulites and their impingement with each other were observed under the HSM by holding the samples at three different isothermal temperatures (95,110 and 125 °C) for various periods (see Figures 3.19-3.21).

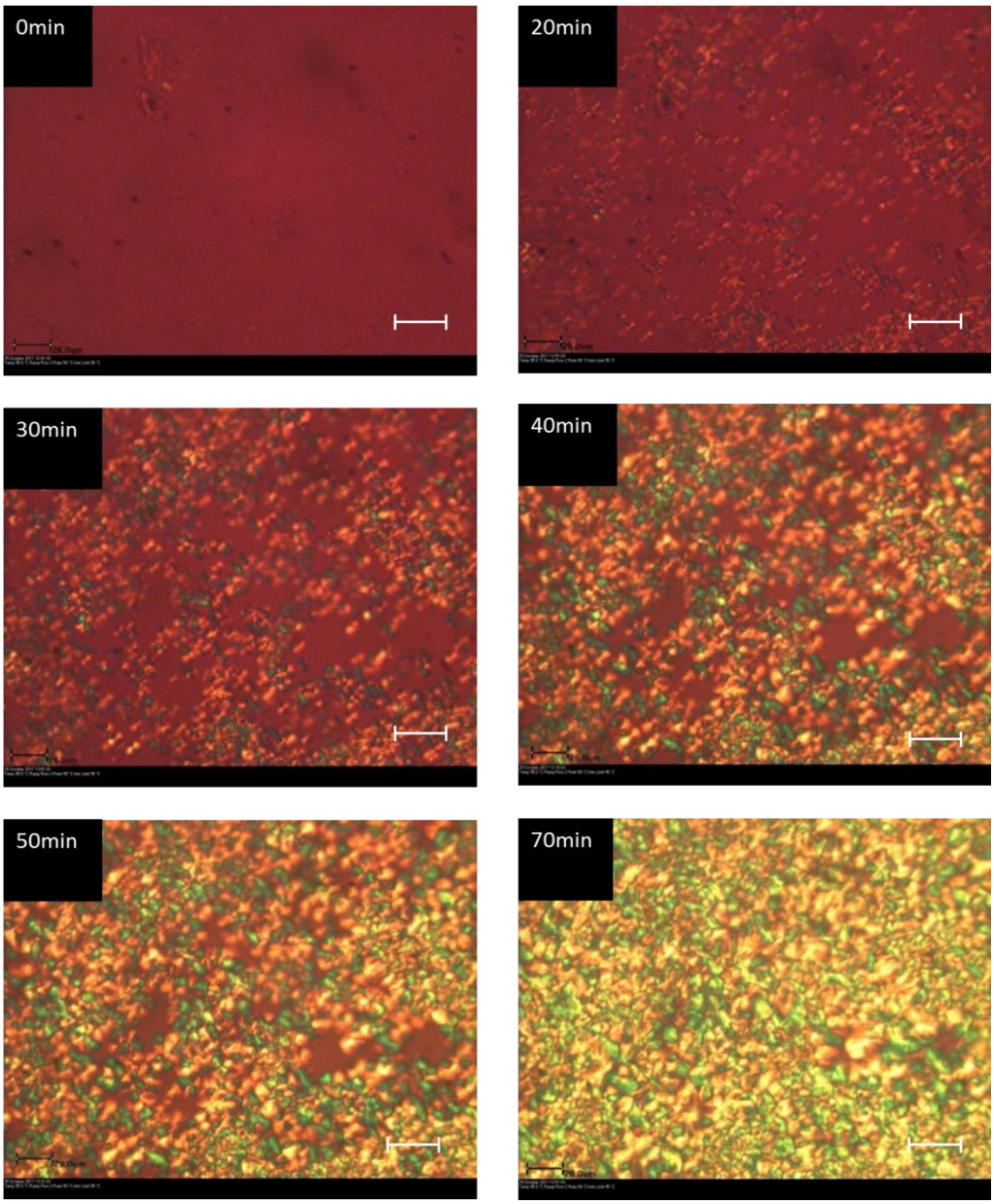


Figure 3.19 HSM micrographs showing growth of spherulites during melt crystallisation at 95 °C. The white scale bars represent 40 μm

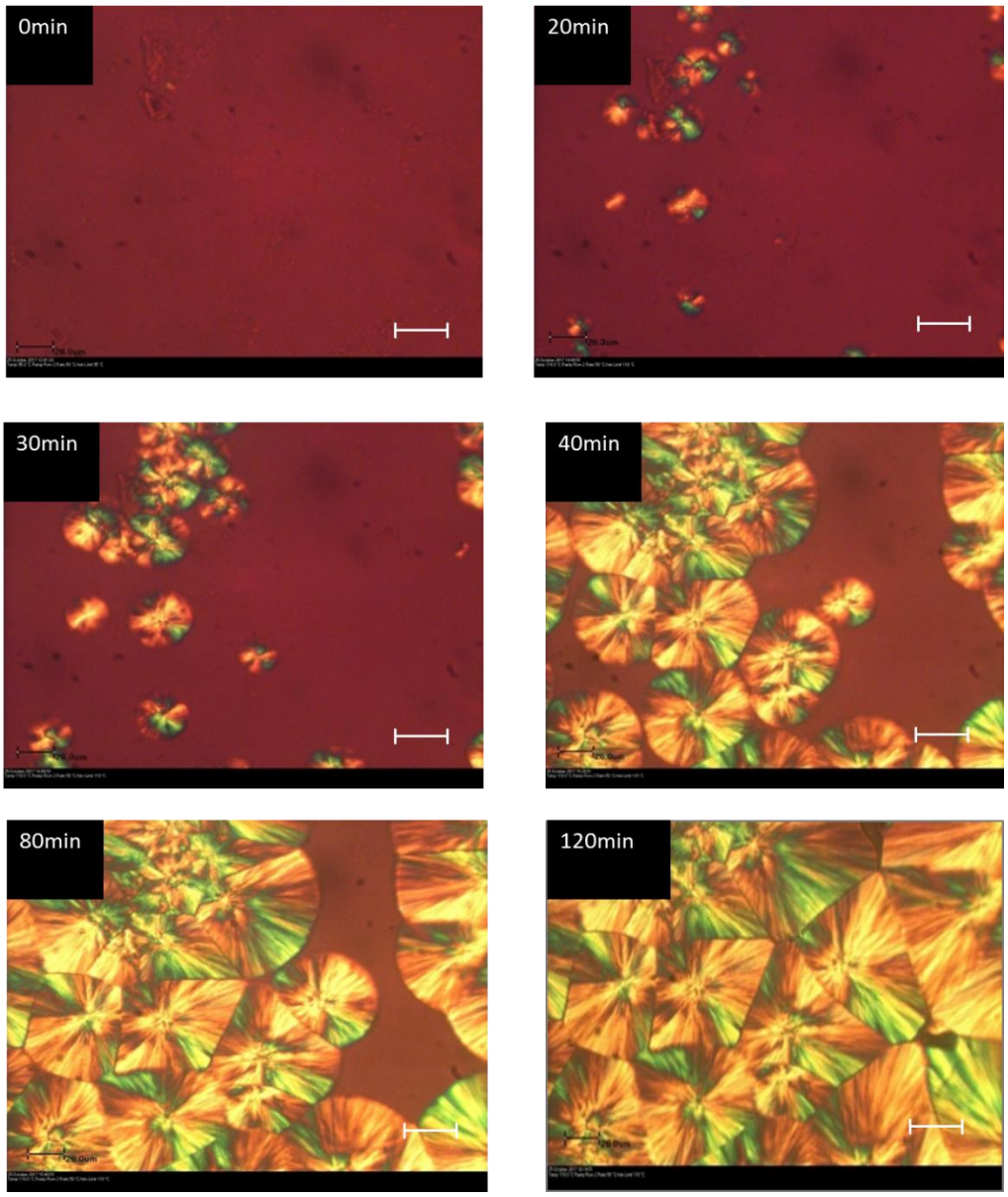


Figure 3.20 HSM micrographs showing growth of spherulites during melt crystallisation at 110 °C. The white scale bars represent 40 μm

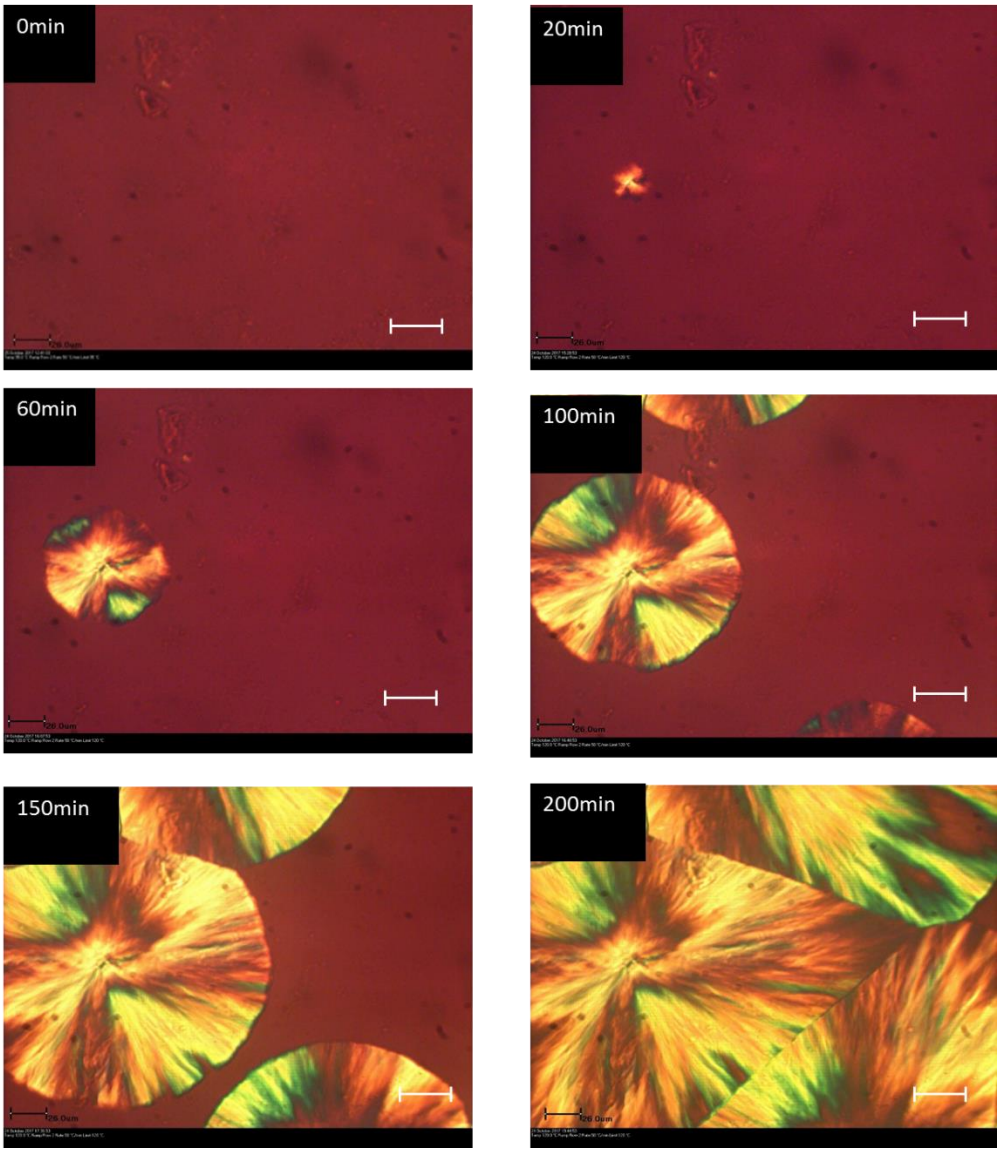


Figure 3.21 HSM micrographs showing growth of spherulites during melt crystallisation at 125 °C. The white scale bars represent 40 μm

As can be seen from micrographs above (Figures 3.19-3.21), the microstructure and size of spherulites were controlled and manipulated by holding the samples at different isothermal temperatures for various periods. As the isothermal temperature went up the size of spherulites increased while their number decreased. This can be associated with the relationship between the nucleation and growth rate, which was mentioned earlier. At higher isothermal temperatures, the nucleation density decreased. Therefore, the number of crystalline structures decreased, but the size of them increased as the temperature went up. Small spherulites (approx.

15-20 μm in diameter) were formed at the low temperature of 95 °C shown by Figure 3.19 whereas the larger spherulites samples with a range of around 60-100 μm and 200-250 μm in diameter were grown at 110 °C and 125 °C, respectively (see Figures 3.20 and 3.21). Similar experiments were performed by Abdul Aziz et al. for PLA at 95 and 125 °C [51]. However, the whole crystallisation process of the sample from the melt state at 95 °C (less than 60 minutes) and 125 °C (around 1 hour) occurred faster in that report [51] in comparison with this study in which the time required for completing the crystallisation process were 70 minutes at 95 °C and 200 minutes at 125 °C. This might be because of using a different grade of PLA and applying a different melting temperature (210 °C) in this study compared to that report in which the results were recorded after melting the polymer at a lower temperature (180 °C), which could influence the nucleation process (triggered residual crystal components to act as the nucleating agents) and consequently have an effect on the crystallisation kinetics. This point was emphasised by the differences observed for the dimensions of formed spherulites for PLA at 125 °C between these two studies. The diameters of spherulites in this study (200-250 μm) were slightly greater than the size of spherulites (175 μm) formed by Abdul Aziz et al. at 125 °C.

Overall, these results indicate that the morphology and crystal sizes of polymer samples can be controlled and manipulated by applying different isothermal temperatures for certain time periods.

3.1.8 Isothermal crystallisation kinetics and the Avrami analysis

The isothermal crystallisation process was also performed using the HSM equipped with a light dependent resistance (LDR). The heat treatment process was the same as mentioned above in Section 3.1.7 for the isothermal morphology analysis of the PLA at different temperatures under the HSM. Thin hot pressed PLA samples were heated up to 210 °C and held for 5 minutes. Afterwards, they were cooled down to the pre-set crystallisation temperatures (95-125 °C) and held for various periods. A rate of 50 °C min^{-1} was used for both heating and cooling rates.

Figure 3.22 illustrates the X_t values of PLA as a function of crystallisation time at various isothermal holding temperatures from 95 to 125 °C. According to this figure, all the curves presented a sigmoidal shape, suggesting that the primary process which occurred during the initial stages of crystallisation was faster in comparison with the secondary one which occurred at later stages of crystallisation process [149]. Furthermore, it is apparent from the same figure that the relative crystallinity firstly increased as the temperature went up. However, after reaching a peak at 110 °C, the crystallinity rate decreased with increasing the temperature. This is because at higher temperatures the polymer chains are more able to crystallise. Nevertheless, much higher temperatures could enhance the mobility of the polymer chains significantly, which leads to a longer period for completing the crystallisation process. Similar results for isothermal crystallisation of PLA for these range of temperatures were reported by Zhou et al. [150].

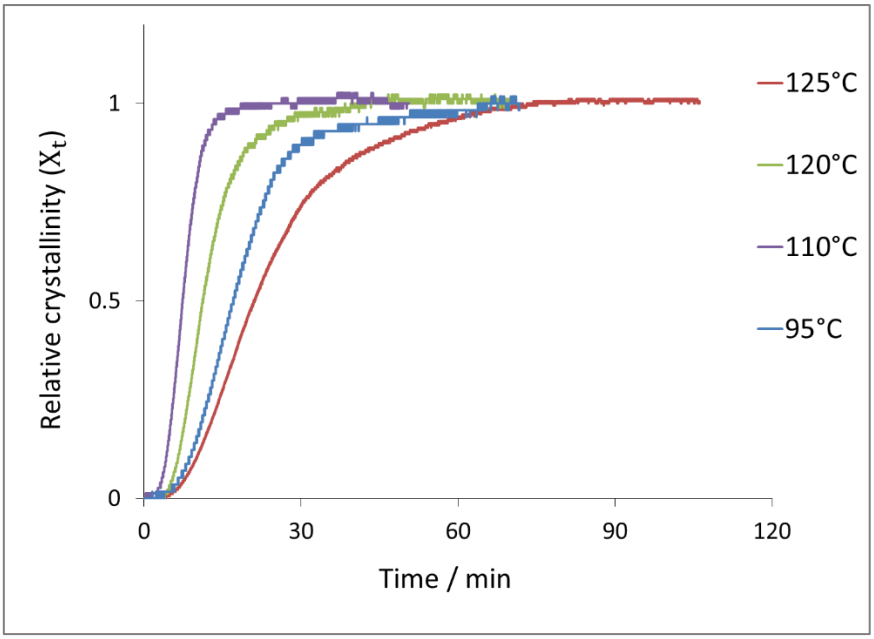


Figure 3.22 Relative crystallinity (X_t) against crystallisation time of PLA held at different isothermal temperatures

Half-time values are usually applied in order to describe the crystallisation rate of the polymers [150]. There was an induction time with all the sigmoidal curves shown in Figure 3.22. The induction time was deducted from the initial half time obtained from the sigmoidal curves at different isothermal temperatures and the final results compared and shown in Figure 3.23. As it is apparent from this figure, the half time of the crystallisation of the PLA sample was highly dependent on the crystallisation temperature and it approached its minimum level at 110 °C. At high temperatures (T>120 °C), the molecular chains were too active; thus, there was little chance for the formation of stable nuclei. However, as the temperature decreased further and the viscosity increased more, the rate of crystallisation approached its maximum level at the halfway of the curve between the T_g and T_m (110-120 °C). Near to the T_g (95 °C), the viscosity of the polymer increased significantly which resulted in decreasing the mobility of the chain segments and less possibility of the formation of stable nuclei [67, 75].

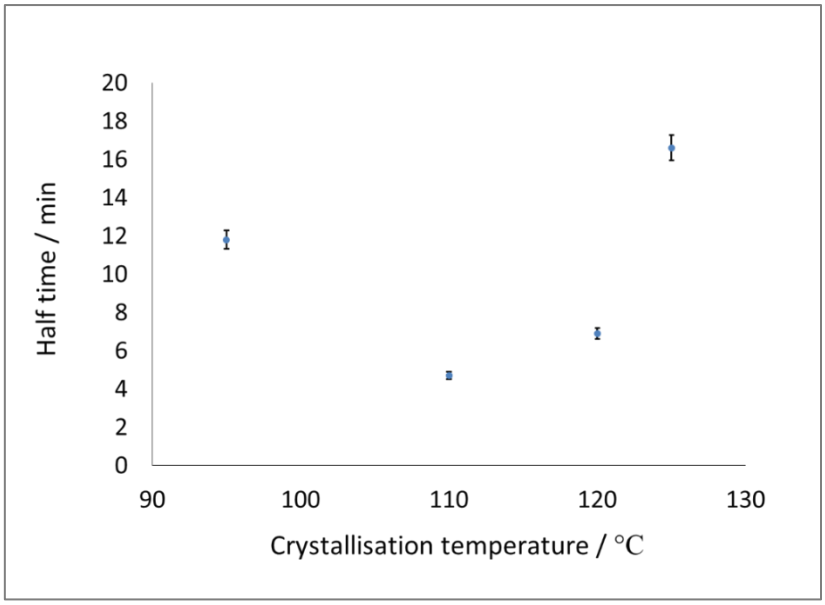


Figure 3.23 Variation in half-life with crystallisation temperature

The Avrami equation was employed for the analysis of the isothermal crystallisation kinetics of the PLA as follows [151]:

$$1 - X_t = \exp(-Zt^n) \text{ [151]} \qquad \textbf{(Equation 3.3)}$$

where X_t is the percentage of relative crystallisation at time t, n is the Avrami exponent that can take different values depending on the crystallisation mechanism and Z is the crystallisation rate constant which contributes to time-dependent properties of nucleation and growth. By taking logarithm to both sides, Equation 3.3 can be transformed to the equation below:

$$log[-ln(1 - X_t)] = logZ + nlogt \qquad \textbf{(Equation 3.4)}$$

By plotting the $log\ [-ln(1 - X_t)]$ against $logt$ as shown in Figure 3.24 and getting the linear regression of these data the values of n (the slope of the line) and the Ln (z) (the intercept of the line) can be determined.

The half time of crystallisation can be also calculated using the equation below:

$$t_{0.5}^{n} = \frac{ln2}{Z} \quad [150] \qquad \textbf{(Equation 3.5)}$$

The value of the Avrami exponent (n value) varied between 2.6 and 3.1 (see Table 3.4) which is in good agreement with other reports for PLA and its copolymers [59, 150–152]. In terms of the crystallisation models adopted by the Avrami, the growth of spherulites are in accordance with the growth of spherical particles from heterogeneous nuclei, for which n=3 [153]. According to a report by Hay et al. [83], the Avrami model can describe the crystallisation mechanism of a polymer only when the nucleation is either predetermined or sporadic with a constant radial growth. In this condition, the Avrami exponent (n value) is 3 and 4, respectively. In other words, the exponent value must be an integer to be described accurately by the Avrami model. However, as can be seen from the results of this work, that is not the case. Nevertheless, fractional Avrami exponents (n values) which are close to integer values acceptable by the Avrami model have been widely observed during the crystallisation process of the polymers. These fractional values might be as a result of variation in the nucleation density across the polymer sample [153].

The variation in half-life with temperature obtained from the Avrami equation is illustrated in Figure 3.25. The results for both Figures 3.23 and 3.25 followed a similar trend. However, the halftime values obtained from the Avrami equation (Figure 3.25) were lower in comparison with the ones obtained previously (Figure 3.23). The halftime values obtained from the Avrami model might be less accurate because of the limitations of this model such as comprising only the primary crystallisation process (not the secondary) as well as the fluctuations existed in n and Z values which obtained from the regression of the lines.

The variation in the growth rate constant, Z, is shown in Figure 3.26. Although Z is a reciprocal function of half time value, in this figure, it did not exhibit a linear reciprocal relationship with halftime trendlines (Figure 3.25).

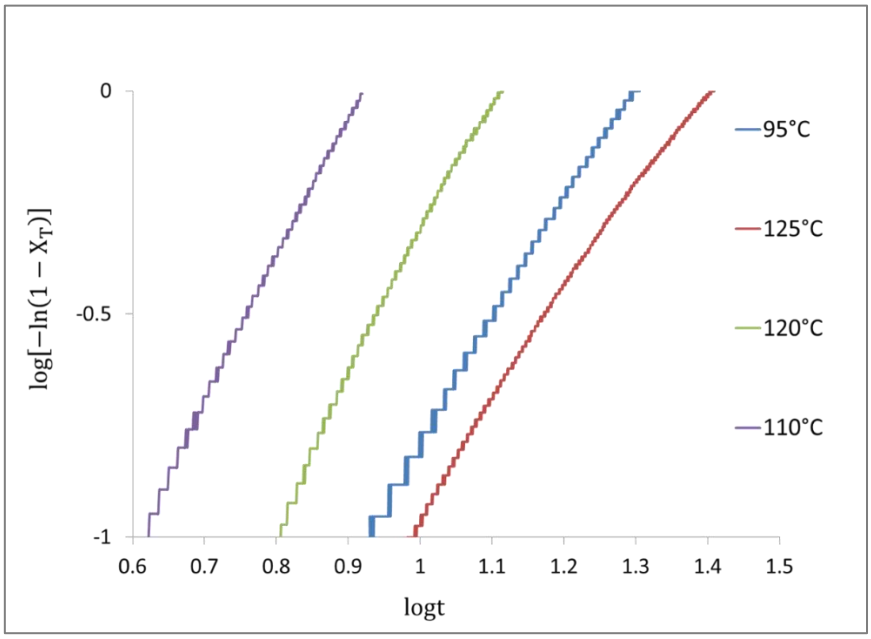


Figure 3.24 The Avrami plots of PLA at different isothermal temperatures

Table 3.4 The n values of PLA at different isothermal temperatures obtained from Avrami ± standard deviation

T (°C)	n
95	2.6 ± 0.07
110	3.23 ± 0.09
120	3.18 ± 0.09
125	2.36 ± 0.07

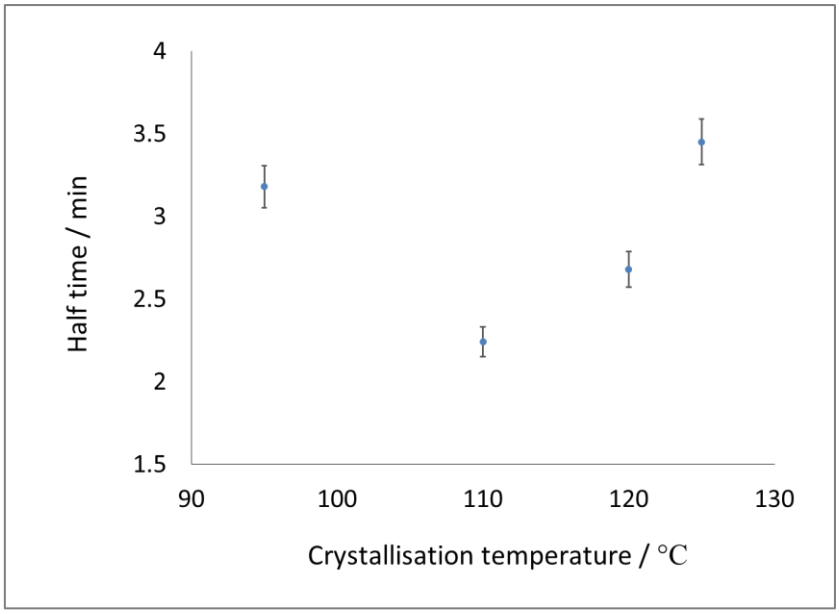


Figure 3.25 Variation in half-life with crystallisation temperature obtained from the Avrami

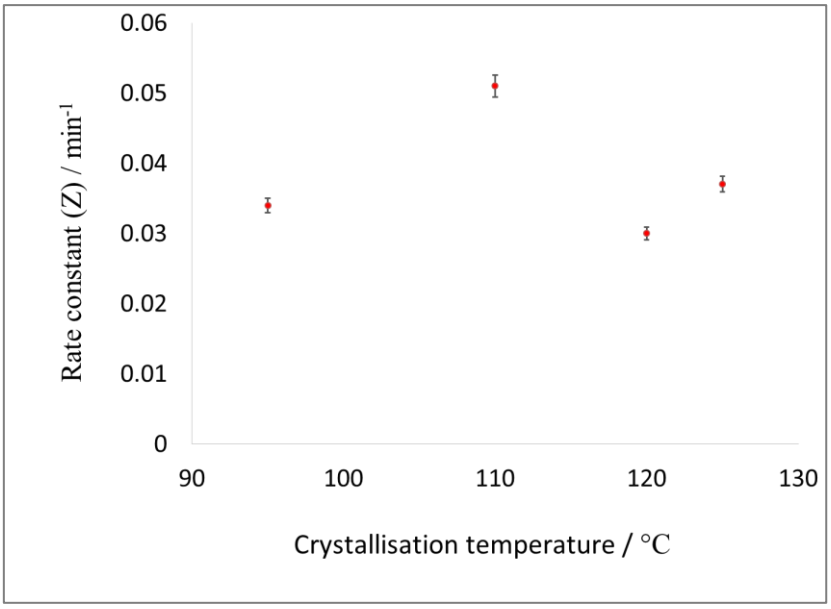


Figure 3.26 Crystallisation rate constant (Z) of PLA at different isothermal temperatures

3.2 Conclusions

Studies into the crystallisation kinetics of PLA were conducted under nonisothermal and isothermal conditions. According to the results from nonisothermal studies, the degree of crystallinity of PLA samples can be controlled and manipulated by using different cooling rates. Additionally, by applying different cooling rates polymers with various spherulite dimensions and microstructures can be produced. Both cooling and heating rates could influence the glass transition temperature of the polymer. In isothermal conditions, the crystallinity behavior, morphology and crystal sizes of the polymer were manipulated at different isothermal temperatures. The isothermal crystallisations were analysed using the Avrami model and produced n values of around 3, indicating a three-dimensional crystal growth mechanism with sphere geometry.

Chapter 4: Controlling the microstructure and crystallisation behaviour of PLA-HA composites

4.0 Introduction

In this chapter, PLA-HA composites were fabricated using three different procedures, including hot pressing, injection moulding and solution casting. The advantageous and shortcomings of each technique were discussed. In order to investigate the effect of HA particles on the morphology, thermal behaviour, crystallisation kinetics and mechanical properties of the PLA matrix, composite samples were characterised using different techniques including SEM, DSC, HSM, TGA, tensile and flexural tests as well as DMTA. Additionally, a novel approach for producing porous structures using DCM solvent was introduced.

4.1 Results and discussion

4.1.1 SEM morphology of PLA and HA powders as well as hot pressed samples

In order to produce composite samples with a suitable dispersion, PLA pellets were cryogenically ground into powders. The scanning electron microscopy (SEM) was used for the morphological study of both PLA powders obtained by cryogenic grinding and the as-received HA powders. Figure 4.1 illustrates the SEM images of PLA powders. As can be seen from this figure, the average size of the PLA powders is around 970 ± 190 μm. The SEM morphology of the as-received HA powders shown in Figure 4.2. It is apparent that HA powders have an average size of 19 ± 0.5 μm with an irregular shape.

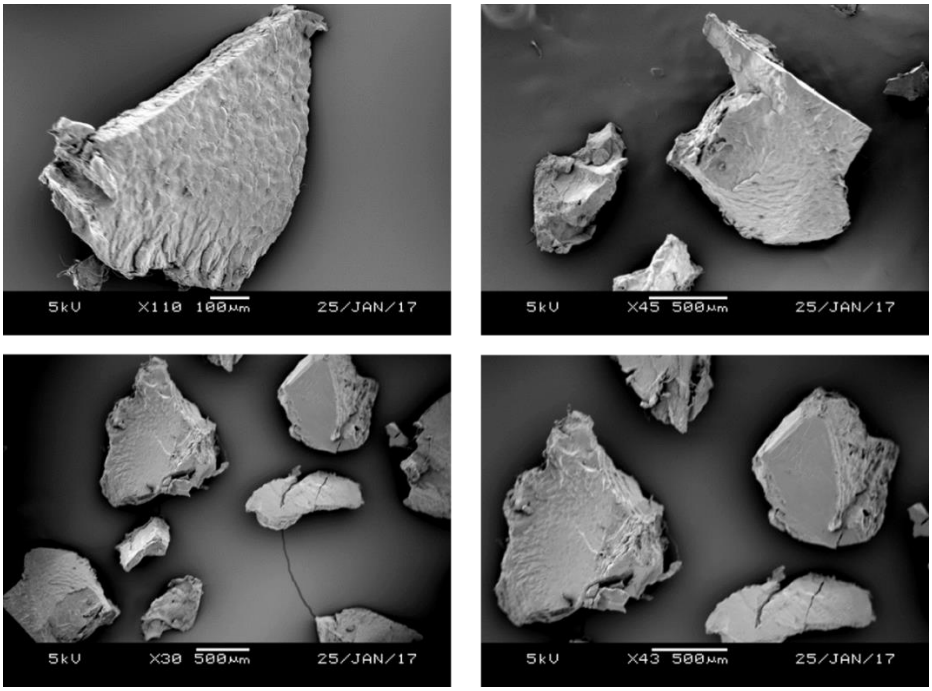


Figure 4.1 SEM images of PLA powders obtained via cryogenic grinding

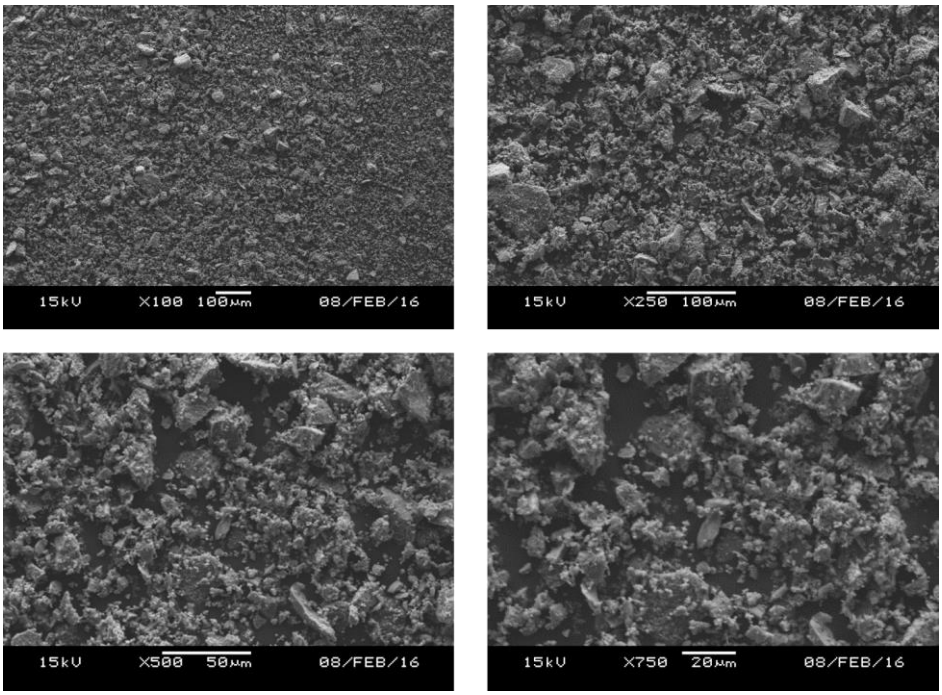


Figure 4.2 SEM images of the as-received HA powders

Figure 4.3 demonstrates the SEM micrographs of fracture surfaces of the hot pressed composite samples containing different amount of HA (0-40 wt%). It is apparent from this figure that HA particles with sharp edges (Figure 4.2) are not obviously recognisable even at 40 wt% loading of HA. This indicates that HA particles were successfully integrated within the PLA matrix. No agglomeration of HA powders was observed in the pictures showing that the dispersion of the filler within the polymer matrix was quite well. As the percentage of HA particles increased through the composite, a rougher surface was observed under the microscope. This is in accordance with previous reports which suggest that by adding HA into PLA the surface roughness of the composite could be increased [154, 155].

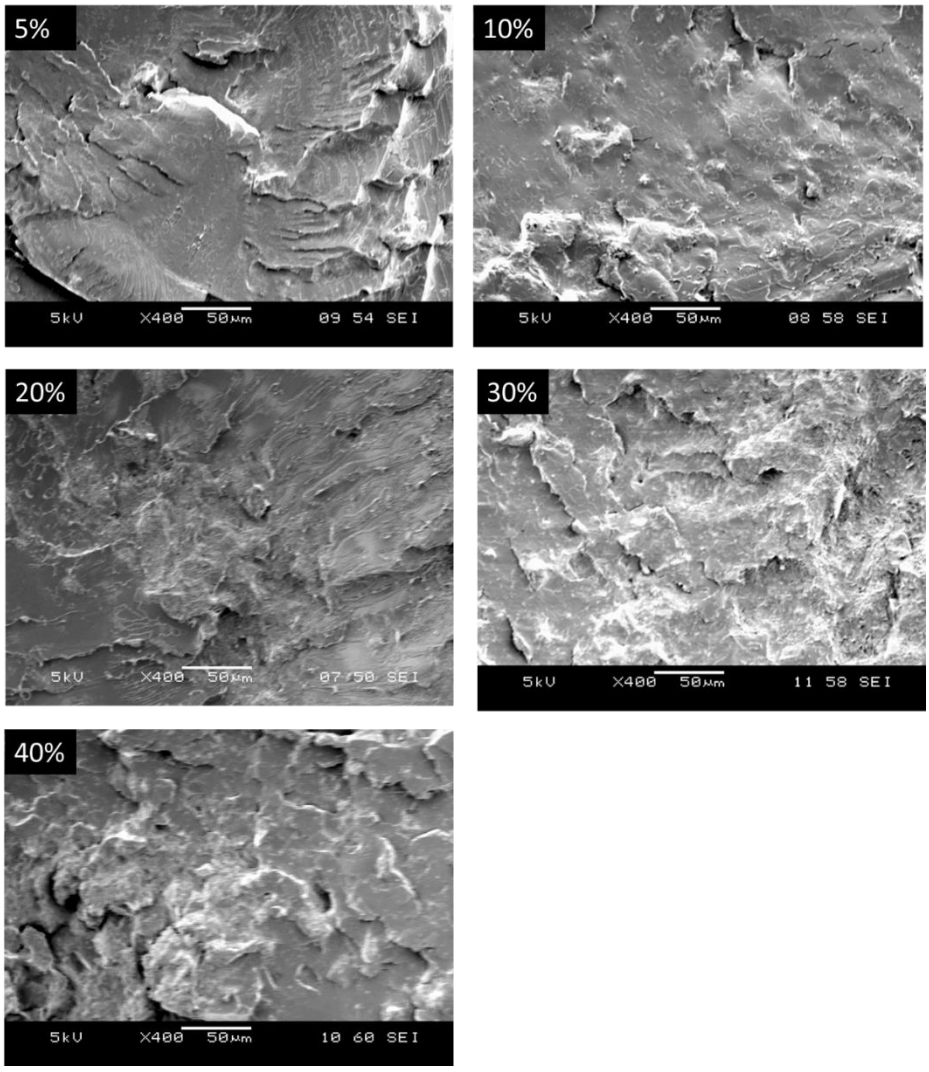


Figure 4.3 SEM micrographs of hot pressed PLA-HA samples with different wt% of HA

4.1.2 Nonisothermal DSC studies of PLA powder and hot pressed samples

In order to investigate the effect of cryogenic grinding on the crystallinity and thermal behaviour of the as-received PLA pellets, both PLA pellets and powder (after grinding) were analysed by DSC. In the first run, PLA pellets and powders were heated up to 210 ºC at a heating rate of 20 ºC min^{-1} and held for 5 minutes. Afterwards, they were cooled to the RT at 20 ºC min^{-1} before being reheated to the melt temperature at the same heating rate (Figure 4.4). The degree of crystallinity and glass transition temperature of both PLA pellet and powder were almost similar during the first and second heating scans (Table 4.1). According to both Figure 4.4 and Table 4.1, the cryogenic process did not change the properties and thermal behaviour of the original PLA pellet.

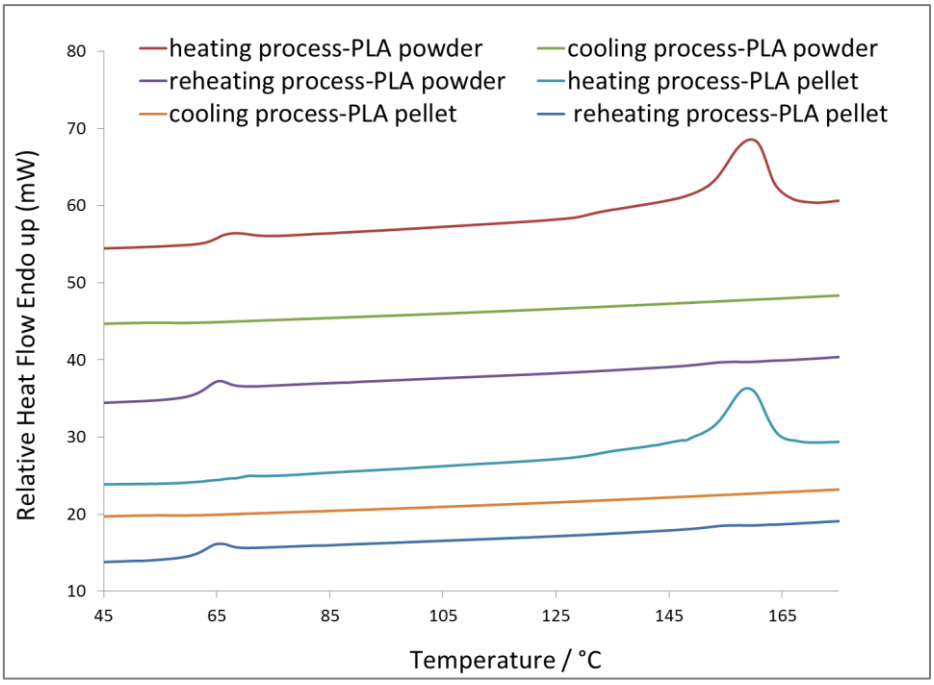


Figure 4.4 DSC graphs of as-received PLA pellet and powder (after cryogenic grinding) first heating, cooling and second heating (reheating) processes

Table 4.1 Comparison of properties of PLA before and after cryogenic grinding process ± standard deviation

Type of sample	X_c (%) -heat 1	X_c (%) -heat 2	T_g (°C) -heat 1	T_g (°C) -heat 2
PLA pellet	38 ± 0.3	0	65 ± 0.5	61 ± 0.6
PLA powder	38 ± 0.5	0	64.5 ± 0.8	61 ± 0.7

A nonisothermal DSC process was performed on PLA and PLA-HA hot pressed samples to investigate the effect of HA and hot pressing process on the crystallinity and thermal behaviour of the samples. The process involved heating the samples (around 10 mg) up to 210 ºC and held for 5 minutes to eliminate any thermal history. Afterwards, they were cooled to the RT before being reheated to the melt temperature. The heating and cooling rates applied during the processes were 20 ºC min^{-1}. Figure 4.5 illustrates the reheating processes of all composite samples (0-40 wt%) HA. As it is apparent from this figure, there was evidence of some crystallisation and melting during all reheating processes. However, according to Figure 4.6, no melting peak or crystallisation appeared during the reheating process when a heating rate of 50 ºC $min^{-1}$was applied (PLA and 10 wt% HA). This suggests that the crystallisation and melting peaks observed during the reheating processes in Figure 4.5 were not related to the pre-existing crystallinity of the pure PLA due to hot pressing process or the HA content of the composite, but, they could be related to the crystallisation that occurred during the reheating process due to the low heating rate [156]. Furthermore, as can be seen from Figure 4.5, a peak appeared on the T_g for all samples suggesting that some physical ageing occurred during the process. However, physical ageing tends to happen in amorphous materials and not in semi-crystalline [144]. This further supports the hypothesis that all samples achieved through hot pressing were totally amorphous and HA did not seem to influence the crystallinity behaviour of the samples.

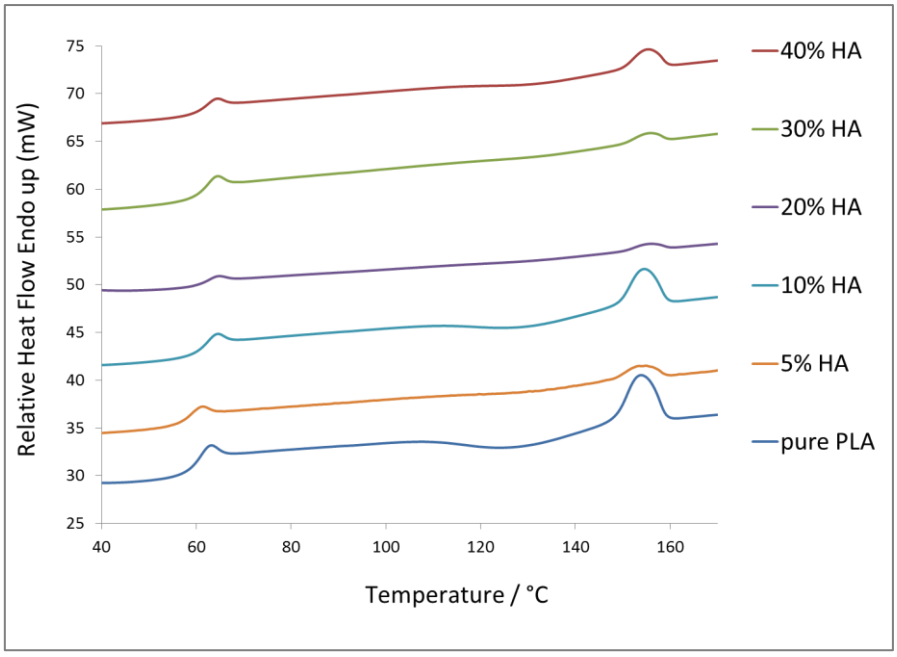


Figure 4.5 Subsequent heating scans of hot pressed HA-PLA composites with different HA loadings after cooling at 20 ºC min^{-1}

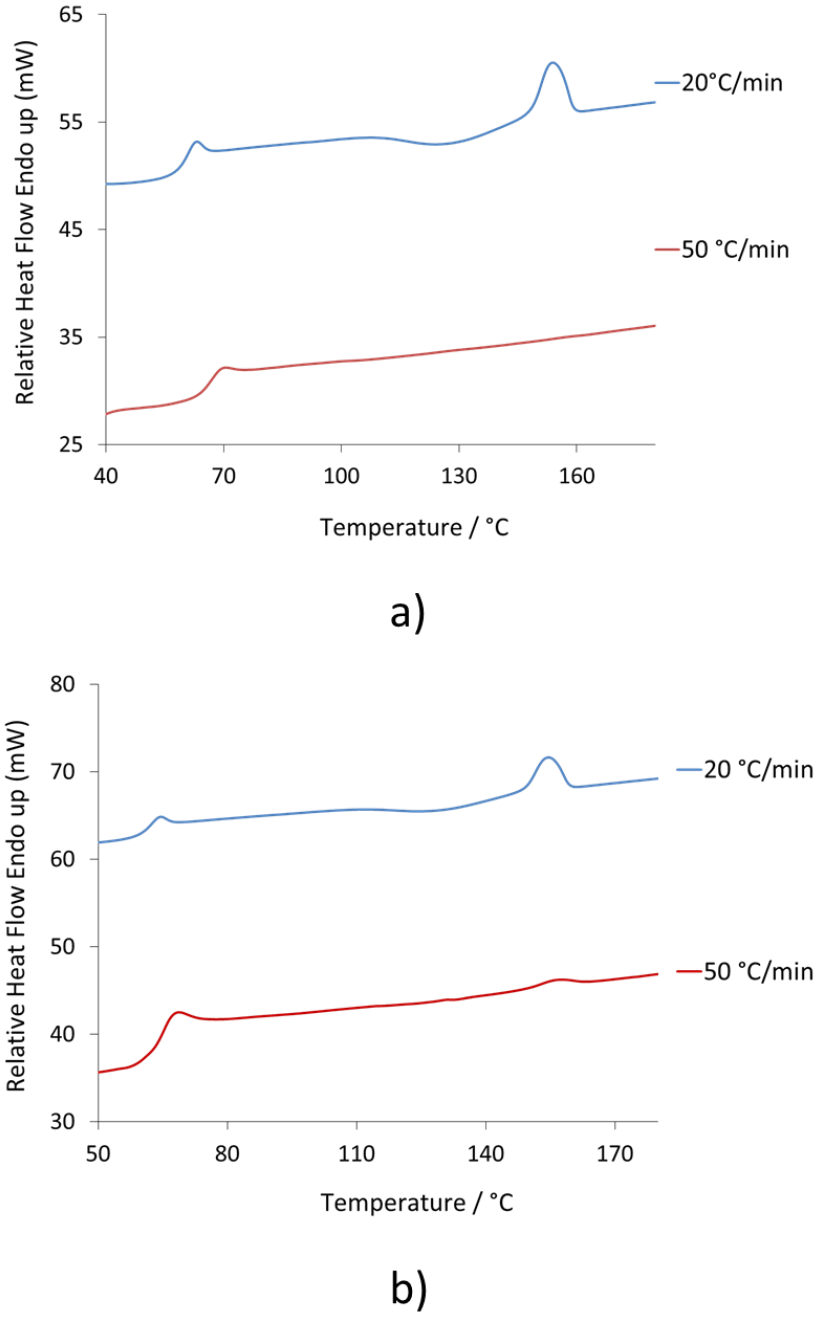


Figure 4.6 Subsequent heating scans of hot pressed a) pure PLA and b) 10% HA-PLA after cooling at 20 ºC min^{-1} using different heating rates (20 and 50 ºC min^{-1})

The glass transition temperatures of the samples with different HA loadings were compared and shown in Figure 4.7. As it is apparent from this figure, the glass transition temperature increased slightly with increasing the HA content in the samples (except for 5 wt% HA). However, the variance of the T_g was not significant (according to the error bars). Nevertheless, the shifting of the T_g into a higher temperature due to the increase in the filler content has been reported previously by other authors [121, 125, 128, 129]. This could be attributed to the agglomeration of HA particles, which restricted the chain mobility of the polymer. Thus, in order to mobilise the polymer chains, more energy was required resulting in an increase in the T_g [125].

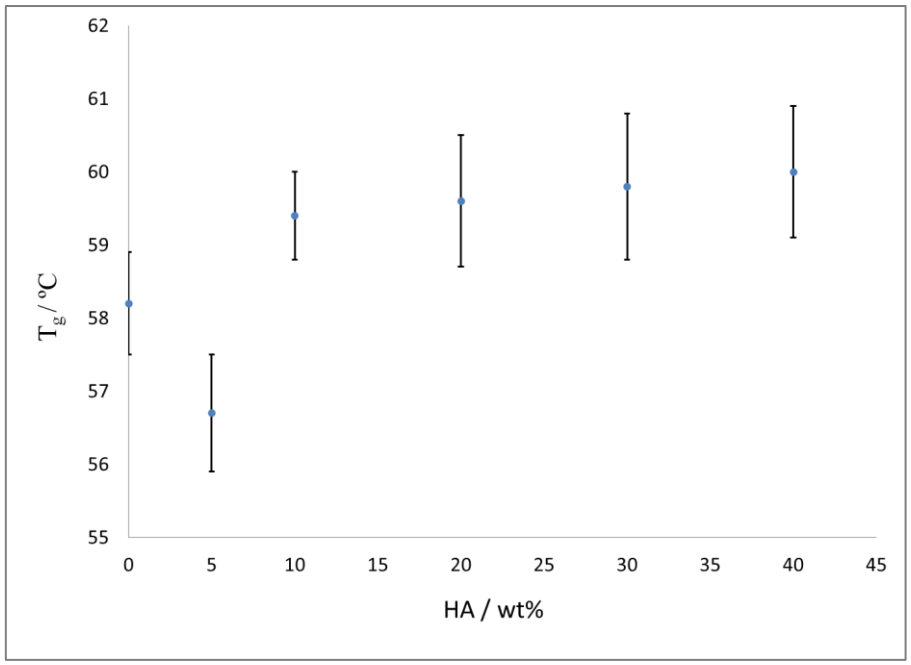


Figure 4.7 The effect of HA loading on the T_g of hot pressed composite samples

4.1.3 Isothermal crystallisation studies of hot pressed samples by DSC

In order to explore the effect of HA particles on the crystallisation behaviour of PLA under isothermal conditions, PLA and PLA-HA samples with different loadings of HA were isothermally treated under the DSC at three different isothermal temperatures (95,110 and 125 °C). The heat treatment process was repeated the same as for the pure PLA in Chapter 3 (Section 3.1.6).

Figures 4.8.a-4.8.f show the melting endotherms of subsequent heating processes that were performed on the PLA and PLA-HA samples (5-40 wt% HA loading) after being held at 95 °C for various periods. As can be seen from these figures, double melting peaks due to the melting-recrystallisation-remelting process, which was mentioned previously (Chapter 3), appeared during the heating processes of all samples. The general trend of these figures shows that storing a sample at a longer period resulted in stabilising the double melting peaks and converting them into one single peak. Furthermore, the area under the melting region for all samples increased over time. It is also apparent that adding more HA led to double melting peaks converting faster into one single melting peak, indicating that HA could accelerate the crystallisation process. Nevertheless, according to these figures, by adding a larger amount of HA particles in the polymer samples (30 and 40 wt% HA), melting peaks with a small shoulder appeared suggesting that the rate of crystallinity could be reduced by the addition of HA (Figures 4.8.e and 4.8.f). This observation might be attributed to the fact that at high loadings, the filler particles can generate a physical barrier or steric hindrance to the growth of crystal lamellae and consequently limit the crystallisation process [157].

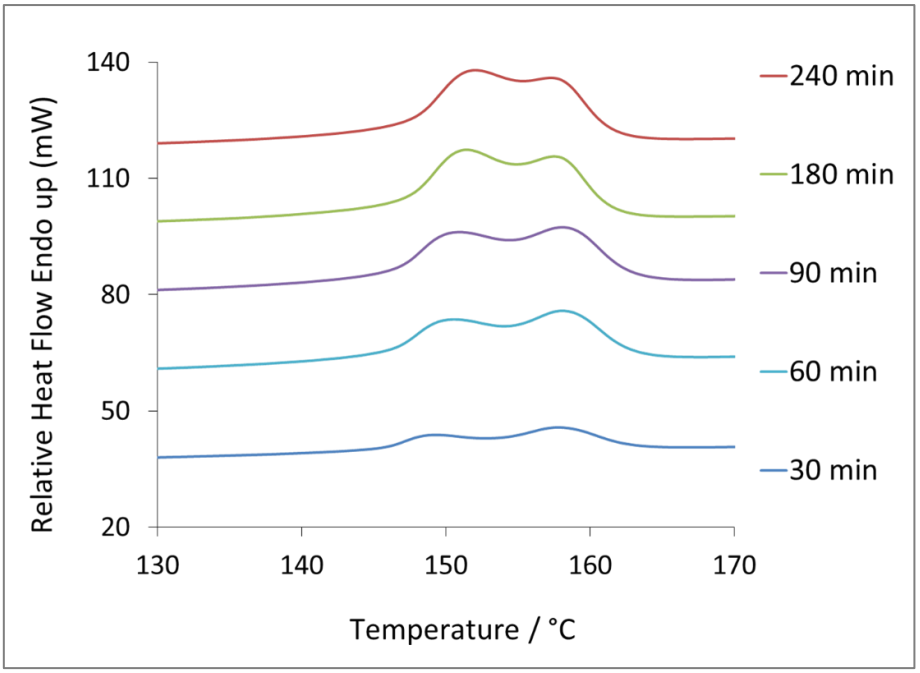


Figure 4.8.a Melting endotherms produced after Isothermal crystallisation process at 95 °C. PLA

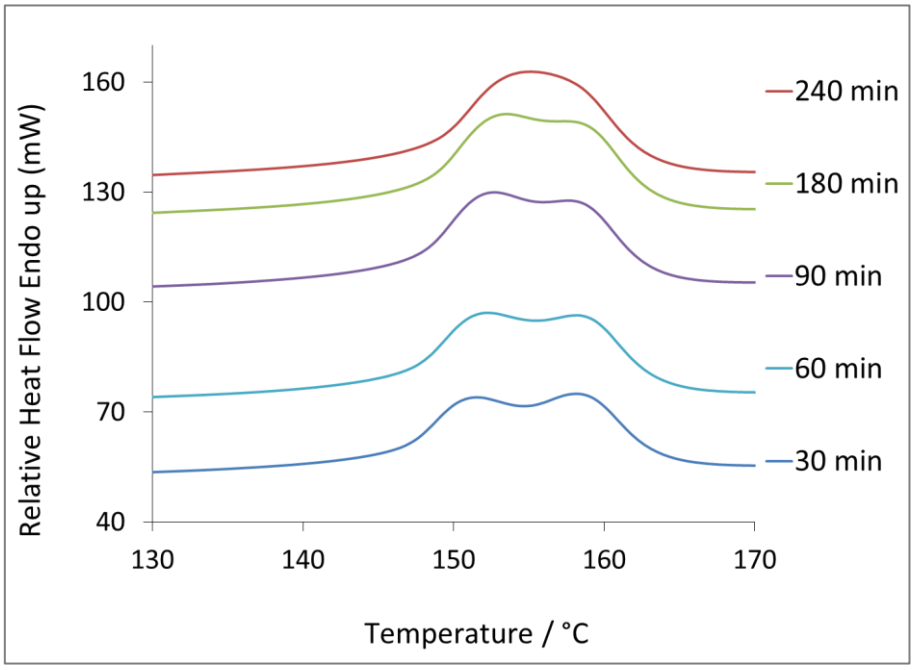


Figure 4.8.b Melting endotherms produced after Isothermal crystallisation process at 95 °C. PLA-HA (5 wt%)

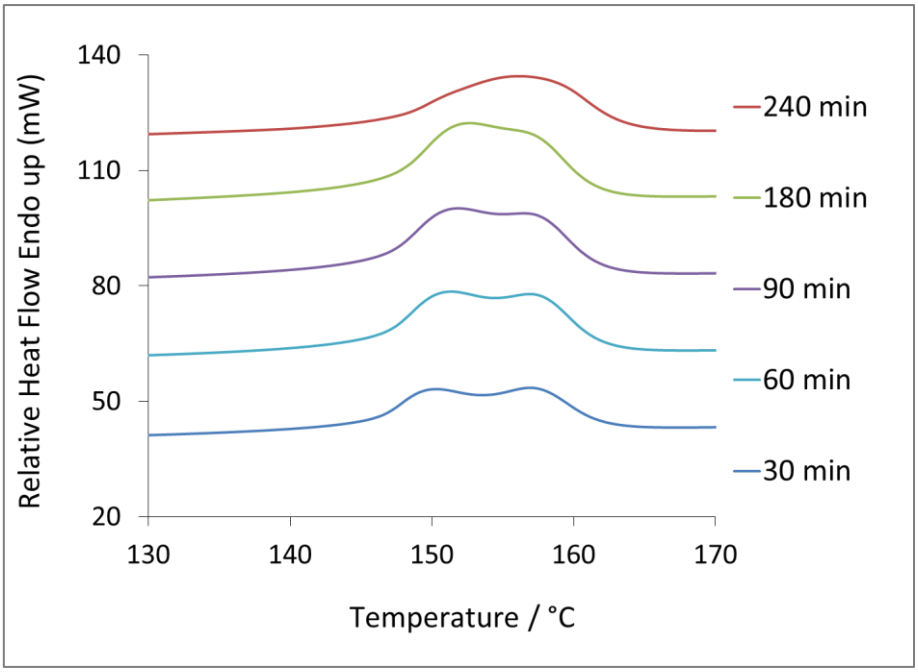


Figure 4.8.c Melting endotherms produced after Isothermal crystallisation process at 95 °C. PLA-HA (10 wt%)

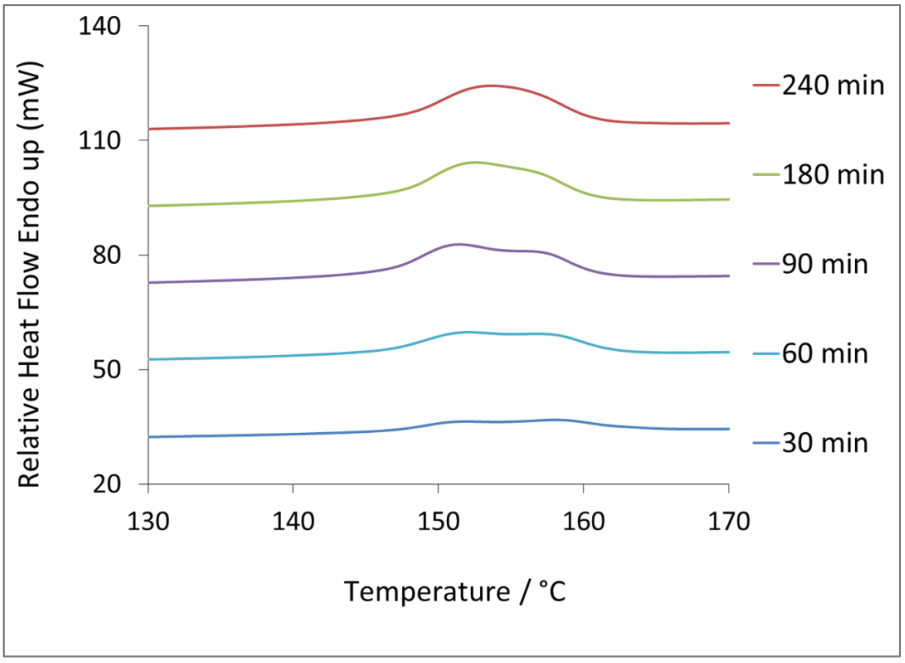


Figure 4.8.d Melting endotherms produced after Isothermal crystallisation process at 95 °C. PLA-HA (20 wt%)

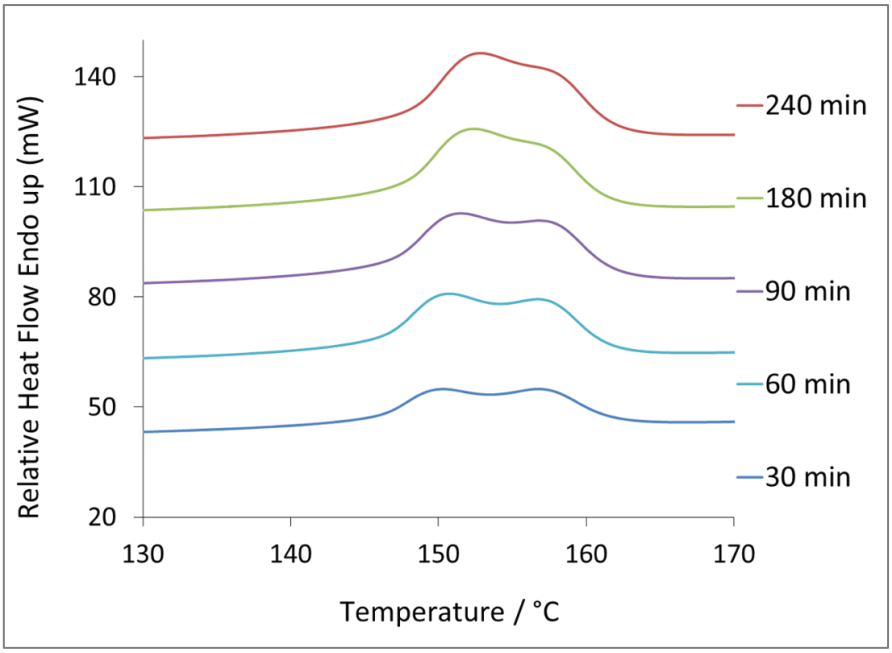


Figure 4.8.e Melting endotherms produced after Isothermal crystallisation process at 95 °C. PLA-HA (30 wt%)

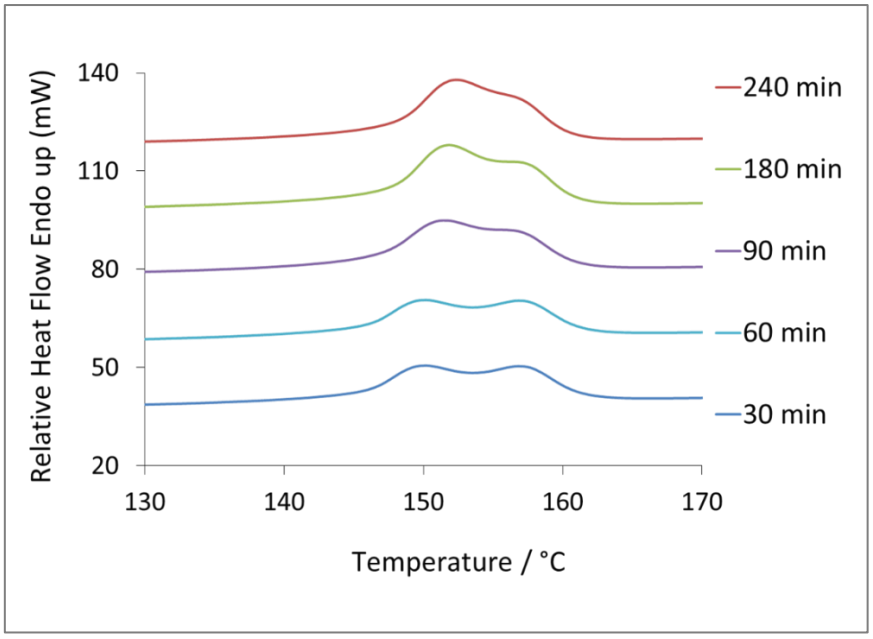


Figure 4.8.f Melting endotherms produced after Isothermal crystallisation process at 95 °C. PLA-HA (40 wt%)

Figures 4.9 and 4.10 illustrate the melting endotherms of subsequent heating processes, which were performed on the PLA and PLA-HA samples (10-40 wt% HA loading) after being held at 110 and 125 °C, respectively, for various periods.

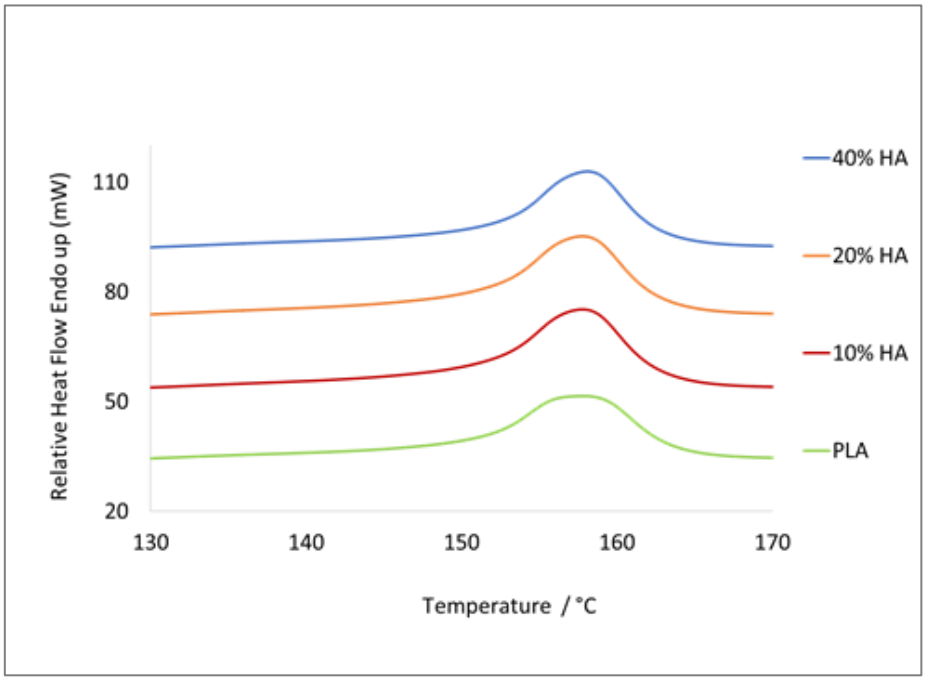


Figure 4.9 Melting endotherms produced after 60 minutes of Isothermal crystallisation process at 110 °C for PLA-HA samples with different HA loadings

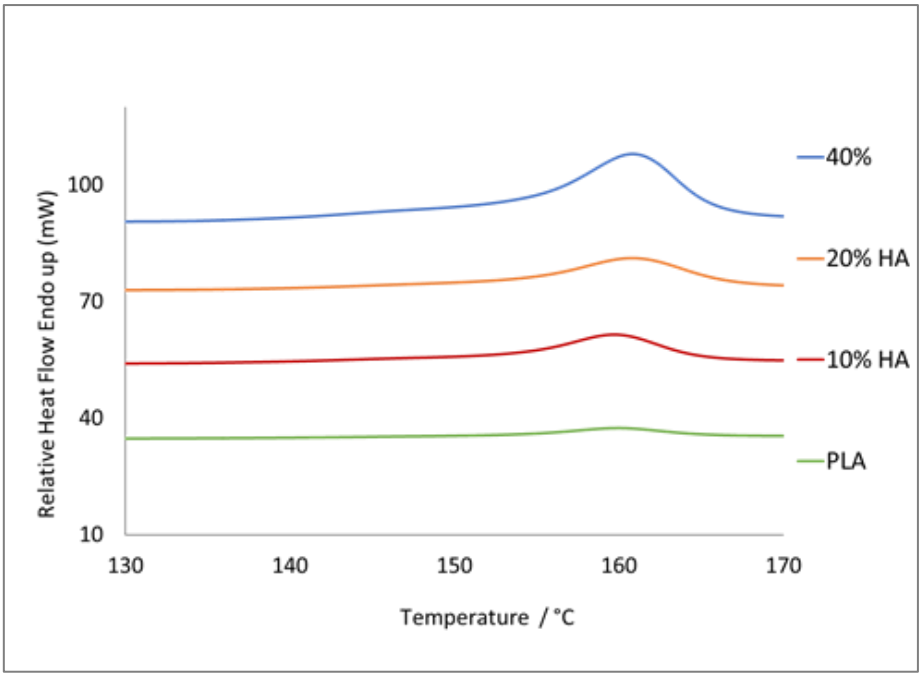


Figure 4.10.a Melting endotherms produced after 60 minutes of Isothermal crystallisation process at 125 °C for PLA-HA samples with different HA loadings

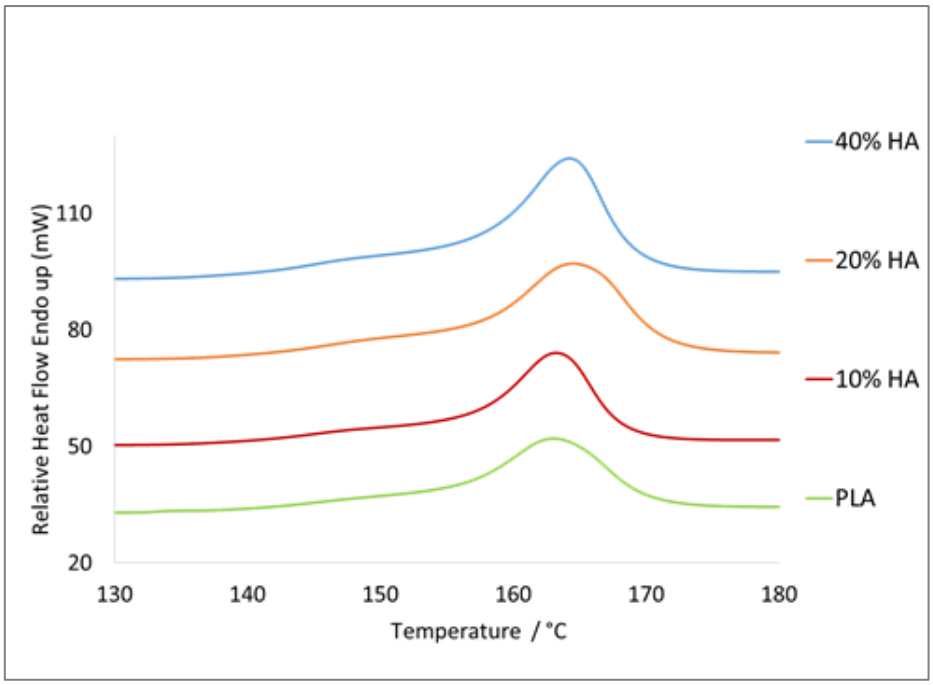


Figure 4.10.b Melting endotherms produced after 180 minutes of Isothermal crystallisation process at 125 °C for PLA-HA samples with different HA loadings

The degree of crystallinity of the samples treated under the DSC at 110 and 125 °C for various times was determined using Equation 3.1 in Chapter 3 and is shown in Table 4.2. As can be seen from this table, the degree of crystallinity (X_c) increased considerably by adding more HA through the structure of the composites for various periods at both temperatures. However, the gap between the degree of crystallinity of pure PLA and PLA-HA composites which were heat treated isothermally at 125 °C for 60 minutes was considerably more in comparison with the samples which were heat treated isothermally at 110°C and 125 °C for 60 and 180 minutes, respectively. This might be because in the latter cases, the degree of crystallinity of pure PLA was very high. According to previous reports, the effect of a filler as a nucleating agent on the degree of crystallinity in a polymer can be much less when the material is highly crystalline [157].

Table 4.2 Measurement of X_c of PLA-HA samples at 110 and 125 °C for various isothermal times ± standard deviation

HA (%)	110 °C for 60 min (%)	125 °C for 60 min (%)	125 °C for 180 min (%)
0	27 ± 0.9	2 ± 0.2	29 ± 0.9
10	35 ± 0.2	9 ± 0.8	44 ± 0.5
20	38 ± 0.6	12 ± 07	45 ± 0.5
40	50 ± 0.3	36 ± 0.5	51 ± 0.8

4.1.4 Isothermal crystallisation kinetics and Avrami analysis of hot pressed samples

The isothermal crystallisation process for PLA-HA composite samples was also performed using HSM equipped with a light dependent resistance (LDR). The procedure was repeated the same as for the pure PLA, which was described in Chapter 3 (Section 3.1.8).

Figure 4.11 illustrates the relative crystallinity (X_t) values of the samples with various HA loadings as a function of the crystallisation time at various isothermal holding temperatures from 95 to 125 °C. The general trend for the variation of crystallinity over isothermal crystallisation time for all samples was quite similar to each other. The crystallinity of all samples was firstly increased by increasing the temperature up to reaching its peak at 110 °C. Afterwards, there was a reduction in crystallinity by increasing the temperature up to 125 °C.

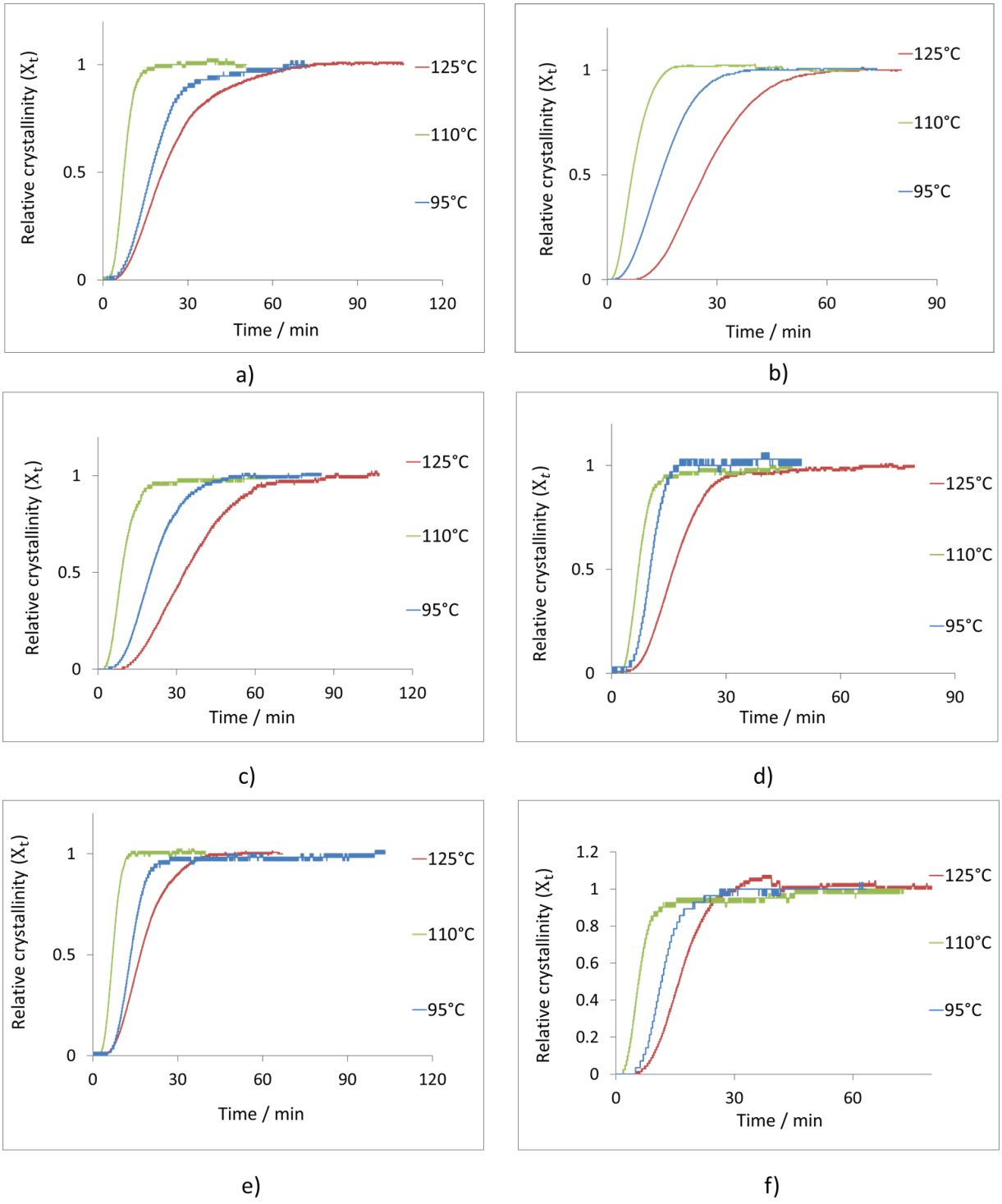


Figure 4.11 Relative crystallinity (Xt) against crystallisation time of samples with different HA wt% loadings, a) 0% b) 5% c) 10% d) 20% e) 30% f) 40% held at different isothermal temperatures

The halftime crystallisation values of all samples at different isothermal temperatures obtained from Figure 4.11 are compared and shown in Figure 4.12. As can be seen from this figure, the addition of HA particles in PLA can increase the crystallisation rate for all isothermal temperatures. However, the crystallisation rate did not vary too much by increasing HA content at 110 °C. This was because the rate of crystallisation was too fast at this temperature such that the light dependent resistance (LDR) procedure was not capable of detecting the differences in the crystallisation rate for different samples. Composite samples contain 5 and 10 wt% HA showed a negative effect on the crystallinity of the PLA matrix. This might be due to the composition variance of HA particles in the polymer matrix. According to this figure, there was no linear relationship between the crystallisation rate and the amount of HA in the sample. Nevertheless, the general trend showed that PLA-HA composites could reach 50% of relative crystallinity (X_t) in a shorter time in comparison with the pure PLA indicating that HA could act as a nucleating agent to facilitate the crystallisation process of PLA. Similar results were also reported by Liuyun et al., who found that HA acted as a nucleating agent in PLGA [158].

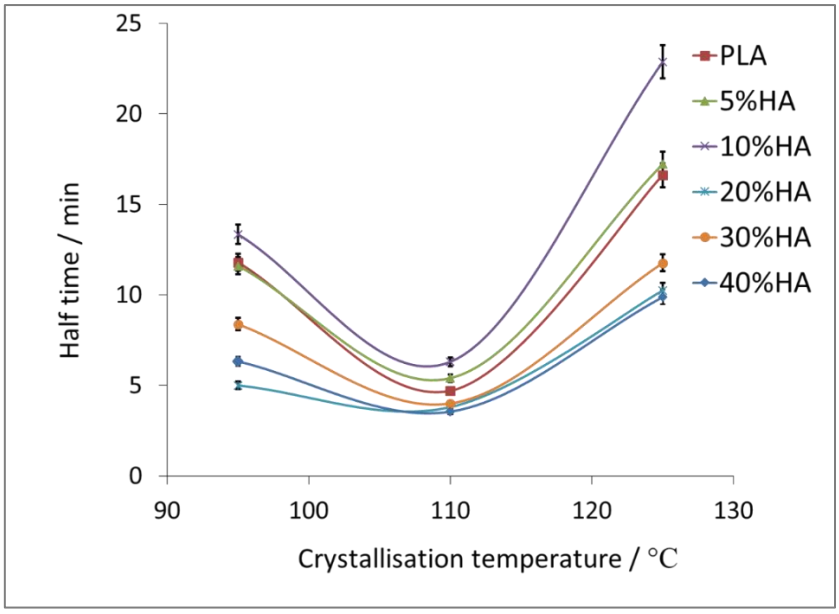


Figure 4.12 Half time crystallisation of hot pressed PLA-HA composites at different isothermal temperatures

The Avrami equation, which was described previously in Chapter 3, was applied for the analysis of the isothermal crystallisation kinetics of the PLA-HA composites. The Avrami graphs of all samples were obtained by plotting the $log[-ln(1-X_t)]$ against $logt$ and are shown in Figure 4.13. The rate constant Z and n values of the samples at different isothermal temperatures were determined by getting the linear regression of the Avrami graphs and are shown in Figure 4.14 and Table 4.3, respectively. The Z constant for the composites containing different amount of HA did not follow any trend. The n values obtained at 95 and 125 °C seem to increase by increasing the HA loading without any linear relationship. However, at 110 °C, the n values were almost similar for all samples comprising different percentages of HA. The halftime values obtained from the Avrami equation are illustrated in Figure 4.15. The general trend for the variation of the halftime crystallisation at different isothermal temperatures for all samples was very similar to the one observed in Figure 4.12. As previously mentioned in Chapter 3, the discrepancy between the halftime values obtained from the Avrami equation and the ones obtained from the crystallisation-time graph might be related to the limitations of the Avrami method.

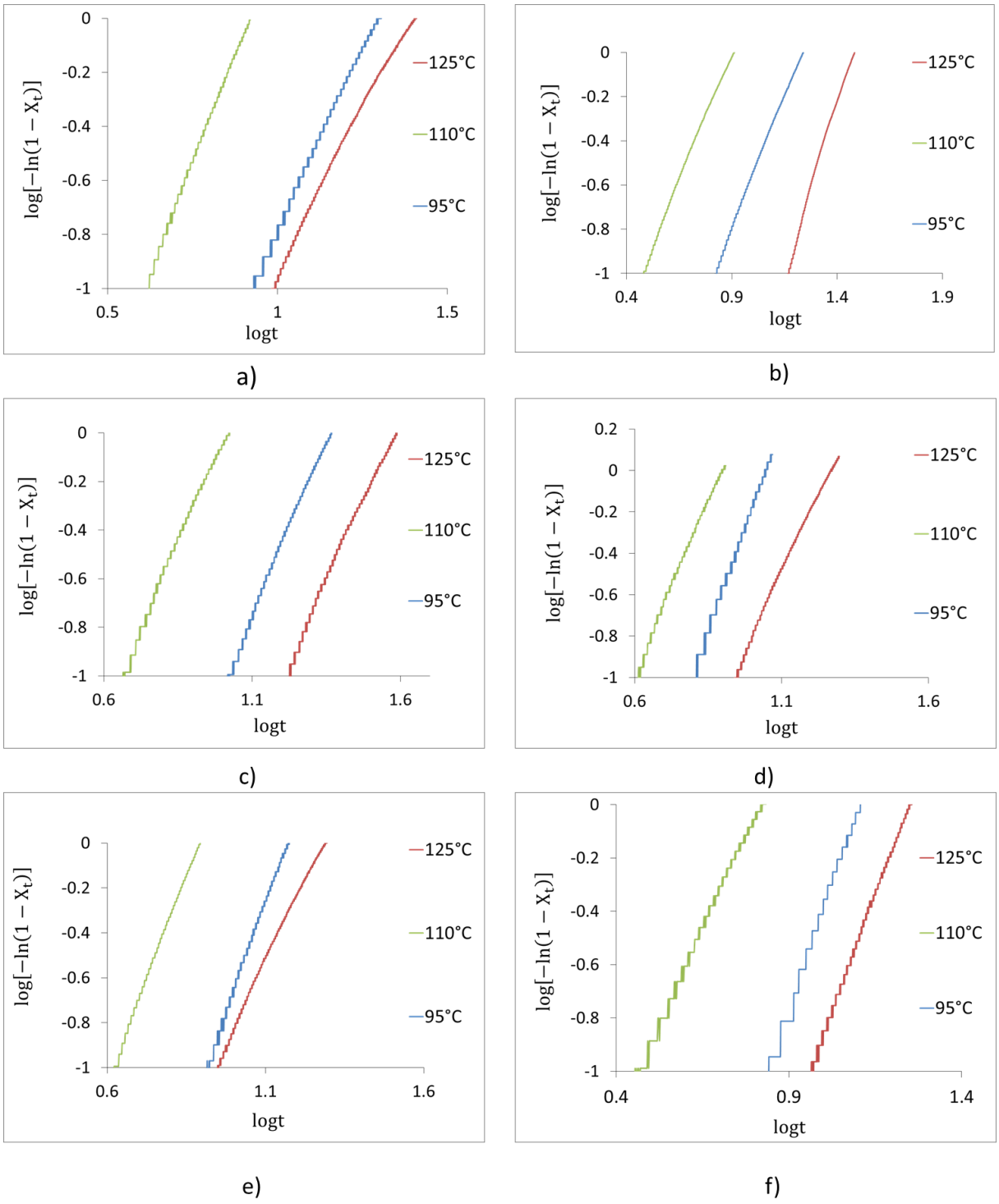


Figure 4.13 Avrami plots of the hot pressed PLA-HA composites with different HA wt% loadings, a) 0% b) 5% c) 10% d) 20% e) 30% f) 40% held at different isothermal temperatures

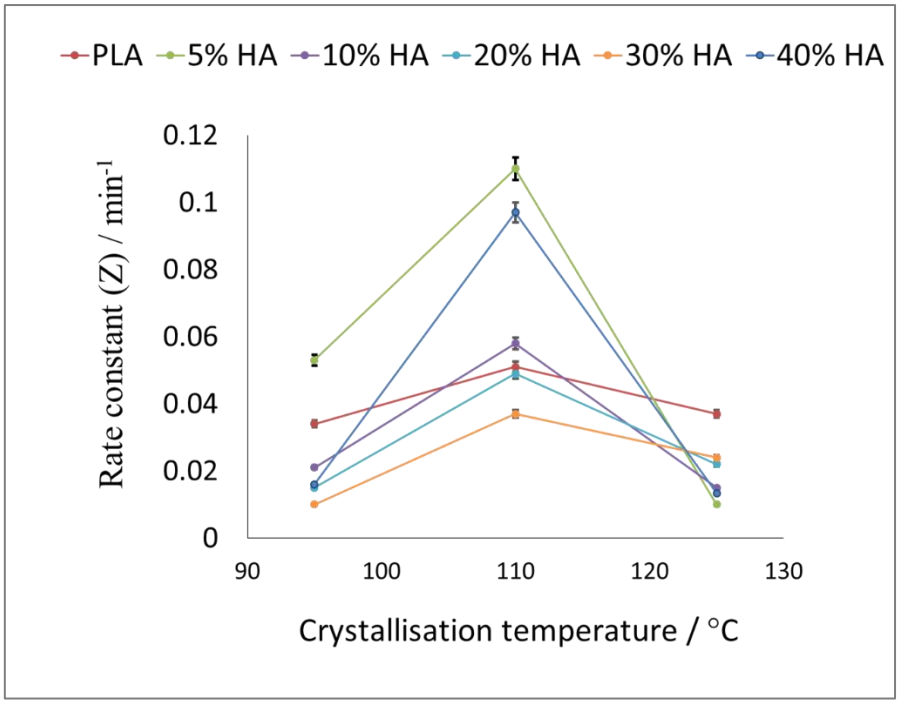


Figure 4.14 Crystallisation rate constant of hot pressed PLA-HA composites at different isothermal temperatures. The error bars are small (around 3%).

Table 4.3 The n values of hot pressed PLA-HA composites at different isothermal temperatures obtained from Avrami ± standard deviation

T (°C)	**HA %**					
	0%	**5%**	**10%**	**20%**	**30%**	**40%**
95	2.6 ± 0.07	2.4 ± 0.07	2.8 ± 0.08	4 ± 0.1	3.9 ± 0.1	3.7 ± 0.1
110	3.23 ± 0.09	2.5± 0.07	2.8 ± 0.08	3.4 ± 0.1	3.7 ± 0.1	2.9 ± 0.09
125	2.36 ± 0.07	3 ± 0.09	2.62 ± 0.07	3 ± 0.09	2.9 ± 0.08	3.4 ± 0.1

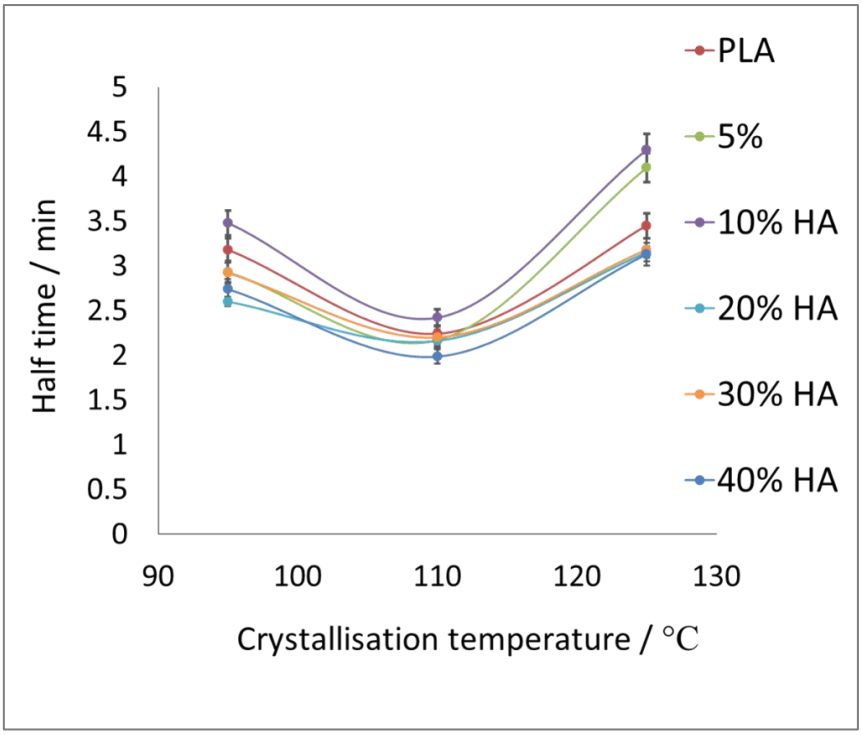


Figure 4.15 Half time crystallisation of hot pressed PLA-HA composites at different isothermal temperatures obtained from the Avrami equation. The error bars are small (around 4%).

4.1.5 Isothermal crystallisation kinetics of PLA-HA samples via HSM

In order to investigate the effect of the HA particles on the microstructure of the samples, the final morphology of PLA and PLA-HA samples after completing the isothermal crystallisation process at 95, 110 and 125 °C were recorded and shown in Figure 4.16. The isothermal crystallisation process was repeated the same as for pure PLA in Chapter 3 (Section 3.1.7). The general trend of the figure shows that in all samples by increasing the holding temperature, the size of the spherulites increased while their number decreased. This is associated with the relationship between the nucleation and growth rate, which was previously explained. At lower temperatures, the mobility of polymer chains was not high enough to grow into crystalline lamellae structures from the amorphous state. As the temperature went up, the nucleation sites decreased, resulting in a reduction in the number of spherulites. However, higher temperatures could offer better chain mobility leading to larger spherulites. It is also apparent from this figure that by increasing the HA loading in the polymer matrix, the size of spherulites became smaller

while their number increased. Furthermore, the crystallisation process completed earlier at all temperatures by adding the HA particles in the polymer matrix. For instance, by introducing 20 wt% HA into the PLA matrix, the time required for completing the crystallisation process at the isothermal temperature of 125 °C was reduced by more than 2 hours. According to these optical microscopy images, the addition of HA had a typical heterogeneous nucleating effect for the isothermal crystallisation of PLA matrix because of the randomly distributed nucleating sites.

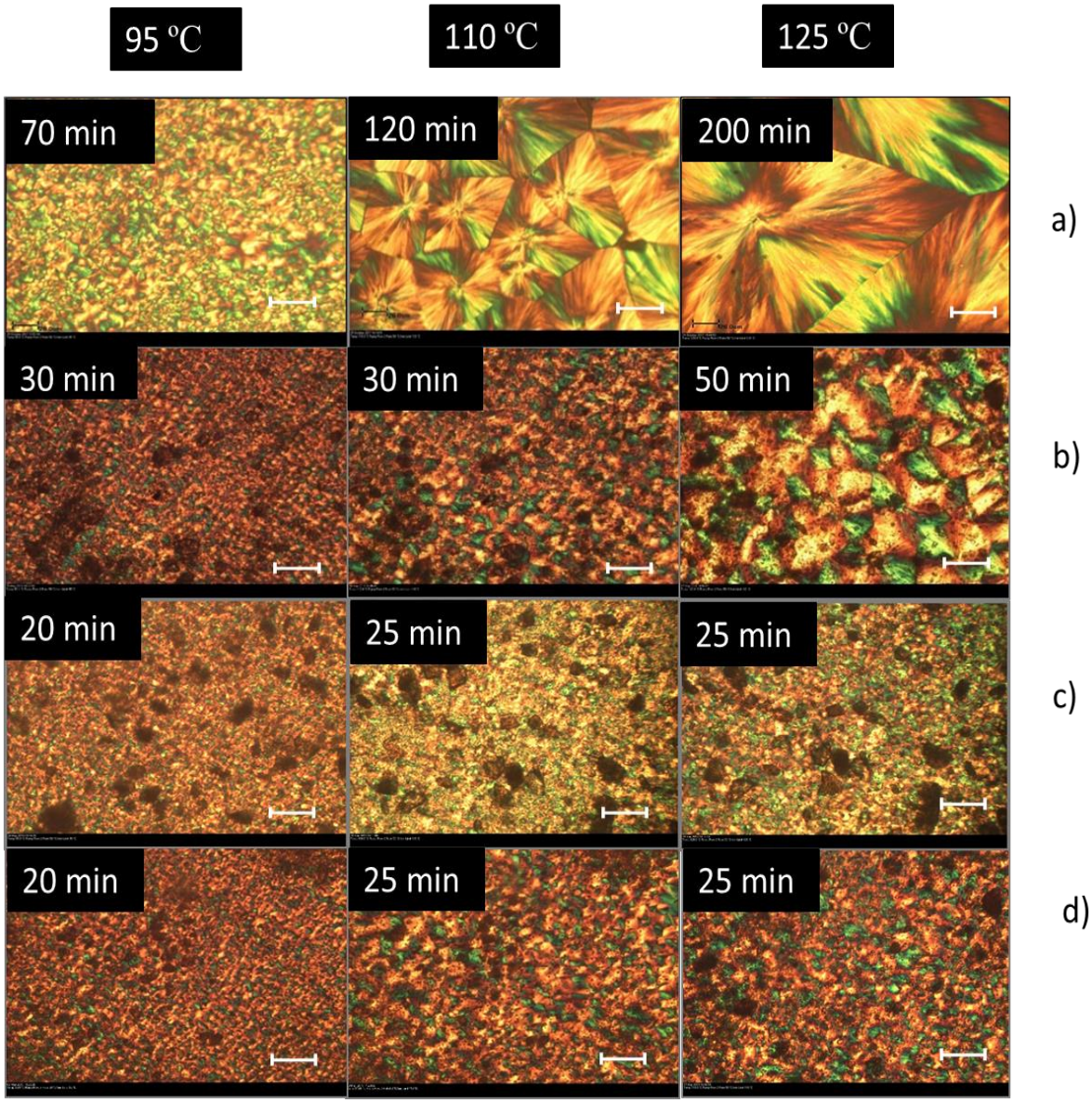


Figure 4.16 Final microstructure of hot pressed PLA-HA composites with different HA wt% loadings under HSM, a) 0 % HA, b) 10 % HA c) 20 % HA d) 40 % HA at 95, 110 and 125 °C from left to the right - The white scale bars represent 40 μm.

4.1.6 Thermogravimetric analysis (TGA) of hot pressed samples

PLA and PLA-HA hot pressed samples were analysed by TGA in order to confirm and determine the presence of HA within the PLA matrix and explore the effect of HA particles on thermal decomposition and stability of the PLA matrix. Figures 4.17 and 4.18 demonstrate the weight loss and derivative weight loss curves of the samples, respectively. TGA plots of the samples show that decomposition of the samples initiated at around 300 °C and was complete around 400 °C. According to the previous reports, HA did not undergo any thermal decomposition within this range of temperatures [159]. Therefore, it was expected that HA particles played a vital role in the enhancement of the thermal stability of the PLA. However, as it is apparent from both Figures 4.17 and 4.18, the decomposition of PLA was catalysed by additional loadings of HA particles. The weight loss values at different temperatures where 5% (T_5), 50% (T_{50}) and 80% (T_{80}) of the initial weight were lost were obtained from the TGA plots and shown in Table 4.4. According to this table, the thermal stability of PLA decreased (around 40 °C) with increasing HA loading in the initial stages of thermal degradation (T_5). At later stages of decomposition, the decrease in thermal stability was not significant compared with that of pure PLA. The slight increase in T_{80} and T_p (the peak temperature obtained from the first derivative-Figure 4.18) at 40 wt% HA compared to 20 wt% HA might be due to the restriction of the PLA molecular mobility as a result of high loading concentration of the filler. Previous studies have shown that low loadings of HA had the potential to enhance the thermal stability of thermoplastic polymers such as poly(methyl methacrylate) and polyamide [160], although this study verified that the thermal stability of the polymers could be also decreased by addition of HA particles. Having said that, the effect of calcium phosphates, including β-TCP and HA fillers on decreasing the thermal stability of the PLA was also reported by other authors [125, 159–163]. This could be attributed to the high hydrophilicity of HA and its tendency to absorb moisture. On the other hand, PLA is a type of polyester polymer, which is

very sensitive to hydrolysis. Consequently, the hydrolytic scission of PLA could result in promoting a plasticization process and formation of lactic acid as well as oligomers which possess less thermal stability at high temperatures in comparison with the long PLA molecular chains [163]. According to previous reports, HA particles could enhance the thermal stability of PLA when they are at very low concentration (less than 5 wt % HA) within the matrix [159, 160]. However, higher loadings of the filler could shift the onset of degradation to the lower temperatures. The residual percentage weight of the composites did not correspond to the actual weight of HA in each sample (see Table 4.4). This might be due to the HA variations in the composite. Overall, these results indicate that high concentration of HA loadings could accelerate the decomposition of PLA at the initial stage; however, the reduction of the thermal stability of the polymer at later stages of the decomposition process was insignificant. Furthermore, in general, the thermal degradation of the hot pressed composites was almost invariable, and decomposition had occurred at approximately the same temperature.

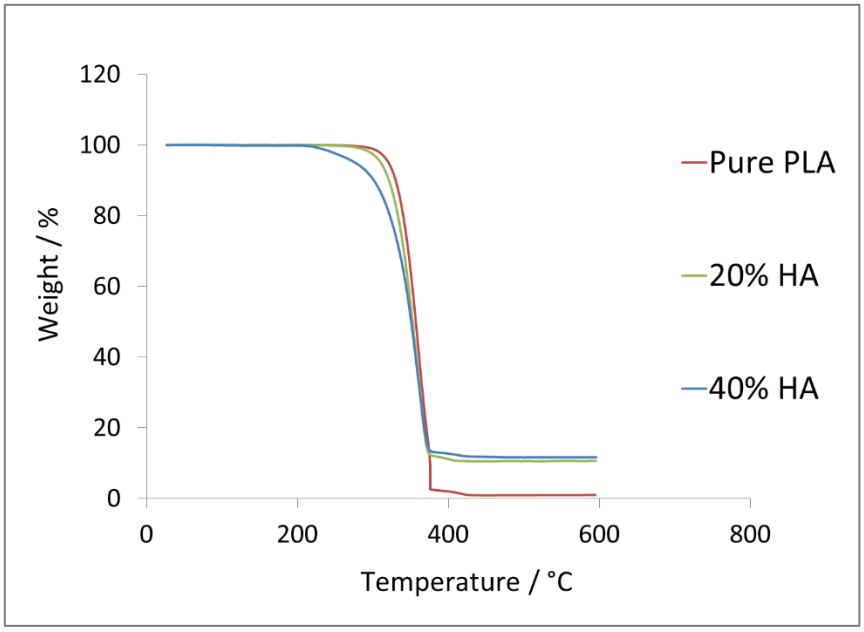


Figure 4.17 TGA of hot pressed PLA-HA composites, Mass loss (%) versus temperature

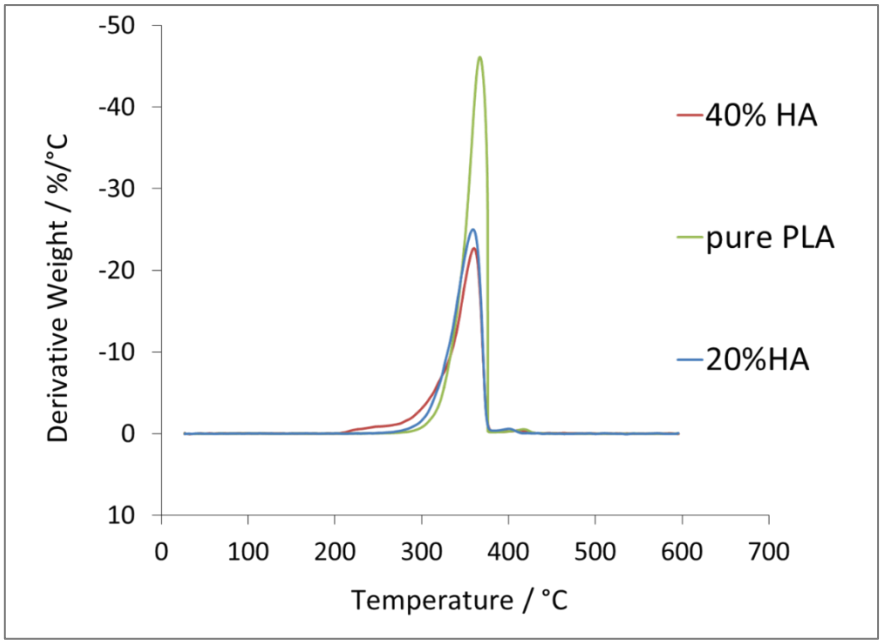


Figure 4.18 First derivative mass loss (%/°C) versus temperature for hot pressed PLA-HA composites

Table 4.4 Characteristic temperatures of the thermal decomposition of hot pressed PLA-HA Composites ± standard deviation, T_x = temperature at which x % of the initial mass is lost.

Sample	T_5/°C	T_{50}/°C	T_{80}/°C	T_p/°C	Residual weight percentage
Pure PLA	320 ± 0.5	356 ± 0.9	370 ± 0.5	366 ± 0.5	1 ± 0.3
20% HA	310 ± 0.3	352 ± 0.5	367 ± 0.5	360 ± 0.1	10± 0.5
40 % HA	279 ± 0.5	350 ± 0.6	368 ± 0.1	364 ± 0.1	12 ± 0.4

4.1.7 SEM of injection moulded samples

In order to investigate the effect of HA particles on the mechanical properties of PLA matrix, samples of HA-PLA with 0-35 wt% HA were prepared via injection moulding. Figure 4.19 illustrates the SEM morphology of the fracture surfaces of the injection moulded samples containing different loadings of HA. The results showed that HA particles were homogeneously dispersed within the matrix at lower concentration loadings of HA (5 and 12 wt%) without containing any lumps. However, at higher loadings (20 and 35 wt% HA) large HA particles were observed clearly. Additionally, there were several gaps and voids within the matrix. Agglomeration of HA at high loadings could be associated with the orientation

phenomenon, which usually occurred during the injection moulding process of polymers [164–166]. During the injection process, the viscous polymer matrix was forced through the mould or die under high pressure and temperature, resulting in some molecular orientation of the samples. Consequently, this orientation could cause non-uniform distribution of the filler within the polymer matrix. In addition, from Figure 4.19, it was observed that some HA particles were located on the surface of the polymer composite. This might be advantageous as the HA particles are bioactive and would be exposed to cells and tissues in the body forming a chemical bond. Furthermore, agglomeration of HA particles on the surface can increase the roughness of the composite's surface. According to previous reports, by increasing the surface roughness cell adhesion could be improved [159]. This is because the rough substrates possess more topographical features with more surface area, which is beneficial for the interactions within cells and proteins.

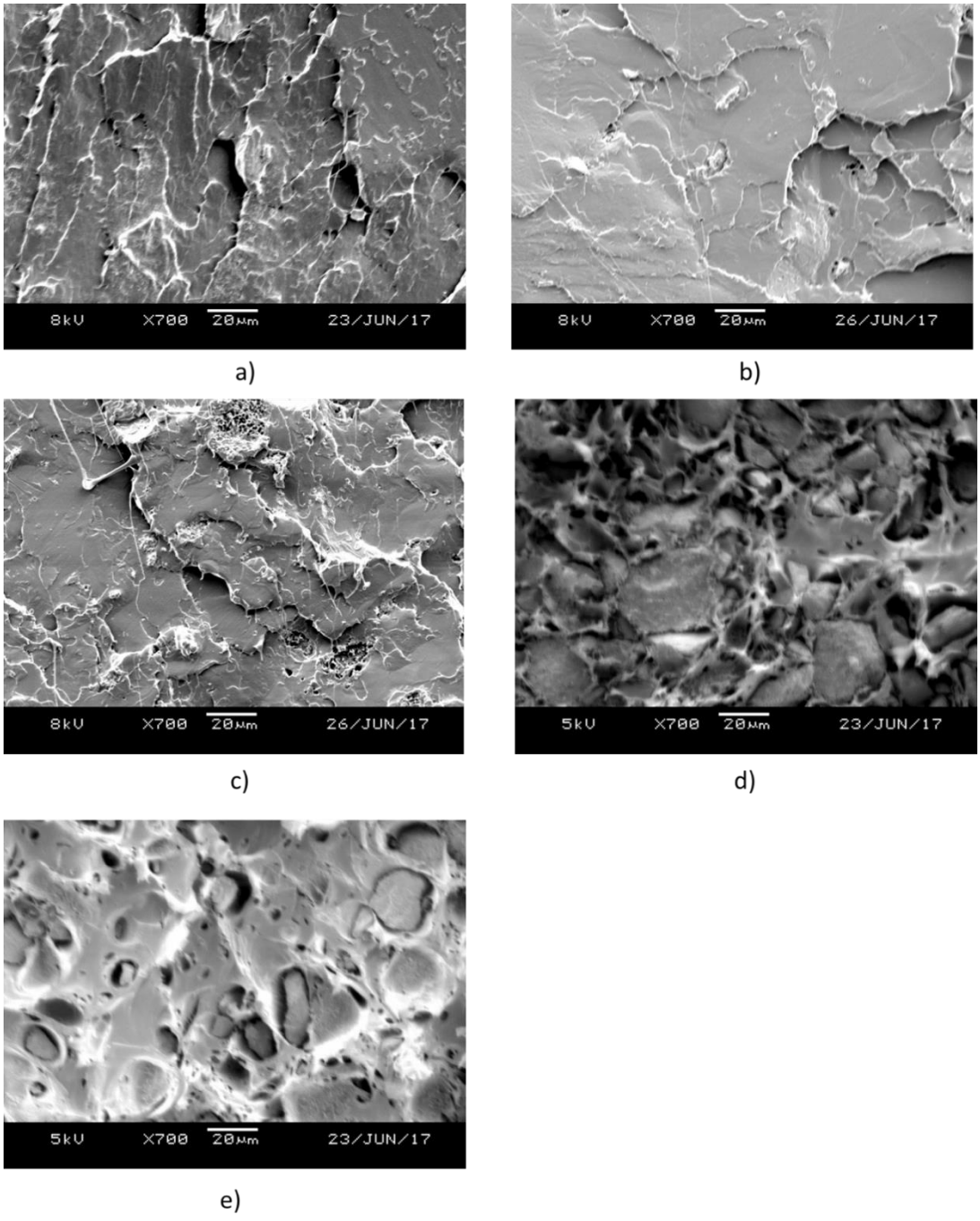


Figure 4.19 SEM micrographs of fracture surfaces of the injection moulded PLA-HA composites with different HA wt% loadings a) 0 % HA, b) 5 % HA c) 12 % HA d) 20 % HA and e) 35 % HA

4.1.8 DSC analysis of injection moulded samples

A nonisothermal DSC process (the same as hot pressed samples) was performed on all injection moulded samples to explore the effect of HA loading and injection moulding process on the crystallisation and thermal behaviour of samples. The subsequent heating process (after one heating and cooling) of all injection moulded samples is shown in Figure 4.20. The DSC traces of the injection moulded samples were quite similar to the hot pressed samples. Crystallisation and melting were observed during the subsequent heating scans of all specimens, including pure PLA. This was previously attributed to the crystallisation process that occurred during the heating procedure due to the low heating rate [156]. The value of T_g for all samples was quite similar and the HA content of the samples did not influence it (see Figure 4.21). Overall, there was no significant difference between the nonisothermal DSC results of injection moulded samples and the ones observed for hot pressed samples.

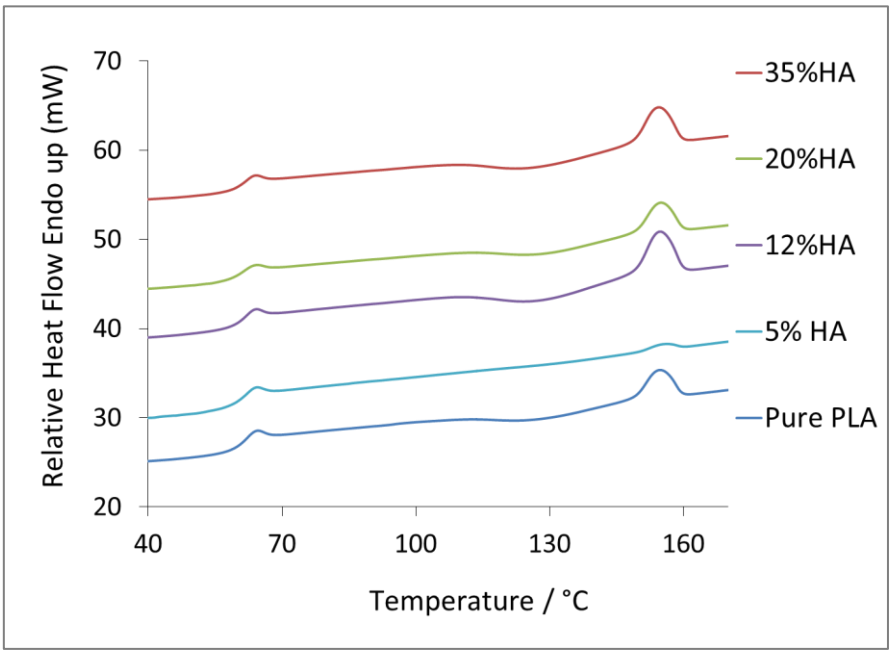


Figure 4.20 Second heating DSC scan of injection moulded HA-PLA composites with different HA loadings

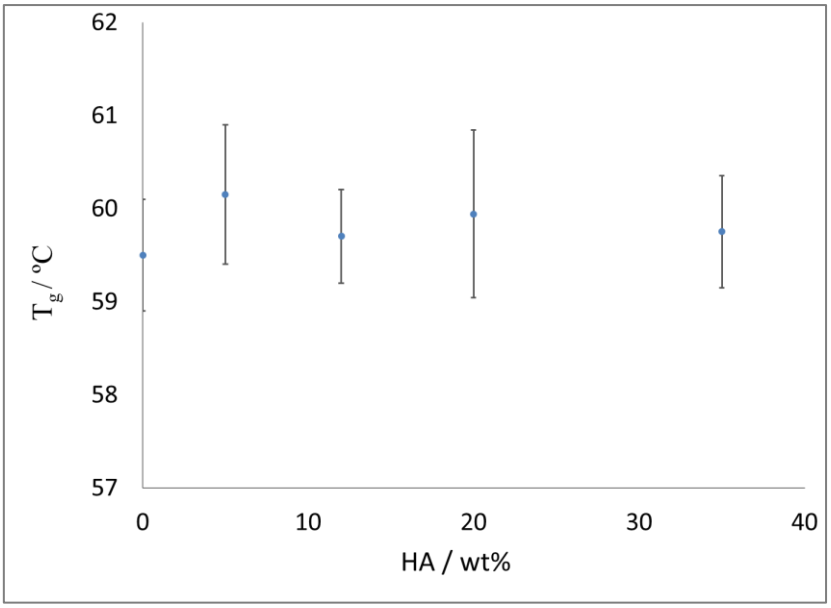


Figure 4.21 The effect of HA content on the Tg of injection moulded PLA-HA composites

4.1.9 Mechanical properties of injection moulded samples

In order to explore the effect of HA on the mechanical properties of PLA-HA composite samples, both tensile and flexural strength tests were performed for all injection moulded samples. Figures 4.22-4.24 demonstrate the effect of the amount of HA in the sample on the ultimate tensile strength (UTS), elongation at break and tensile modulus (Young's Modulus), respectively. The range of values obtained for the UTS and elongation at break for the pure PLA were in accordance with previous reports [125, 129, 163]. There was a decrease in both UTS and elongation at break as the amount of HA increased. The reduction in UTS by the incorporation of more inorganic fillers through the structure of the thermoplastic polymer is typical and was previously reported by other authors [125, 129, 132, 163, 167]. This might be due to a decrease of the cross-sectional area of the load-bearing polymer by adding more fillers into the matrix [129]. Furthermore, according to the literature, the mechanical strength of a PLA-HA composite made from non-modified HA particles can be reduced because of the weak interface between the PLA matrix and HA particles [120].

The reduction of elongation at break with higher loadings of HA was expected as in all polymer composites elongation mostly arises from the polymer rather than the inorganic filler, which is more rigid. Higher loadings decreased the amount of polymer required for the elongation and eventually reduced the final value for elongation at break [129]. As expected there was a proportional increase in the tensile modulus (stiffness) of the matrix by increasing HA loadings (Figure 4.24) indicating that by adding more fillers more rigid materials were obtained.

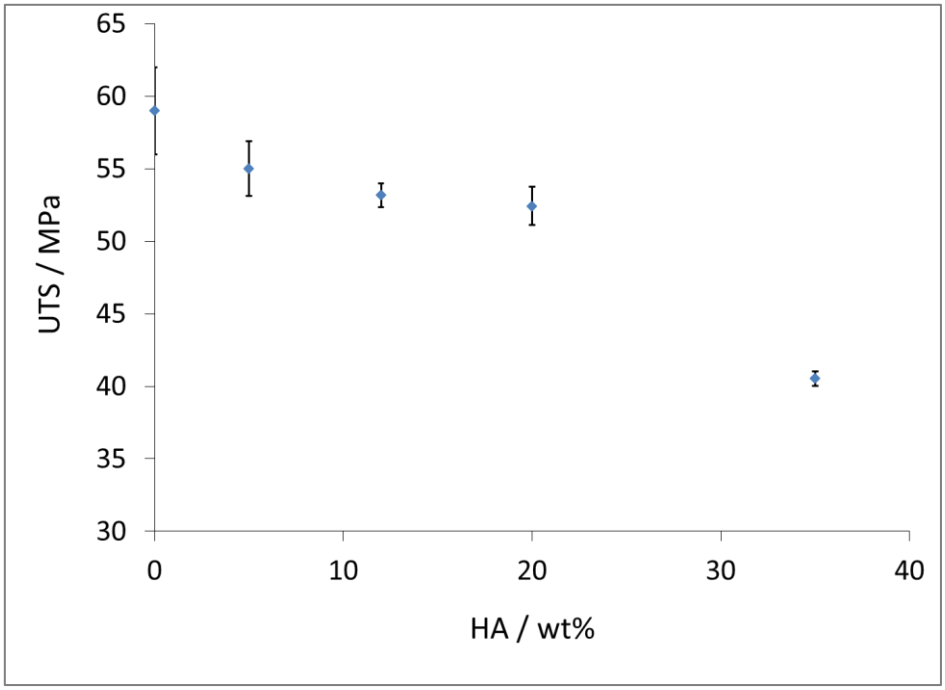


Figure 4.22 Evolution of the tensile strength as a function of HA wt%

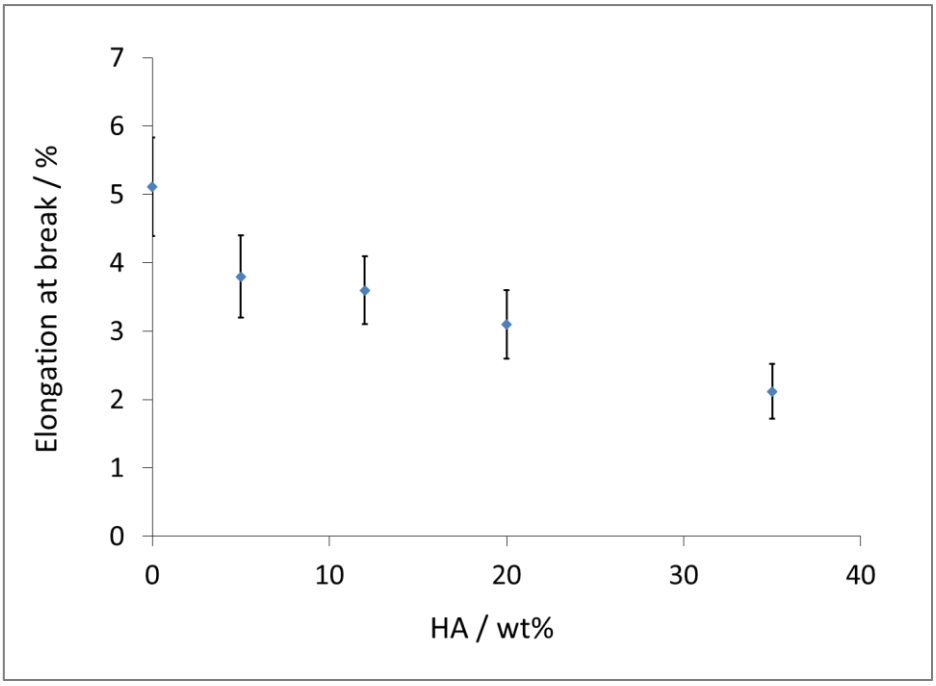


Figure 4.23 Evolution of the elongation at break as a function of HA wt%

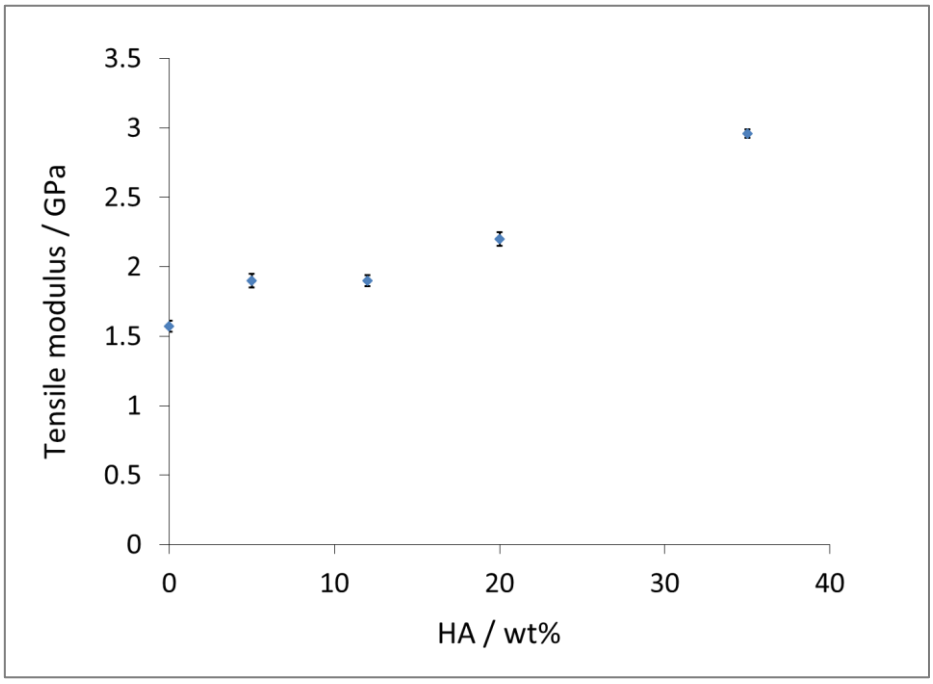


Figure 4.24 Evolution of tensile modulus as a function of the HA wt%. The error bars are very small (± 0.03-0.05) and are not recognisable in the figure.

Similar trends were observed for the flexural behaviour of composite samples. As the HA loading increased, the flexural modulus increased due to the higher stiffness of the material (Figure 4.25). The flexural modulus increased considerably from 3.7 GPa for the pure PLA up to around 5 GPa for the composites containing 35 wt% HA. The range of values for the flexural modulus was in accordance with values obtained for PLA composites in the literature [162, 163]. In contrast, the flexural strength of PLA decreased around 10 MPa by increasing the HA loading to 35 wt% HA (Figure 4.26).

Generally, the results for both flexural and tensile tests followed a similar trend. PLA-HA composites containing 10-20 wt% of HA are considered as the most appropriate choice in terms of maintaining a good balance between all mechanical properties as they offer a high stiffness with slightly lower deformation ability in comparison with pure PLA.

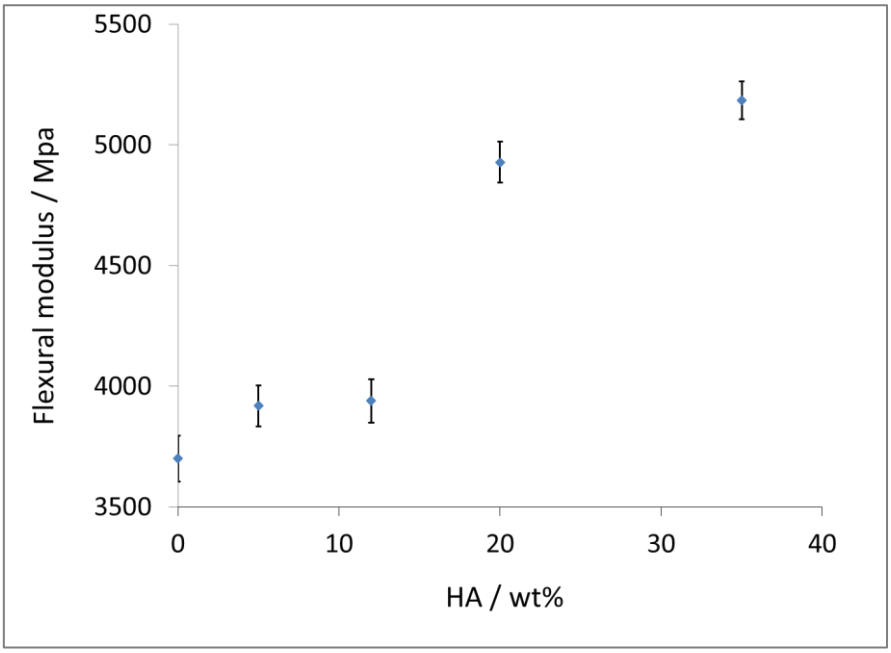


Figure 4.25 Evolution of flexural modulus as a function of the HA wt%

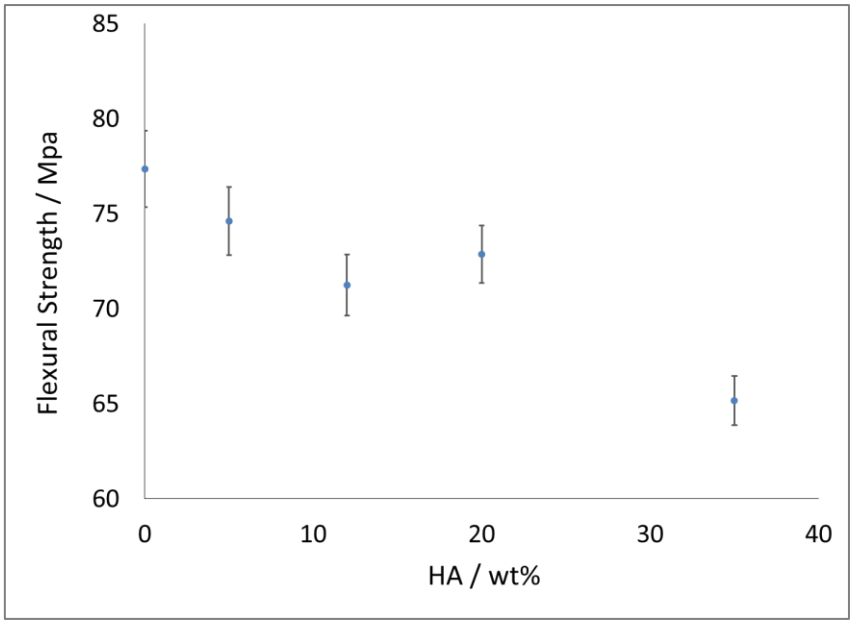


Figure 4.26 Evolution of flexural strength as a function of the HA wt%

4.1.10 Dynamic mechanical thermal analysis (DMTA) of injection moulded samples

PLA and PLA-HA injection moulded samples were analysed by DMTA in the range of temperatures from RT to 130 °C, in order to explore the viscoelastic behaviour and glass transition temperature changes of PLA and its composites. Figure 4.27 illustrates the values of storage modulus (E') as a function of temperature for different HA loadings. As can be seen from this figure, a peak appeared on the curves for all samples except for 12 wt% HA as the samples reached to their T_g. This observation was unexpected. This might be associated with the orientation that occurred during the injection moulding process. During the heat treatment (during DMTA testing) as the samples reached to near their T_g, the oriented molecular chains obtained from the injection moulding process should be relaxed. However, the samples were clamped in a dual cantilever during the DMTA experiment which may have inhibited the process of chain relaxation and therefore higher heat flux was required to overcome the situation leading to the relaxation of highly oriented polymer chains. This higher force which could be considered as an apparent stiffness appeared as a peak on the curves for all samples around their T_g. However, this phenomenon (the peak on the T_g due to the orientation) was not

observed previously in similar experiments (DMTA of injection moulded samples of PLA-HA composites) [125].

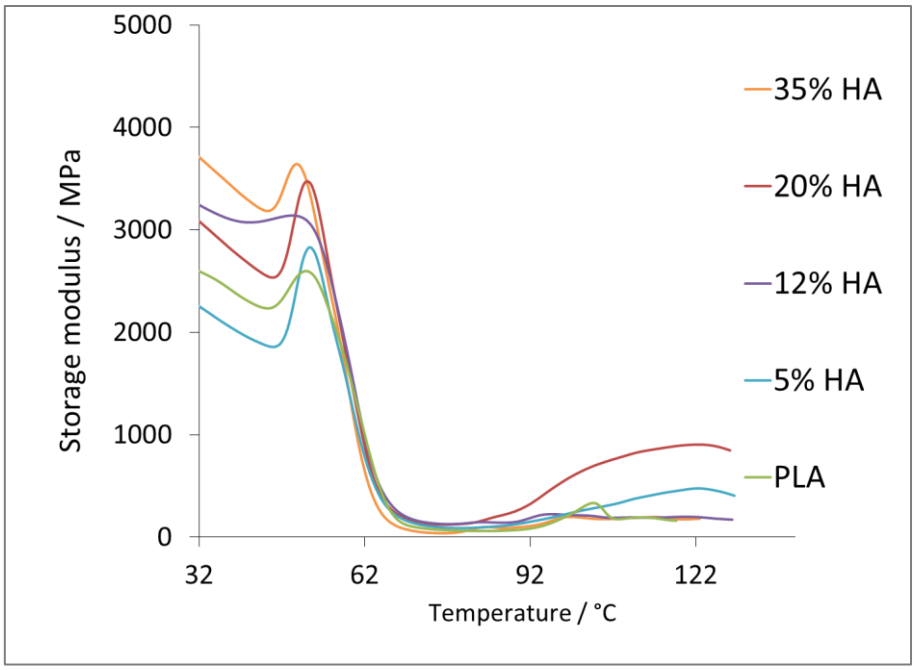


Figure 4.27 Storage modulus vs. temperature for PLA and PLA-HA injection moulded samples

Figure 4.28 shows the trend of E' (storage modulus) as a function of temperature for 20 wt% HA before and after the heat treatment at 70 °C in an oven for 1 hour. As it is apparent from this figure, the peak on the T_g disappeared after the heat treatment of the sample. This is because the sample above the T_g was a liquid during equilibrium and all the polymer chain orientation disappeared. Therefore, the peak on the T_g could be considered as an artifact from the injection moulding process, which could be removed by annealing the samples above their T_g and below their crystallisation temperature. A new increase in E' was detected at temperatures around 90-120 °C in both Figures 4.27 and 4.28 which could be attributed to the crystallisation process due to the low heating rate (1 ºC min^{-1}) applied during the experiment. Therefore, higher crystallinity led to a higher stiffness of the sample. The increase in crystallinity started slightly earlier (around 80 °C) for 20 wt% HA sample which was heat treated at 70 °C compared to the one which was not heat treated (Figure 4.28). This could be due to the preheating process at 70

°C. The E' started to decrease again after an increase due to the crystallinity in both Figures 4.27 and 4.28. This could be due to the melting out of a proportion of the material and producing some mobile chains.

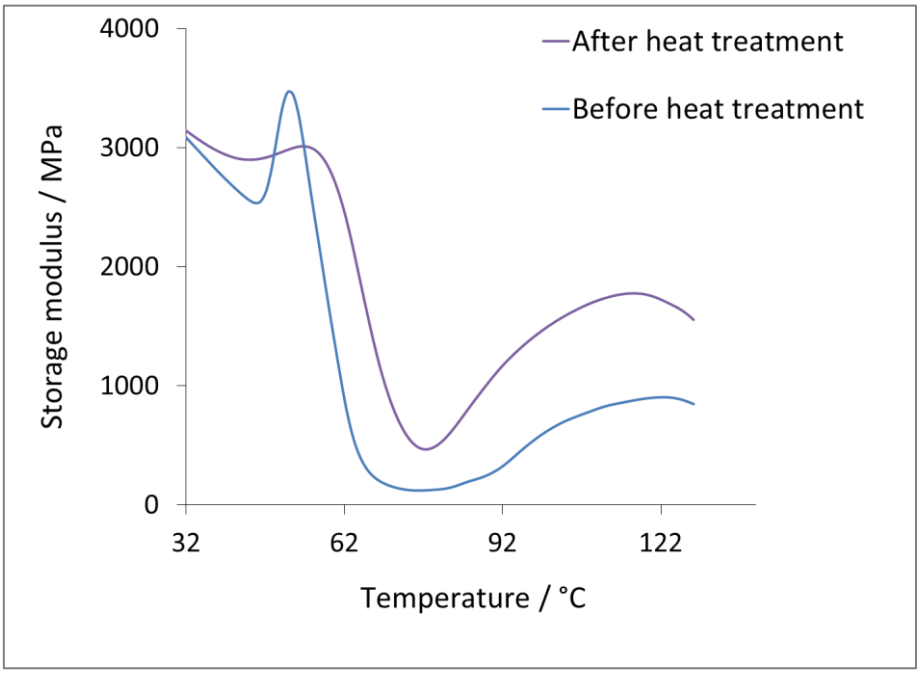


Figure 4.28 Comparing the storage modulus of 20 wt% HA before and after heat treatment at 70 ºC

The effect of HA loading on the storage modulus for the samples is shown in Figure 4.29. The general trend of this figure shows that the E' values for the samples became greater as the HA loading increased, indicating that the material became more rigid by adding more HA. This is in accordance with previous results in this study regarding tensile and flexural mechanical properties of the injection moulded samples where it was shown that by increasing the HA loading, the material became stiffer. A similar range of values for E' of PLA and PLA-HA samples were reported by Liu et al. [125].

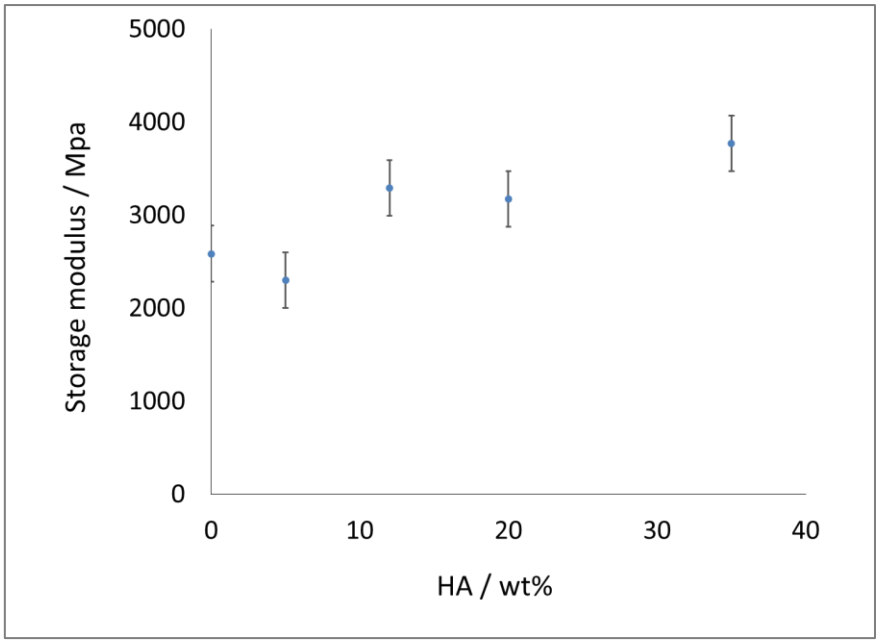


Figure 4.29 The effect of HA wt % loading on the storage modulus for injection moulded samples

By plotting tan δ versus temperature (Figure 4.30), the glass transition temperature (T_g) was obtained. Tan δ generally remained constant up to the onset of T_g. The main peak observed at around 65-70 ºC was considered as the range for the glass transition temperature (T_g) of the sample. The second peaks observed for some of the samples could be due to the mobilisation of another less mobile region of the amorphous phase. The T_g values were obtained from the main peaks of the curves of figure 4.30 and compared with each other (Figure 4.31). The range of values of T_g for samples with different HA wt% loading is quite similar and the HA did not seem to influence it.

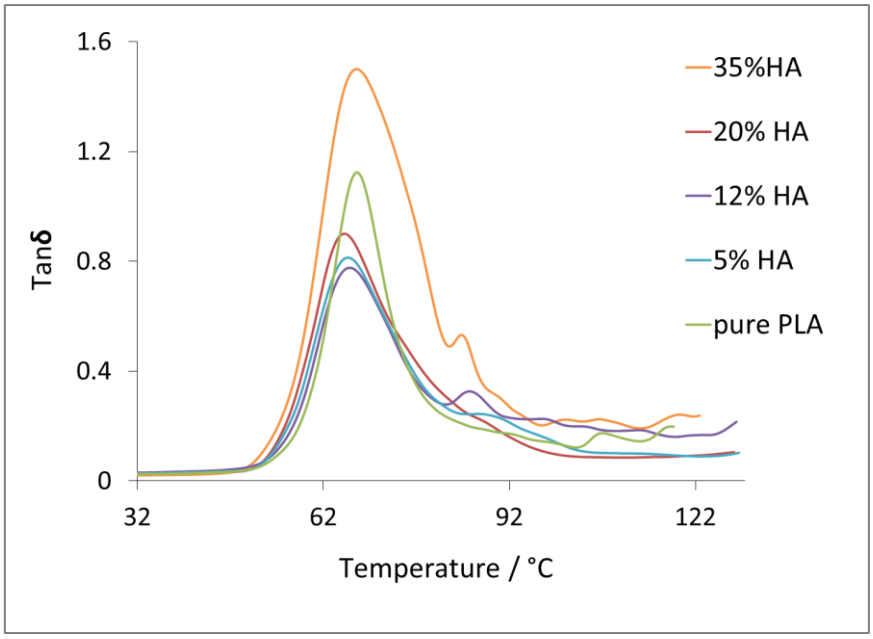


Figure 4.30 Tan Delta vs. temperature for PLA and PLA-HA injection moulded samples

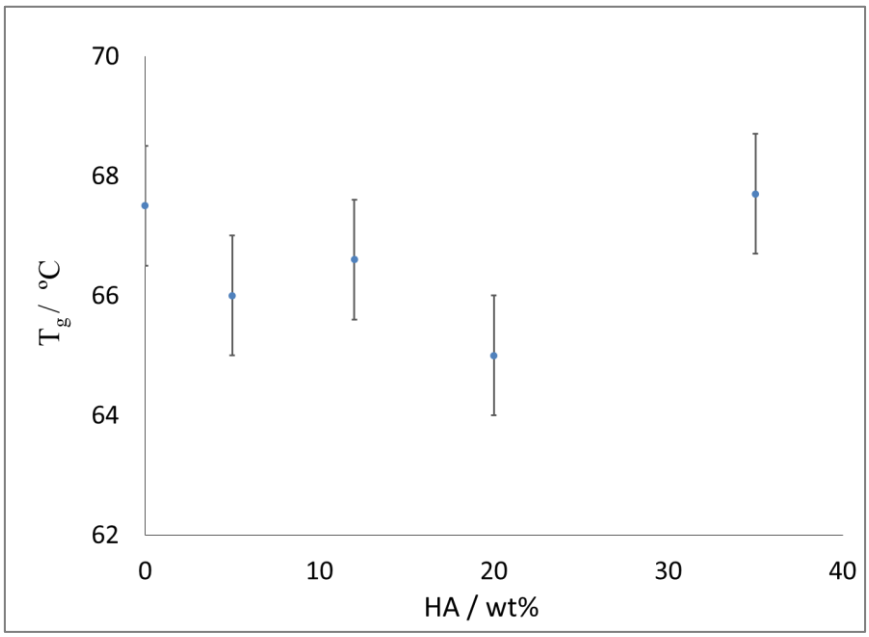


Figure 4.31 The effect of HA content on the T_g of injection moulded PLA-HA composites obtained from DMTA

4.1.11 TGA analysis of injection moulded samples

PLA and PLA-HA injection moulded samples were analysed by TGA (the same procedure as hot pressed samples in Section 4.1.6) in order to confirm and determine the presence of HA within the PLA matrix and explore the effect of HA particles on the thermal stability of the polymer. The results of weight loss and derivative weight loss for injection moulded samples were quite similar to the ones observed for the hot pressed samples (see Figures 4.32 and 4.33). According to Figure 4.32, decomposition of all samples occurred between around 300 and 400 °C. It is quite apparent from this figure that the decomposition of PLA was accelerated by additional HA loadings. The general trend of the data presented in Table 4.5 indicates that the thermal stability of the PLA was decreased by increasing the amount of HA within the samples due to the hydrolysis, which was mentioned earlier (Section 4.1.6). However, there are some exceptions to this trend. For example, at T_{50} the decomposition was delayed by adding more HA in the composite, which was previously attributed to the aggregation of HA powders within the matrix and restriction of the PLA molecular mobility. The residual percentage of the composites were approximately equal to the weight percentage of the filler within the sample (Table 4.5). For example, composites that contained 20 wt% HA had a residual percentage weight of 24%, which corresponded to the weight of HA particles and the residual PLA in the sample.

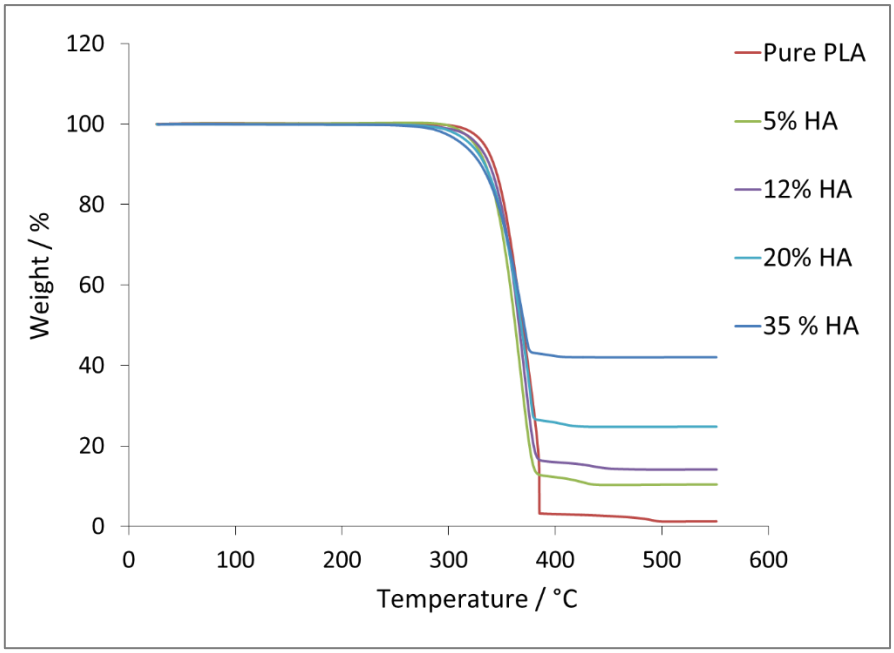


Figure 4.32 TGA of injection moulded PLA/HA composites, Mass loss (%) versus temperature

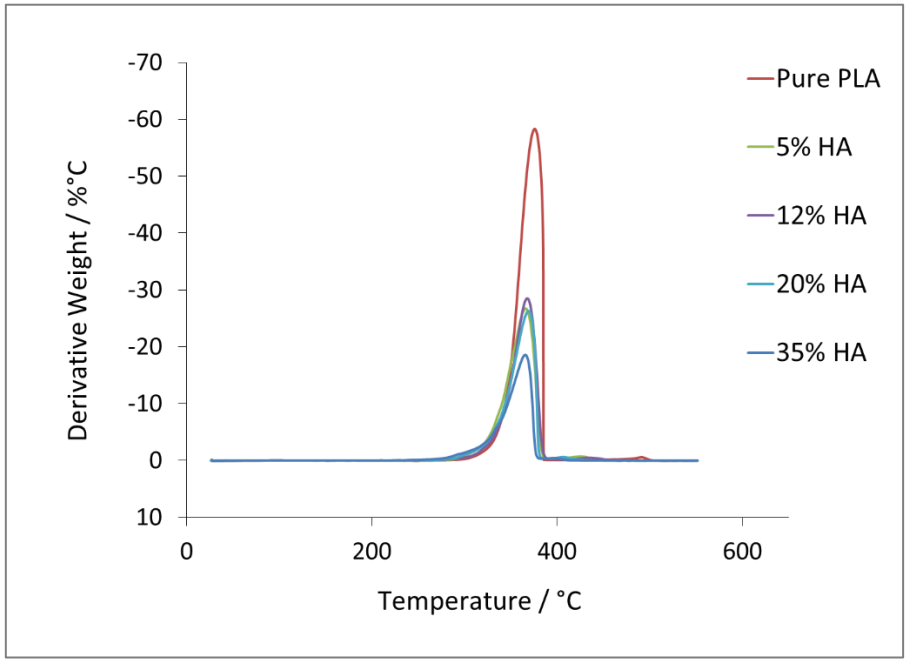


Figure 4.33 First derivative mass loss (%/°C) versus temperature for hot pressed PLA-HA composites

Table 4.5 Characteristic temperatures of the thermal decomposition of injection moulded PLA-HA Composites ± standard deviation , T_x = temperature at which x % of the initial mass is lost.

HA wt% loading	T_5 (°C)	T_{50} (°C)	T_{80} (°C)	T_p (°C)	Residual percentage %
0	333 ± 0.5	369 ± 0.4	383 ± 0.5	375 ± 0.1	1.3 ± 0.02
5	324 ± 0.4	362 ± 0.2	375 ± 0.8	365 ± 0.5	10 ± 0.5
12	327 ±0.5	365 ± 0.9	379 ± 0.7	367 ± 0.1	14 ± 0.2
20	320 ± 0.5	367 ± 0.1	-	368 ± 0.8	24 ± 0.8
35	313 ± 0.3	369 ± 0.7	-	365 ± 0.7	42 ± 0.05

4.1.12 Imaging and SEM analysis of samples achieved by solution casting

PLA and PLA-HA samples with various HA loadings (5-40 wt% HA) were produced via the solution casting method. Figure 4.34 illustrates the photo of a PLA film obtained by dissolving the PLA pellets in DCM. The white regions in the film indicated that crystallisation had occurred within the PLA matrix during the experiment. Furthermore, the colour of the whole surface of the film was white and cloudy suggesting that the sample was partially crystalline. Inducing the crystallisation of PLA by organic solvents has been previously reported in the literature [168]. Figure 4.35 shows photos of two PLA-HA composite films (5 and 20 wt% HA) obtained by solution casting. It is apparent from this figure that the HA particles were not uniformly dispersed within the PLA matrix and instead were agglomerated around the edges of the film. This could be due to the crystallisation of PLA that occurred during the evaporation of the solvent resulting in the migration of HA particles towards the edges of the sample and preventing their integration within the matrix. The SEM images of PLA and PLA-HA (40 wt% HA) also revealed spherulites (through the appearance of polyhedral boundaries) that were formed during the evaporation of the solvent (Figure 4.36). These observations suggest that the solution casting might not be an appropriate method for production of a PLA-HA composite with a suitable dispersion of the filler within the matrix.



Figure 4.34 PLA film sample obtained by solution casting

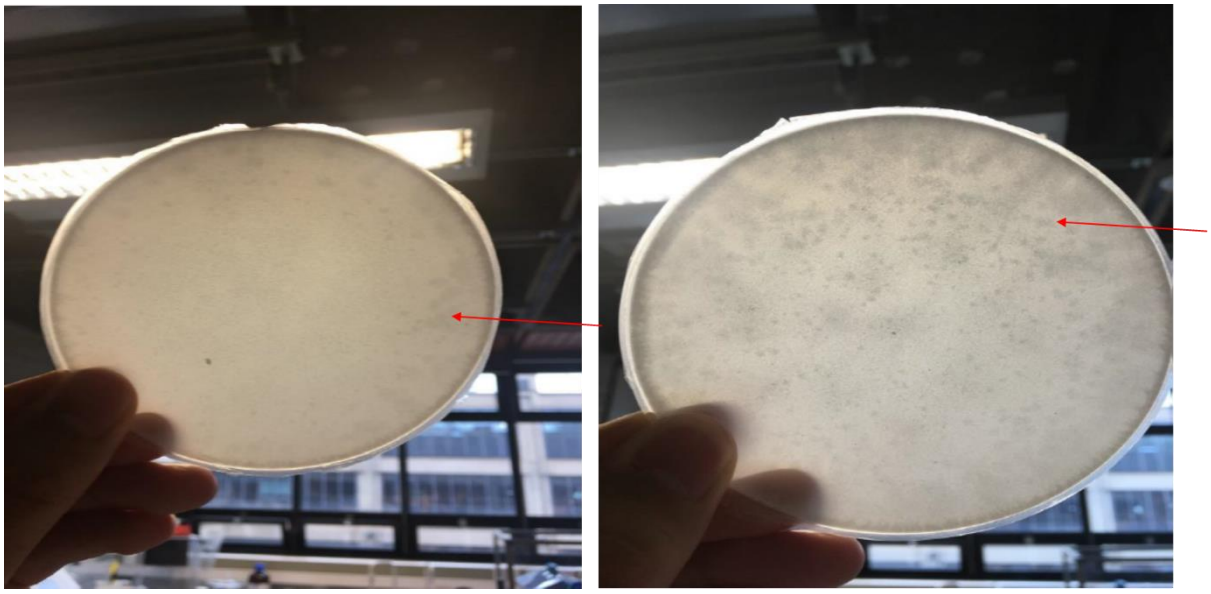


Figure 4.35 PLA-HA film samples with 5 and 20 wt% HA from left to right obtained by solution casting

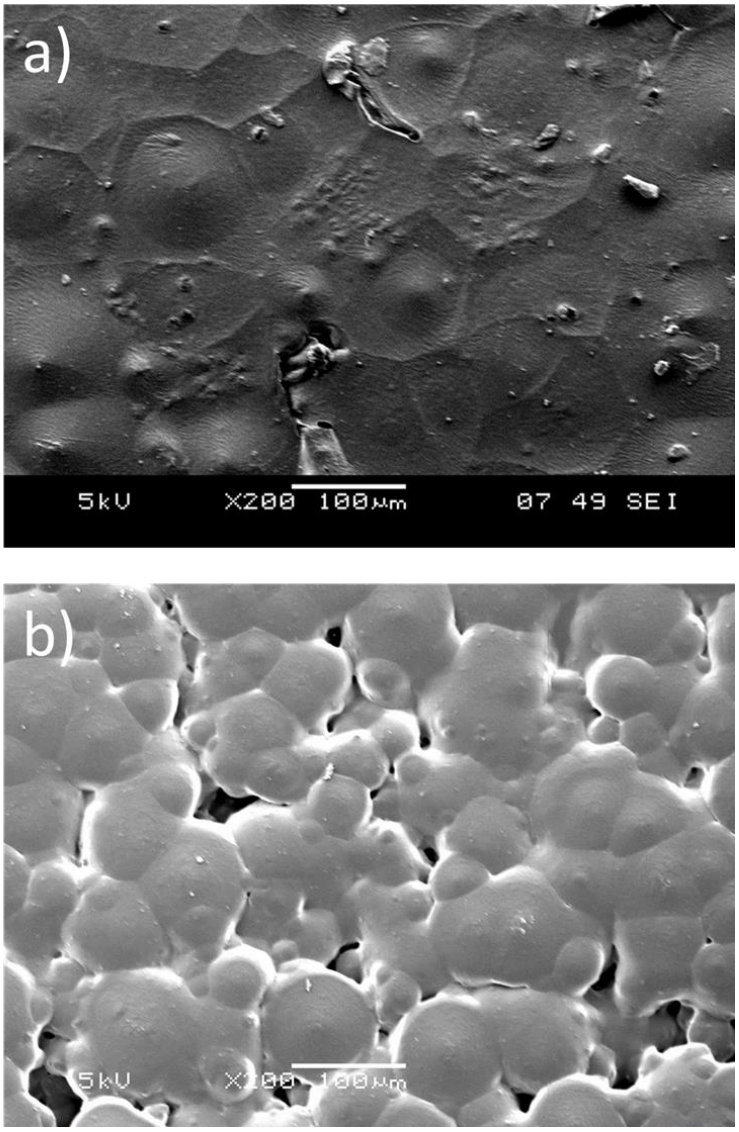


Figure 4. 36 SEM images of a) PLA and b) PLA-HA (40 wt% HA) film samples obtained by solution casting

4.1.13 Etching the samples in DCM

The HA particles were not distinguishable in the SEM images of the surface area of the PLA-HA (40 wt% HA) composite (Figure 4.36). Hence, it was decided that the samples should be etched using DCM in order to remove the surface skin and find out if HA particles could be discovered. However, the SEM images of the etched composite samples (40 wt% HA) revealed that a polymer matrix with a uniform porous surface structure could be created through etching the samples with DCM (Figure 4.37). This was a surprise allowing us to further investigate the

relationship between the etching of the samples and the formation of porosities within the samples.

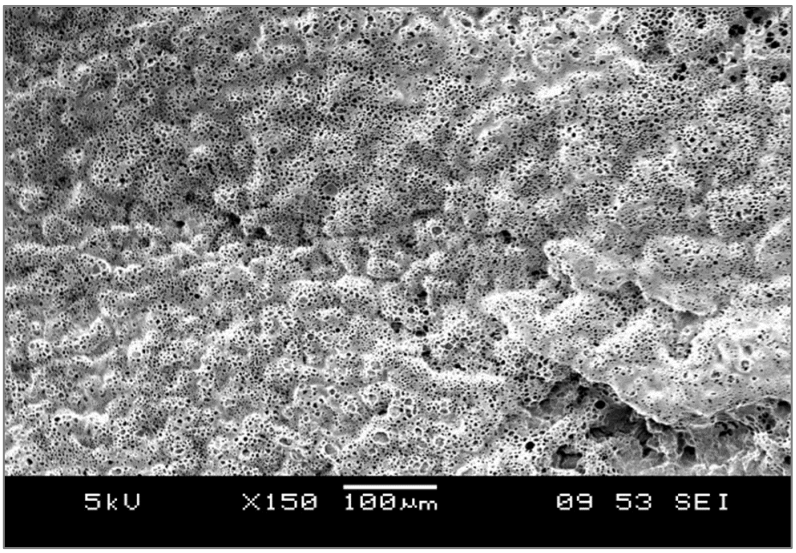


Figure 4.37 SEM images of PLA-HA (40 wt% HA) film sample obtained by solution casting after 10 minutes etching in DCM

4.1.13.1 Investigation of the Porous Surface Structure

An amorphous hot pressed plaque of PLA was cut into small pieces and put in 50 mL of DCM inside a glass beaker (DCM temperature: 20.5ºC) for various periods. It was discovered that the samples were dissolved and disappeared entirely after 5 minutes etching in DCM. Figure 4.38 illustrates the SEM morphology of the amorphous PLA samples after etching in DCM for various periods. It can be observed that a uniform distribution and size of pores covering all the samples after etching in DCM were present. It was also apparent that as the samples were held in DCM for a longer period of time, the average pore diameters and their depth within the samples increased. According to the literature, the nucleation sites for the polymer foams could occur in random locations in a polymer [169]. Therefore, it could be speculated that the nucleation sites for different pores and the locations where DCM dissipate through the PLA sample occurred randomly within the surface of the polymer. DCM might have acted as a lubricant inducing the molecular chains of the polymer to slide over each other and cluster in

several different regions near to the nucleation spots. After the removal of the sample from DCM, the molecular chains could settle into new positions and by evaporation of the DCM from the sample, a porous surface structure could be achieved.

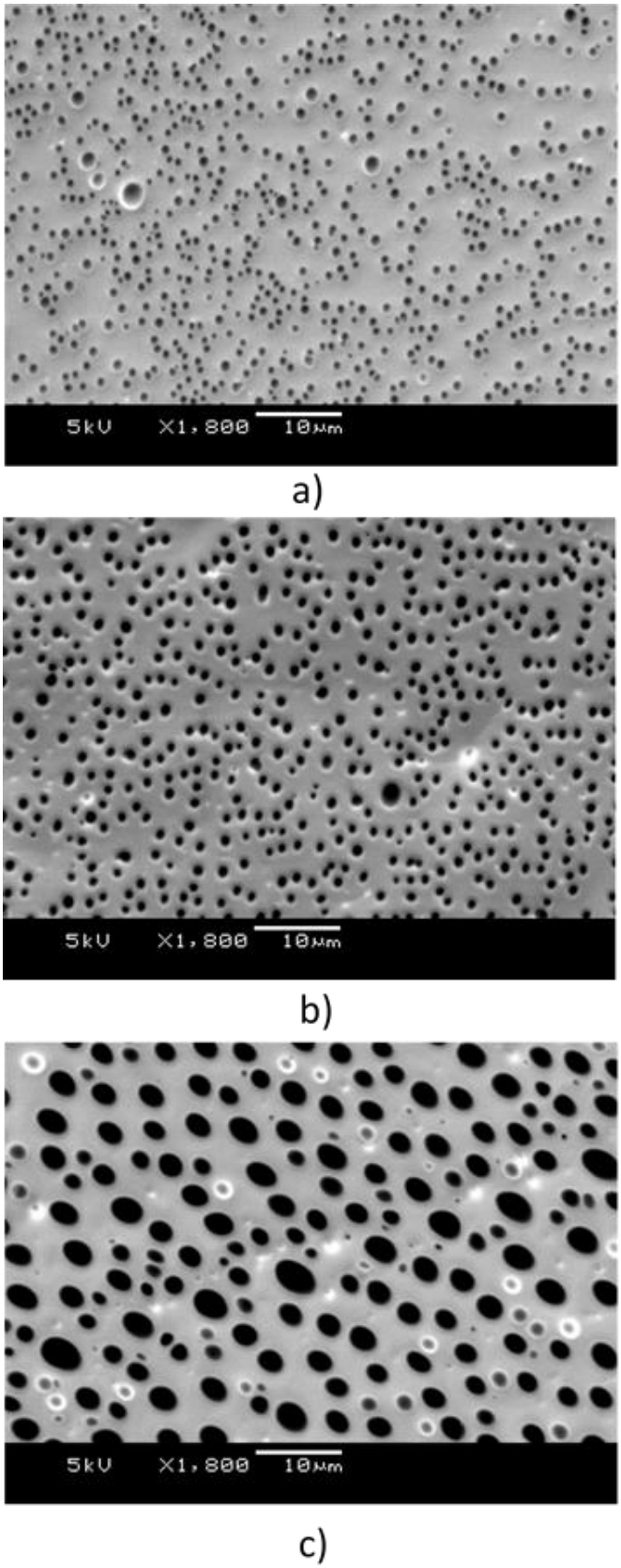


Figure 4.38 SEM images of an etched amorphous hot pressed PLA sample a) after 10 seconds etching, b) after 30 seconds etching and c) after 2 minutes etching

A crystalline PLA film obtained from solution casting was also examined after etching in DCM for 60 seconds. An interesting phenomenon was observed from the SEM micrograph of the etched crystalline PLA sample (see Figure 4.39). As it is apparent from this micrograph, large pores with a diameter of around 3.5 µm surrounded by several smaller pores with the average size of around 1 µm and less were observed. The interesting point was that the large pores were surrounded with a halo of no pores, which span the surface around 15 µm. This might indicate that the driving mechanic behind the formation of pores within the samples is based around a concentration gradient of DCM such that the pores with larger diameters pushing away the DCM from the surrounding region. Consequently, the growth of smaller pores within that area was prevented and the large pores could get the chance to grow even larger.

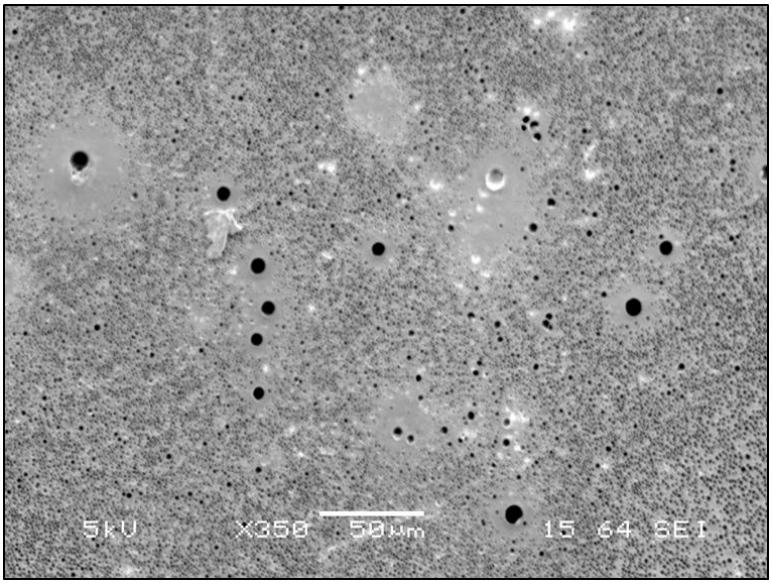


Figure 4.39 Semi-crystalline PLA obtained by solution casting, etched in DCM for 60 seconds

In order to investigate the penetration depth of the pores within the samples, the fracture surfaces of the amorphous hot pressed PLA samples after etching through DCM for various periods were observed under the microscope. This could allow calculating the dissolution rate of DCM through the PLA sample. However, as can be seen from all micrographs in Figure 4.40, there were no internal pores through the sample after etching for various times. Therefore, according to these images, the porous structure was only present at the surface of the polymer and it did not penetrate deeper into the sample. This could be considered as an advantageous feature for bone applications as the polymer can maintain most of its original stability and mechanical properties, while providing enough porosity for migration, penetration and proliferation of the cells into the structure of the scaffold.

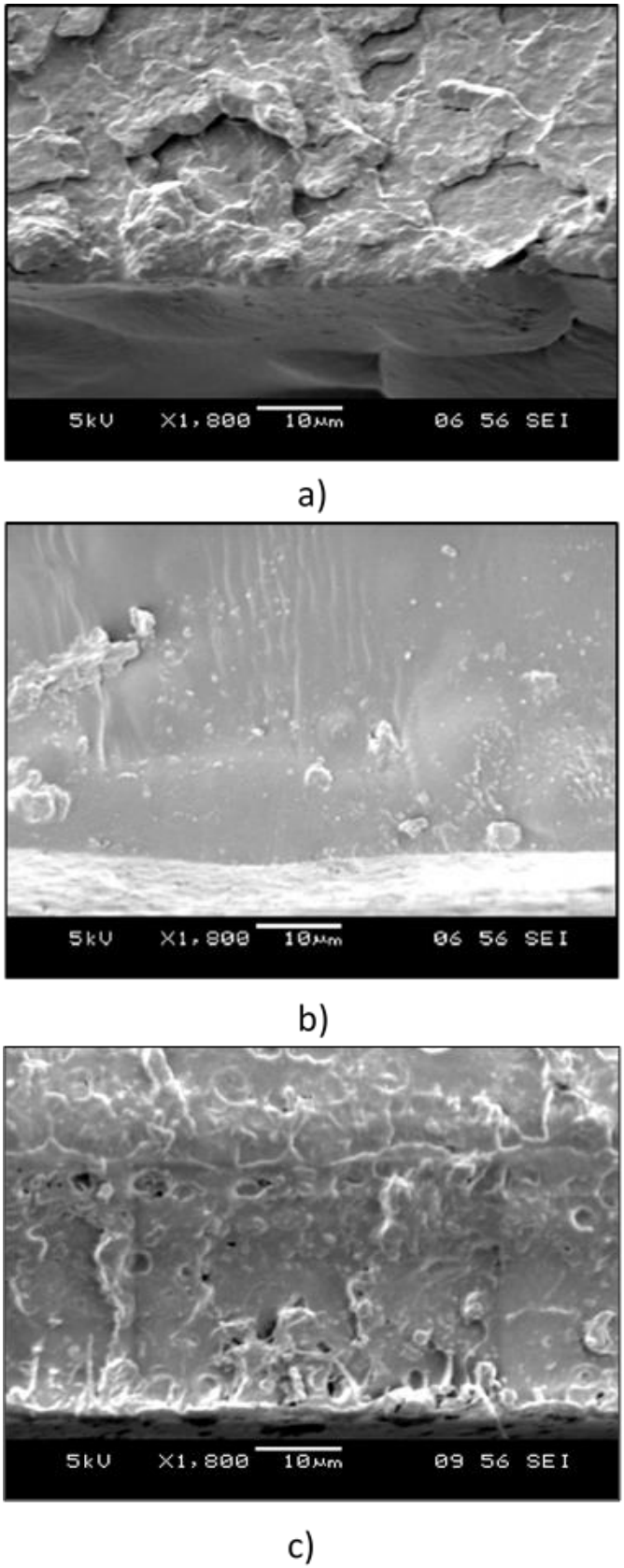


Figure 4.40 SEM morphology of the fracture surfaces of PLA after etching in DCM for various periods including a) 1 min, b) 2 min and c) 4 min

4.2 Conclusions

PLA-HA composite samples were fabricated using three different procedures, including hot pressing, injection moulding and solution casting. SEM micrographs revealed that the HA particles were homogeneously distributed within the PLA matrix in all hot pressed samples. However, the dispersion of HA particles with PLA was poor in both injection moulding and solution casting techniques due to the orientation and crystallisation phenomena occurring during these processes. Isothermal DSC results showed that the degree of crystallinity went up by increasing the HA loading. Furthermore, the double melting peaks converted into a single peak by incorporation of HA particles through the sample. HSM images revealed that HA particles had a heterogeneous nucleating effect on PLA. This was also confirmed by the Avrami analysis, where it was observed that the crystallisation rate increased by increasing the HA content of samples. However, there was no linear relationship between the HA loading and the rate of crystallinity. According to the results of mechanical tests PLA-HA composites with 10-20 wt% HA could be considered as the most appropriate samples in terms of maintaining a good balance between all mechanical properties, including stiffness and deformation simultaneously. It was expected that the HA particles increased the thermal stability of PLA; however, according to the TGA results, the decomposition of PLA was catalysed by the incorporation of HA particles due to hydrolysis. By etching the samples in DCM, a structure with uniform pore size and distribution was produced. Furthermore, by manipulating the time of etching, the diameter of the pores could be controlled. This porous structures could be beneficial as bone scaffolds for migration and attachment of the cells and proteins.

Chapter 5: The effect of microstructure on the hardness and tribology behaviour of PLA

5.0 Introduction

In this chapter, the effect of spherulitic microstructure on nano-hardness (nano-indentation) characteristics of PLA was explored. Firstly, by using hot stage microscopy (HSM) the spherulitic microstructure was investigated. Secondly, appropriate samples required for nano-hardness testing were produced by the DSC. Furthermore, the effect of secondary crystallisation on tribological behaviour of PLA was investigated.

5.1 Results and discussion

5.1.1 Hot Stage Microscopy (HSM)

According to the HSM micrographs recorded during the isothermal process, the size of spherulites can be controlled and manipulated at different isothermal temperatures. Figure 5.1 shows the samples with small spherulites (approx. 5 μm in diameter) produced at 95 °C via cold crystallisation. The process involved heating amorphous thin film hot pressed samples (15-20 μm) at a rate of 50 °C min^{-1} up to 210 °C, holding them for 5 minutes before cooling them back to RT at a rate of 50 °C min^{-1}. Afterwards, samples were heated up at the same heating rate to 95 °C and the spherulites formation at this temperature for a certain period (up to achieving a semi-crystalline sample with approx. 40% crystallinity) was recorded. As it is apparent from this figure, the spherulites formation was entirely finished after 20 minutes. It seems that the crystallisation process occurred more quickly through this procedure (cold crystallisation) compared to the melt crystallisation at the same temperature in Section 3.1.7 in Chapter 3 (Figure 3.19). This is in accordance with the literature where it was shown that the isothermal crystallisation process at a certain temperature was slower from the molten state

than from the amorphous (glassy) state [170]. Furthermore, the size of spherulites grown via this method (cold crystallisation) was more uniform and slightly smaller than those previously achieved at 95 °C from the molten state (approx. 15-20 μm in diameter) demonstrated in Chapter 3. Samples with large spherulites (200-250 μm in diameter) were grown isothermally at a higher temperature (125 °C) from the molten state, as illustrated in Section 3.1.7 in Chapter 3 (Figure 3.21).

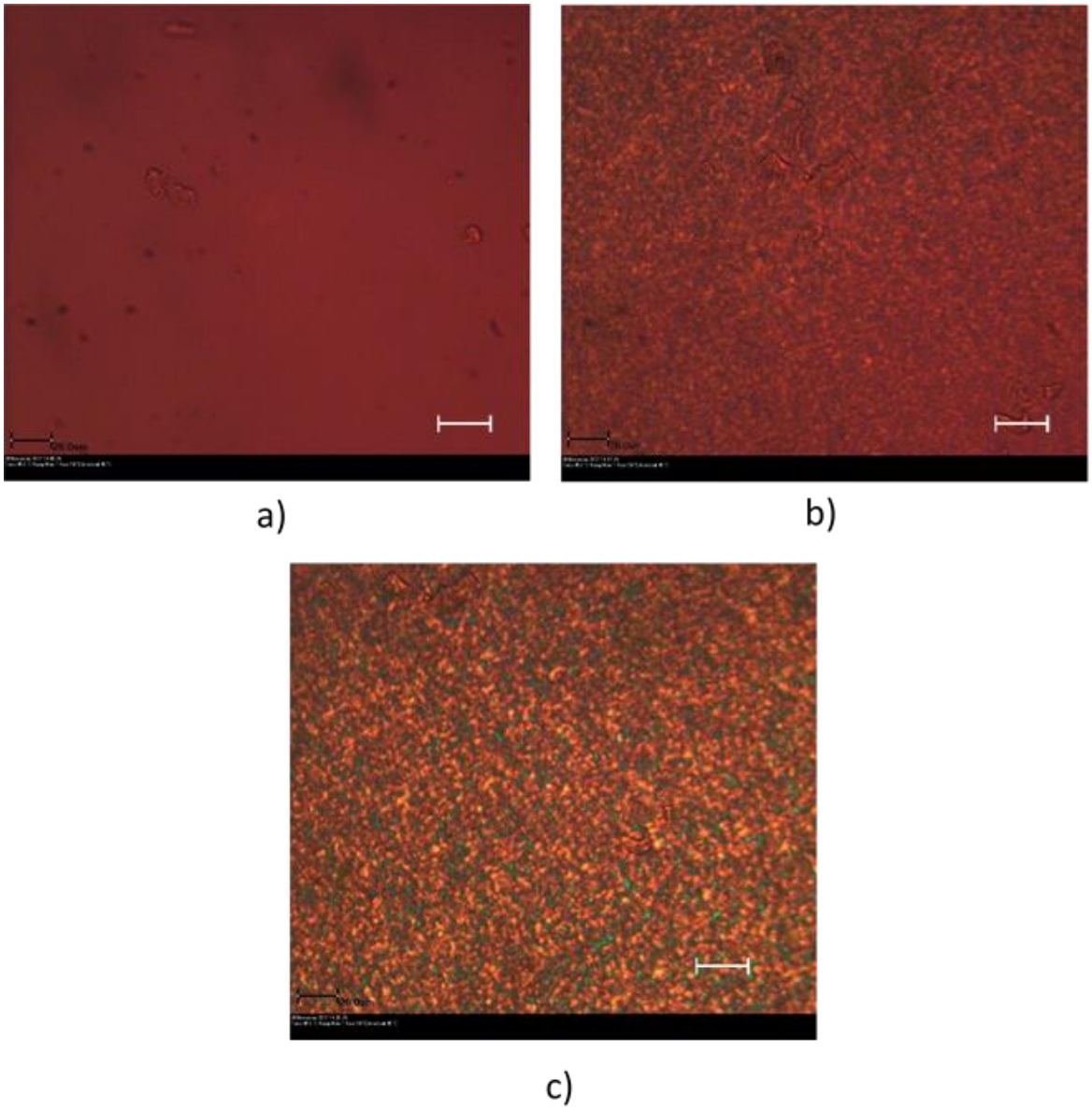
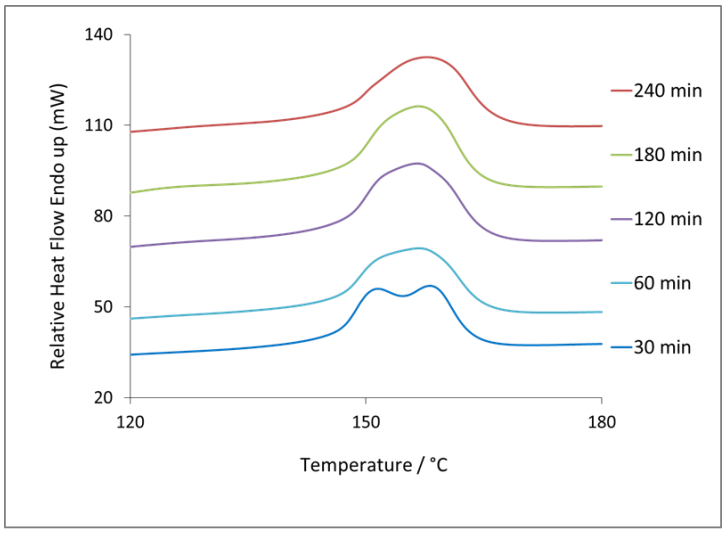


Figure 5.1 HSM images of spherulites formation at 95 °C via cold crystallisation for different periods: a) 0 minutes, b) 10 minutes, and c) 20 minutes. The white scale bars represent 40 μm.

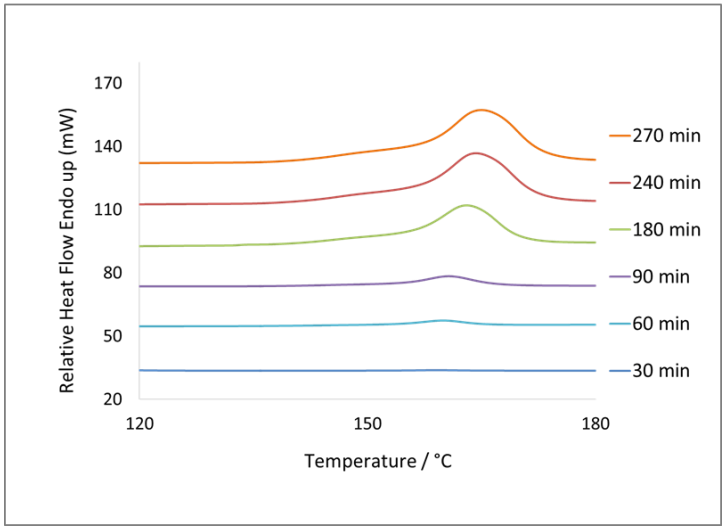
5.1.2 Differential scanning calorimetry (DSC)

By analysing the samples via HSM, the crystalline microstructure could be observed and measured accurately. However, HSM was not capable of making the samples with appropriate geometry that can be applied for the nano-hardness experiment. On the other hand, DSC was able to produce suitable samples for the nano-hardness experiment, whereas the microstructure could not be observed through this method. Therefore, the actual samples for the nano-hardness experiment were prepared via DSC by considering the assumption that the same microstructures as shown in HSM micrographs could be obtained for the samples via this method. The amorphous hot pressed samples were dried in the oven for 24 hours at 60 °C before applying them in the DSC in accordance with literature to remove moisture and prevent any degradation [170]. Samples with small spherulites were produced through the DSC by heating the samples up to 210 °C and held for 5 minutes before cooling them back to 25 °C. Afterwards, the samples were removed from the DSC and were put in an oven at 95 °C for various periods up to achieving semi-crystalline samples with approximately 40% crystallinity. The procedure for making large spherulites samples involved heating the samples in the DSC to the melting temperature (210 °C) and held for 5 minutes to erase the previous thermal history. Then, the samples were cooled down straight to 125 °C and held at this temperature for a certain period to obtain semi-crystalline samples with around 40% crystallinity. In both procedures, heating and cooling rates of 50 °C min^{-1} were used to avoid additional crystallisation.

The degree of crystallinity of both types of samples, including small and large spherulites was measured by heating the samples in the DSC at a heating rate of 50 °C min^{-1} (Figure 5.2). The required hold time to produce semi-crystalline samples (around 40% crystallinity) via the DSC was longer compared to the HSM. This might be due to the differences that existed in the sample sizes and geometries.



a)



b)

Figure 5.2 Melting peaks of PLA samples produced (a) via cold crystallisation at 95°C and (b) via melt crystallisation at 125°C

The double melting peaks which are visible in Figure 5.2.a for 30 minutes at the isothermal hold of 95 °C is due to the melting-recrystallisation mechanism, which was previously explained (in Chapters 3 and 4). These double melting peaks were disappeared after holding the sample for 1 hour. However, multiple melting peaks produced via melt crystallisation at the same temperature (95 °C) were in all DSC traces up to 4 hours (Figure 3.17.a in Chapter 3). This is in accordance with the previous results from HSM where it was shown that the crystallisation kinetics were faster via cold crystallisation compared to the melt crystallisation at the same isothermal temperature. Therefore, the double melting peaks for PLA could convert into one single peak in a shorter period when the crystallisation occurred from the glassy state compared to the molten state.

The degree of crystallinity increased with increasing isothermal heat treatment holding times, as shown in Table 5.1. The semi-crystalline samples (X_c:~40%) with small spherulites were achieved at 95 °C via cold crystallisation after an isothermal holding time of 4 hours whereas the 40% large spherulites semi-crystalline samples were obtained through melt crystallisation at 125 °C after a holding time of 4.5 hours. Therefore, these samples were produced through the DSC to be applied for the nano-hardness testing.

Table 5.1 X_c values obtained for cold crystallisation at 95 °C and melt crystallisation at 125 °C for different periods ± standard deviation

Temperature (°C)	Isothermal hold time (min)	X_c (%)
95	30	-
	60	24 ± 0.4
	120	30 ± 0.3
	180	36 ± 0.4
	240	39.5 ± 0.3
125	30	0.20 ± 0.005
	60	2 ± 0.2
	90	6 ± 0.9
	180	29 ± 0.9
	240	37 ± 0.35
	270	39.5 ± 0.5

5.1.3 Nano-Indentation (nano-hardness) analysis

Semi-crystalline hot pressed samples with different sizes of spherulites (small and large diameters) obtained from the DSC and amorphous hot pressed sample (without any heat treatment) as the reference were used for the nano-indentation testing. Only one epoxy disc contains (one amorphous, one small spherulites, one large spherulites) samples were tested due to time constraints. The indentation was also conducted on Epofix™ resin as a control measure.

Table 5.2 shows the mean values for hardness and elastic modulus (Young's modulus) for all PLA samples and Epofix™ resin. As can be seen from this table, the amount of hardness and Young's modulus for Epofix™ resin were significantly less and quite distinguishable compared to PLA samples suggesting that the indentation test was properly done on the samples (not on the resin as the top layer of the samples). Furthermore, samples with large spherulites demonstrated a greater value for both hardness and Young's modulus in comparison with the smaller spherulites samples and both of the semi-crystalline samples displayed higher hardness and Young's modulus compared to the amorphous sample.

These differences in the amount of both hardness and Young's modulus among the PLA samples with different microstructures indicate that the top amorphous layer of all samples was removed successfully through polishing.

According to Table 5.2 and Figure 5.3, the standard deviation for both hardness and Young's modulus for semi-crystalline samples were relatively higher than the amorphous sample.

Table 5.2 Hardness and Young's modulus of Epofix™ resin and PLA samples with different microstructures ± standard deviation

Sample type	**Hardness (GPa)**	**Young's Modulus (GPa)**
Epofix™ resin	0.185 ± 0.021	4.2 ± 0.25
Amorphous PLA	0.285 ± 0.022	6.79 ± 0.29
Small Spherulites PLA	0.343 ± 0.028	7.31 ± 0.35
Large Spherulites PLA	0.377 ± 0.036	7.79 ± 0.42

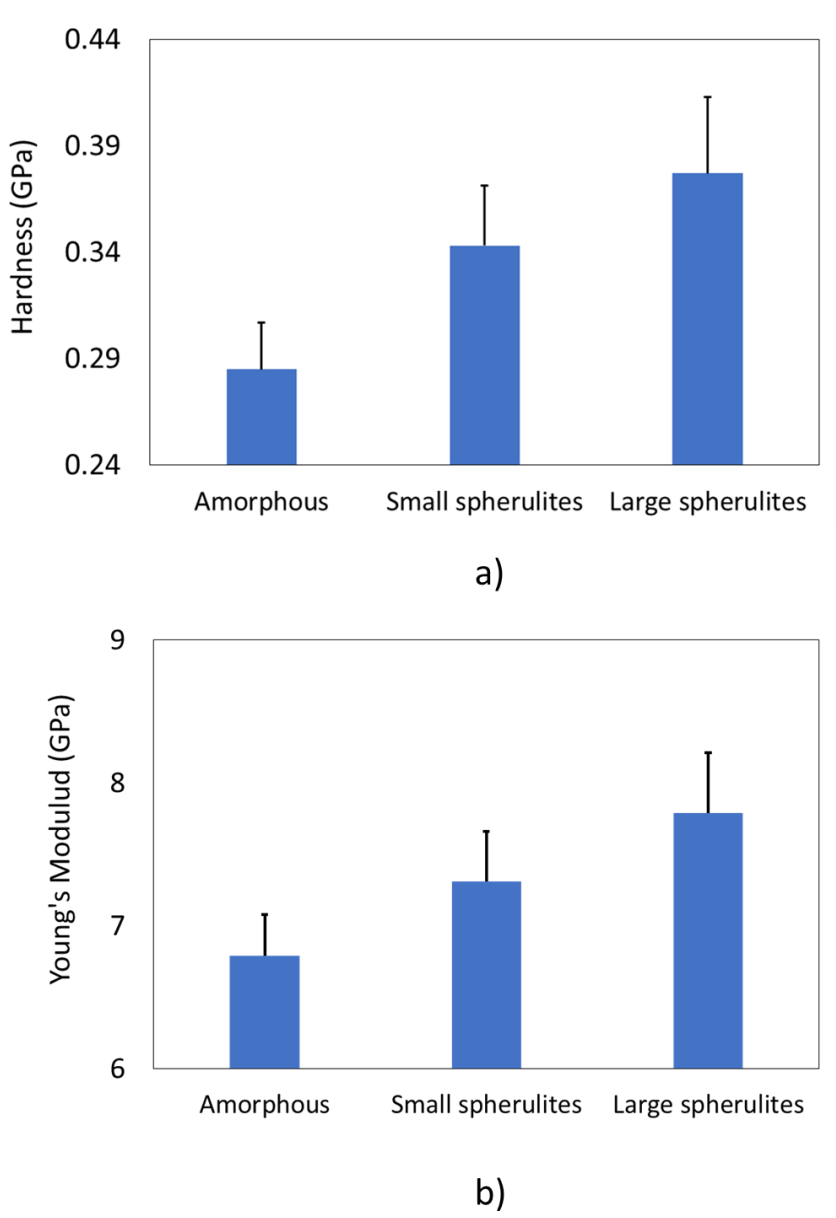


Figure 5.3 The values obtained for a) nano-hardness and b) Young's modulus for PLA samples with different microstructures

Achieved hardness values from the nano-indentation experiment were plotted against the location of indentations for all samples (Figures 5.4-5.6) to explore precisely the relationship between the spherulitic microstructure and nano-indentation results. As it is apparent from these figures, the indentations were applied at different locations in each sample in a rectangular pattern.

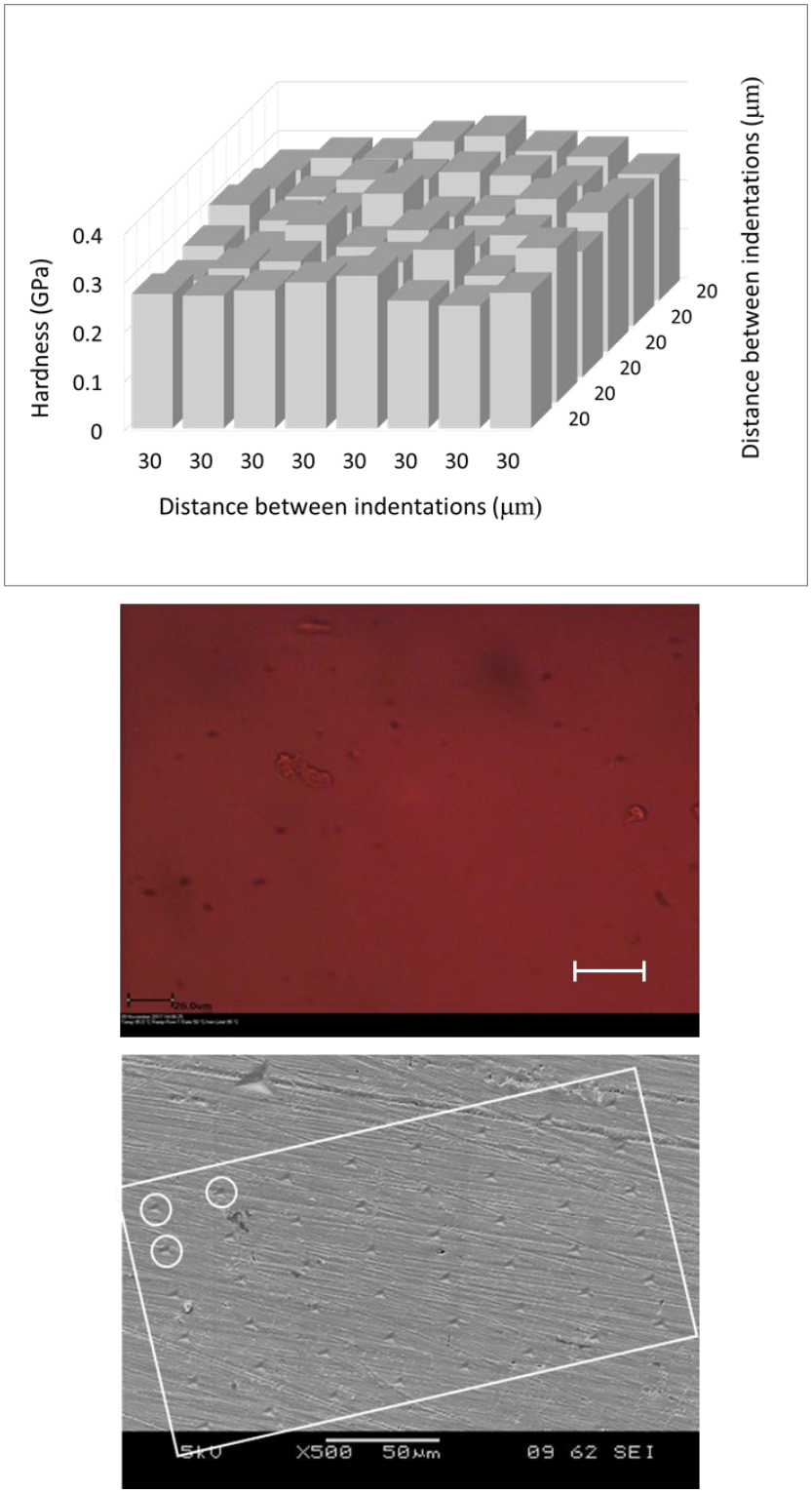
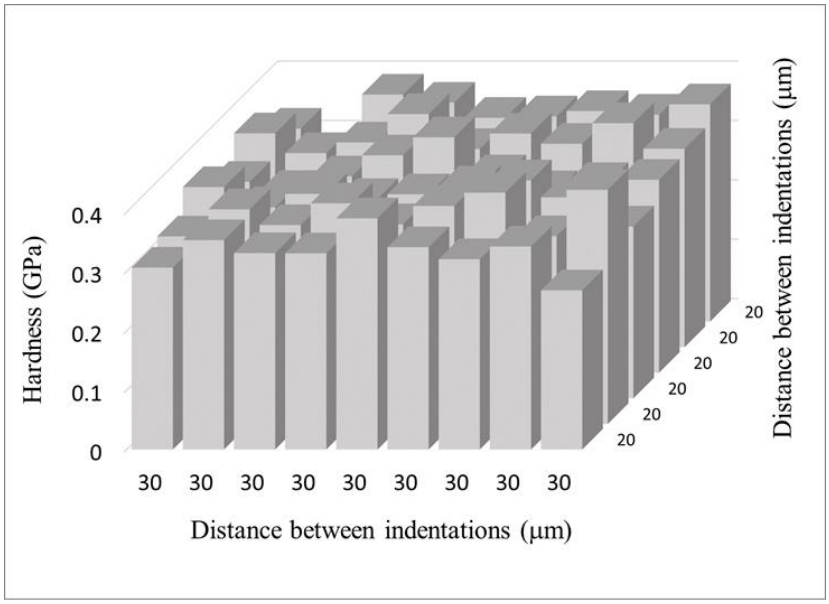
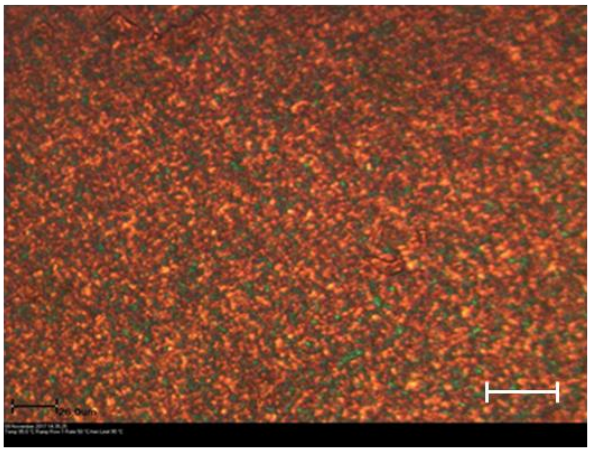


Figure 5.4 Amorphous sample. Graph of nano-hardness values against the location of indentations on the sample (top), the HSM micrograph of the sample (middle) – (The white scale bars represent 40 µm) and SEM micrograph of the indentations on the polymer surface (bottom)





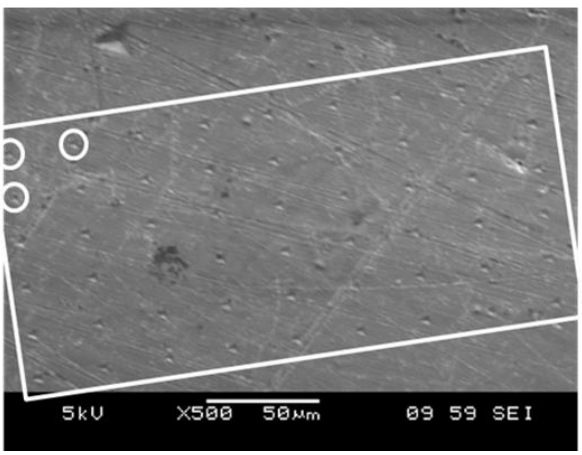


Figure 5.5 Small spherulites sample. Graph of nano-hardness values against the location of indentations on the sample (top), the HSM micrograph of the sample (middle) – (The white scale bars represent 40 μm) and SEM micrograph of the indentations on the polymer surface (bottom)

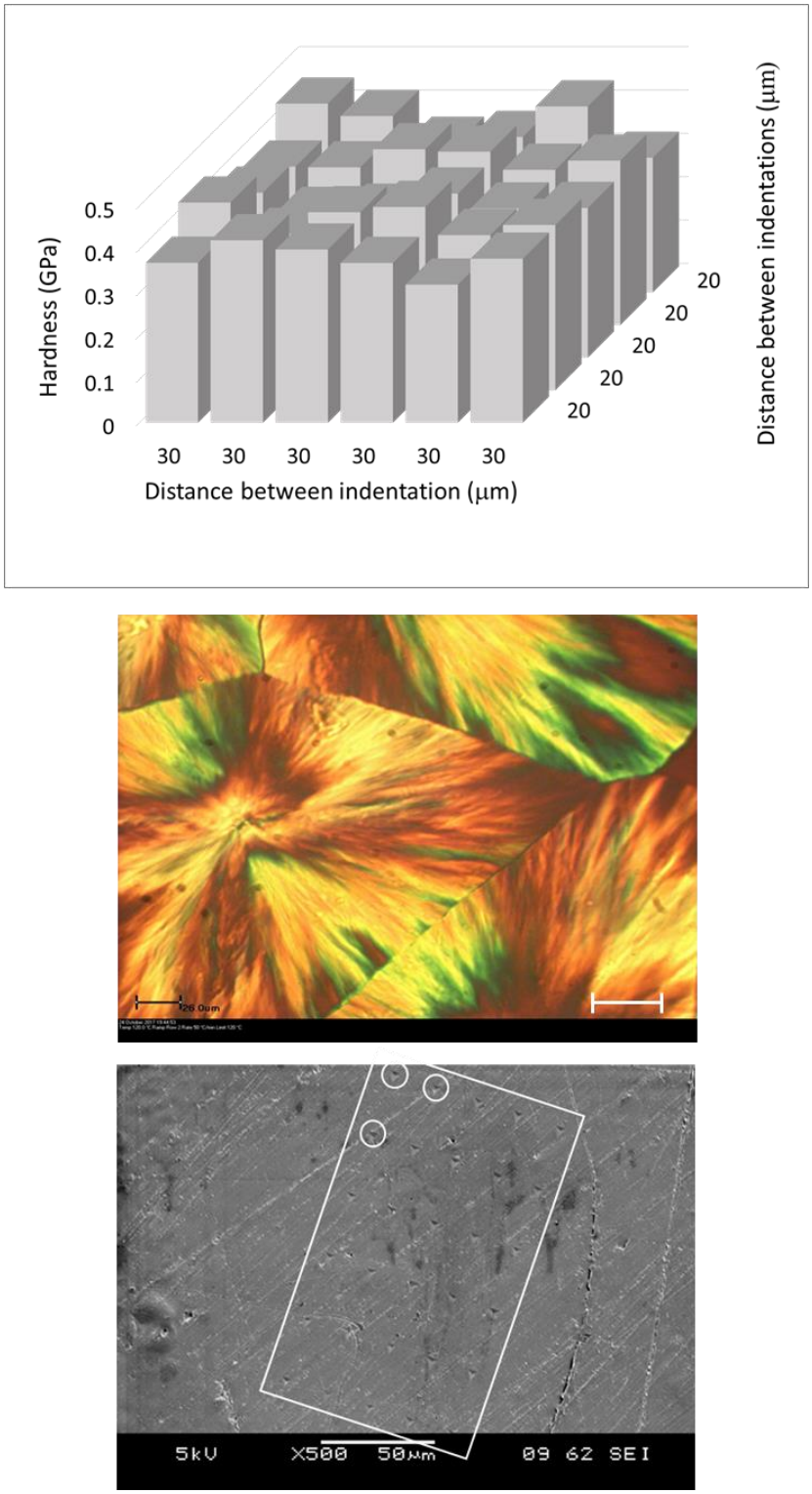


Figure 5.6 Large spherulites sample. Graph of nano-hardness values against the location of indentations on the sample (top), the HSM micrograph of the sample (middle) – (The white scale bars represent 40 μm) and SEM micrograph of the indentations on the polymer surface (bottom)

Smaller deviations observed for both hardness and Young's modulus for the amorphous sample compared to the semi-crystalline ones could be due to the more uniform and homogenous microstructure of the amorphous sample (Figure 5.4) in comparison with the semi-crystalline structures (Figures 5.5 and 5.6). A semi-crystalline polymer contains three different microstructures, including the soft amorphous areas, harder crystalline lamellae regions and softer inter-spherulitic boundaries. Therefore, the results for values of indentation in a semi-crystalline polymer could be various depending on the location of testing [143, 171]. However, according to Figure 5.6 (large spherulites samples), the full area of nano-indentation block (180 μm ×100 μm) was smaller than the area of a single spherulite (approx. 200 μm × 200 μm) indicating that the indentation experiment could be conducted across the surface of a single spherulite (not on the amorphous boundary layers in between them). However, the hardness value is usually greater in the center of a spherulite and becomes smaller outwards towards the boundaries [107]. Therefore, the large variations in the results could be related to the differences in the amount of hardness across the surface of a single spherulite. Nevertheless, no visible pattern was observed in the values of hardness corresponding to different areas where the nano-indentation experiment was applied to them (Figure 5.6). Although the microstructure of the amorphous sample was more uniform, shown by the smaller standard deviations of hardness values, it still had some variations as illustrated in Figure 5.4. This might be because of the hot pressing procedure by which the polymer chains were oriented in the polymer matrix and the final microstructure of the polymer became anisotropic [172]. Therefore, it could be beneficial to do the same nano-indentation testing on a PLA pellet (before any process) to explore whether the standard deviation values decreased or if any change could be observed in the amount of hardness overall.

According to the results, a lower hardness was obtained for small spherulites samples compared to the samples with large spherulites showing that by increasing the diameter of spherulites, the hardness value went up. This observation disputed the theory that declares the hardness value is not influenced directly by the spherulite size [109, 171]. The differences in hardness values between small and large spherulites samples might be originated from the variations in the thickness of lamellae [109, 171]. According to the Gibbs-Thomson equation, there is a

direct relationship between the thickness of lamellae and the melting point in a polymer [173]. According to the results of DSC shown in Figure 5.2, small spherulites samples had a melting point of around 159 °C. The DSC traces displayed a higher melting point (around 163 °C) for large spherulites samples, which proposes that there was an increase in lamellar thickness for these samples compared to the samples with small spherulites. These results suggest that the increase in hardness values for larger spherulites samples derived from the increase in lamellar thickness, which is in accordance with the literature [171, 174, 175]. An increase in the lamellar thickness could be also derived from the increase in crystallisation temperature [176]. In this study, samples with large spherulites were prepared at a temperature of 30 °C higher than the samples with small spherulites. This could further support the proposal that the increase in nano-hardness results for larger spherulite samples was associated with an increase in the lamellar thickness.

In all SEM micrographs of the samples (Figures 5.4-5.6), some scratches could be observed. This could be as a result of using a coarse grit paper during polishing of the samples. Thus, the results might have been affected by these scratches, particularly in the case of measuring the hardness on top of these scratches. However, since the hardness measurements were made on a single stub, which contained all samples that were cold mounted and polished in the same way, the issue could be ignored. Furthermore, according to the SEM micrographs, a permanent plastic deformation had occurred in all samples.

5.1.4 The effect of secondary crystallisation on tribology behaviour of PLA

In order to determine the effect of secondary crystallisation on tribology behaviour of PLA, amorphous hot pressed PLA samples were conditioned in the oven at 95 °C for various times. The degree of crystallinity for these samples was measured by using the DSC through heating the samples at 50 °C min^{-1} (Figure 5.7) and the results shown in Table 5.3. It is surprising that the degree of crystallinity of the nano-indentation PLA samples that were heat treated at 95 °C for 2 hours in the oven (Figure 5.2.a) was around 13% less than the degree of crystallinity achieved here at the same condition. However, the nano-indentation samples were melted in the DSC at 210 °C for 5 minutes before conditioning them in the oven whereas the specimens for wear testing were put in the oven straight away (the dimensions of the specimens were not appropriate to put them in the DSC for melting).

The secondary crystallisation was attributed to the lamellae thickening via secondary nucleation on the surface and the growth occurrence perpendicular to the surface of the lamellae. The thickness of lamella started to increase linearly with the square root of the isothermal heat treatment time just from the moment that the primary process started to produce the lamellae [177]. According to Figure 5.8, there was a significant positive relationship between the degree of crystallinity and isothermal heat treatment time at 95 °C, indicating the occurrence of secondary crystallisation.

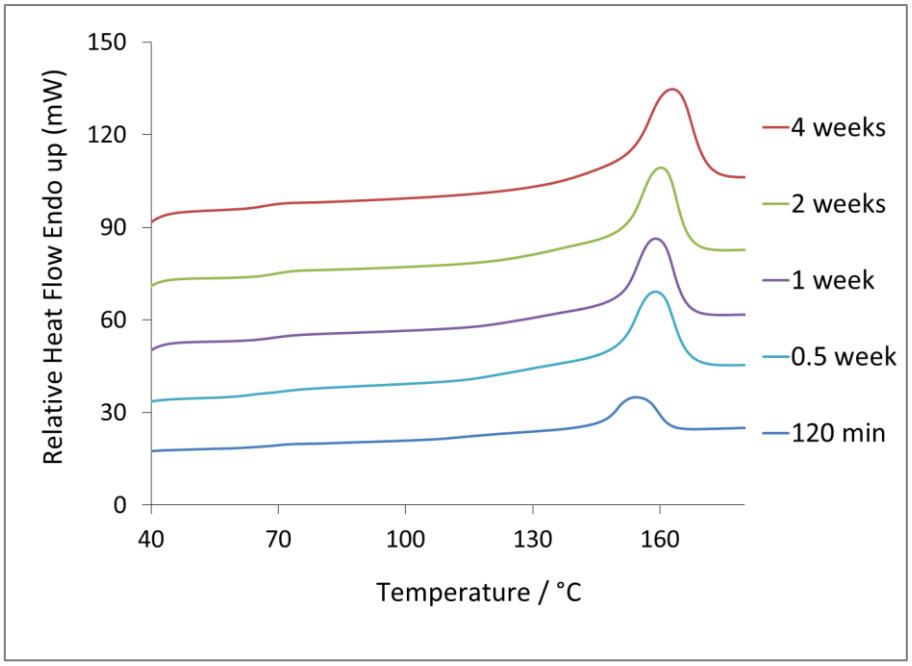


Figure 5.7 Melting peaks of PLA samples produced via secondary crystallisation

Table 5.3 Different Percentages of crystallinity at various periods at 95°C ± standard deviation

Isothermal treatment time (at 95°C)	Mean crystallinity (%)
None (Amorphous)	0.45 ± 0.05
2 hours	43.0 ± 0.2
3.5 days	45.12 ± 1.4
7 days	46.15 ± 3.1
14 days	48.7 ± 0.5
28 days	52.0 ± 2.1

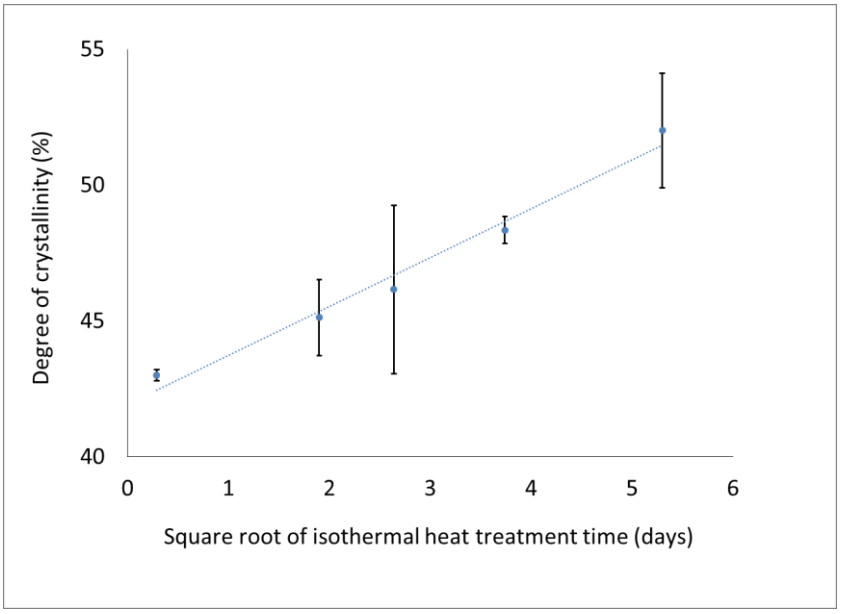


Figure 5.8 The relationship between the extent of secondary crystallisation and the square root of the isothermal heat treatment time

During the experiment for some samples the coefficient of friction did not follow the trend of an increase in friction with sliding time (see Figure 5.9 polyamide 6, POM and UHMWPE as an example from the literature) [178]. This included four samples; number 2 of amorphous samples, number 1 of 3.5 days samples, number 3 of 14 days samples and number 1 of 28 days samples, all of which were shattered during the experiment. Therefore, these samples were not included in the following data analysis.

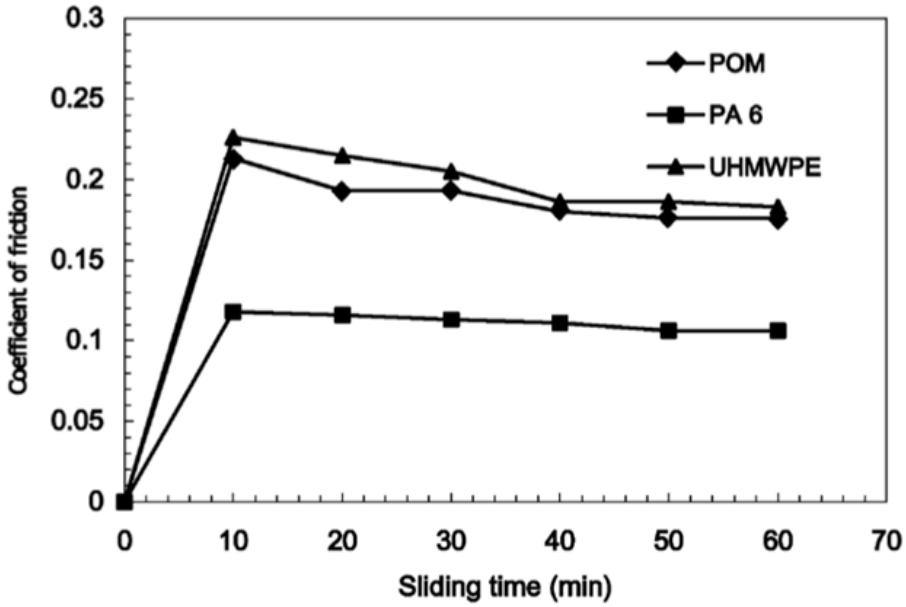


Figure 5.9 Relationship between coefficient of friction and sliding time for polyamide 6, POM and UHMWPE (load 30N, sliding speed = 0.88m/s) [178]

Wear rate was determined by calculating the percentage of mass loss and the results shown in Table 5.4. As can be seen from this table, the percentage of mass loss for amorphous samples was almost equal to the semi-crystalline samples, which were held at 95 °C for 2 hours. This point opposed the previous literature that illustrated the semi-crystalline polymers were more wear resistant than the amorphous polymers [179, 180]. However, this low difference observed here could be because of the small number of samples (three samples of each type) which wear tested suggesting that by increasing the number of samples for the experiment a more significant difference might be observed. The SEM micrographs of wear scars shown in Figures 5.10 and 5.11 supported this proposal. As it is apparent from these micrographs, the width of wear scars for amorphous samples was around 3.5 mm which was wider than the width of wear scars for semi-crystalline samples (around 2.8mm) suggesting a lower mass loss for the latter group (semi-crystalline samples). Moreover, according to the SEM micrographs, there was a larger difference between the wear tested and non-wear tested regions in amorphous

samples compared to the semi-crystalline ones suggesting that the semi-crystalline samples were less worn (Figure 5.11).

Table 5.4 Mass Losses for heat-treated PLA samples (secondary crystallisation) for different periods ± standard deviation

Isothermal treatment time (95 °C)	Mean mass loss (%)
None (Amorphous)	1.24 ± 0.36
2 hours	0.59 ± 0.13
3.5 days	0.71 ± 0.20
7 days	0.98 ± 0.06
14 days	0.92 ± 0.22
28 days	1.35 ± 0.36

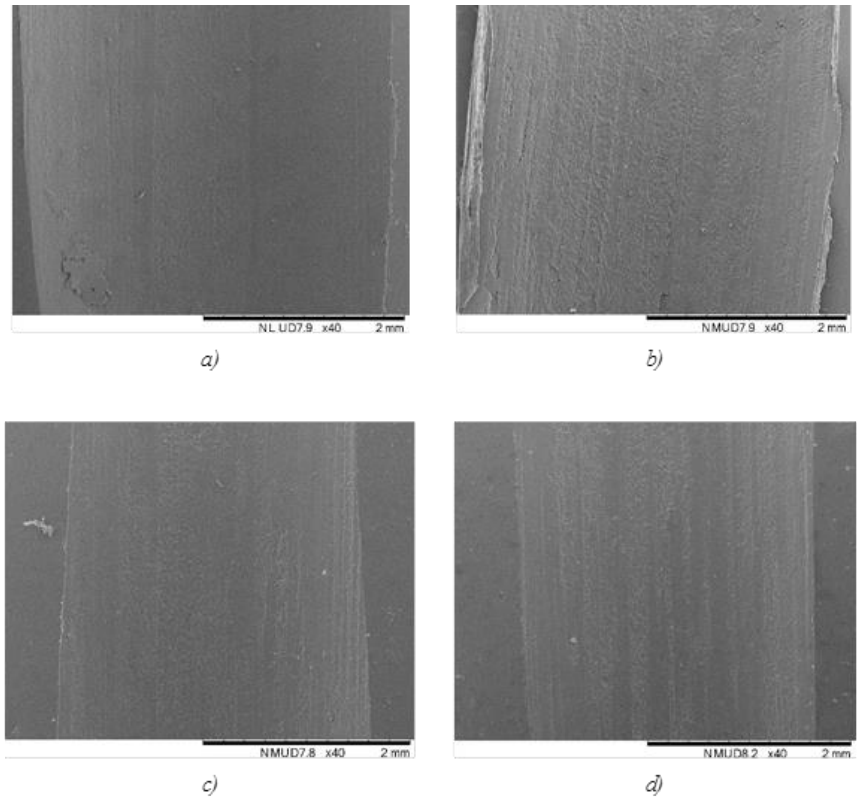


Figure 5.10 SEM micrographs of the middle of the wear scar; a) amorphous sample 1, b) amorphous sample 3, c) semi-crystalline 2 hours at 95°C sample 2, d) semi-crystalline 2 hours at 95°C sample 3 (direction of friction from top to bottom), x40 magnification

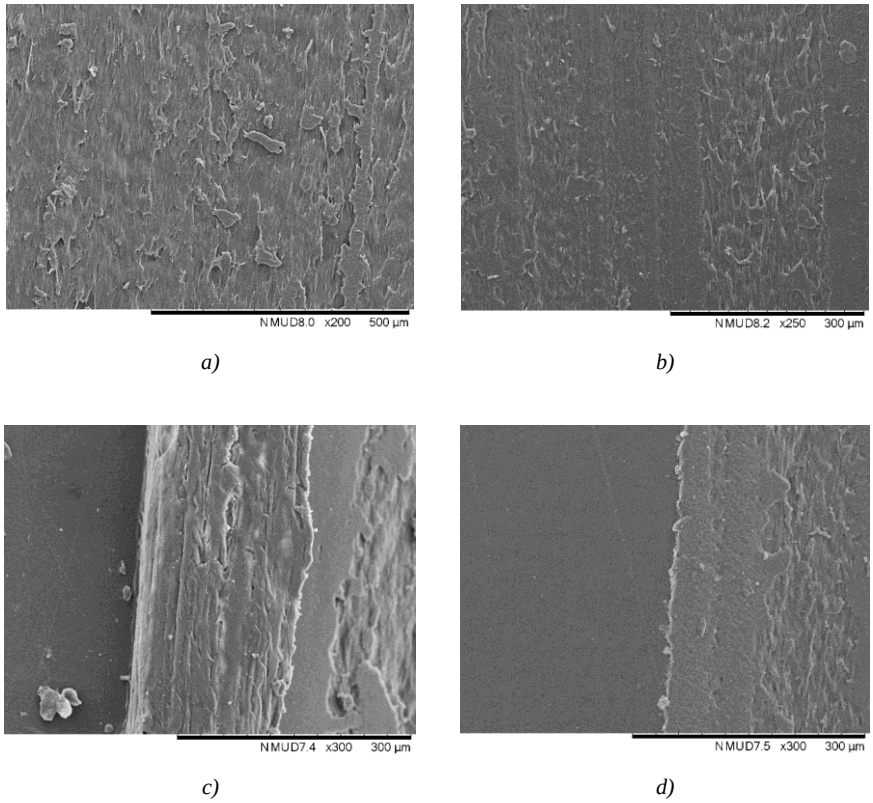


Figure 5.11 SEM micrographs of the middle of the wear scar; a) amorphous sample 3, b) semi-crystalline 2 hours at 95°C sample 3, and SEM micrographs of the wear scar boundary; c) amorphous sample 3, d) semi-crystalline 2 hours at 95°C sample 2 (direction of friction from top to bottom), x200-300 magnification

Figure 5.12 illustrates a linear relationship between the isothermal heat treatment times and wear mass loss for semi-crystalline PLA samples. As can be seen from this figure, longer isothermal heat treatment time increased wear mass loss, indicating clearly that the wear resistance of polymer samples decreased by the development of the secondary crystallisation. This is in accordance with previous literature, which reported that the introduction of secondary crystallisation could increase the embrittlement in polymer samples. This is because by increasing the crystallinity, the chain mobility of the polymer decreases, resulting in increasing the embrittlement in polymer samples [181]. Subsequently, by increasing the embrittlement, the tensile strength, which plays a vital role in determining the wear properties decreases [182]. Therefore, the possibility for the fracture of the polymer samples increases by developing the tensile stresses in embrittled areas of them [62] which leads to the breaking off some sections

of the polymer surface and consequently increases the wear mass loss. Furthermore, the development of secondary crystallisation could introduce thermal degradation into the polymer samples [137], which possibly leads to an increase in wear mass loss.

As mentioned earlier, two pieces of samples, including sample 1 from 2 weeks and sample 3 from 4 weeks secondary crystallisation were broken during the experiment. The degree of crystallinity for these two samples were around 50%. According to the literature, the critical stress intensity factor (K_{IC}) for PLA could be decreased when its degree of crystallinity reaches beyond 50% [183]. This could explain clearly the reason for the shattering of these samples during the experiment. Nevertheless, it is surprising that the other samples with approximately the same degree of crystallinity did not destroy. For example, sample 3 from 4 weeks secondary crystallisation process, which had the highest degree of crystallinity (54%) among all specimens did not break.

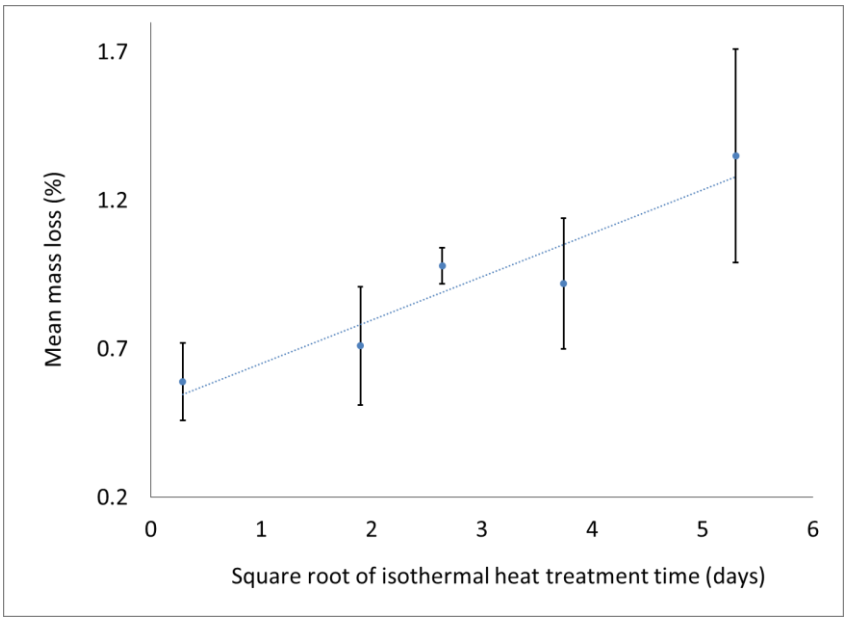


Figure 5.12 The relationship between increasing isothermal treatment time and wear mass loss (Amorphous samples are not included)

5.2 Conclusions

HSM experiments showed that samples with small and uniform diameters could be produced at 95 °C from the amorphous state. The crystallisation kinetics was faster via cold crystallisation compared to the melt crystallisation at the same temperature (95 °C). Larger spherulites samples were produced at a higher temperature (125 °C) via melt crystallisation.

According to the results from nano-indentation samples, the spherulite dimensions could influence the nano-hardness of PLA, but only when the thickness of lamellae is considered specifically. The results showed that the lamellar thickness increased as the size of spherulites became larger, resulting in an increase in the amount of nano-hardness of the samples.

The results from wear testing suggest that there was an increase in mass loss in PLA when it was amorphous compared to its semi-crystalline structure. However, introducing the secondary crystallisation caused an increase in embrittlement within the PLA sample resulting in a reduction in wear resistance of the sample.

Chapter 6: The effect of hydrolytic degradation on different microstructures of PLA

6.0 Introduction

In this chapter, the effect of hydrolytic degradation on the mass change of PLA pellets in both static and dynamic conditions was investigated and compared. Furthermore, the effect of the hydrolytic degradation process on the changes in the molecular weight and the microstructural behaviour of PLA and PLA-HA samples under dynamic conditions was explored using SEC, DSC and XRD techniques.

6.1 Results and discussion

6.1.1 Mass loss measurements under static and dynamic conditions

The *in vitro* degradation experiment was performed on an as-received PLA pellet of 500 mg (as the reference) at three different temperatures including 37, 50 and 70 °C in 5 mL Tris-buffer for a period of two months in static conditions. During the hydrolysis process, water or buffer can penetrate into the polymer chains randomly. Consequently, the molecular weight could be reduced, resulting ultimately in producing water soluble oligomers. Therefore, the hydrolysis rate could be indirectly followed by mass loss measurements during a specific period of time [184]. No weight loss was observed for the PLA at 37 °C (the average temperature of the human body) indicating that this period was not enough for the degradation of the sample. According to the literature, the hydrolysis rate of PLA is very slow. Therefore the degradation experiments are usually carried out at higher temperatures (50 °C and above) in order to accelerate the process [184–187]. By increasing the temperature of the degradation medium, the degradation rate could be accelerated significantly, while the overall mechanism of degradation was reported to be similar at different temperatures [187].

Figure 6.1 shows the mass change of a PLA pellet as a function of time during 60 days of degradation at 50 °C. The percentage of the remaining mass decreased with degradation time. From the same figure, it is also apparent that the mass loss of the polymer at the initial stages of hydrolysis was very small up to 30 days. Afterwards, the degradation of the polymer increased dramatically. This is in accordance with a report by Beslikas et al. who stated that at the initial stages of hydrolysis, only small parts of the material could be removed. The authors speculated that this might be because the hydrolysis rate was very small and occurred only at the end of the polymer chains resulting in the formation of polymer chains with low molecular weight [184]. However, Fukuzaki et al. reported that the low mass loss of the polymer at the first days of hydrolysis could be due to the fact that the hydrolysis of polyesters occurs randomly along the polymer chain resulting in the decrease of the molecular weight without significant mass loss [188]. This is because the oligomers, which are formed at the initial stages of hydrolysis, are not small enough to be water soluble and diffuse through the bulk material. Therefore, only after a long period of time, when the size of oligomers decreased sufficiently to become water soluble, they could be diffused out, resulting in reducing the weight considerably [184]. PLA is generally hydrophobic and the polymer chains can become water soluble only when the molecular weight ranges between 5000 and 8000 g mol^{-1}. Nevertheless, this could be varied according to the thickness of the material. For instance, in the case of samples with high thickness, the polymer chains could not be diffused out from the sample even after decreasing their molecular weight sufficiently (soluble point). On the other hand, the degradation products could migrate easily from thin specimens, mainly from the surface [189].

According to Figure 6.1, there is a weight loss of 9% and 25% after 30 and 60 days of the degradation process, respectively. The values obtained for the weight loss reported by Beslikas et al. (0.5% after 30 days and around 3.5% after 60 days) [184] were much smaller compared to the ones observed in this study. This is because the PLA grade used in the report by Beslikas

et al. contained only L-lactide, whereas the PLA in this study included also 4% of D-lactide. According to the literature, the degradation rate of copolymer bonds is greater than the homo-polymer bonds and generally, the more L-D bonds can lead to faster degradation rates. The reason why L-D bonds can degrade faster than L-L bonds is not very clear. The difference might be attributed to the concept of collective steric effects [189]. These effects from L-L and D-D bonds could be different from the L-D configuration, which ultimately can influence the rate of degradation.

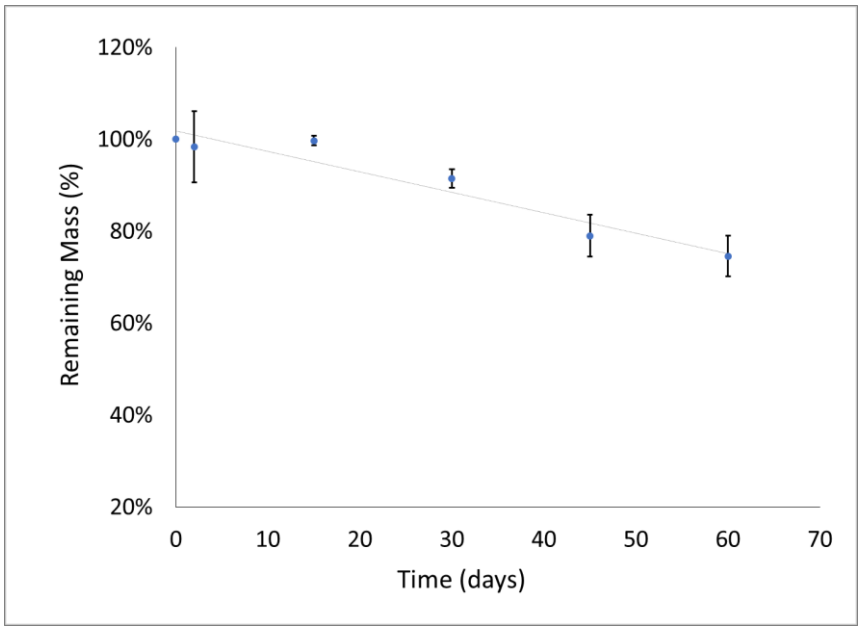


Figure 6.1 Mass % as a function of time during 60 days of the degradation of the PLA pellet at 50 °C

Figure 6.2 illustrates the percentage of the remaining mass as a function of time during 60 days of the degradation process of the PLA pellet at 70 °C. The amount of weight loss at this temperature was 32% and 51% after 1 and 2 months, respectively. The values for the weight loss and the hydrolysis rate are much higher (around 2 times more) in comparison with the ones observed at 50 °C. This is because by increasing the temperature; the diffusion rate of the buffer could be increased, resulting in increasing the amount of soluble oligomers. Furthermore, at the temperature of 70 °C (which is above the T_g of the PLA in this study) the molecules of the

buffer could penetrate through the amorphous region of the polymer easier, resulting in a faster rate of hydrolysis [186, 187].

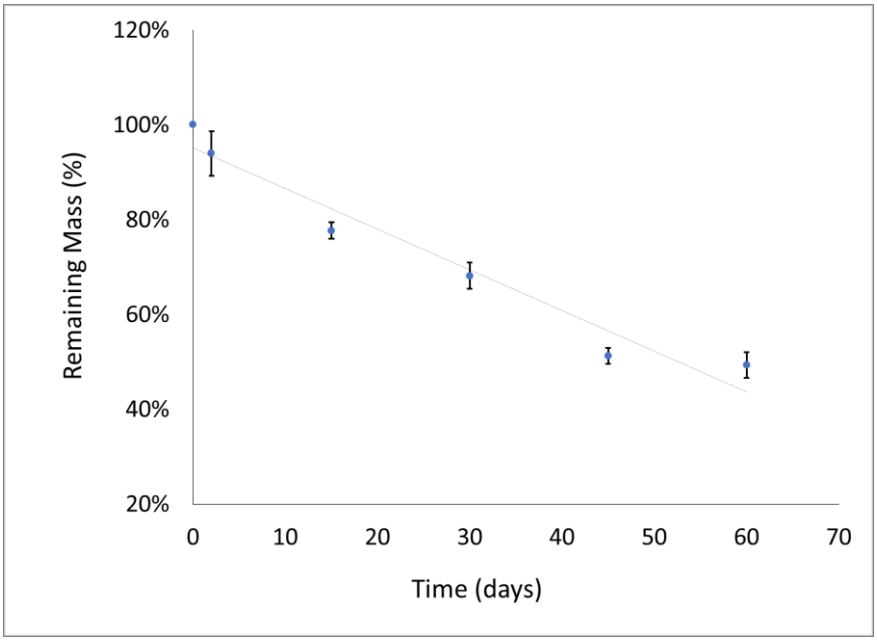


Figure 6.2 Mass % as a function of time during 60 days of the degradation process of the PLA pellet at 70 °C

A degradation study under dynamic conditions was conducted for all samples (as described in the experimental Chapter 2, Table 2.4) at 50 °C for 30 days. No change was observed in the weight and dimensions of all samples, including the as-received PLA pellet during the experiment, in contrast to the degradation observed under static conditions for the as-received PLA pellet as discussed above. The reason that no weight change was observed during the dynamic degradation testing could be related to the heterogeneous hydrolysis as well as the auto-acceleration phenomenon, which could influence the degradation process. In other words, the monomers which are generated during the hydrolysis process (e.g., lactic acid) can reduce the amount of pH locally [189], [190]. This means that under static conditions, there was a local decrease of pH that could accelerate the degradation rate of the polymer. The changes of pH as a function of degradation time for PLA pellet at 50 °C in static conditions shown in Figure 6.3. As it is apparent from this figure, the amount of pH decreased significantly (from

8.17 to 3.93) after a month. However, during the degradation study under dynamic conditions, there was no localised change of pH as the pH was almost constant during the experiment owing to the aqueous environment being regenerated continuously (circulation of the buffer) and therefore any small changes in the pH did not have any effect on the degradation rate. Consequently, during degradation under dynamic conditions, the effect of the auto-acceleration degradation mechanism was eliminated resulting in a decrease in degradation rate and lower weight loss compared with the weight loss observed during the degradation study under the static conditions.

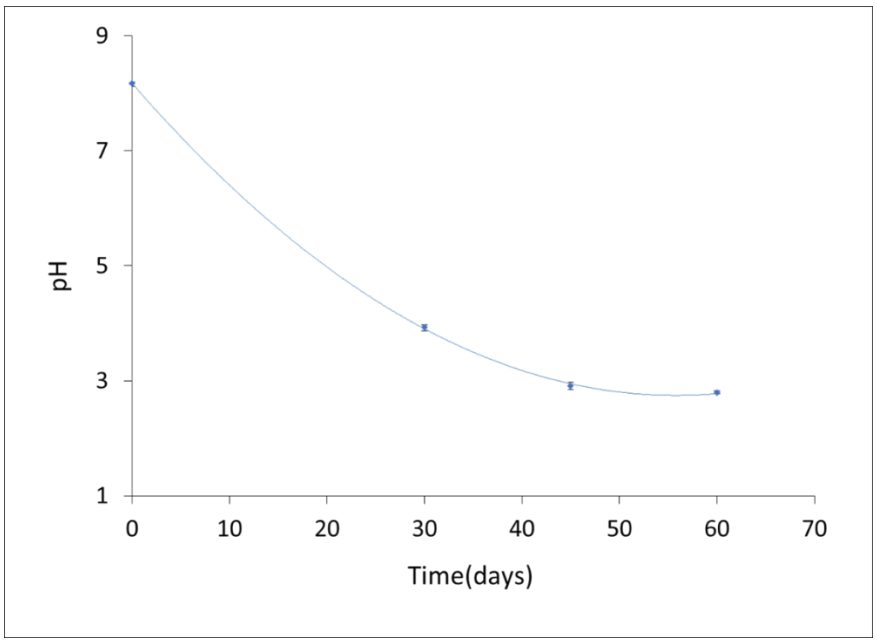


Figure 6.3 pH changes as a function of time during 60 days of degradation process at 50 degree for PLA pellet in static conditions. The error bars are very small (± 0.04) and are not recognisable in the graph.

6.1.2 Size exclusion chromatography (SEC) analysis

Size exclusion chromatography (SEC) analysis was performed on the samples before and after the degradation process under dynamic conditions in order to investigate the effect of the degradation process on the molecular weight behaviour of the samples. Table 6.1 shows the amount of the molecular weight measured by SEC on the samples before the degradation process. As it was explained previously in the experimental chapter (Chapter 2), most of the samples (PLA pellet, amorphous PLA, PLA-5 wt% HA and PLA-20 wt% HA) were analysed by SEC using THF as the solvent. However, the semi-crystalline samples with around 40% crystallinity degree (small and large spherulites, the preparation was the same as the nono-indentation samples in a DSC which was explained in Chapter 5) were not soluble in THF; thus, $CHCl_3$ was used as the solvent for their analysis. However, according to Table 6.1, different values of molecular weight were obtained for the amorphous PLA sample (as the reference) using the two different solvents (THF and $CHCl_3$). Therefore, it was decided to compare the results for each group of the samples (according to the solvent) separately. According to Table 6.1, the amount of the molecular weight of the as-received PLA pellet was 86,920 g mol^{-1}. It is also apparent from this table that there was a reduction in the amount of molecular weight of PLA and PLA-HA composite samples after the hot pressing process (amorphous PLA, PLA-5 wt% HA and PLA-20 wt% HA). The decrease in the molecular weight of the PLA after a melting manufacturing process (hot pressing in this study) due to the thermal degradation is usual and it has been reported previously by other authors [136, 191]. However, there was a significant reduction in the molecular weight of PLA-5 wt% HA sample (compared to the other hot pressed samples) after hot pressing, which was unexpected. This could be due to an error occurred during the SEC measurement of the samples.

The amount of molecular weight of the semi-crystalline samples with 40% crystallinity (small and large spherulites) is smaller than the amorphous PLA sample (Table 6.1). This might be

because the crystalline phase of the polymer was not dissolved entirely during the SEC analysis; thus, the obtained molecular weight was mostly related to the dissolved amorphous part of the semi-crystalline polymers.

Semi-crystalline samples (around 40% crystallinity) with large spherulites illustrated a larger value of molecular weight (around 18000 g mol^{-1}) in comparison with small spherulites with the same degree of crystallinity. As previously mentioned in Chapter 5, the thickness of lamellae in the large spherulites sample was greater than the small spherulites sample with the same degree of crystallinity. According to the literature, increasing the average lamellar thickness in a semi-crystalline polymer can result in increasing its molecular weight [192].

Table 6.1 SEC analysis of polymer samples before degradation under dynamic conditions

Solvent	Sample	M_n /gmol^{-1}	M_w/ gmol^{-1}	PDI= M_w / M_n
THF	PLA pellet	51,602	86,920	1.7
	Amorphous PLA	45,014	77,428	1.7
	PLA- 5% HA	31,322	60,207	1.9
	PLA-20% HA	47,469	85,245	1.8
$CHCl_3$	Amorphous PLA (reference)	48,800	62,900	1.3
	Semi-crystalline PLA-Small spherulites	25,030	36,150	1.4
	Semi-crystalline PLA-Large spherulites	41,650	54,050	1.3

Table 6.2 illustrates the amount of molecular weight measured via SEC for the samples after the degradation process. As it is apparent from this table, the molecular weight of all samples was reduced significantly suggesting that hydrolytic degradation occurred within all samples in accordance with the literature [15, 184, 187, 189, 193]. The percentages of reduction of M_w and M_n for the as-received PLA pellet and the amorphous PLA (after hot pressing) are quite similar. However, according to the results, it seems that by increasing the amount of HA particles within the polymer (5 and 20 wt% HA), the percentage of the decrease in both M_w and M_n of PLA was reduced (see Table 6.2). According to the literature, by incorporating the HA particles into the structure of PLA, the degradation rate was reduced as a result of ion exchange between the alkaline HA particles and the aqueous environment neutralising the effect the degradation by-products (such as L-lactic acid) on the hydrolysis of the polymer [133].

In the case of the semi-crystalline samples with a similar degree of crystallinity, the reduction in the molecular weight was more in the case of large spherulites samples compared to the samples with small spherulites (see Table 6.2). This might be due to the fact that samples containing small spherulites were more densely packed compared to the samples containing larger spherulites. Therefore, the buffer molecules could not penetrate deeply inside the small spherulite samples containing more densely packed microstructures compared to the samples containing larger spherulites. However, Tomasi et al. reported that the enzymatic degradation rate of Poly(3-hydroxybutyrate) (PHB) increased by decreasing the average size of spherulites [194].

Table 6.2 SEC analysis of polymer samples after degradation under dynamic condition

Solvent	Sample	M_n /gmol^{-1}	M_w/ gmol^{-1}	PDI= M_w / M_n	Reduction of M_n %	Reduction of M_w %
THF	PLA pellet	13,793	24,789	1.8	73	71
	Amorphous PLA	13,386	24,506	1.8	70	68
	PLA- 5% HA	14,759	22,840	1.6	53	62
	PLA-20% HA	18,772	38,677	2	60	54
$CHCl_3$	Semi-crystalline PLA-Small spherulites	12,020	21100	1.7	52	42
	Semi-crystalline PLA-Large spherulites	14,160	19,090	1.4	66	65

As it was explained in the experimental chapter, SEC analysis was also performed on the liquid (Tris buffer) at different points of the experiment to investigate the amount of polymer release (dissolution of the polymer) during the experiment. However, as it was expected, no polymer was detected in good agreement with the fact that no mass change was observed during the polymer degradation study.

The values of the polydispersity index (PDI) for all samples before hydrolysis were similar and they remained the same after hydrolysis (Tables 6.1 and 6.2). There is a debate in the literature about how polymer hydrolytic degradation occurs. According to some authors, during hydrolysis, the reactivity of the polymer bonds at the end of the polymer chains is higher [195]. However, others believe that hydrolysis takes place by random chain scission and the reactivity for all bonds is equal. In the latter case, when all bonds have equal reactivity, a larger polymer

chain containing more bonds, could react with water and degrade faster in comparison with smaller polymer chains. Therefore, the size of polymer chains can become similar and consequently, the polydispersity (PDI) can approach 1. On the other hand, if the reactivity of the bonds at the chain ends is higher the degradation occurs more quickly for smaller polymer chains compared to the larger ones resulting in increasing the PDI of the samples during hydrolytic degradation. In this study, the amount of PDI did not increase after degradation, indicating that all polymer bonds had identical reactivity and degradation occurred randomly rather than at the chain ends [189].

6.1.3 The effect of degradation on the microstructure of polymers

DSC analysis was carried out on the samples before and after the degradation process under dynamic conditions in order to explore the effect of the degradation process on the crystallinity and microstructure of the polymer samples. The DSC traces (1st heating scans) of the samples before and after degradation are presented in Figures 6.4-6.9.

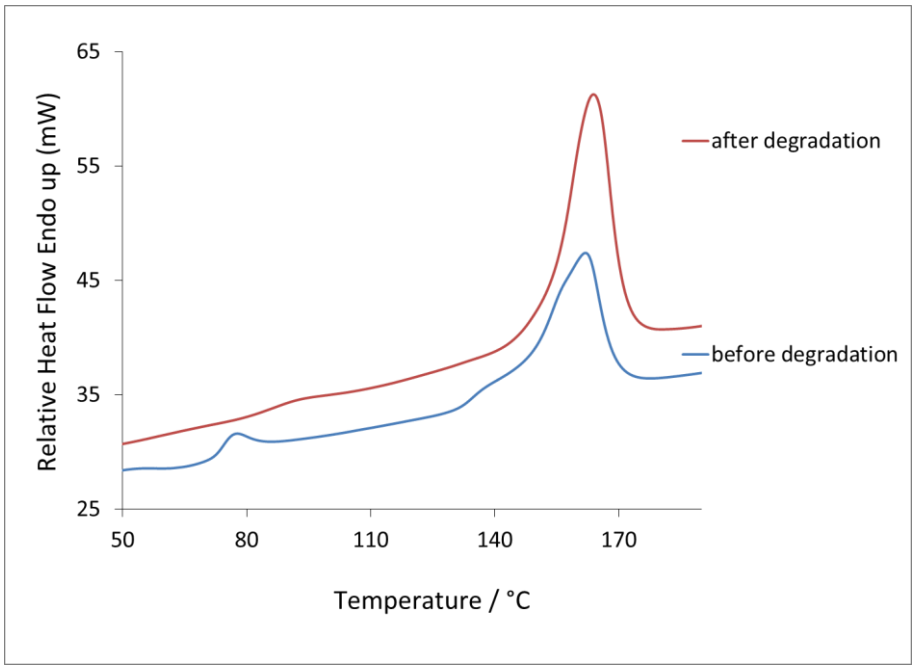


Figure 6.4 DSC scans (first heating scans) of as-received PLA pellet before and after degradation

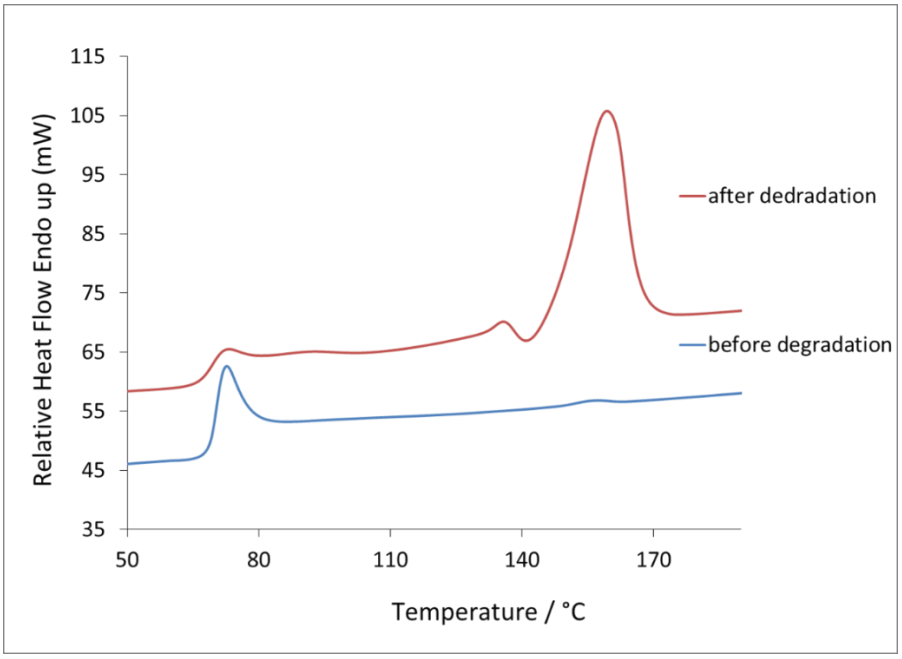


Figure 6.5 DSC scans (first heating scans) of amorphous PLA obtained via hot pressing before and after degradation

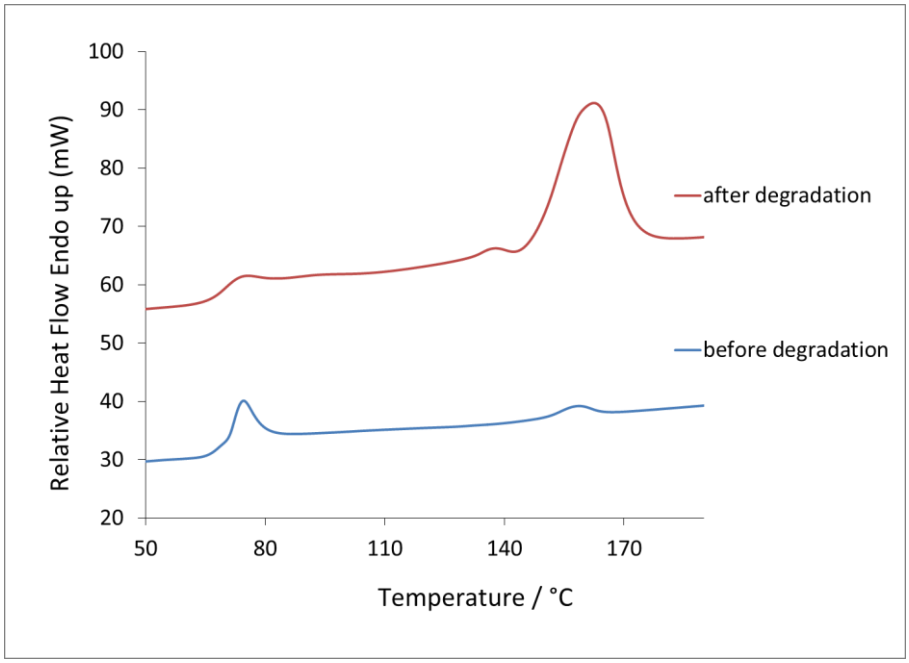


Figure 6.6 DSC scans (first heating scans) of amorphous PLA-5 wt% HA obtained via hot pressing before and after degradation

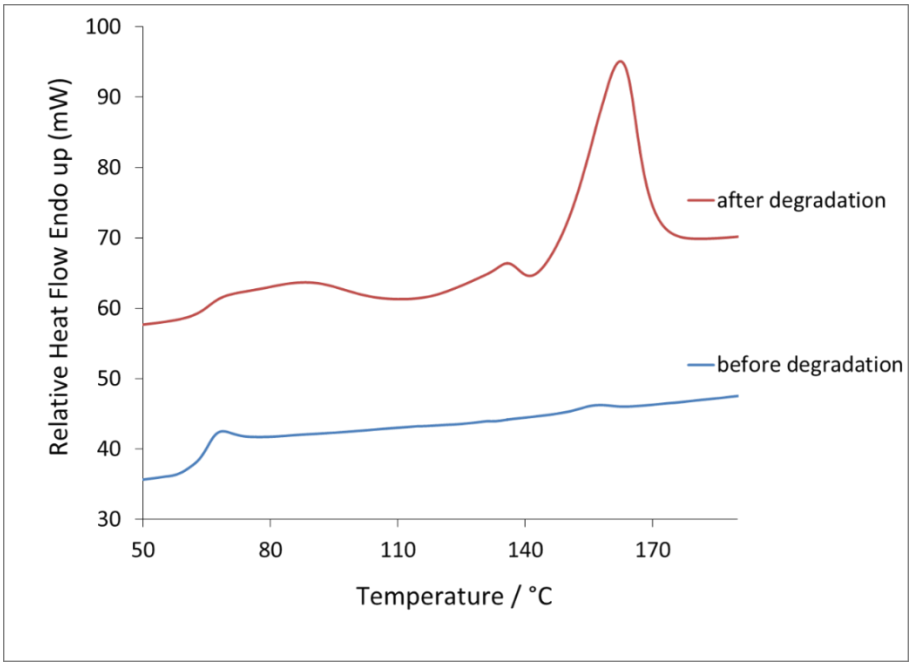


Figure 6.7 DSC scans (first heating scans) of amorphous PLA-20 wt% HA obtained via hot pressing before and after degradation

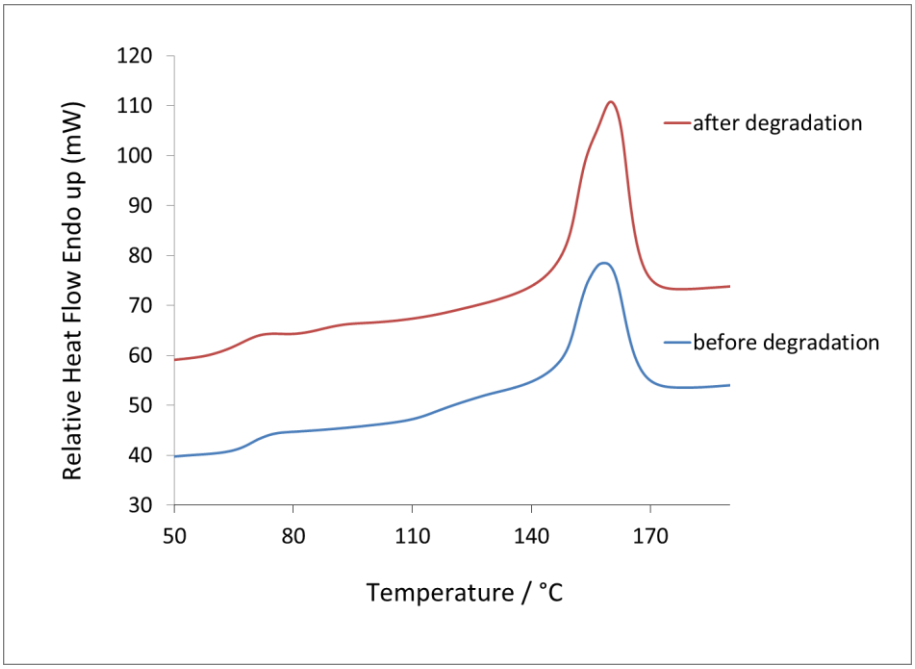


Figure 6.8 DSC scans (first heating scans) of 40% semi-crystalline sample with small spherulites before and after degradation

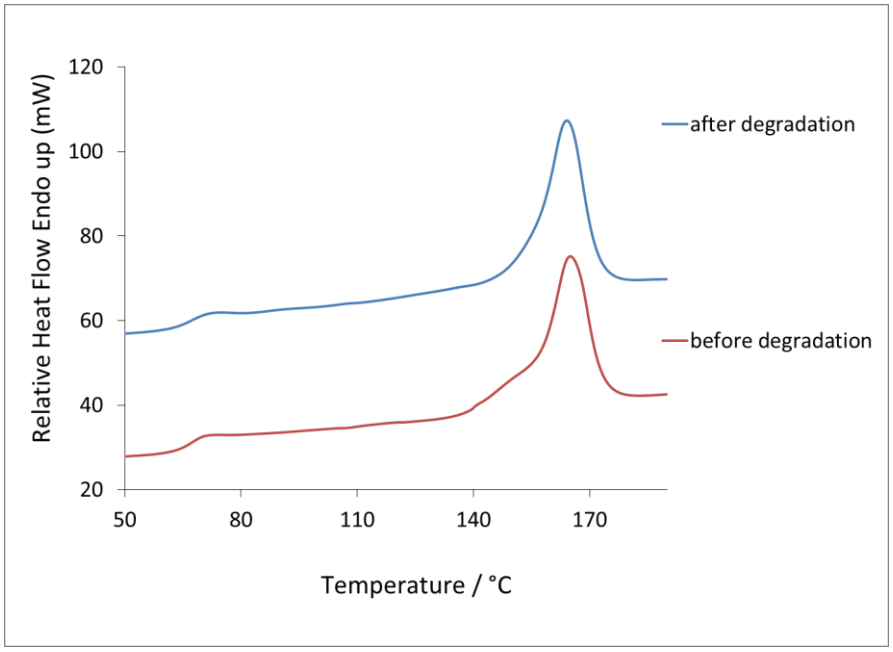


Figure 6.9 DSC scans (first heating scans) of 40% semi-crystalline sample with large spherulites before and after degradation

According to Figure 6.4 (DSC traces of the as-received PLA pellet), the area under the melting peak increased significantly after degradation compared to the DSC trace of the sample before the degradation process, suggesting that the degree of crystallinity increased during degradation. Regarding the samples obtained via hot pressing (Figures 6.5-6.7), no melting peak was observed in the DSC traces before hydrolysis indicating that all samples were totally amorphous. However, after degradation, two melting peaks (one small and a larger second one) appeared in the DSC traces of all three samples demonstrating that the amorphous material was crystallised during degradation. As previously explained (in Chapters 3 and 4), double melting peaks usually appear during the heating process when samples are treated at low temperatures or low heating rates. The maximum heating rate which was possible to use in the DSC was 50 ^{o}C min^{-1}. However, multiple melting peaks were observed in the DSC trace of samples attributed to the crystallisation during the heating of the polymer in accordance with the literature [136]. It can be assumed that some part of the amorphous phase were crystallised during hydrolysis and when a sample of the hydrolysed polymer was heated in the DSC, the

crystalline part acted as a nucleating agent resulting in further crystallisation. Consequently, this crystallinity is associated with the heating process and the only way to prevent it is to run the DSC experiment at a much faster heating rate which was not possible. In the DSC trace of PLA-20 wt% HA after degradation (Figure 6.7) an exothermic peak can be observed between 90 and 130 ºC attributed to cold crystallisation. Therefore, it can be presumed that HA may act as a nucleating agent to promote the crystallisation of PLA after the degradation process. On the other hand, there was no exothermic peak in the DSC graphs of PLA-20 wt% HA composite before the degradation process (see Figure 6.7). Consequently, it can be speculated that HA might act as a more effective nucleating agent when the molecular weight is decreased due to degradation. The area under the melting peaks was also increased for both semi-crystalline samples with small and large spherulites indicating that the heat of fusion was increased for the degraded samples (Figures 6.8 and 6.9).

The degree of crystallinity (X_c), melting point (T_m) and glass transition temperature (T_g) for all samples were measured and shown in Table 6.3.

Table 6.3 Xc, Tm and Tg of the samples before (B) and after (A) the degradation process under dynamic conditions ± standard deviation

Sample		**X_c %**	**T_m °C**	**T_g °C**
PLA pellet	B	38.20 ± 0.04	161 ± 0.8	70 ± 1
	A	48 ± 0.1	169 ± 0.7	Not detectable
Amorphous PLA	B	0.45 ± 0.05	156 ± 0.2	60 ± 0.9
	A	37 ± 0.4	159 ± 0.3	67 ± 1
PLA-5 wt% HA	B	1.2 ± 0.06	158 ± 0.2	60 ± 1
	A	35.8 ± 0.03	162 ± 0.3	67 ± 1
PLA-20 wt% HA	B	0.52	156 ± 0.3	62 ± 0.8
	A	31 ± 0.2	162 ± 0.3	67 ± 0.9
Semi-crystalline PLA with small spherulites	B	39.5 ± 0.3	162.8 ± 0.04	69 ± 1
	A	45 ± 0.5	163 ± 0.1	70 ± 0.8
Semi-crystalline PLA with large spherulites	B	39.5 ± 0.5	163 ± 0.2	67 ± 0.9
	A	48 ± 0.5	164 ± 0.2	68 ± 0.8

The degree of crystallinity (X_c) of the semi-crystalline samples (PLA pellet, 40% small spherulites and 40% large spherulites) was increased after degradation in accordance with the literature [15, 184, 190, 196, 197]. During the hydrolytic degradation process, the polymer chains reacted with water molecules resulting in chain scissions. Consequently, the polymer chains became more mobile resulting in polymer crystallisation and leading to a gradual increase in the heat of fusion and degree of crystallinity of the samples [184, 197]. Due to the faster hydrolytic degradation of the amorphous region compared to the crystalline region, the overall degree of crystallinity of the semi-crystalline samples increased during hydrolysis [190]. Beslikas et al. reported that the degree of crystallinity of PLA increased up to 60 days of hydrolytic degradation and it was stabilised afterwards. This is because after a while (e.g., 60 days in that report) when the molecular weight of the polymer decreased severely, the crystalline region of the semi-crystalline polymer also started to degrade [184].

The degree of crystallinity for all amorphous samples (PLA, PLA-5wt% HA and PLA-20wt% HA) shown in Table 6.3 increased from almost 0% up to more than 30%. This observation is in good agreement with the literature [190, 198]. Goepferich et al. reported that the degree of crystallinity was increased in degraded amorphous polymers (e.g., quenched polymer samples). This is because, during hydrolysis when the polymer chains reacted with the buffer or water, the mobility of polymer chains increased (the T_g of the polymer decreased) owing to the plasticization effect of water which led to the recrystallisation of the polymer [190, 198].

The melting points of the peaks for all samples increased after degradation due to the increase in the crystallinity during degradation (Table 6.3). However, according to Beslikas et al., the increase of the melting point of the semi-crystalline samples was temporary and after a certain period of time, when the crystalline part of the polymer started to hydrolyse, the melting points shifted to lower temperatures [184].

According to Table 6.3, the T_g was not detectable during the DSC analysis of the PLA pellet sample after the degradation indicating that the amorphous part of the sample was reduced significantly or was not present and therefore the T_g of the amorphous phase was not possible to be measured by the DSC.

The T_g values for all amorphous samples were shifted to higher temperatures after degradation. This observation cannot be explained by the Fox-Flory equation (Equation 6.1) that clearly states the relationship of the glass transition temperature with the average number of molecular weight and predicts that the glass transition temperature decreases with the average number of molecular weight of the polymer due to degradation [199]:

$$T_g = T_{g,\infty} - \frac{k}{M_n} \quad [199] \qquad \textbf{(Equation 6.1)}$$

where K (k.kg.mol^{-1}) is the Fox-Flory constant, $T_{g,\infty}$ is the glass transition temperature of a polymer having an infinite molar mass and M_n is the average number of molecular weight of the polymer.

As mentioned above, our results did not show the same dependence of T_g to the molecular weight as predicted by the Fox-Flory equation. This is very surprising and therefore, it was thought that the way the T_g was calculated might have had an effect on the data presented in this thesis. According to Figures 6.5-6.7, there is an ageing peak on the T_g for all amorphous samples before the degradation process. As it was explained in the experimental chapter (Section 2.3), when an endotherm peak appears on the T_g, the T_g of the sample must be determined according to the Richardson's method [135]. The value obtained for the T_g through the Richardson's method is usually smaller in comparison with the normal procedure (mid-point) for the calculation of T_g. Therefore, since the T_g was determined through two different procedures (mid-point before degradation and Richardson's method after degradation), the comparison might be within a range of errors. Furthermore, according to the literature, the

value of $T_{g,\infty}$ can be increased with more D-isomer for the amorphous samples [200]. Therefore, it can be presumed that the copolymer (4% D-isomer in this study) has a lower dependence of T_g on the average number of molecular weight (M_n) when it is in its amorphous phase compared to the semi-crystalline sample in accordance with the literature [198].

The ageing peaks for all samples disappeared after degradation (see Figures 6.4-6.9). As previously explained (in Chapter 4), physical ageing peaks tend to occur in amorphous materials, but not in partially crystalline ones [144]. This further supports the hypothesis that the amorphous phase of the samples during the hydrolytic degradation process was removed and the crystallinity within the samples was increased.

Figure 6.10 illustrates the DSC traces (1st heating scans) of the hot pressed amorphous PLA plaques, which were conditioned in the oven at 50 °C for different periods from 1 to 28 days. According to this figure, ageing of all samples occurred, but no melting point was observed suggesting that no secondary crystallisation occurred during the degradation process at 50 °C. This finding reinforces the argument that the thermal behaviour of all samples was not affected by the temperature of 50 °C during the degradation, no secondary crystallisation was observed and therefore any changes in the DSC curves after degradation were only caused by the hydrolytic degradation process.

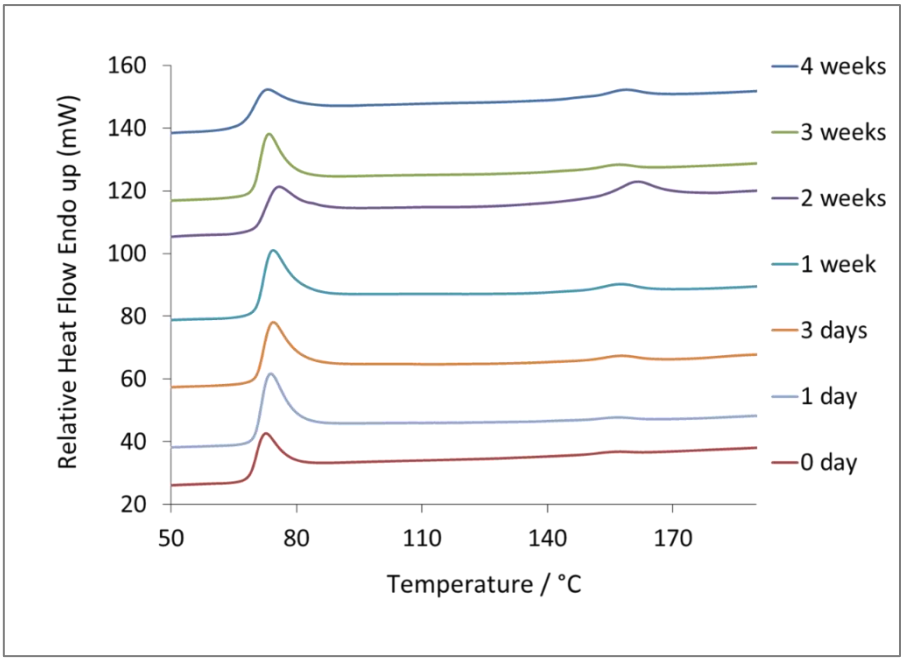


Figure 6.10 DSC scans (first heating scans) of amorphous PLA sample conditioned in the oven at 50 °C for different periods (0 day-28 days)

Figure 6.11 shows the XRD spectra of the hot pressed PLA sample before and after the degradation process under dynamic conditions. The hot pressed PLA before degradation was totally amorphous (a broad peak shown in Figure 6.11 in blue colour). However, after degradation, two diffraction peaks (110)/(200) and (203) at 19.3° and 22.3°, respectively, appeared in the XRD pattern of the sample corresponding to the crystalline structure of PLA in accordance with the literature [201, 202]. This result further confirms that the amorphous sample was crystallised during degradation.

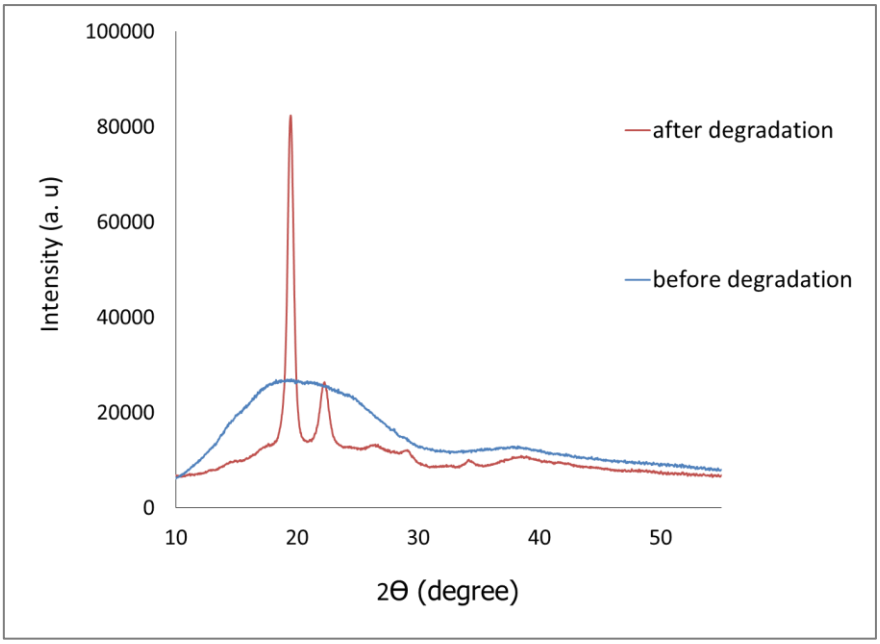


Figure 6.11 XRD spectra of hot pressed amorphous PLA before and after degradation

6.2 Conclusions

The amount of weight loss and hydrolysis rates after degradation under static conditions were doubled with increasing the temperature from 50 to 70 °C. No weight loss was observed at 37 °C during the degradation process for the total time of 2 months, indicating that this time period was not sufficient for the degradation of the PLA samples at 37 °C.

No change was observed in the mass and dimensions of the samples after degradation under dynamic conditions. This was attributed to the fact that there was no local reduction of pH during the experiments because the average value of pH was constant as the degradation medium was recycled and mobile.

According to the SEC results, there was a significant reduction in the molecular weight of all samples, indicating that degradation occurred under dynamic conditions. By increasing the amount of HA within the polymer samples, the change in the molecular weight was reduced due to the alkaline nature of HA particles. Regarding the semi-crystalline samples with the same degree of crystallinity, it seems that samples containing small spherulites and exhibiting more densely packed microstructures were more stable in reaction with the buffer compared to the samples with larger spherulites. The values of PDI for all samples before and after degradation were almost similar, indicating that the degradation occurred randomly through all polymer chains.

DSC studies showed that the degree of crystallinity increased for all samples after the degradation under dynamic conditions. In addition, XRD studies revealed that the amorphous sample crystallised during the degradation. According to the DSC results, HA might act as a more effective nucleating agent for PLA samples after the degradation process (when the molecular weight of PLA decreased significantly).

Chapter 7: Conclusions and Future Work

7.1 Conclusions

DSC and HSM techniques were used to study the crystallisation kinetics and thermal behaviour of the PLA samples. It was possible to produce both totally amorphous and semi-crystalline polymer samples with controlled fractional crystallinity under nonisothermal conditions by controlling the cooling rates from the melting point via these techniques. HSM revealed that the spherulites dimensions could be controlled and manipulated using various cooling rates. By decreasing the cooling rate, the size of the spherulites was increased significantly. Furthermore, the effect of the cooling rate on the glass transition temperature of both semi-crystalline and amorphous samples was studied by DSC. Regarding the semi-crystalline samples, which were produced via low cooling rates (less than 5 ^{o}C min^{-1}), the T_g increased as the cooling rates decreased, whereas the T_g of the amorphous samples made at faster cooling rates (5 ^{o}C min^{-1} and above) became larger by increasing the cooling rate. These two different types of behaviour were attributed to the fact that the T_g of partially crystalline samples was mainly influenced by the degree of crystallinity, while the cooling rate was found to be the dominant factor in determining the T_g of the amorphous samples.

The morphology and crystallisation behaviour of the polymer samples was also controlled under isothermal conditions by holding the samples at three different temperatures, including 95, 110 and 125 ^{o}C after their melting. Double melting peaks appeared during the isothermal heating process of the samples at the low isothermal temperature of 95 ^{o}C even after 4 hours of heat treatment in the DSC due to the melt-recrystallisation-remelting process. However, these multiple melting peaks disappeared after holding the samples for 1 hour at the same temperature (95 ^{o}C) in the DSC when the crystallisation occurred from the amorphous state. Furthermore, generally, the crystallisation rate was faster through cold crystallisation compared

to the melt crystallisation at the same temperature (95 ºC). According to the HSM isothermal crystallisation experiments, by increasing the isothermal temperature, the size of spherulites increased, while their number decreased due to the relationship between the nucleation and growth rate. The fastest rate of crystallisation occurred between 110 and 120 ºC. The isothermal crystallisation was also analysed using the Avrami equation and produced n values of around 3, indicating a three-dimensional crystal growth mechanism with spherical crystals geometry.

PLA-HA composites were fabricated using three different procedures, including hot pressing, injection moulding and solution casting. According to the SEM micrographs of fracture surfaces of hot pressed samples, the HA particles were homogeneously distributed within the PLA matrix. However, the dispersion of HA particles with PLA matrix was poor in both injection moulding and solution casting techniques due to orientation and crystallisation occurred during these processes.

Isothermal DSC results of PLA-HA composites at 95 ºC revealed that the double melting peaks converted to a single peak by the incorporation of a low amount of HA particles (5-20 wt% HA) into the polymer sample, indicating that HA accelerated the crystallisation process. However, at higher loadings of HA (30 and 40 wt% HA), melting peaks with a small shoulder appeared suggesting that the rate of crystallinity can be also reduced by the addition of HA. Nevertheless, the degree of crystallinity was increased linearly by increasing HA content through the composites at both 110 and 125 ºC. According to the HSM micrographs, HA particles had a heterogeneous nucleating effect on PLA. This was also confirmed by the Avrami analysis, where it was observed that the crystallisation rate increased by increasing the HA content of the samples. However, there was no linear relationship between the HA loading and the rate of crystallinity.

Mechanical testing results showed that generally by increasing the amount of filler (HA wt%) within the polymer matrix, the material became stiffer, while its elongation decreased. Composite samples containing 10-20 wt% HA were considered as the most appropriate in terms of maintaining a good balance between all mechanical properties, including stiffness and deformation simultaneously.

It was expected that the HA particles increased the thermal stability of PLA. However, according to the TGA results, the decomposition of PLA was catalysed by the incorporation of HA particles due to hydrolysis.

By etching the samples in DCM, polymer structures with a uniform pore size and distribution were produced. Furthermore, by manipulating the time of etching, the diameter of the pores was controlled.

The results of the nano-indentation testing revealed that as the size of spherulites increased, the thickness of lamella became larger, resulting in an increase in the amount of the nano-hardness of samples. According to the results of tribology studies of PLA samples, the amount of mass loss was increased by introducing secondary crystallisation due to an increase in the embrittlement of the polymer samples. Nevertheless, according to the SEM micrographs and the calculated weight loss of the polymer samples, the wear resistance of polymer samples was lower in the amorphous phase compared to the semi-crystalline phase.

Hydrolytic degradation results under static conditions showed that no weight loss was identified at 37 °C during the degradation process for the total time of 2 months, suggesting that this period was not sufficient for the degradation of PLA samples at the average temperature of the human body. However, the mass loss and hydrolysis rates were increased with increasing the temperature from 50 to 70 °C due to an increase in the diffusion rate of the buffer at a higher temperature. On the other hand, no change was observed in the mass and

dimensions of the samples after degradation under dynamic conditions. This was attributed to the fact that there was no local reduction of pH during the experiments because the average value of pH was constant as the degradation medium was mobile and recycled.

According to the SEC results, there was a significant reduction in the molecular weight of all samples, indicating that degradation occurred under dynamic conditions. By increasing the amount of HA in the polymer samples, the change in the molecular weight was reduced due to the alkaline nature of HA particles resulting in neutralising the effect of the degradation by-products on the hydrolysis rate of the polymer. Regarding the semi-crystalline samples, it was observed that samples containing small spherulites were more stable during the reaction with the buffer compared with the samples containing larger spherulites. This was attributed to the fact that small spherulites samples had a more densely packed microstructure compared to the larger spherulites samples. Consequently, the buffer could not penetrate deeply inside the samples containing small spherulites. The values of PDI for all samples before and after the degradation was almost similar, indicating that the degradation occurred randomly through all polymer chains.

According to the DSC results, the degree of crystallinity increased for all samples during the hydrolytic degradation under dynamic conditions. In addition, XRD studies revealed that the amorphous sample crystallised during the degradation.

7.2 Future Work

PLA-HA composites within this study were produced using three different techniques; hot pressing, injection moulding and solution casting. However, by using an extruder (which can produce filaments of the composite samples) followed by a 3D printing device (Fused Deposition Modelling (FDM)), 3D components of composites with greater effectiveness of blending of PLA and HA particles can be obtained. Furthermore, it would be very interesting to control the cooling rate of polymer samples during the 3D printing process by using a cooling system by which the cooling rate can be adjusted. Consequently, 3D specimens with different degree of crystallinity and microstructures can be produced and the results can be compared with the results of different microstructures of the polymers in this study. Additionally, the crystallinity studies and thermal characterisations of PLA and its composites with HA, which was the main focus of this work can be repeated for the samples obtained via 3D printing with the expectation that likely they will exhibit an improvement in blending. Subsequently, the effect of HA particles as nucleating agents on the PLA matrix could be further investigated and analysed. Furthermore, in this study, only one type of HA powder with a specific particle size was used for all experiments. It would be interesting to repeat all thermal characterisations and crystallisation studies of this work for different particle sizes of HA powder to investigate the effect of various HA particle sizes on the crystallisation behaviour of PLA. In this thesis, the crystallinity of polymer samples was only analysed by DSC. It would be also beneficial to study and analyse the crystallisation behaviour of the samples via XRD and compare the results with DSC.

In this work, it was shown that by etching the samples using DCM, specimens with uniform porosities were produced. Further investigations could be performed in this area. Firstly, the samples could be dried by heating the samples in the oven above the evaporation point of DCM (39.6 °C) until all DCM is removed. Secondly, cell culture growth experiments could be

conducted on the heat treated and etched samples to investigate how well the living cells can interact and adhere to the surface of these samples.

The effect of spherulite dimensions on the nano-hardness of PLA samples was investigated in this thesis. It would be quite useful to explore the effect of secondary crystallisation on the nano-hardness of PLA samples as well. Similarly, regarding the wear testing; only the effect of secondary crystallisation on the mass loss of polymer samples was explored. However, the study could be expanded to investigate the effect of spherulitic microstructures on the wear resistance of polymer samples. Consequently, specimens containing large spherulites can be produced on a scale large enough to be appropriate for wear testing followed by comparing these results with samples containing small spherulites.

Hydrolytic degradation experiments under both static and dynamic conditions must be accomplished for a longer period until weight loss could be observed. SEC analysis must be performed on the liquid (Tris buffer) at different points of the experiment to explore the amount of polymer release (dissolution of the polymer) during the hydrolysis experiment under dynamic conditions. In this study, the characterisations were performed for the samples before (initial point) and after (final point) degradation. However, by characterising the buffer (e.g., SEC analysis) at different periods during hydrolysis, a better understanding of the degradation process can be obtained and the effect of different microstructures of the polymer on the hydrolysis can be further investigated. Furthermore, the exact rate of hydrolysis could be determined for different samples and the results can be analysed and then compared with each other. It would be also beneficial to examine the effect of secondary crystallisation of PLA samples on their hydrolytic degradation. Furthermore, the study could be expanded to explore the effect of different microstructures of PLA on the enzymatic degradation behaviour of PLA.

References

[1] P. Jamshidi, "The formulation of novel calcium phosphate containing culture beads for cell therapy, PhD thesis," University of Birmingham, 2012.

[2] S. C. Cox, "Synthesis and 3D Printing of Hydroxyapatite Scaffolds for Applications in Bone Tissue Engineering, PhD thesis," University of Warwick, 2013.

[3] P. Netti, *Biomedical foams for tissue engineering applications ,P 214*. Woodhead Publishing, 2014.

[4] F. Sefat, "The Role of ECM Proteins, TGFβ-1, 2 and 3 and HCl/ BSA in Cellular Adhesion, Wound Healing and Imaging of the Cell Surface Interface with the Widefield Surface Plasmon Microscope, PhD thesis," University of Bradford, 2013.

[5] B. Clarke, "Normal bone anatomy and physiology.," *Clin. J. Am. Soc. Nephrol.*, vol. 3 Suppl 3, pp. 131–139, 2008.

[6] R. Cancedda, B. Dozin, P. Giannoni, and R. Quarto, "Tissue engineering and cell therapy of cartilage and bone," *Matrix Biol.*, vol. 22, no. 1, pp. 81–91, 2003.

[7] J. Salgado, O. P. Coutinho, and R. L. Reis, "Bone Tissue Engineering : State of the Art and Future Trends," *Macromol. Biosci.*, pp. 743–765, 2004.

[8] R. K. Fuchs, S. J. Warden, and C. H. Turner, *Bone anatomy, physiology and adaptation to mechanical loading*. Woodhead Publishing Limited, 2009.

[9] X. Feng, "Chemical and Biochemical Basis of Cell-Bone Matrix Interaction in Health and Disease," *NIH Public Access*, vol. 64, no. 12, pp. 2391–2404, 2008.

[10] A. Bandyopadhyay, S. Bernard, W. Xue, and S. Bose, "Calcium Phosphate-Based Resorbable Ceramics: Influence of MgO, ZnO, and SiO 2 Dopants," *Am. Ceram. Soc.*,

vol. 2688, no. 21673, 2006.

[11] W. Wang and K. W. K. Yeung, “Bone grafts and biomaterials substitutes for bone defect repair: A review,Biactive Materials,” vol. 2, no. 4, pp. 224–247, 2017.

[12] Z. Sheikh, S. Najeeb, Z. Khurshid, V. Verma, H. Rashid, and M. Glogauer, “Biodegradable Materials for Bone Repair and Tissue Engineering Applications,OPEN ACCESS materials,” pp. 5744–5794, 2015.

[13] S. H. Jo, Y. K. Kim, and Y. H. Choi, “Histological evaluation of the healing process of various bone graft materials after engraftment into the human body,” *Materials (Basel).*, vol. 11, no. 5, 2018.

[14] G. E. J. Poinern, X. T. Le, P. K. Nicholls, M. A. Cake, and D. Fawcett, “The synthesis, characterisation and in vivo study of a bioceramic for potential tissue regeneration applications,SCIENTIFIC REPORTS,” pp. 1–9, 2014.

[15] O. Ô. Ero-Phillips, “DEVELOPMENT OF BI- AND MULTICOMPONENT FIBRES FOR TISSUE ENGINEERING BY ELECTROSPINNING, PhD thesis,” University of Birmingham, 2012.

[16] F. J.O’Brien, “Biomaterials & scaffolds for tissue engineering,” *MaterialsToday*, vol. 14, no. 3, pp. 88–95, 2011.

[17] Z. Wang *et al.*, “Role of the porous structure of the bioceramic scaffolds in bone tissue engineering jin,” *Nat. Preced.*, pp. 1–19, 2010.

[18] L. Polo-Corrales, M. Latorre-Esteves, and J. E. Ramirez-Vick, “Scaffold design for bone regeneration.,” *J. Nanosci. Nanotechnol.*, vol. 14, no. 1, pp. 15–56, Jan. 2014.

[19] F. Zhao, J. Wang, H. Guo, S. Liu, and W. He, “The Effects of Surface Properties of

Nanostructured Bone Repair Materials on Their Performances," *J. Nanomater.*, vol. 2015, pp. 1–11, May 2015.

[20] T. Winkler, F. A. Sass, G. N. Duda, and K. Schmidt-Bleek, "A review of biomaterials in bone defect healing, remaining shortcomings and future opportunities for bone tissue engineering," *Bone Joint Res.*, vol. 7, no. 3, pp. 232–243, Mar. 2018.

[21] F. Matassi, L. Nistri, D. Chicon Paez, and M. Innocenti, "New biomaterials for bone regeneration.," *Clin. cases Miner. bone Metab.*, vol. 8, no. 1, pp. 21–24, Jan. 2011.

[22] B. Stevens, Y. Yang, A. Mohandas, B. Stucker, and K. T. Nguyen, "A review of materials, fabrication methods, and strategies used to enhance bone regeneration in engineered bone tissues," *J. Biomed. Mater. Res. Part B Appl. Biomater.*, vol. 85B, no. 2, pp. 573–582, May 2008.

[23] K. Prasad *et al.*, "Metallic Biomaterials: Current Challenges and Opportunities.," *Mater. (Basel, Switzerland)*, vol. 10, no. 8, Jul. 2017.

[24] F. N. Alaribe, S. L. Manoto, and S. C. K. M. Motaung, "Scaffolds from biomaterials: advantages and limitations in bone and tissue engineering," *Biologia (Bratisl).*, vol. 71, no. 4, pp. 353–366, Jan. 2016.

[25] K. Alvarez and H. Nakajima, "Metallic Scaffolds for Bone Regeneration," *Materials (Basel).*, vol. 2, no. 3, pp. 790–832, Jul. 2009.

[26] K. Mallick, *Bioceramics for skeletal bone regeneration,Bone substitute biomaterials*. 2014.

[27] F. Baino, G. Novajra, and C. Vitale-Brovarone, "Bioceramics and Scaffolds: A Winning Combination for Tissue Engineering,Frontiers in bioengineering and biotechnology,"

vol. 3, 2015.

[28] C. Gao *et al.*, “Current progress in bioactive ceramic scaffolds for bone repair and regeneration, International journal of molecular sciences,” vol. 15, no. 3, pp. 4714–4732, Mar. 2014.

[29] M.-P. Ginebra, M. Espanol, Y. Maazouz, V. Bergez, and D. Pastorino, “Bioceramics and bone healing.,” *EFORT open Rev.*, vol. 3, no. 5, pp. 173–183, May 2018.

[30] J. C. Middleton and A. J. Tipton, “Synthetic biodegradable polymers as orthopedic devices,” *Biomaterials*, vol. 21, no. 23, pp. 2335–2346, Dec. 2000.

[31] D. Zhang, X. Wu, J. Chen, and K. Lin, “The development of collagen based composite scaffolds for bone regeneration,” *Bioact. Mater.*, vol. 3, no. 1, pp. 129–138, Mar. 2018.

[32] J. F. Mano *et al.*, “Natural origin biodegradable systems in tissue engineering and regenerative medicine: present status and some moving trends.,” *J. R. Soc. Interface*, vol. 4, no. 17, pp. 999–1030, Dec. 2007.

[33] S. Gomes, I. B. Leonor, J. F. Mano, R. L. Reis, and D. L. Kaplan, “Natural and Genetically Engineered Proteins for Tissue Engineering.,” *Prog. Polym. Sci.*, vol. 37, no. 1, pp. 1–17, Jan. 2012.

[34] D. Bhattarai, L. Aguilar, C. Park, and C. Kim, “A Review on Properties of Natural and Synthetic Based Electrospun Fibrous Materials for Bone Tissue Engineering,” *Membranes (Basel).*, vol. 8, no. 3, p. 62, Aug. 2018.

[35] M. E. Gomes and R. L. Reis, “Biodegradable polymers and composites in biomedical applications: from catgut to tissue engineering. Part 1 Available systems and their properties,” *Int. Mater. Rev.*, vol. 49, no. 5, pp. 261–273, Oct. 2004.

[36] Z. Heydari, D. Mohebbi-Kalhori, and M. S. Afarani, “Engineered electrospun polycaprolactone (PCL)/octacalcium phosphate (OCP) scaffold for bone tissue engineering,” *Mater. Sci. Eng. C*, vol. 81, pp. 127–132, Dec. 2017.

[37] A. Gregor *et al.*, “Designing of PLA scaffolds for bone tissue replacement fabricated by ordinary commercial 3D printer.,” *J. Biol. Eng.*, vol. 11, p. 31, 2017.

[38] J. P. Zambon *et al.*, “Histological changes induced by Polyglycolic-Acid (PGA) scaffolds seeded with autologous adipose or muscle-derived stem cells when implanted on rabbit bladder.,” *Organogenesis*, vol. 10, no. 2, pp. 278–288, 2014.

[39] H. Eslami *et al.*, “Poly(lactic-co-glycolic acid)(PLGA)/TiO 2 nanotube bioactive composite as a novel scaffold for bone tissue engineering: In vitro and in vivo studies,” *Biologicals*, vol. 53, pp. 51–62, May 2018.

[40] L. P. Gabriel *et al.*, “Bio-based polyurethane for tissue engineering applications: How hydroxyapatite nanoparticles influence the structure, thermal and biological behavior of polyurethane composites,” *Nanomedicine Nanotechnology, Biol. Med.*, vol. 13, no. 1, pp. 201–208, Jan. 2017.

[41] B. Dhandayuthapani, Y. Yoshida, T. Maekawa, and D. S. Kumar, “Polymeric Scaffolds in Tissue Engineering Application: A Review,” *Int. J. Polym. Sci.*, vol. 2011, pp. 1–19, Sep. 2011.

[42] A. Neto and J. Ferreira, “Synthetic and Marine-Derived Porous Scaffolds for Bone Tissue Engineering,” *Materials (Basel).*, vol. 11, no. 9, p. 1702, Sep. 2018.

[43] B. Huang, G. Caetano, C. Vyas, J. J. Blaker, C. Diver, and P. Bártolo, “Polymer-Ceramic Composite Scaffolds: The Effect of Hydroxyapatite and β-tri-Calcium Phosphate.,” *Mater. (Basel, Switzerland)*, vol. 11, no. 1, Jan. 2018.

[44] H. Zhang *et al.*, "Three dimensional printed macroporous polylactic acid/hydroxyapatite composite scaffolds for promoting bone formation in a critical-size rat calvarial defect model.," *Sci. Technol. Adv. Mater.*, vol. 17, no. 1, pp. 136–148, 2016.

[45] G. Turnbull *et al.*, "3D bioactive composite scaffolds for bone tissue engineering," *Bioact. Mater.*, vol. 3, no. 3, pp. 278–314, Sep. 2018.

[46] K. Rezwan, Q. Z. Chen, J. J. Blaker, and A. R. Boccaccini, "Biodegradable and bioactive porous polymer/inorganic composite scaffolds for bone tissue engineering," *Biomaterials*, vol. 27, no. 18, pp. 3413–3431, Jun. 2006.

[47] I. J. Macha, B. Ben-Nissan, J. Santos, S. Cazalbou, and B. Milthorpe, "Hydroxyapatite/PLA Biocomposite Thin Films for Slow Drug Delivery of Antibiotics for the Treatment of Bone and Implant-Related Infections," *Key Eng. Mater.*, vol. 696, pp. 271–276, May 2016.

[48] V. Guarino *et al.*, "Polylactic acid fibre-reinforced polycaprolactone scaffolds for bone tissue engineering," *Biomaterials*, vol. 29, no. 27, pp. 3662–3670, Sep. 2008.

[49] P. Saini, M. Arora, and M. N. V. R. Kumar, "Poly(lactic acid) blends in biomedical applications," *Adv. Drug Deliv. Rev.*, vol. 107, pp. 47–59, Dec. 2016.

[50] A. Södergård and M. Stolt, "Industrial Production of High Molecular Weight Poly(Lactic Acid)," in *Poly(Lactic Acid)*, Hoboken, NJ, USA: John Wiley & Sons, Inc., 2010, pp. 27–41.

[51] A. Bin Abdul Aziz, "Crystallization and enthalpic relaxation studies on a Copolymer of lactic acid, PhD thesis," University of Birmingham, 2017.

[52] Z. Jin, Y. Tian, and J. Wang, "Chemistry and Thermodynamic Properties of Lactic Acid

and Lactide and Solvent Miscibility in Poly(lactic acid) Synthesis, Structures, Properties, Processing, and Applications, R. Auras, L.-T Lim, S. E. M Selke, and H. Tsuji, Eds," in *Poly(Lactic Acid)*, Hoboken, NJ, USA: John Wiley & Sons, Inc., 2010, pp. 19–25.

[53] J. Lunt, "Large-scale production, properties and commercial applications of polylactic acid polymers," *Polym. Degrad. Stab.*, vol. 59, no. 1–3, pp. 145–152, Jan. 1998.

[54] R. L. Madan, *stereochemistry of organic compounds in Organic chemistry*. Tata McGraw-Hill, 2013.

[55] V. Siracusa, P. Rocculi, S. Romani, and M. D. Rosa, "Biodegradable polymers for food packaging: a review," *Trends Food Sci. Technol.*, vol. 19, no. 12, pp. 634–643, Dec. 2008.

[56] L.-T. Lim, R. Auras, and M. Rubino, "Processing technologies for poly(lactic acid)," *Prog. Polym. Sci.*, vol. 33, no. 8, pp. 820–852, Aug. 2008.

[57] M. Mihai, M. A. Huneault, and B. D. Favis, "Crystallinity development in cellular poly(lactic acid) in the presence of supercritical carbon dioxide," *J. Appl. Polym. Sci.*, vol. 113, no. 5, pp. 2920–2932, Sep. 2009.

[58] S. Baratian, E. S. Hall, J. S. Lin, R. Xu, and J. Runt, "Crystallization and Solid-State Structure of Random Polylactide Copolymers: Poly(l -lactide- *co* - d -lactide)s," *Macromolecules*, vol. 34, no. 14, pp. 4857–4864, Jul. 2001.

[59] J. J. Kolstad, "Crystallization kinetics of poly(L-lactide-co-meso-lactide)," *J. Appl. Polym. Sci.*, vol. 62, no. 7, pp. 1079–1091, Nov. 1996.

[60] W. Groot, J. van Krieken, O. Sliekersl, and S. de Vos, "Production and Purification of

Lactic Acid and Lactide in Poly(lactic acid) Synthesis, Structures, Properties, Processing, and Applications, R. Auras, L.-T Lim, S. E. M Selke, and H. Tsuji, Eds," Hoboken, NJ, USA: John Wiley & Sons, Inc., 2010, pp. 1–18.

[61] R. T. MacDonald, A. Stephen P. McCarthy, and R. A. Gross*, "Enzymatic Degradability of Poly(lactide): Effects of Chain Stereochemistry and Material Crystallinity," *Macromolecules*, 1996.

[62] R. J. Young, Robert J and P. A. P. A. Lovell, *Introduction to polymers*. Chapman & Hall, 1991.

[63] F. Cardarelli, *Polymers and Elastomers in Materials handbook : a concise desktop reference*. Springer, 2008.

[64] G. Pertici, *Chapter2-The effect of molecular structure on the properties of biomedical polymers in Durability and reliability of medical polymers,M.Jenkins,A.Stamboulis,Eds*. Woodhead Pub, 2012.

[65] M. Muthukumar, "Chapter 1-Nucleation in Polymer Crystallization,in Advances in Chemical Physics,S.A.Rise,Ed.," Wiley-Blackwell, 2004, pp. 1–63.

[66] L. Sabbatini, *Chapter 1-Introductory remarks on polymers and polymer surfaces, in Polymer surface characterization*. .

[67] J. M. G. Cowie, *Polymers chemistry and physics of modern materials.2nd ed. London:* Blackie Academic and Professional, 1991.

[68] M. Day, Y. Deslandes, J. Roovers, and T. Suprunchuk, "Effect of molecular weight on the crystallization behaviour of poly(aryl ether ether ketone): a differential scanning calorimetry study," *Polymer (Guildf).*, vol. 32, no. 7, pp. 1258–1266, Jan. 1991.

[69] L. H. (Leslie H. Sperling, *Introduction to physical polymer science*. Wiley, 2006.

[70] M. Salmerón Sánchez, V. B. F. Mathot, G. Vanden Poel, and J. L. Gómez Ribelles, "Effect of the Cooling Rate on the Nucleation Kinetics of Poly(l -Lactic Acid) and Its Influence on Morphology," *Macromolecules*, vol. 40, no. 22, pp. 7989–7997, Oct. 2007.

[71] H. Xiao, L. Yang, X. Ren, T. Jiang, and J.-T. Yeh, "Kinetics and crystal structure of poly(lactic acid) crystallized nonisothermally: Effect of plasticizer and nucleating agent," *Polym. Compos.*, vol. 31, no. 12, pp. 2057–2068, Dec. 2010.

[72] P. Cebe and S.-D. Hong, "Crystallization behaviour of poly(ether-ether-ketone)," *Polymer (Guildf).*, vol. 27, no. 8, pp. 1183–1192, Aug. 1986.

[73] S. Andjelic, R. Scogna, S. Sa, A. Andjelic´, and R. C. Scogna, "Polymer crystallization rate challenges: The art of chemistry and processing," *J. Appl. Polym. Sci.*, vol. 132, pp. 42066–42067, 2015.

[74] Z. Chen, "The crystallization of Poly(ethylene terephthalate) studied by thermal analysis and FTIR spectroscopy.PhD thesis," University of Birmingham, 2013.

[75] M. L. Di Lorenzo and C. Silvestre, "Non-isothermal crystallization of polymers," *Prog. Polym. Sci.*, vol. 24, no. 6, pp. 917–950, Aug. 1999.

[76] M. Avrami, "Kinetics of Phase Change. II Transformation-Time Relations for Random Distribution of Nuclei," *J. Chem. Phys.*, vol. 8, no. 2, pp. 212–224, Feb. 1940.

[77] M. Avrami, "Granulation, Phase Change, and Microstructure Kinetics of Phase Change. III," *J. Chem. Phys.*, vol. 9, no. 2, pp. 177–184, Feb. 1941.

[78] D. Dudić, V. Djoković, and D. Kostoski, "The high temperature secondary crystallisation of aged isotactic polypropylene," *Polym. Test.*, vol. 23, no. 6, pp. 621–

627, Sep. 2004.

[79] W. Xie, N. Jiang, and Z. Gan, “Effects of Multi-Arm Structure on Crystallization and Biodegradation of Star-Shaped Poly(ε -caprolactone),” *Macromol. Biosci.*, vol. 8, no. 8, pp. 775–784, Aug. 2008.

[80] Y. He, Z. Fan, Y. Hu, T. Wu, J. Wei, and S. Li, “DSC analysis of isothermal melt-crystallization, glass transition and melting behavior of poly(l-lactide) with different molecular weights,” *Eur. Polym. J.*, vol. 43, no. 10, pp. 4431–4439, Oct. 2007.

[81] A. T. Lorenzo, M. L. Arnal, J. Albuerne, and A. J. Müller, “DSC isothermal polymer crystallization kinetics measurements and the use of the Avrami equation to fit the data: Guidelines to avoid common problems,” *Polym. Test.*, vol. 26, no. 2, pp. 222–231, Apr. 2007.

[82] J. N. Hay and Z. J. Przekop, “On a nonexponential transformation equation for spherulitic crystallization,” *J. Polym. Sci. Polym. Phys. Ed.*, vol. 16, no. 1, pp. 81–89, Jan. 1978.

[83] J. N. Hay, “Crystallisation from the melt, Flow-Induced Crystallisation,” *Gordon Breach Sci. Publ. Ltd London; Gt. Britain*, Mar. 1979.

[84] Z. Dechun, “Chemical and photophysical properties of materials for OLEDs,” *Org. Light. Diodes*, pp. 114–142, Jan. 2013.

[85] C. T. Moynihan, A. J. Easteal, J. Wilder, and J. Tucker, “Dependence of the glass transition temperature on heating and cooling rate,” *J. Phys. Chem.*, vol. 78, no. 26, pp. 2673–2677, Dec. 1974.

[86] Y. (Writer on solid dosage forms) Qiu, Y. Chen, and G. G. Z. Zhang, *Chapter 9-polymer*

properties and characterization in Developing solid oral dosage forms : pharmaceutical theory and practice. Academic, 2009.

[87] A. Rudin, P. Choi, A. Rudin, and P. Choi, "Mechanical Properties of Polymer Solids and Liquids," *Elem. Polym. Sci. Eng.*, pp. 149–229, Jan. 2013.

[88] J. M. Hutchinson, "Physical aging of polymers," *Prog. Polym. Sci.*, vol. 20, no. 4, pp. 703–760, Jan. 1995.

[89] J. R. White, "Polymer ageing: physics, chemistry or engineering? Time to reflect," *Comptes Rendus Chim.*, vol. 9, no. 11–12, pp. 1396–1408, Nov. 2006.

[90] M. Martina and D. W. Hutmacher, "Biodegradable polymers applied in tissue engineering research: a review," *Polym. Int.*, vol. 56, no. 2, pp. 145–157, Feb. 2007.

[91] P. A. Gunatillake and R. Adhikari, "Biodegradable synthetic polymers for tissue engineering.," *Eur. Cell. Mater.*, vol. 5, p. 1–16; discussion 16, May 2003.

[92] A. Göpferich, "Mechanisms of polymer degradation and erosion.," *Biomaterials*, vol. 17, no. 2, pp. 103–104, Jan. 1996.

[93] T. Niemelä and M. Kellomäki, *Bioactive glass and biodegradable polymer composites in Bioactive glasses : materials, properties and applications,Heimo O. Ylänen,Ed,* Woodhead Publishing, 2011.

[94] J. A. Tamada and R. Langer, "Erosion kinetics of hydrolytically degradable polymers.," *Proc. Natl. Acad. Sci. U. S. A.*, vol. 90, no. 2, pp. 552–556, Jan. 1993.

[95] R. van Dijkhuizen-Radersma, L. Moroni, A. van Apeldoorn, Z. Zhang, and D. Grijpma, "Degradable polymers for tissue engineering in tissue engineering,Clemens van Blitterswijk, Peter Thomsen, Jérôme Sohier,Eds," *Acad. Press Ser. Biomed. Eng.*, pp.

193–221, Jan. 2008.

[96] C. R. Gajjar and M. W. King, *Chapter 2,Degradation Process in Resorbable Fiber-Forming Polymers for Biotextile Applications*. Cham: Springer International Publishing, 2014.

[97] F. von Burkersroda, L. Schedl, and A. Göpferich, "Why degradable polymers undergo surface erosion or bulk erosion.," *Biomaterials*, vol. 23, no. 21, pp. 4221–4231, Nov. 2002.

[98] A. Finniss, S. Agarwal, and R. Gupta, "Retarding hydrolytic degradation of polylactic acid: Effect of induced crystallinity and graphene addition," *J. Appl. Polym. Sci.*, vol. 133, no. 43, Nov. 2016.

[99] S. Affatato and L. Grillini, *Topography in bio-tribocorrosion in Biomaterials and Medical Implants,Yu Yan,Ed*. Woodhead Publishing, 2013.

[100] Y. Yamaguchi, *Chapter 2 Wear in Tribology of Plastic Materials Their Characteristics and Applications to Sliding Components*, vol. 16. Elsevier, 1990.

[101] N. K. Myshkin, M. I. Petrokovets, and A. V. Kovalev, "Tribology of polymers: Adhesion, friction, wear, and mass-transfer," *Tribol. Int.*, vol. 38, no. 11–12, pp. 910–921, Nov. 2005.

[102] N. Axén, S. Hogmark, and S. Jacobson, "Friction and Wear Measurement Techniques," 2001.

[103] G. W. (Gwidon W. . Stachowiak and A. W. (Andrew W. . Batchelor, *Tribology of polymers in Engineering tribology*. .

[104] I. V. Gofman, V. E. Yudin, O. Orell, J. Vuorinen, A. Y. Grigoriev, and V. M.

Svetlichnyi, “Influence of the Degree of Crystallinity on the Mechanical and Tribological Properties of High-Performance Thermoplastics Over a Wide Range of Temperatures: From Room Temperature up to 250°C,” *J. Macromol. Sci. Part B*, vol. 52, no. 12, pp. 1848–1860, Dec. 2013.

[105] Jong Hyun Yoo and N. S. Eiss, “Tribological behavior of blends of polyether ether ketone and polyether imide,” *Wear*, vol. 162–164, pp. 418–425, Apr. 1993.

[106] S. V Bely V, “Effect of Structure on Polymer Friction.Wear,” vol. 18, no. 4, pp. 11–18, 1971.

[107] S. B. Ainbinder and K. I. Alksne, “The effect of friction on the distribution of the spherulite structure of polypropylene,” *Polym. Mech.*, vol. 8, no. 4, pp. 570–574, 1974.

[108] F. J. Balta Calleja and S. Fakirov, *Microhardness determination in polymeric materials.Microhardness of polymers*. Cambridge: Cambridge University Press, 2000.

[109] E. J. Balta -Calleja and H.-G. Kilian, “A novel concept in describing elastic and plastic properties of semicrystalline polymers: polyethylene,” *Colloid Polym. Sci.*, vol. 263, no. 9, pp. 697–707, Sep. 1985.

[110] D. Garlotta, “A Literature Review of Poly(Lactic Acid),” *J. Polym. Environ.*, vol. 9, no. 2, pp. 63–84, 2001.

[111] R. von Oepen and W. Michaeli, “Injection moulding of biodegradable implants.,” *Clin. Mater.*, vol. 10, no. 1–2, pp. 21–28, 1992.

[112] Y. He, Z. Fan, J. Wei, and S. Li, “Morphology and melt crystallization of poly(L-lactide) obtained by ring opening polymerization ofL-lactide with zinc catalyst,” *Polym. Eng. Sci.*, vol. 46, no. 11, pp. 1583–1589, Nov. 2006.

[113] M. Yasuniwa, S. Tsubakihara, Y. Sugimoto, and C. Nakafuku, “Thermal analysis of the double-melting behavior of poly(L-lactic acid),” *J. Polym. Sci. Part B Polym. Phys.*, vol. 42, no. 1, pp. 25–32, Jan. 2004.

[114] E. Urbanovici, H. A. Schneider, and H. J. Cantow, “Some considerations concerning the temperature dependence of the bulk crystallization rate constants of polymeric materials,” *J. Polym. Sci. Part B Polym. Phys.*, vol. 35, no. 2, pp. 359–369, Jan. 1997.

[115] J. Ahmed, J.-X. Zhang, Z. Song, and S. K. Varshney, “Thermal properties of polylactides,” *J. Therm. Anal. Calorim.*, vol. 95, no. 3, pp. 957–964, Mar. 2009.

[116] S. B. Ghosh and S. Mohini, *Composites in Poly(lactic acid) : synthesis, structures, properties, processing, and applications, R. Auras, L.-T Lim, S. E. M Selke, and H. Tsuji, Eds,*. Wiley, 2010.

[117] H. Zhou, J. G. Lawrence, and S. B. Bhaduri, “Fabrication aspects of PLA-CaP/PLGA-CaP composites for orthopedic applications: A review,” *Acta Biomater.*, vol. 8, no. 6, pp. 1999–2016, Jul. 2012.

[118] S. M. Zhang, J. Liu, W. Zhou, L. Cheng, and X. D. Guo, “Interfacial fabrication and property of hydroxyapatite/polylactide resorbable bone fixation composites,” *Curr. Appl. Phys.*, vol. 5, no. 5, pp. 516–518, Jul. 2005.

[119] Y. Cui, Y. Liu, Y. Cui, X. Jing, P. Zhang, and X. Chen, “The nanocomposite scaffold of poly(lactide-co-glycolide) and hydroxyapatite surface-grafted with l-lactic acid oligomer for bone repair,” *Acta Biomater.*, vol. 5, no. 7, pp. 2680–2692, Sep. 2009.

[120] T. Wang *et al.*, “Improve the Strength of PLA/HA Composite Through the Use of Surface Initiated Polymerization and Phosphonic Acid Coupling Agent.,” *J. Res. Natl. Inst. Stand. Technol.*, vol. 116, no. 5, pp. 785–796.

[121] C. R. Kothapalli, M. T. Shaw, and M. Wei, “Biodegradable HA-PLA 3-D porous scaffolds: Effect of nano-sized filler content on scaffold properties,” *Acta Biomater.*, vol. 1, no. 6, pp. 653–662, Nov. 2005.

[122] S. Koutsopoulos, “Synthesis and characterization of hydroxyapatite crystals: A review study on the analytical methods,” *J. Biomed. Mater. Res.*, vol. 62, no. 4, pp. 600–612, Dec. 2002.

[123] G. Ma and X. Y. Liu, “Hydroxyapatite: Hexagonal or Monoclinic?,” *Cryst. Growth Des.*, vol. 9, no. 7, pp. 2991–2994, Jul. 2009.

[124] H. Zhou and J. Lee, “Nanoscale hydroxyapatite particles for bone tissue engineering,” *Acta Biomater.*, vol. 7, no. 7, pp. 2769–2781, Jul. 2011.

[125] X. Liu, T. Wang, L. C. Chow, M. Yang, and J. W. Mitchell, “Effects of Inorganic Fillers on the Thermal and Mechanical Properties of Poly(lactic acid).,” *Int. J. Polym. Sci.*, vol. 2014, 2014.

[126] L. Borum-Nicholas and O. C. Wilson, “Surface modification of hydroxyapatite. Part I. Dodecyl alcohol.,” *Biomaterials*, vol. 24, no. 21, pp. 3671–9, Sep. 2003.

[127] M. Kaavessina, F. Khanifatun, I. Ali, and S. M. Alzahrani, “In Vitro</i> Biodegradability of Poly(lactic Acid)/Hydroxyapatite Biocomposites Prepared by Solvent-Blending Technique,” *Adv. Mater. Res.*, vol. 626, pp. 631–635, Dec. 2012.

[128] S. N. Nazhat, M. Kellomäki, P. Törmälä, K. E. Tanner, and W. Bonfield, “Dynamic mechanical characterization of biodegradable composites of hydroxyapatite and polylactides.,” *J. Biomed. Mater. Res.*, vol. 58, no. 4, pp. 335–343, 2001.

[129] N. C. Bleach, S. N. Nazhat, K. E. Tanner, M. Kellomäki, and P. Törmälä, “Effect of

filler content on mechanical and dynamic mechanical properties of particulate biphasic calcium phosphate--polylactide composites.," *Biomaterials*, vol. 23, no. 7, pp. 1579–1585, Apr. 2002.

[130] T. Ferringo, "Principles of filler selection and use. In:Handbook of fillers and reinforcements for plastics, Harry S. Katz and John V. Milewski, Eds., Van Nostrand Reinhold, New York, 1978, 652 pp.," *J. Polym. Sci. Polym. Lett. Ed.*, vol. 16, no. 10, pp. 551–552, Oct. 1978.

[131] Y. Shikinami and M. Okuno, "Bioresorbable devices made of forged composites of hydroxyapatite (HA) particles and poly-L-lactide (PLLA): Part I. Basic characteristics.," *Biomaterials*, vol. 20, no. 9, pp. 859–877, May 1999.

[132] M. Hiljanen-Vainio, M. Heino, and J. V. Seppälä, "Reinforcement of biodegradable poly(ester-urethane) with fillers," *Polymer (Guildf).*, vol. 39, no. 4, pp. 865–872, Feb. 1998.

[133] G. Sui *et al.*, "Poly-L-lactic acid/hydroxyapatite hybrid membrane for bone tissue regeneration," *J. Biomed. Mater. Res. Part A*, vol. 82A, no. 2, pp. 445–454, Aug. 2007.

[134] "https://pslc.ws/macrog/dsc.htm." .

[135] L. Aras and M. J. Richardson, "The glass transition behaviour and thermodynamic properties of amorphous polystyrene," *Polymer (Guildf).*, vol. 30, no. 12, pp. 2246–2252, Dec. 1989.

[136] S. H. Murphy, "CARBON ' DIOXIDE ' ASSISTED ' BLENDING ' OF ' BIODEGRADABLE ' POLYESTERS ' ', PhD thesis," University of Birmingham, 2014.

[137] K. E. Robbins, “Secondary crystallisation and degradation during long term aging of P(HB-co-HV), PhD thesis,” University of Birmingham, 2017.

[138] J. K. Nielsen, J. K. Nielsen, J. Maiboe, H. K. Denmark, and K. Denmark, “EPOFIX AND VACUUM: AN EASY METHOD TO MAKE CASTS OF HARD SUBSTRATES,” 1999.

[139] N. Fotaki, *Flow-Through Cell Apparatus (USP Apparatus 4): Operation and Features*, vol. 18, no. 4. Dissolution Technologies Inc, 2011.

[140] D. Battegazzore, S. Bocchini, and A. Frache, “Crystallization kinetics of poly(lactic acid)-talc composites,” *Express Polym. Lett.*, vol. 5, no. 10, pp. 849–858, 2011.

[141] J. Foreman, S. R. Sauerbrunn, and C. L. Marcozzi, “Exploring the Sensitivity of Thermal Analysis Techniques to the Glass Transition Thermal Analysis & Rheology,” 2013.

[142] Pengju Pan, A. Bo Zhu, and Y. Inoue, “Enthalpy Relaxation and Embrittlement of Poly(l-lactide) during Physical Aging,” *Macromolecules*, 2007.

[143] A. Saiter, “RIGID AND MOBILE AMORPHOUS FRACTIONS IN TWO POLY(LACTIC ACID).” 2015.

[144] J. N. Hay, “The physical ageing of amorphous and crystalline polymers,” *Pure Appl. Chem.*, vol. 67, no. 11, pp. 1855–1858, Jan. 1995.

[145] S. K. Burgess, J. E. Leisen, B. E. Kraftschik, C. R. Mubarak, R. M. Kriegel, and W. J. Koros, “Chain Mobility, Thermal, and Mechanical Properties of Poly(ethylene furanoate) Compared to Poly(ethylene terephthalate),” *Macromolecules*, vol. 47, no. 4, pp. 1383–1391, Feb. 2014.

[146] M. L. Di Lorenzo, “The Crystallization and Melting Processes of Poly(L-lactic acid),”

Macromol. Symp., vol. 234, no. 1, pp. 176–183, Feb. 2006.

[147] T. Liu and J. Petermann, "Multiple melting behavior in isothermally cold-crystallized isotactic polystyrene," *Polymer (Guildf).*, vol. 42, no. 15, pp. 6453–6461, Jul. 2001.

[148] M. Bonnet, K.-D. Rogausch, and J. Petermann, "The endothermic ``annealing peak'' of poly(phenylene sulphide) and poly(ethylene terephthalate," *Colloid Polym. Sci.*, vol. 277, no. 6, pp. 513–518, Jun. 1999.

[149] E. Freire, O. Bianchi, J. N. Martins, E. E. C. Monteiro, and M. M. C. Forte, "Non-isothermal crystallization of PVDF/PMMA blends processed in low and high shear mixers," *J. Non. Cryst. Solids*, vol. 358, no. 18–19, pp. 2674–2681, Sep. 2012.

[150] W. Y. Zhou, B. Duan, M. Wang, and W. Lam, "Isothermal and Non-isothermal Crystallization Kinetics of Poly(L-Lactide)/Carbonated Hydroxyapatite Nanocomposite Microspheres," in *Advances in Diverse Industrial Applications of Nanocomposites*, InTech, 2011.

[151] H. Tsuji, H. Takai, and S. K. Saha, "Isothermal and non-isothermal crystallization behavior of poly(l-lactic acid): Effects of stereocomplex as nucleating agent," *Polymer (Guildf).*, vol. 47, no. 11, pp. 3826–3837, May 2006.

[152] S. Iannace and L. Nicolais, "Isothermal crystallization and chain mobility of poly(L-lactide)," *J. Appl. Polym. Sci.*, vol. 64, no. 5, pp. 911–919, May 1997.

[153] K. Phillipson, "Ageing and crystallisation of polycaprolactone, PhD thesis," University of Birmingham, 2016.

[154] C. Chen *et al.*, "Graphene Oxide-Templated Synthesis of Hydroxyapatite Nanowhiskers To Improve the Mechanical and Osteoblastic Performance of Poly(lactic acid) for Bone

Tissue Regeneration," *ACS Sustain. Chem. Eng.*, vol. 6, no. 3, pp. 3862–3869, Mar. 2018.

[155] J.-Y. Bae, J.-E. Won, J.-S. Park, H.-H. Lee, and H.-W. Kim, "Improvement of surface bioactivity of poly(lactic acid) biopolymer by sandblasting with hydroxyapatite bioceramic," *Mater. Lett.*, vol. 65, no. 19, pp. 2951–2955, Oct. 2011.

[156] Y. Furushima, C. Schick, and A. Toda, "Crystallization, recrystallization, and melting of polymer crystals on heating and cooling examined with fast scanning calorimetry," *Polym. Cryst.*, vol. 1, no. 2, Aug. 2018.

[157] A. Makhlouf, H. Satha, D. Frihi, S. Gherib, and R. Seguela, "Optimization of the crystallinity of polypropylene/submicronic-talc composites: The role of filler ratio and cooling rate," *Express Polym. Lett.*, vol. 10, no. 3, pp. 237–247, 2016.

[158] J. Liuyun, X. Chengdong, J. Lixin, and X. Lijuan, "Effect of hydroxyapatite with different morphology on the crystallization behavior, mechanical property and in vitro degradation of hydroxyapatite/poly(lactic-co-glycolic) composite," *Compos. Sci. Technol.*, vol. 93, pp. 61–67, Mar. 2014.

[159] M. Persson, G. S. Lorite, S.-W. Cho, J. Tuukkanen, and M. Skrifvars, "Melt Spinning of Poly(lactic acid) and Hydroxyapatite Composite Fibers: Influence of the Filler Content on the Fiber Properties," *ACS Appl. Mater. Interfaces*, vol. 5, no. 15, pp. 6864–6872, Aug. 2013.

[160] S. Yavarpanah, J. Seyfi, S. M. Davachi, I. Hejazi, and H. A. Khonakdar, "Evaluating the effect of hydroxyapatite nanoparticles on morphology, thermal stability and dynamic mechanical properties of multicomponent blend systems based on polylactic acid/Starch/Polycaprolactone," *J. Vinyl Addit. Technol.*, Aug. 2018.

[161] S. I. Jeong, E. K. Ko, J. Yum, C. H. Jung, Y. M. Lee, and H. Shin, “Nanofibrous Poly(lactic acid)/Hydroxyapatite Composite Scaffolds for Guided Tissue Regeneration,” *Macromol. Biosci.*, vol. 8, no. 4, pp. 328–338, Apr. 2008.

[162] J. Ferri, I. Gisbert, D. García-Sanoguera, M. Reig, and R. Balart, “The effect of beta-tricalcium phosphate on mechanical and thermal performances of poly(lactic acid),” *J. Compos. Mater.*, vol. 50, no. 30, pp. 4189–4198, Dec. 2016.

[163] J. Ferri, J. Jordá, N. Montanes, O. Fenollar, and R. Balart, “Manufacturing and characterization of poly(lactic acid) composites with hydroxyapatite,” *J. Thermoplast. Compos. Mater.*, vol. 31, no. 7, pp. 865–881, Jul. 2018.

[164] Z. Tadmor, “Molecular orientation in injection molding,” *J. Appl. Polym. Sci.*, vol. 18, no. 6, pp. 1753–1772, Jun. 1974.

[165] R. Zheng, P. Kennedy, N. Phan-Thien, and X.-J. Fan, “Thermoviscoelastic simulation of thermally and pressure-induced stresses in injection moulding for the prediction of shrinkage and warpage for fibre-reinforced thermoplastics,” *J. Nonnewton. Fluid Mech.*, vol. 84, no. 2–3, pp. 159–190, Aug. 1999.

[166] S. S. Katti and M. Schultz, “The microstructure of injection-molded semicrystalline polymers: A review,” *Polym. Eng. Sci.*, vol. 22, no. 16, pp. 1001–1017, Nov. 1982.

[167] Y. Shikinami and M. Okuno, “Bioresorbable devices made of forged composites of hydroxyapatite (HA) particles and poly-L-lactide (PLLA): Part I. Basic characteristics.,” *Biomaterials*, vol. 20, no. 9, pp. 859–877, May 1999.

[168] S. Sato, D. Gondo, T. Wada, S. Kanehashi, and K. Nagai, “Effects of various liquid organic solvents on solvent-induced crystallization of amorphous poly(lactic acid) film,” *J. Appl. Polym. Sci.*, vol. 129, no. 3, pp. 1607–1617, Aug. 2013.

[169] N. J. (Nigel J. . Mills, *Polymer foams handbook : engineering and biomechanics applications and design guide*. Butterworth Heinemann, 2007.

[170] F. De Santis, R. Pantani, and G. Titomanlio, "Nucleation and crystallization kinetics of poly(lactic acid)," *Thermochim. Acta*, vol. 522, no. 1–2, pp. 128–134, Aug. 2011.

[171] F. J. Baltá-Calleja and S. Fakirov, *Microhardness of polymers*. Cambridge Univ. Press, 2007.

[172] P. Ding, J. Zhang, N. Song, S. Tang, Y. Liu, and L. Shi, "Anisotropic thermal conductive properties of hot-pressed polystyrene/graphene composites in the through-plane and in-plane directions," *Compos. Sci. Technol.*, vol. 109, pp. 25–31, Mar. 2015.

[173] Koji Yamada, Masamichi Hikosaka, Akihiko Toda, and Shinichi Yamazaki, and K. Tagashira, "Equilibrium Melting Temperature of Isotactic Polypropylene with High Tacticity. 2. Determination by Optical Microscopy," 2003.

[174] R. Popli and L. Mandelkern, "Influence of structural and morphological factors on the mechanical properties of the polyethylenes," *J. Polym. Sci. Part B Polym. Phys.*, vol. 25, no. 3, pp. 441–483, Mar. 1987.

[175] B. Crist, C. J. Fisher, and P. R. Howard, "Mechanical properties of model polyethylenes: tensile elastic modulus and yield stress," *Macromolecules*, vol. 22, no. 4, pp. 1709–1718, Jul. 1989.

[176] C. V. D'Alkaine and H. Otaguro, "The Effect of Step Isothermal Crystallization on the Polymer Crystalline Morphology: The Case of Isotactic Polystyrene," *Polímeros*, vol. 11, no. 4, pp. 234–239, 2001.

[177] A. A. Aziz, S. A. Samsudin, J. N. Hay, and M. J. Jenkins, "The effect of a secondary

process on polymer crystallization kinetics – 3. Co-poly (lactic acid)," *Eur. Polym. J.*, vol. 94, pp. 311–321, Sep. 2017.

[178] H. Unal and A. Mimaroglu, "Friction and wear behaviour of unfilled engineering thermoplastics," *Mater. Des.*, vol. 24, no. 3, pp. 183–187, May 2003.

[179] K. Hornbogen, E., Schäfer, *Friction and wear of thermoplastic polymers, in Fundamentals of Friction and Wear of Materials. Rigney D.A. Ohio.* 1981.

[180] K. S. Kanaga Karuppiah *et al.*, "Friction and wear behavior of ultra-high molecular weight polyethylene as a function of polymer crystallinity," *Acta Biomater.*, vol. 4, no. 5, pp. 1401–1410, Sep. 2008.

[181] F. Biddlestone, A. Harris, J. N. Hay, and T. Hammond, "The Physical Ageing of Amorphous Poly(hydroxybutyrate)," *Polym. Int.*, vol. 39, no. 3, pp. 221–229, Mar. 1996.

[182] D. Harris, "Active-Screen Plasma Surface-Modification of Polyamide 6,6 (PA6,6) and Polytetrafluoroethylene (PTFE). PhD [thesis],University of Birmingham," 2006.

[183] S.-D. PARK, M. TODO, and K. ARAKAWA, "Effects of isothermal crystallization on fracture toughness and crack growth behavior of poly (lactic acid)," *J. Mater. Sci.*, vol. 40, no. 4, pp. 1055–1058, Feb. 2005.

[184] T. Beslikas, I. Gigis, V. Goulios, J. Christoforides, G. Z. Papageorgiou, and D. N. Bikiaris, "Crystallization Study and Comparative in Vitro–in Vivo Hydrolysis of PLA Reinforcement Ligament," *Int. J. Mol. Sci.*, vol. 12, no. 10, pp. 6597–6618, Oct. 2011.

[185] A. Höglund, M. Hakkarainen, and A.-C. Albertsson, "Migration and Hydrolysis of Hydrophobic Polylactide Plasticizer," *Biomacromolecules*, vol. 11, no. 1, pp. 277–283,

Jan. 2010.

[186] Q. Zhou and M. Xanthos, “Nanoclay and crystallinity effects on the hydrolytic degradation of polylactides,” *Polym. Degrad. Stab.*, vol. 93, no. 8, pp. 1450–1459, Aug. 2008.

[187] N. A. Weir, F. J. Buchanan, J. F. Orr, D. F. Farrar, and G. R. Dickson, “Degradation of poly-L-lactide. Part 2: Increased temperature accelerated degradation,” *Proc. Inst. Mech. Eng. Part H J. Eng. Med.*, vol. 218, no. 5, pp. 321–330, May 2004.

[188] H. Fukuzaki *et al.*, “In vivo characteristics of high, molecular weight copoly(l-lactide/glycolide) with S-type degradation pattern for application in drug delivery systems,” *Biomaterials*, vol. 12, no. 4, pp. 433–437, May 1991.

[189] S. Lyu and D. Untereker, “Degradability of polymers for implantable biomedical devices.,” *Int. J. Mol. Sci.*, vol. 10, no. 9, pp. 4033–4065, Sep. 2009.

[190] A. Göpferich, “Mechanisms of polymer degradation and erosion,” *Biomaterials*, vol. 17, no. 2, pp. 103–114, Jan. 1996.

[191] A. Rothen-Weinhold *et al.*, “Injection-molding versus extrusion as manufacturing technique for the preparation of biodegradable implants,” *Eur. J. Pharm. Biopharm.*, vol. 48, no. 2, pp. 113–121, Sep. 1999.

[192] S. K. Mallapragada and N. A. Peppas, “Dissolution mechanism of semicrystalline poly(vinyl alcohol) in water,” *J. Polym. Sci. Part B Polym. Phys.*, vol. 34, no. 7, pp. 1339–1346, May 1996.

[193] S. Farah and D. G. Anderson, “Physical and mechanical properties of PLA, and their functions in widespread applications — A comprehensive review,” *Adv. Drug Deliv.*

Rev., vol. 107, pp. 367–392, Dec. 2016.

[194] G. Tomasi, M. Scandola, B. H. Briese, and D. Jendrossek, "Enzymatic Degradation of Bacterial Poly(3-hydroxybutyrate) by a Depolymerase from *Pseudomonas lemoignei*," *Macromolecules*, vol. 29, no. 2, pp. 507–513, Jan. 1996.

[195] C. F. van Nostrum, T. F. J. Veldhuis, G. W. Bos, and W. E. Hennink, "Hydrolytic degradation of oligo(lactic acid): a kinetic and mechanistic study," *Polymer (Guildf).*, vol. 45, no. 20, pp. 6779–6787, Sep. 2004.

[196] M. Kaavessina, A. Chafidz, I. Ali, and S. M. Al-Zahrani, "Characterization of poly(lactic acid)/hydroxyapatite prepared by a solvent-blending technique," *J. Elastomers Plast.*, vol. 47, no. 8, pp. 753–768, Dec. 2015.

[197] A. Gleadall, J. Pan, and H. Atkinson, "A simplified theory of crystallisation induced by polymer chain scissions for biodegradable polyesters," *Polym. Degrad. Stab.*, vol. 97, no. 9, pp. 1616–1620, Sep. 2012.

[198] G. Gorrasi and R. Pantani, "Effect of PLA grades and morphologies on hydrolytic degradation at composting temperature: Assessment of structural modification and kinetic parameters," *Polym. Degrad. Stab.*, vol. 98, no. 5, pp. 1006–1014, May 2013.

[199] D. Rasselet, A. Ruellan, A. Guinault, G. Miquelard-Garnier, C. Sollogoub, and B. Fayolle, "Oxidative degradation of polylactide (PLA) and its effects on physical and mechanical properties," *Eur. Polym. J.*, vol. 50, pp. 109–116, Jan. 2014.

[200] D. M. Bigg, "Polylactide copolymers: Effect of copolymer ratio and end capping on their properties," *Adv. Polym. Technol.*, vol. 24, no. 2, pp. 69–82, 2005.

[201] T. Tabi, I. E. Sajo, F. Szabo, A. S. Luyt, and J. G. Kovacs, "Crystalline structure of

annealed polylactic acid and its relation to processing," *Express Polym. Lett.*, vol. 4, no. 10, pp. 659–668, 2010.

[202] S. D. Hsu and Y. L. Yao, "EFFECT OF FILM FORMATION METHOD AND ANNEALING ON CRYSTALLINITY OF POLY (L-LACTIC ACID) FILMS." 2011.